An investigation into the self-assembly of aromatic amino acids: Structural polymorphism, unusual stability, and detection of the metastable intermediates

Ph.D. Thesis

By

DEBANJAN BAGCHI

DEPARTMENT OF CHEMISTRY

INDIAN INSTITUTE OF TECHNOLOGY INDORE

JULY 2024

An investigation into the self-assembly of aromatic amino acids: Structural polymorphism, unusual stability, and detection of the metastable intermediates

A THESIS

Submitted in partial fulfillment of the
requirements for the award of the degree
of
DOCTOR OF PHILOSOPHY

by

DEBANJAN BAGCHI

DEPARTMENT OF CHEMISTRY
INDIAN INSTITUTE OF TECHNOLOGY INDORE
JULY 2024

INDIAN INSTITUTE OF TECHNOLOGY INDORE

I hereby certify that the work which is being presented in the thesis entitled **An investigation into the self-assembly of aromatic amino acids: Structural polymorphism, unusual stability, and detection of the metastable intermediates** in the partial fulfillment of the requirements for the award of the degree of **DOCTOR OF PHILOSOPHY** and submitted in the **DEPARTMENT OF CHEMISTRY, Indian Institute of Technology Indore**, is an authentic record of my own work carried out during the time period from **JULY 2019** to **JULY 2024** under the supervision of **Prof. ANJAN CHAKRABORTY**, Professor, Department of Chemistry, Indian Institute of Technology Indore.

The matter presented in this thesis has not been submitted by me for the award of any other degree of this or any other institute.

Debanjan Bagchi

DEBANJAN BAGCHI

This is to certify that the above statement made by the candidate is correct to the best of my knowledge.

A Chakraborty

Prof. ANJAN CHAKRABORTY

DEBANJAN BAGCHI has successfully given his/her Ph.D. Oral Examination held on 05.12.2024

A Chakraborty

Prof. ANJAN CHAKRABORTY

ACKNOWLEDGEMENTS

This thesis would not have been possible without the guidance and encouragement of several individuals who contributed and extended their valuable assistance in the thesis works; it is a pleasure to thank those who made the thesis works possible.

I am profoundly grateful to my supervisor, Professor Anjan Chakraborty, for his constant support, invaluable guidance, encouragement, and help throughout the whole course of the thesis work. I could not have completed this journey without his thorough knowledge, superior command over the subject, precious advice, and constant enthusiasm. His ideologies have been a constant source of inspiration, which have made me cruise through the Ph.D. journey much more efficiently. Moreover, he stood firmly by my side whenever I needed it the most. I will forever be grateful and indebted to him for his moral support, motivation, and guidance.

Additionally, I am highly thankful to my PSPC members, Dr. Tridib K. Sarma and Prof. Apurba K. Das, for their valuable suggestions and guidance. Without their feedback, this endeavor wouldn't have been possible. I would also like to thank Prof. Tushar Kanti Mukherjee, HOD Department of Chemistry IIT Indore, Professor Suhas Joshi, Director IIT Indore, and all the faculty members of the Department of Chemistry, IIT Indore, for their guidance and valuable insights about my thesis work. I would like to thank the Sophisticated Instrument Centre (SIC), Indian Institute of Technology Indore, for providing in-house research equipment.

I want to express my heartfelt thanks to Mr. Kinny Pandey, Mr. Ghanshyam Bhavsar, Mr. Manish Kushwaha, Mrs. Vinita Kothari, and Mr. Rameshwar Dauhare for their technical support, without which it would not be possible to continue my work. I am very much thankful to Dr. Ravinder Kumar for his selfless cooperation and guidance during confocal microscopy experiments. I would like to

acknowledge all the technical and non-technical staff of IIT Indore for their assistance and service.

I want to express my heartfelt thanks to all the members of our Laboratory. I personally extend my heartiest gratitude to my seniors, Dr. Soumya Kanti De and Dr. Nishu Kanwa, for their constant guidance, support, and love during my Ph.D. journey. Besides, I want to convey my deepest thanks to my colleagues who are no less than friends: Mr. Avijit, Ms. Huma, Ms. Priyanka, Mr. Naveen, Mr. Suman, Ms. Kavana M, Mr. Abhinav, Mr. Saikat, Mr. Sachin Debnath, Mr. Khushwant, Mr. Sachin Vishwakarma, Ms. Sheetal for their selfless co-operation and help to make my work successful.

I have been lucky enough to have some people in my life, without whom this journey would have been incomplete. I want to thank Argha, Sayantan, Shivendra, Nirmiti, Shivendu, Achena, Ekta, Vaishnavi, Ritabrata, Swagata, Mallar, Moumita, Sukanya, Sampurna, Amitabha, Surya, Aditya, Anjali, Ravindra, Suryakamal, and Tarun, for their love and support. In the never-ending list, I would like to mention a few more names: Mr. Tushar, Mr. Subhra, Dr. Lona Dutta, Ms. Ankana Roy, Ms. Pritha Pal, Ms. Ipsita Negel, Dr. Tanushree Ghosh, Ms. Swarna Chatterjee, and Ms. Sweta Agarwal for their love and support. I want to especially thank Mr. Avijit Maity for his support and insights, Ms. Amrita Chakraborty for her good wishes, and Ms. Vidhi Agarwal for believing in me and making me stronger.

Last, but not least, I would finally and with all my heart thank my father, Mr. Ranjan Bagchi, my mother, and Mrs. Monika Bagchi for all the non-repayable hard work they have done to make me who I am today. I am thankful for my brother, Mr. Agniv Bagchi who constantly believed in me and supported me and the endless love I received from him. I end here by thanking all the people mentioned here and others whose names I might have omitted unwillingly.

Debanjan Bagchi

Dedicated to My Family,
Friends and Teachers

SYNOPSIS

Biomolecular self-assembly is a ubiquitous process in nature. Among all the biomolecules, the self-assembly of proteins and peptides has attracted immense interest due to their ability to form various nanostructures with important cellular organizations and functions *[1,2]*. However, their uncontrolled aggregation can lead to the formation of amyloid fibrillar structures, which are associated with several diseases like Alzheimer's disease, type II diabetes, Parkinson's disease, and many more *[3,4]*. Several attempts were made to understand the fundamental principles that govern the self-assembly process, but the mechanism of structural transitions of the proteins and peptides remains elusive. In this context, a reductionist approach can be targeted at understanding the self-assembly of the amino acids, as they serve as the simplest building blocks of proteins or peptides. Recently, amyloid-like fibrillar structures with cytotoxic effects have been reported for single amino acids like phenylalanine, tryptophan, and tyrosine *[5,6]*. This thesis summarizes the experimental results of the self-assembly process of aromatic amino acids and the effect of several external stimuli, like metal ions, pH, temperature, etc., on the self-assembly process using several spectroscopic and microscopic techniques. The thesis also provides a detailed study of how the emission properties of carbon dots can be exploited for the visual detection of different intermediates during self-assembly formation by amino acids.

Summary of the Thesis Work

The contents of each chapter included in the thesis are discussed as follows:

Chapter 1. General Introduction and Background

This chapter briefly introduces the background of the self-assembly process of biomolecules and the origin of the self-aggregation behavior of proteins and peptides. It addresses the effect of several

external stimuli on the self-assembly of peptides and proteins. Further, it describes the importance of understanding the aggregation behavior of amino acids, which serve as the basic building blocks of proteins and peptides. As the visual detection of the self-assembly and its dynamics is of utmost importance, the introduction section also includes how the emission of nanoparticles and carbon dots can be used for the visual detection of the self-assembly formation of amino acids.

Chapter 2. Effect of Metal Ions on the Intrinsic Blue Fluorescence Property and Morphology of Aromatic Amino Acid Self-Assembly

This chapter describes the effect of metal ions of different nuclear charges and sizes on the intrinsic blue luminescence of the amino acids (phenylalanine and tryptophan) and their self-assembled structures with the help of several spectroscopic techniques like steady-state fluorescence, TCSPC, and different imaging techniques like CLSM, and FESEM. The study reveals that the intrinsic blue fluorescence of amino acid assemblies is influenced by the charge and size of the metal ions and their pK_a values. Monovalent Na^+ ($pK_a \sim 14$) and divalent Mg^{2+} and Ca^{2+} ($pK_a \sim 11-12$) do not significantly alter the emission behavior and morphology of the self-assemblies. In contrast, Zn^{2+} ($pK_a \sim 9$), Al^{3+} ($pK_a \sim 5$), and Ga^{3+} ($pK_a \sim 3$) inhibit the usual fibrillation and lead to the formation of nano aggregates, as evident from the imaging studies. These metal ions with a higher charge-to-radius ratio (low pK_a) promote clusterization, which results in the enhancement of the intrinsic fluorescence, an effect known as "clusteroluminescence" of the amino acids aggregates. The inhibition of the large fibrillation of aromatic amino acids and the formation of small nonfibrillar aggregates is attributed to the extensive clusterization of amino acids that take place due to dehydration and enhanced hydrophobic interaction in the presence of metal ions, particularly of lower pK_a values. The clusterization and subsequent formation of diverse nano aggregates in the presence of metal ions

significantly increase the local concentration of amino acids, therefore enhancing the clusteroluminescence as compared to native aggregates.

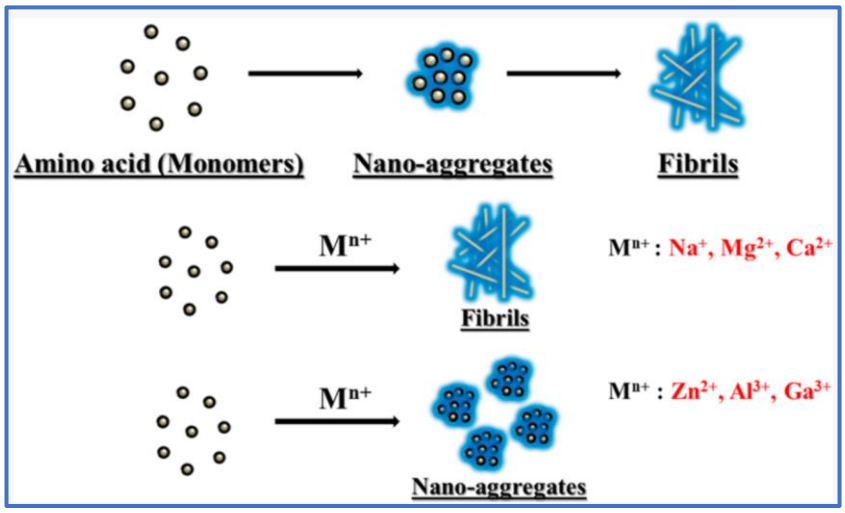

Figure 1. *Schematic representation of the effect of metal ions on the amino acid self-assembly*

Chapter 3. Metal-Ion-Induced Evolution of Phenylalanine Self-Assembly: Structural Polymorphism of Novel Metastable Intermediates

This chapter describes the metal-ion-induced structural polymorphism observed during the self-assembly process of aromatic amino acids. It discusses the existence of different metastable intermediate states of diverse morphologies, for example, droplets, spheres, vesicles, flowers, and toroids, that are sequentially formed in the aqueous medium during the self-assembly process of phenylalanine in the presence of different divalent (Zn^{2+}, Cd^{2+}, and Hg^{2+}) and trivalent (Al^{3+}, Ga^{3+}, and In^{3+}) metal ions having low pK_a values. At the very beginning stage of the self-assembly process, entropy favors the formation of droplet and microsphere, owing to the strong hydrophobic Phe⋯Phe interaction and metal coordination with amino acids. The microspheres subsequently transform into different intermediate structures at the later stage, such as vesicles, flowers, or toroids, due to Phe⋯solvent interactions. For trivalent metal ions, the spherical nano aggregates formed at the initial stage

are much stabilized. They can sustain longer due to stronger hydrophobic interactions than those with divalent metal ions.

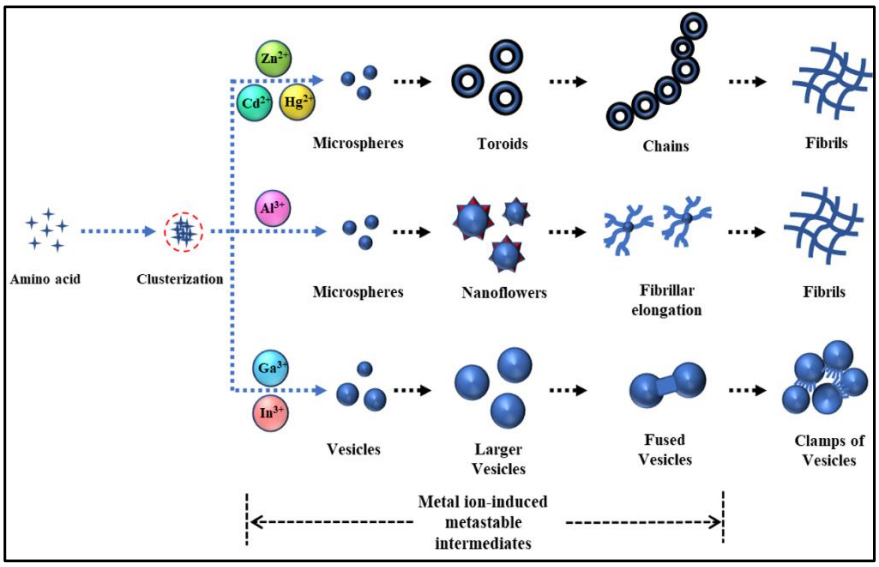

Figure 2. *Schematic representation of the structural polymorphism observed during the phenylalanine self-assembly process under the influence of different metal ions.*

Chapter 4. Metal Ion-Induced Unusual Stability of the Metastable Vesicle-like Intermediates Evolving during the Self-Assembly of Phenylalanine: Prominent Role of Surface Charge Inversion

In this chapter, the self-assembly formation of carboxybenzyl (Z)-protected phenylalanine (ZF) by exchanging the good solvent for a bad solvent and the effect of different metal ions and other factors several factors, like concentration of amino acid, metal ions, incubation temperature, etc., on the self-assembly process are investigated. During the self-assembly of ZF, the fibrillar network is formed that passes through vesicle-like spherical intermediates after phase separation. Microscopic and spectroscopic investigations reveal that the bivalent metal ions like Mg^{2+}, Ca^{2+}, Zn^{2+}, Cd^{2+}, and Hg^{2+} do not affect the fibrillation kinetics. On the contrary, a few specific trivalent metal ions, Al^{3+}, Ga^{3+}, and In^{3+}, stabilize the early-stage vesicle-type intermediates and completely inhibit fibril formation. The metal ions-stabilized microspheres do not undergo

coalescence and remain stable for more than seven days. The unusual stability of the vesicle-like intermediates in the presence of selective metal ions is well rationalized with the metal ion coordination, metal ion-specific entropy factor, and excess hydrophobicity induced by the trivalent metal ions. The time-lapse measurement of surface charge reveals that the surface charge of blank ZF and in the presence of bivalent metal ions changes from a negative value to zero, implying unstable intermediates leading to the fibril network. Strikingly, a prominent charge inversion from an initial negative value to a positive value in the presence of trivalent metal ions imparts unusual stability to the metastable intermediates.

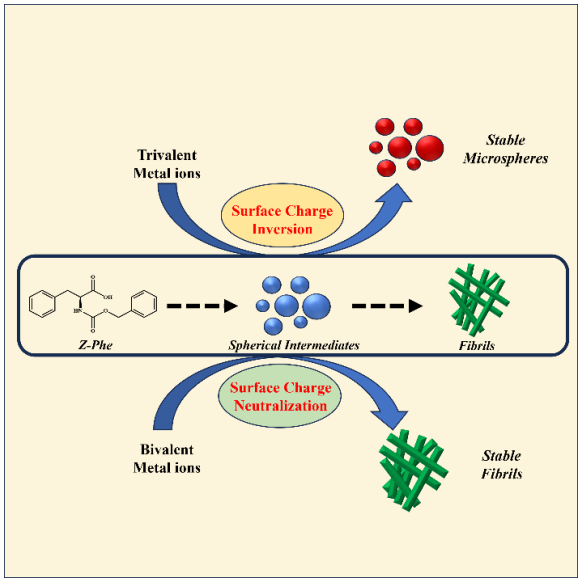

Figure 3. *Schematic representation of the formation of metastable vesicle-like intermediates during ZF self-assembly and their unusual stability in the presence of trivalent metal ions.*

Chapter 5. Distinct and Dynamic Emission Behavior of Hydrophobic Carbon Dots during the Biomolecular Self-Assembly Process

This chapter explores the unique emission behavior of a special hydrophobic carbon dot (HCD) that identifies the distinct intermediates formed during the self-assembly formation of amino acids. It is observed that the restricted rotation of the S-S bond of the

carbon dot synthesized from dithiosalicylic acid and melamine leads to exhibit different emission behaviors in the multistep transformation from the amino acid droplets to fibrils. The HCD shows blue emission during the initial stage of self-assembly, and with the progression of time, it turns into intense red emission, which can be visualized by the naked eye under a UV lamp. The HCD showed the potential to become an excellent biomarker to monitor the self-assembly dynamics of biomolecules. It has advantages over the traditional dyes (like Thioflavin-T, Nile red, etc.), which have their own limitations. The ability to monitor the self-assembly dynamics of the HCD can be used for the visual detection of uncontrolled aggregation of proteins and peptides related to neurodegenerative diseases like Alzheimer's and Parkinson's disease.

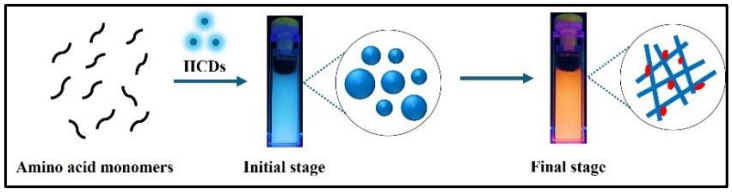

Figure 4. *Schematic representation of the distinct emission behavior of the hydrophobic carbon dot (HCD) during the stepwise transformation of the amino acid droplets to fibrils.*

Chapter 6. Materials, Methods, and Instrumentation

In this chapter, the materials used in the thesis works, various protocols regarding the self-assembly formation, carbon dots synthesis, and various fabrication and characterization techniques that were used throughout the thesis have been discussed in detail.

Chapter 7. Conclusion and Future Aspects

The thesis provides a detailed investigation of the effect of various metal ions, pH, temperature, and carbon dots on the self-assembly process of aromatic amino acids. Our study demonstrates how external stimuli hugely affect the self-assembled structures and account for the unusual stability of the metastable intermediates

formed. This study may facilitate understanding of the role of metal ions in the amino acid self-assembly process and broaden future applications of the obtained nanostructures in drug delivery, tissue engineering, bioimaging, biocatalysis, and other fields.

As a future prospect, these studies may add new dimensions to understanding the self-assembly of biomolecules and their potential application in various bio-inspired applications.

References

[1] Haines L. A., Rajagopal K., Ozbas B. *et al.* (2005), Light-Activated Hydrogel Formation via the Triggered Folding and Self-Assembly of a Designed Peptide, J. Am. Chem. Soc. 127, 17025–17029 (DOI: 10.1021/ja054719o)

[2] Rudra J. S., Tian Y. F., Jung J. P. *et al.* (2010), A Self-Assembling Peptide Acting as an Immune Adjuvant, Proc. Natl. Acad. Sci. U. S. A. 107, 622–627 (DOI: 10.1073/pnas.0912124107)

[3] Knowles T. P., Vendruscolo M., Dobson, C. M. (2014), The amyloid state and its association with protein misfolding diseases, Nat Rev Mol Cell Biol 15, 384−396 (DOI: 10.1038/nrm3810)

[4] Aguzzi A., O'Connor T. (2010), Protein aggregation diseases: pathogenicity and therapeutic perspectives, Nat Rev Drug Discovery 9, 237−248 (DOI: 10.1038/nrd3050)

[5] Adler-Abramovich L., Vaks L., Carny O., *et al.* (2012), Phenylalanine assembly into toxic fibrils suggests amyloid etiology in phenylketonuria, Nat Chem Biol 8, 701−706 (DOI: 10.1038/nchembio.1002)

[6] Shaham-Niv S., Rehak P., Vuković L. *et al.* (2017), Formation of apoptosis-inducing amyloid fibrils by tryptophan, Isr J Chem 57, 729−737 (DOI: 10.1002/ijch.201600076)

LIST OF PUBLICATIONS

Thesis work:

1. **Debanjan Bagchi**, Avijit Maity, Soumya Kanti De, Anjan Chakraborty, Effect of Metal Ions on the Intrinsic Blue Fluorescence Property and Morphology of Aromatic Amino Acid Self-Assembly, J. Phys. Chem. B, 2021, 125, 12436-12445 (DOI: 10.1021/acs.jpcb.1c07392) (Impact factor 2.8)

2. **Debanjan Bagchi**, Avijit Maity, Soumya Kanti De, Anjan Chakraborty, Metal-Ion-Induced Evolution of Phenylalanine Self-Assembly: Structural Polymorphism of Novel Metastable Intermediates, J. Phys. Chem. Lett., 2022, 13, 10409-10417 (DOI: 10.1021/acs.jpclett.2c02882) (Impact factor 4.8)

3. **Debanjan Bagchi**, Avijit Maity, Anjan Chakraborty, Metal Ion-Induced Unusual Stability of the Metastable Vesicle-like Intermediates Evolving during the Self-Assembly of Phenylalanine: Prominent Role of Surface Charge Inversion, J. Phys. Chem. Lett., 2024, 15, 4468-4476 (DOI: 10.1021/acs.jpclett.4c00444) (Impact factor 4.8)

4. **Debanjan Bagchi**, Khushwant Saini, Avijit Maity, Huma Tabassum, Priyanka Nath, Sachin Vishwakarma, Anjan Chakraborty, Distinct and Dynamic Emission Behavior of Hydrophobic Carbon Dots during the Biomolecular Self-Assembly Process (Manuscript Submitted)

Other works:

1. Soumya Kanti De, Avijit Maity, **Debanjan Bagchi**, Anjan Chakraborty, Lipid phase dependent distinct emission behaviour of hydrophobic carbon dots: C-dot based membrane probes, Chem.

Commun., 2021, 57, 9080– 9083 (DOI: 10.1039/d1cc01941d) (Impact factor 4.9)

2. Avijit Maity, Soumya Kanti De, **Debanjan Bagchi**, Hwankyu Lee, Anjan Chakraborty, Mechanistic Pathway of Lipid Phase-Dependent Lipid Corona Formation on Phenylalanine-Functionalized Gold Nanoparticles: A Combined Experimental and Molecular Dynamics Simulation Study, J. Phys. Chem. B, 2022, 126, 11, 2241-2255 (DOI: 10.1021/acs.jpcb.2c00356) (Impact factor 2.8)

3. Avijit Maity, **Debanjan Bagchi**, Soumya Kanti De, Anjan Chakraborty, Insight into the Lysozyme-Induced Aggregation of Aromatic Amino Acid-Functionalized Gold Nanoparticles: Impact of the Protein Conjugation and Lipid Corona on the Aggregation Phenomena, Langmuir 2023, 39, 14, 4881-4894 (DOI: 10.1021/acs.langmuir.2c03077) (Impact factor 3.7)

4. Avijit Maity, Priyanka Nath, **Debanjan Bagchi**, Sachin Debnath, Huma Tabassum, Saikat Sinha, Anjan Chakraborty, Formation of lipid corona on Ag nanoparticles and its impact on Ag^{+} ion dissolution and aggregation of Ag nanoparticles against external stimuli, Chemical Physics Impact, 2024, 8, 100445 (DOI: 10.1016/j.chphi.2023.100445) (Impact factor 2.2)

5. Huma Tabassum, Avijit Maity, Krishna Singh, **Debanjan Bagchi**, Abhinav Prasad, Anjan Chakraborty, Effect of Lipid Corona on Phenylalanine-Functionalized Gold Nanoparticles to Develop Stable and Corona-Free Systems, Langmuir 2024, 40, 8, 4531–4543 (DOI: 10.1021/acs.langmuir.4c00019) (Impact factor 3.7)

TABLE OF CONTENTS

LIST OF FIGURES

LIST OF SCHEMES

LIST OF TABLES

NOMENCLATURE

α	Alpha
β	Beta
τ	Fluorescence Lifetime
a_i	Relative Amplitude
ϕ	Quantum Yield
Å	Angstrom
χ	Chi
λ	Wavelength
μ	Micro
π	Pi
Σ	Summation
ns	Nanosecond
ps	Picosecond
nM	Nano Molar
mM	Milli Molar
μM	Micro Molar
ε	Molar Extinction coefficient
cm	Centimeter
μm	Micrometer
nm	Nanometer
pm	Picometer

a_i	Relative Amplitude
°	Degree
K	Kelvin
mL	Milliliter
mV	Mili Volt
μL	Microliter
a. u.	Arbitrary Unit
λ_{ex}	Excitation Wavelength
λ_{em}	Emission Wavelength
pH	The negative logarithm of hydronium-ion concentration
pK_a	The dissociation constant of an acid in the ground state
ζ	Zeta Potential

ACRONYMS

AA	Amino acid
Aβ	Amyloid β
AD	Alzheimer’s disease
AFM	Atomic force microscopy
AIE	Aggregation-induced emission
Arg	Arginine
Asp	Aspartic acid
BSA	Bovine serum albumin
CA	Citric acid
CAY CD	Citric acid-tyrosine carbon dots
CD	Circular dichroism
CDs	Carbon dots
CLSM	Confocal laser scanning microscopy
CQD	Carbon quantum dot
CR	Congo red
CTE	Clustering-triggered emission
DDS	Drug delivery systems
DNA	Deoxyribonucleic acid
DSC	Differential Scanning Calorimetry
DTSA	Dithiosalicylic acid

ECM	Extracellular matrix
FESEM	Field emission scanning electron microscopy
FL	Fluorescence
FTIR	Fourier transformed infrared
FW	Phenylalanine-tryptophan
FY	Phenylalanine-tyrosine
FWHM	Full Width Half Maxima
Gly	Glycine
GTP	Guanosine triphosphate
HCD	Hydrophobic carbon dot
HEPES	4-(2-hydroxyethyl)-1-piperazineethanesulfonic acid
HR-TEM	High-resolution Transmission Electron Microscope
IAPP	Islet amyloid polypeptide
IEM	Inborn error of metabolism
IRF	Instrument Response Function
Lys	Lysine
MD	Molecular dynamics
NMR	Nuclear Magnetic Resonance
NPs	Nanoparticles
OM	Optical microscopy

PA	Peptide amphiphiles
Phe	Phenylalanine
Phe-Phe or FF	Diphenylalanine
PKU	Phenylketonuria
RNA	Ribonucleic acid
TCSPC	Time-correlated Single Photon Counting
TEM	Transmission Electron Microscope
ThT	Thioflavin T
Trp	Tryptophan
TSC	Through-space conjugation
Tyr	Tyrosine
UV	Ultraviolet–visible
WF	Tryptophan-phenylalanine
WW	Tryptophan-tryptophan
XPS	X-ray photoelectron spectroscopy
ZF	Carboxybenzyl protected phenylalanine

Chapter 1

Introduction and General Background

1.1 Introduction

The story of evolution spans over approximately 4 billion years. Over the years of evolution, biological systems have optimized their complex structures and developed abilities to unravel many biological and natural challenges, including energy transfer and storage, mass transport, and various chemical transformations. These complex functionalities are aided by the hierarchical structures generated from the biomolecular building blocks through self-assembly *[1–3]*. Biomolecular self-assembly is a process where several biomolecular units form an ordered structure or pattern assisted by local interactions. It is a ubiquitous process that allows individual molecules to organize into a wide range of supramolecular structures. In this fashion, nature capitalizes on the self-association process to transform simple biomolecular building blocks into sophisticated, complex materials. Biomolecules like peptides, proteins, lipids, nucleic acids, and various other cellular components self-assemble to form the cell, the elementary biological unit. Some examples of naturally occurring self-assemblies found in biological systems are the lipid bilayer membrane of cells *[4]*, RNA *[5]*, and DNA complexes *[6]*. Organized self-assembled structures play significant roles in physiological functions and life activities, such as amyloid fibril formation *[7]*, chromatin assembly *[8]*, antigen-antibody recognition *[9,10]*, and membrane formation *[11]*. Inspired by these observations, researchers are working on the molecular self-assembly of supramolecular entities that can mimic biomolecular nanostructures and their activities. The distinctive properties of the biomolecules and the tuneable functions of the hierarchical self-assembled structures are exploited for their promising applications in various fields. Inspired by the self-assembled structures, a wide range of materials have been fabricated and utilized in the applications of tissue engineering *[12]*,

biomedicine *[13]*, energy storage *[14]*, optical materials *[15]*, and so on (**Figure 1.1**).

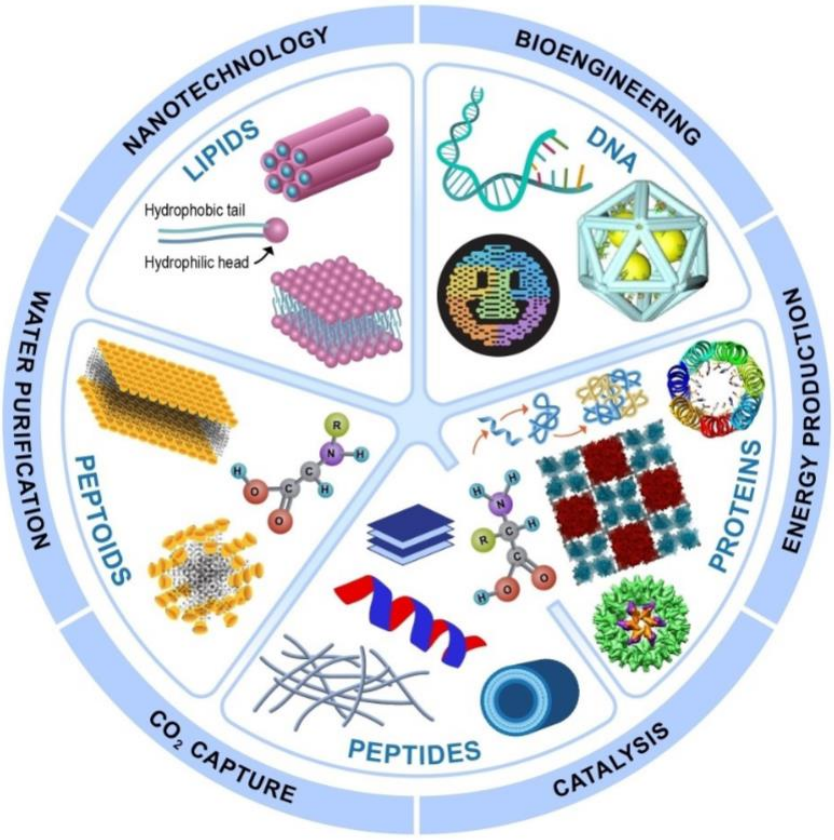

Figure 1.1 *Illustration of various biomolecular self-assembly with their importance and potential applications. Figure reproduced with permission from [16] (Copyright 2023 John Wiley and Sons)*

1.2 Examples of Biomolecular Self-assembled Structures and Their Significance:

Many types of nano- and microstructures are observed in biological systems, such as microtubules, clathrin, flagella, actin filaments, viruses, chromatins, etc. These structures are spontaneously formed by the self-assembly process of various biomolecules like proteins, nucleic acids, and lipids. Examples of some of the important self-assemblies are given as:

1.2.1 Microtubules: The microtubules are natural nanotubes with filamentous structures. They are formed by the self-association of proteins tubulin α & β and GTP. They are involved in forming cell structure, motility, intracellular transport, and cytoskeleton formation *[17]*.

1.2.2 Clathrin: The clathrin lattice is a polyhedral structure, which is formed by self-assembly of clathrin triskelion that consists of 3 clathrin heavy chains and three light chains *[18,19]*. Clathrin plays an important role in forming coated vesicles that help in the transfer of molecules within the cells (endocytosis and exocytosis).

1.2.3 Viruses: Another example of natural supramolecular assembly is viruses. They possess a discrete size and specific aggregation number. They possess rod-like or spherical morphologies with size ~18–100 nm *[20]*. Their structures comprise genome nucleic acids encapsulated in an outer protein shell that is called the "capsid." The 3D structures of simple spherical viruses were determined by X-ray crystallography studies. Most of the spherical viruses are formed by the self-association of multiples of 60 proteins, having icosahedral symmetry. For example, the STNV (satellite tobacco necrosis virus), one of the smallest viruses reported (diameter ~18 nm), is formed by the self-assembly of 60 equivalent protein subunits. TBSV (Tomato bushy stunt virus, diameter ~33 nm) consists of 180 quasi-equivalent protein subunits *[20,21]*.

The nano-space of the viral capsids has been employed as nano-carriers and nano-reactors *[22,23]*. Douglas *et al.* used the nano-space of the capsid of CCMV (cowpea chlorotic mottle virus) to synthesize polyoxometalates *[24]* and single-crystal ferric hydroxide oxide *[25]* successfully. Cornelissen and Nolte *et al.* reported the incorporation of HRP (horseradish peroxidase enzymes) *[26]* and GFP (green fluorescence protein) *[27]* into the inner cavity of the CCMV capsids.

1.2.4 DNA Self-assembly: DNA is a dynamic and one of the most intelligent molecules that is vital in transmitting genetic information and other cellular processes. DNA self-assembly has been a promising

approach to synthesize hybrid novel biomaterials *[28–30]*. DNA nanotechnology involves the formation of nanostructures by DNA self-assembly and it has made quite a rapid progress over the years. Various complex nanostructures were developed, such as DNA polyhedral *[31]*, DNA origami *[2]*, DNA tweezers *[32]*, etc., and have been utilized as biosensors *[33]*, drug delivery systems *[34,35]*, enzyme reactors *[36]*, and nanophotonics *[37]*.

1.2.5 Lipid Bilayer Membrane and Liposome: The lipid bilayer membrane is a thin membrane comprised of two layers of lipid molecules (usually phospholipids). The cellular membranes of most of the organisms and viruses are made of this lipid bilayer. The lipid bilayer is the barrier that controls the permeability of ions, proteins, and other molecules within the cell *[38]*. Liposomes are small artificial vesicles that are formed by the self-assembly of phospholipids in the aqueous medium *[39]*. Liposomes possess similarities with cellular membranes, and therefore, they are often used as simple cell models. Due to their hydrophobic and/or hydrophilic nature, biocompatibility, and size, liposomes are widely used as drug-delivery vehicles for administering drugs and nutrients *[40]*.

From the above-mentioned examples of self-assembled structures, it is evident that the self-aggregations of proteins and peptides, among all other biomolecules, are most crucial from a biological perspective. Therefore, much attention has been given to understanding the essential mechanistic aspects of the self-aggregation process of peptides and proteins.

1.3 The Self-assembly of Peptides and Proteins:

In the past two decades, peptides and proteins have been studied extensively due to their ability to self-assemble into various nanostructures such as tubes *[41]*, spheres *[42]*, fibrils *[43]*, and hydrogels *[44]*. Stupp *et al.* reported that the change in pH can induce the self-assembly of amphiphilic peptides to transform into nanofibers of a high aspect ratio *[45]*. This nanostructured fibrillar scaffold is

reminiscent of the ECM (extracellular matrix) and, therefore, offers the opportunity to mimic the cellular architecture for biomedical applications *[46,47]*. Tirrell *et al.* reported the formation of hydrogels by the self-assembly of artificial proteins triggered by pH and environmental changes *[48]*. These hydrogels can be exploited for wound healing and tissue repairing for medicinal purposes and tissue engineering *[49–51]*. Biodegradable nanofibers of peptides and proteins can serve as target-specific DDS (drug delivery systems) *[52]* with better biocompatibility *[53,54]*. Researchers have also explored the role of self-assemblies of peptides and proteins in the origin of life as self-replicating molecules or catalysts *[55–58]*. In addition, uncontrolled and errant protein and peptide aggregation is associated with several fatal diseases. Protein misfolding leads to self-association into amyloid fibrous structures. These are pathological hallmarks of various devastating neurodegenerative diseases, such as Alzheimer's, Parkinson's, Type II diabetes, and so on *[59]*. Intermolecular interactions between unfolded or partially unfolded proteins can form supramolecular β-sheet structures. This further leads to the abnormal organization where several proteins or polypeptides assemble to form well-organized self-assemblies (**Figure 1.2**).

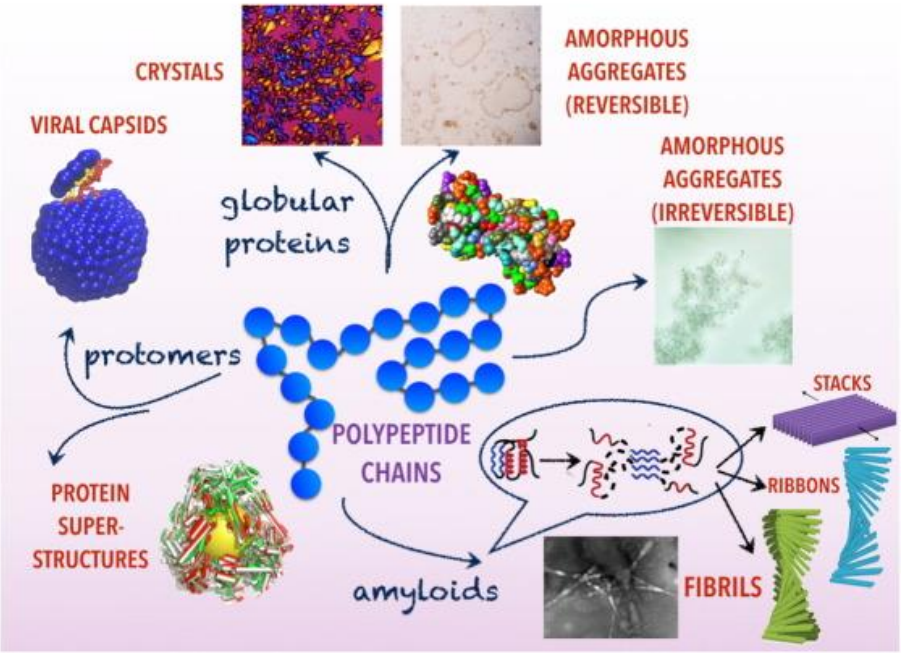

Figure 1.2 *Illustration of various self-assemblies that can be formed by proteins and peptides. Crystals or amorphous aggregates from globular proteins (top), amorphous aggregates or fibrils from peptides and proteins (right), Different twisted structures like stacks, ribbons, and fibrils (bottom right), Higher-ordered structures like viral capsids (with nucleic acid) and protein superstructures (bacterial compartments) (left) [60](Copyright 2016 Elsevier)*

1.3.1 Formation of Amyloid Structures and its Characterization:

Amyloids were first recognized in 1901, over a century ago, by Dr. Eugene Opie. He recognized the deposit formation in the pancreas of patients suffering from type II diabetes *[61]*. In 1906, Alois Alzheimer observed biomaterial deposition in a dementia-affected patient's brain *[62]*. These deposits were termed ''amyloids'' (like starch) for their positive staining by iodine. Later on, the aggregates were recognized to be composed of proteins. Regardless of their source, the structure of amyloids is very typical, consisting of elongated filaments with ~ 10 nm of diameter. The amino acid units are organized into β-strands (separation of ~ 0.4 nm), orthogonally oriented to the fibrillar axes, and closely packed β-sheets running parallel to the fibrillar axes (distance between the sheets ~ 1 nm) *[63, 64]*. Much later, using advanced electron microscopic techniques like AFM (atomic force microscopy) and TEM (transmission electron microscopy), amyloid fibrils having widths of 60 to 130 Å and lengths of 1000 to 16000 Å were observed *[65]*. Amyloid fibrils are known to bind with specific dyes like Thioflavin T (ThT) and Congo red. Thus, these dyes can help in measuring the β-sheet in solution. These dyes are also utilized to monitor the self-aggregation kinetics *[66]*. Infrared spectroscopy is also successfully used for studying amyloid structures and aggregation mechanisms *[67]*. Additionally, solid-state NMR or ss-NMR provides molecular-level information on the formation of amyloid structures *[68]*. X-ray diffraction (XRD) is another sophisticated high-resolution technique that allows the investigation of the molecular structure at the atomic level by obtaining folding information through reflection or

transmission diffraction *[69]*. Amyloid formation is associated with the unfolding of proteins *[70]*, leading to significant changes in the β-structure. Therefore, CD (circular dichroism) spectroscopy is widely used to study amyloidogenesis processes *[71]*.

1.3.2 Peptide-mediated Formation of Amyloid Fibrils:

The amyloid fibrillar structure formation was initially identified in naturally obtained proteins. However, various functional peptides, for example, Amyloid β (36–43 amino acids), human calcitonin (32 amino acids), and IAPP or islet amyloid polypeptide (37 amino acids) were also associated with several neurodegenerative diseases. Aggregated structures of the IAPP were identified in the pancreas of type II diabetes patients *[72]*. While Amyloid β (Aβ) aggregates are found in the brains of patients with Alzheimer's disease. Analogous aggregates composed of calcitonin can be observed in the thyroid of patients suffering from thyroid carcinoma *[73]*. Furthermore, these peptide amyloids exhibited similarities with protein amyloids, which include similar spectroscopic features and binding with specific dyes. With the progression of time, reductionist approaches have been made to recognize the minimal peptide fragments that are able to transform into amyloid fibrils. In this aspect, Tenidis and co-workers identified that the hexapeptide fragments of IAPP can form the amyloid fibrillar structure *[74]*. Further studies recognized the capability of a pentapeptide fragment from calcitonin and a heptapeptide fragment from Aβ to form similar highly-ordered self-assemblies *[75]*.

1.3.3 Self-assembly of Short Peptides:

Researchers made further reductionist approaches to recognize shorter motifs of amyloid-forming peptides. In a pioneering work in 1993, Ghadiri *et al.* reported the formation of short peptide-based nanostructures. They established the generation of nanotubes by the self-association of a cyclic octapeptide having alternating L- and D- amino acids *[76]*. In 2003, Gazit *et al.* discovered that an ultrashort dipeptide, diphenylalanine (Phe-Phe or FF) self-assembled into nanotubes *[77]*

(**Figure 1.3**). The FF motif is the hydrophobic core recognition motif of Aβ polypeptide. It was established that the heptapeptide fragment from Aβ (KLVFFAE or Lys-Leu-Val-Phe-Phe-Ala-Glu) was able to form fibril structures, and two pentapeptide fragments, namely LVFFA and KLVFF act as the inhibitors of amyloid formation *[78]*. Furthermore, FF nanostructures were found to have many similarities in their functional properties with amyloid assemblies *[77]*. This includes the intrinsic luminescence behavior, mechanical rigidity, and their binding with amyloid-specific dyes. Additionally, other FF-based nanostructures, like nanowires, filaments, vesicles, nanotubes, etc., showed potential in various biological and non-biological fields like cell culture, drug delivery, bioimaging, and biosensors *[79–82]*. Further studies indicated the capability of different short peptides to form well-ordered self-assembled structures. Using molecular dynamics (MD) simulations, Frederix and co-workers investigated more than 8000 naturally occurring tripeptides for the formation of self-assembled structures *[83]*. It was found that PFF (Pro-Phe-Phe) was the most aggregation-prone peptide. The rest of the highly aggregation-prone peptides had the FF and other diaromatic motifs like FW, FY, WF, and WW. It showcased the relatively high abundance of aromatic amino acid residues in shorter peptides that are able to generate typical amyloid fibrils.

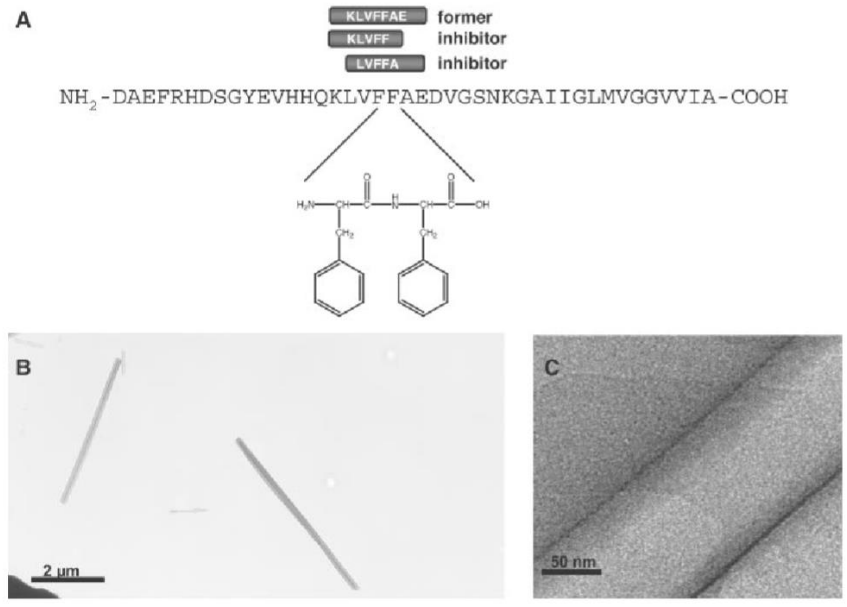

Figure 1.3 *A) Central motif of the Aβ and various other fragments that form amyloid fibrils or inhibit the formation. B) TEM image, (C) HR-TEM image of diphenylalanine peptide nanotubular structures [77] (Copyright 2003 AAAS)*

However, despite the promising applications and ongoing studies on FF-based self-assemblies, the understanding of the mechanism of such self-assembly remains elusive. In this aspect, the report by Gazit *et al.* was quite interesting. They elucidated the significance of aromatic stacking and indicated that the ion-pairing interactions are not a compulsory driving force to form nanotubes *[84]*. Shell *et al.* reported that the balance between electrostatic, side-chain hydrophobic, and hydrogen bonding interactions in the early stages of self-assembly stabilizes the FF nanotubes *[85]*. Bowers *et al.* reported the prominent role of water molecules in stabilizing the FF oligomers *[86]*. In 2014, Levin and Mason *et al.* studied the assembly kinetics of tert-butoxycarbonyl-protected diphenylalanine (Boc-FF) nanotubes, and it was observed that the self-assembly pathway is multistep in nature. This is governed by Ostwald's step rule, in which the soluble Boc-FF monomers coalesce into nanospheres. Further, the nanospheres undergo ripening and eventually transform into nanotubes. DSC (Differential Scanning Calorimetry) measurements showed that the nanotubes are thermodynamically more stable than the spherical structures *[87]* (**Figure 1.4**). FF-based self-assemblies are usually prepared by the dilution of an FF stock solution in a good solvent (such as ethanol or hexafluoroisopropanol) with a poor solvent (water). The obtained structures (nanotubes or nanowires) are stable in boiling water and some organic solvents *[88]*. A molecular dynamics study showed that the self-assembly pathways depend on the peptide concentration. The balance between peptide-peptide and peptide-water H-bonding interactions can result in the forming of different nanostructures *[89]*. Solvent properties like their polarities and the capability of H-bonding can influence local interactions of the self-assembly *[90]*. A study by Yan and Li *et al.* showed the formation of flower-like structures of FF in polar ethanol,

but long nanofibrils were obtained in non-polar toluene. The balance between hydrogen bonding and hydrophobic interactions gets perturbed when toluene is added. Therefore, π-π stacking dominates during the self-assembly process, resulting in the formation of nanofibrils *[91]*. Wang *et al.* showcased that the wall thickness and the diameter of the nanotubes can be controlled by the modulation of the degree of supersaturation of the peptide and the water content *[92]*. These studies mostly focused on the self-assembly of smaller peptides. These peptides, or more precisely, the dipeptides, represent the smallest recognition motif of amyloid formation and their intrinsic nature to form various nanostructures.

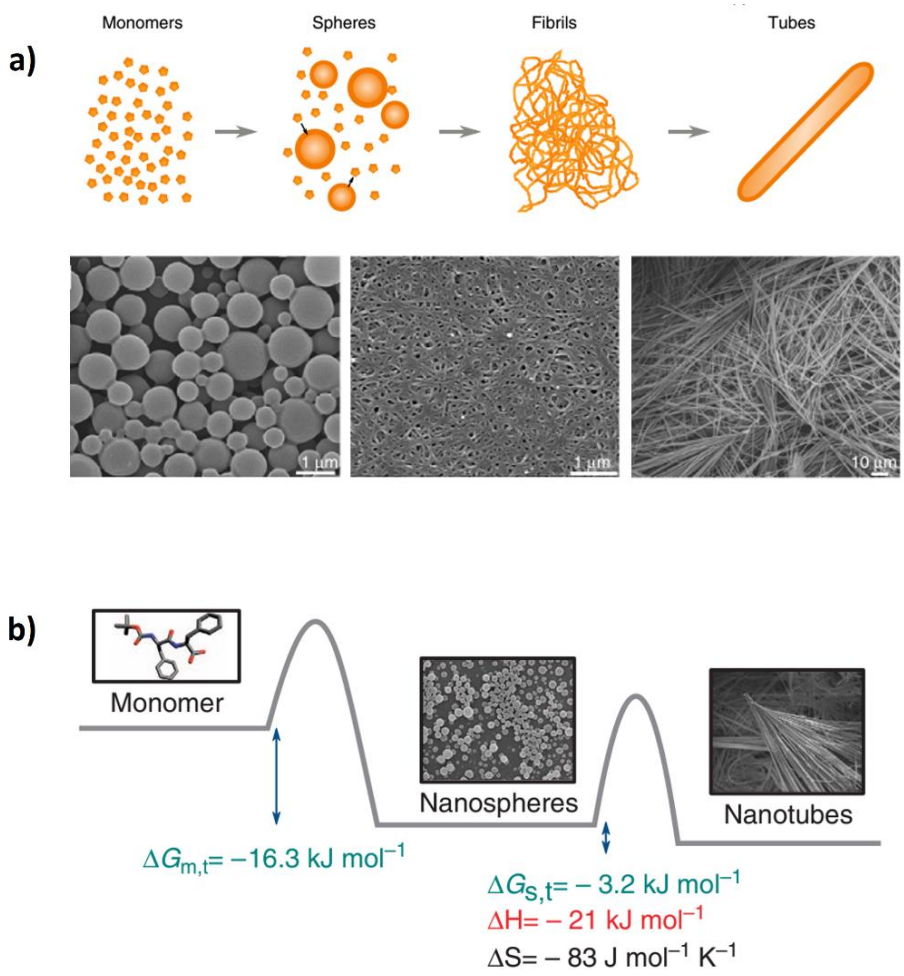

Figure 1.4 *a) Schematic representation and SEM images of morphological transformation, b) The energy diagram representing the free energy changes during the phase transition of Boc-FF [87] (Copyright 2014 Springer Nature)*

1.4 Amino Acid-based Self-assembly:

1.4.1 The Self-assembly of Amino Acids and General Introduction:

Amino acids act as the basic building blocks of peptides and proteins. The composition and sequence of the amino acids control the basic characteristics of these biomolecules. Inspired by the self-assembly of peptides and proteins, current studies have focused on the self-assembly of amino acids. The amino acids can self-aggregate into highly ordered structures that exhibit unique physical and chemical properties *[93–95]*. For example, the simplest amino acid, glycine (Gly) can form crystals that exhibit a high piezoelectric response (d_{16} = 178 pm V^{-1}), indicating their piezoelectric power generation capacity *[96]*. An anhydrase mimicking self-assembly by phenylalanine and Zn^{2+} possesses an excellent catalytic efficiency *[97]*. In a pioneering work in 2012, Adler-Abramovich *et al.* reported the ability of phenylalanine, a single aromatic amino acid, to self-assemble into fibrillar structures with properties similar to the amyloids. The deposition followed by the fibrillation of L-phenylalanine (L-Phe) corresponds to the abnormal neurological state of the body, phenylketonuria (PKU) *[98]* (**Figure 1.5**). PKU is categorized as an inborn error of metabolism (IEM). It results in decreased Phe metabolism. The reduced activity of the enzyme PAH (phenylalanine hydroxylase) has been correlated to the elevated concentrations of Phe that lead to the abnormal processing of the amino acid into further metabolic breakdown products *[99]*.

Further, the Phe fibrils were later found to trigger the protein self-assembly under physiological conditions *[100]*. This can transform the structures of native proteins into β-sheet assemblies. Furthermore, the hemolytic effect was exhibited by both the Phe fibrils and Phe-induced protein aggregates. This characteristic symptom can be observed in patients with phenylketonuria. These observations further strengthened the role of phenylalanine aggregates in the mechanism of PKU. Several attempts were made to modulate the fibrillar structure of Phe for therapeutic purposes. Singh *et al.* observed that the equimolar mixture

of L-Phe and D-Phe led to the formation of unique flake-like structures. In contrast, the individual amino acids formed hydrogel, containing fibrillar structures *[101]*. Sarkar and co-workers reported that the fibrillation of phenylalanine was inhibited by two crown ethers, 15C5 and 18C6, where 18C6 was more effective. The inhibition was associated with the favorable host-guest interaction between the ammonium ($-NH_3^+$) group of Phe and the crown ether 18C6. It was further established that lanthanide cations also arrested the fibrils with an efficiency that follows the order of $Tb^{3+} < Sm^{3+} < Eu^{3+}$ *[102]*. Further studies explored the capability of other amino acids and metabolites to generate ordered self-assembled fibrillar structures associated with several neurodegenerative diseases like tyrosinemia, cystinuria, Hartnup disease, and so on *[103–106]*.

The self-assembly of tyrosine (Tyr) was first documented by Khushalani and co-workers *[107]*. They observed ribbon-like flat fibrillar structures from an aqueous 1 mM Tyr solution. Sarkar and co-workers reported Tyr's distinct self-assembly process compared to that of Phe. They observed that the 18C6 could not inhibit the Tyr fibrillation *[106]*, contrary to the results obtained for Phe *[102]*. They postulated that $-NH_3^+$ did not play a part in the formation of Tyr fibrils; rather, the -COO- and -OH groups were involved in hydrogen bonding. It was also reported that tryptophan (Trp) could form fibrils (**Figure 1.5**) that exhibited typical amyloid-like characteristics like dye-staining capability and substantial toxicity through the induced apoptotic cell death *[104]*.

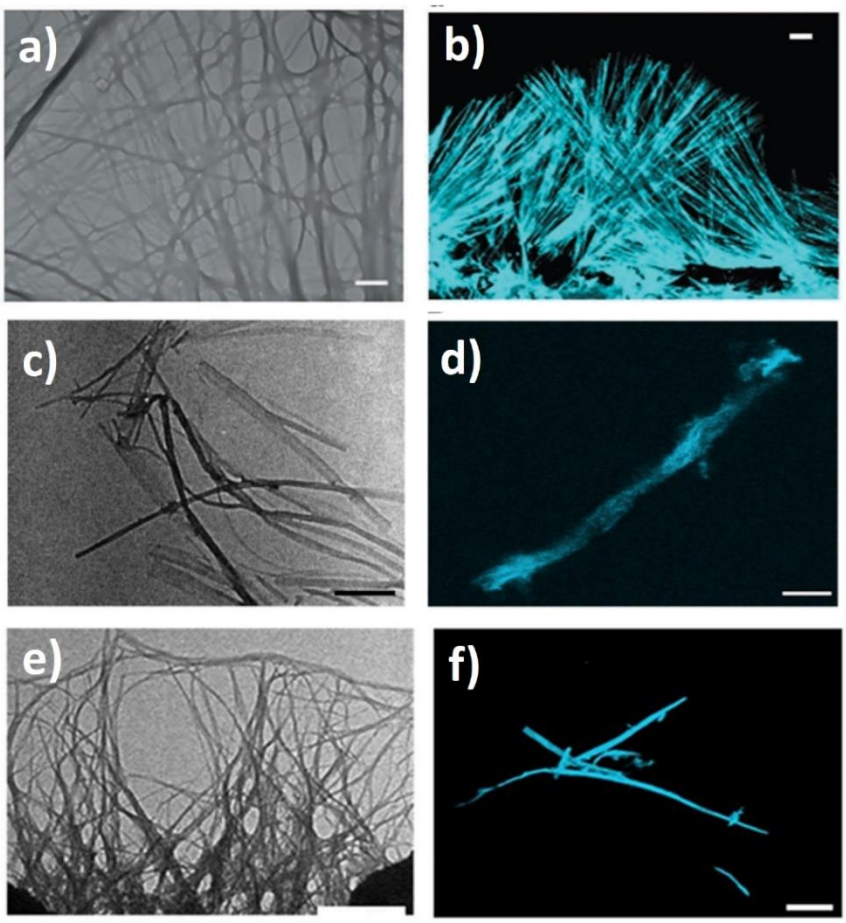

Figure 1.5 *a) TEM image of phenylalanine fibrillar structures (The scale bar is 1 µm), b) CLSM image of the ThT-tagged fibers (scale bar is 10 µm) [98] (Copyright 2012 Springer Nature), c) TEM image of Trp assemblies (scale bar is 500 nm), d) CLSM image of the ThT-tagged fibrils (scale bar is 20 µm) [104] (Copyright 2016 John Wiley and Sons), e) TEM image of Tyr fibrils (scale bar is 500 nm), f) CLSM image of the ThT-tagged fibrils (scale bar is 100 µm) [105].*

Do *et al.* indicated that L-phenylalanine self-associates into oligomers at neutral pH. These oligomeric structures were comprised of several layers of four monomers *[108]*. The structural feature was also detected earlier in the MD simulation study by Hansmann and co-workers *[109]*. Various models, such as single-tube, double-tube, and tetra-tube, were constructed from these layers. Both the lateral π-stacking interactions between the tubes (T-shaped π-stacking) and the π-stacking along the fibrillar axes of the tubes were obtained in this study. It was reported from the MD study that the hydrophilic polar parts of the amino acids

were buried deep in the core with hydrophobic aromatic parts pointing outward *[110]*. These studies also explained the cell toxicity of aromatic amino acid-based fibrils. The outer hydrophobic surface helped penetrate the cellular membrane. In contrast, the polar hydrophilic core, made of zwitterionic terminal groups caused leakage of ions from the cells, leading to cell damage. In a nutshell, the noncovalent interactions, including electrostatic interactions, hydrophobic interactions, π-π interactions, and hydrogen bonding, were found to be the primary driving forces that play a pivotal role in the aggregation mechanism.

1.4.2 Intrinsic Fluorescence of the Amino Acid Self-assembly:

The use of small molecular probes (dyes) is well-established for diagnosing amyloid aggregates formed by proteins and peptides. Several fluorescent dyes have been utilized in binding assays for the in vitro identification of protein misfolding *[111, 112]*. In particular, Congo red (CR) and Thioflavin T (ThT) are the most commonly used dyes to study amyloid aggregation and fibrillar growth kinetics *[113, 114]*. However, it has also been reported that molecular probes or dyes can interfere with the assembly process during the analysis of protein and polypeptide amyloid formation for either diagnosis or treatment *[115]*. Recently, it was observed that several amyloid fibrils display intrinsic luminescent properties in the visible range *[116, 117]*. This remarkable optical feature can be exploited to develop new detection methods for amyloid-related diseases that exclude the need for external dye labeling. In this regard, Shaham-Niv *et al.* reported quite interesting results regarding the intrinsic fluorescence of aromatic amino acids, including phenylalanine, tryptophan, and tyrosine *[118]*. The monomeric amino acids did not exhibit fluorescence in the visual range as they usually emit in the UV region (260-350 nm). Surprisingly, strong fluorescence signals were obtained when they self-assembled to form amyloid-like aggregates. Another study revealed that when Trp was self-assembled into nanotubes in ethanol, it showed multi-color blue, yellow, and red emissions when excited at different wavelengths at 385, 488, and 561 nm, respectively *[119]*. The unique features of the metabolite assemblies

can potentially lead to innovative diagnosis of IEM (Inborn Errors of Metabolism) disorders in patients. The underlying mechanisms of this unique emission behavior of the self-assembled structures are still not understood properly. Therefore, further studies may shed light on the unanswered questions regarding the intrinsic blue emission of the amino acid assemblies.

1.5 Effect of External Factors on the Self-assembly:

1.5.1 Effect of Metal Ions:

Metal ions are fundamental elements in biological systems. They are distributed widely among living organisms that participate in various life activities. Metal ions play significant roles in several physiological functions, like cellular homeostasis and enzymatic activities, by coordinating with important biomolecules. Additionally, metal ions have been linked with amyloid aggregates in various devastating degenerative diseases like Alzheimer's, Parkinson's, and prion diseases *[120-125]*. High levels of Cu^{2+} and Fe^{3+} can be observed in the cerebrospinal fluid and Lewy bodies (intracellular inclusion bodies comprising of α-synuclein aggregates, rich in β-sheet) of patients suffering from Parkinson's disease *[120]*. Metal ions can promote the Aβ aggregation in Alzheimer's disease (AD) *[121, 122]*. Several metal ions (such as Cu^{2+}, Zn^{2+}, Al^{3+}, and Fe^{3+}) are colocalized at unusually elevated concentrations with senile plaques in AD brains *[123–125]*. It was also observed that Aβ underwent aggregation rapidly at physiological concentrations of Zn^{2+} and pH of 7.4 *[126,127]*. The majority of these studies indicated that the metal ions can enhance Aβ fibrillation. However, some studies have shown that copper and zinc ions are non-fibrillogenic under certain conditions *[128,129]*. According to the report by Ha and co-workers, both Zn^{2+} and Cu^{2+} perturb the formation of amyloid fibrils but induce the formation of amorphous aggregates *[130]*. Later, Ji *et al.* showcased that by using different metal ions and variations of the metal ion to dipeptide ratio, the structural transformation from a β-sheet to a superhelical or random coil

can be achieved *[131]*. All these results showcased the importance of metal ions in the self-assembly of peptides and proteins, but the proper understanding of the mechanisms is still in infancy. Also, the influence of metal ions on the self-assembly process of aromatic amino acids is still not well-explored. Particularly, the effect of metal ions on fibril formation and proper understanding of the pathways involved can be very promising fields for researchers. Thus, a systematic investigation may help us to solve the unanswered puzzles regarding metal-amino acid interaction.

1.5.2 Effect of pH:

For the growth of the amyloid fibrils, the pH of the solutions can be a very influential factor. Typically, the formation of protein amyloid fibrils is promoted by decreasing the solution pH. The self-association of short peptides depends on their isoelectric point (pI) and the pK_a of the constituent amino acids. Fibrillation is favored when the peptides possess a low net charge *[132]*. The pH can have a marked influence on the self-assembly of PA or peptide amphiphiles. Stupp and co-workers observed that PAs that contained acidic amino acids were triggered to form nanofibrils at acidic pH *[45]* or using divalent cations *[133]*. Hoyer *et al.* investigated in vitro α-synuclein aggregation and reported the formation of aggregates of different morphologies that depend on both the salt concentration and pH *[134]*. It showed that the self-aggregated α-synuclein morphologies are highly sensitive to both the ionic strength and the pH of the solution. These results cumulatively indicate that pH can play a vital role in the self-aggregation process. However, studies on the influence of pH on the aromatic amino acid self-assembly are lacking in the literature. Therefore, the influence of pH on the simple amino acid self-assembly is subjected to investigation.

1.5.3 Effect of Nanoparticles and Carbon Dots:

Nanoparticles can significantly influence the protein and peptide self-assembly. They can catalyze fibrillation because of the enhanced local concentrations of proteins and peptides or can perturb the self-

association due to the strong binding or a large interaction surface area between particle and protein *[135]*. Polymeric nanoparticles were reported to inhibit the $A\beta_{1-40}$ fibrillization as a result of the binding between nanoparticles and Aβ (monomer or oligomer) *[136]*. The binding and copolymer composition were found to strongly influence the nucleation and the lag time. Kotov and coworkers reported that inorganic CdTe nanoparticles could inhibit the amyloid peptide fibrillation due to multiple binding of Aβ oligomers to CdTe NPs *[137]*. In contrast, TiO_2 nanoparticles promoted Aβ fibrillation through reducing the nucleation period *[138]*; although the detailed mechanism remains elusive.

Another type of nanoparticle widely used for imaging and therapeutic purposes is the carbon quantum dots (CQD) or carbon dots (CD). After the accidental discovery of carbon dots by Xu *et al.* in 2004 *[139]*, the CDs have been studied extensively to exploit their unique fluorescence properties. The graphite core and the hydrophilic functional groups present on the surface of the CD result in a diverse range of physiochemical properties and various applications *[140]*. Studies have shown that CDs can be used as bio-imaging tools. The CD-based labelling for cancer cell imaging *[141]*, stem cell imaging *[142]*, and neuron imaging *[143]* have been developed to understand biological processes. Recently, fluorescent carbon dots (CD) have also been exploited for therapeutic purposes. For example, Shao *et al.* recently reported that the carbon dots synthesized from o-phenylenediamine and $AlCl_3$ can inhibit protein aggregation through hydrophobic and π-π interactions *[144]*. Narayan and coworkers established that the carbon dots synthesized from sodium citrate can prevent the formation of amyloid-like fibrils by interfering with HEWL (Hen-egg white lysozyme) monomers and oligomeric intermediates *[145]*. Malishev *et al.* investigated the effect of enantiomeric carbon dots (synthesized from L-lysine or D-lysine) on the aggregation of Aβ42. It was observed that the L-Lys-CD exhibited higher affinity to Aβ42 and altered the fibrillar structures, as well as inhibited the toxicity *[146]*. Therefore, the

interaction between carbon dots and amino acid self-assembled structures can be a promising field of research. Due to their excellent optical properties, carbon dots can be useful as imaging tools and monitor the biomolecular self-assembly process.

1.6 Motivation and Organization of the Thesis:

The primary aim of the research works comprised in this thesis is to explore the self-assembly process of aromatic amino acids and the effect of several external factors, including metal ions, pH, aliphatic amino acids, and carbon dots. We have studied the effect of different metal ions of varying charge and radius on the intrinsic fluorescence and the morphologies of the self-assembled structures. The effect of pH on the intrinsic emission behavior and morphology of the self-assembled structures has also been explored. The formation of metastable aggregates during the self-aggregation process and their stability have been investigated to get a better insight into the assembly pathway.

The thesis takes the initiative to exploit the distinct emission behavior of a carbon dot and utilize it in monitoring the amino acid self-assembly dynamics. The studies reported here may help in understanding the mechanisms involved in the self-assembly processes of amino acid-based systems and serve to unravel the puzzles unsolved regarding biomolecular self-assembly. The following sections provide a brief description of the contents and organization of the thesis:

Chapter 1 provides a brief introduction to biomolecular self-assembly, its importance, and its applications. It further addresses the significance of aromatic amino acid self-assembly and the effect of different external stimuli on it.

Chapter 2 describes the effect of pH and metal ions of different nuclear charges and sizes on the intrinsic blue luminescence of the aromatic amino acids, i.e., Phe (phenylalanine) and Trp (tryptophan) and their self-assembled structures with the help of several spectroscopic

techniques like steady-state fluorescence, TCSPC, and different imaging techniques like CLSM, and FESEM.

In **Chapter 3**, the metal-ion-induced structural polymorphism is studied during the self-assembling process of aromatic amino acids. The existence of different metastable intermediate states of diverse morphologies, for example, droplets, spheres, vesicles, flowers, and toroids, is investigated using imaging techniques like CLSM, FESEM, and spectroscopic techniques like steady-state FL and TCSPC.

Chapter 4 deals with the self-assembly formation of carboxybenzyl (Z)-protected phenylalanine (ZF) by exchanging the good solvent for a bad solvent and the effect of different metal ions and other factors several factors, like concentration of amino acid, metal ions, incubation temperature, etc., on the self-assembly process are investigated.

Chapter 5 explores the unique emission behavior of a special hydrophobic carbon dot (HCD) that identifies the distinct intermediates formed during the self-assembly formation of amino acids.

In **Chapter 6**, the materials used in the thesis works, various protocols regarding the self-assembly formation, carbon dots synthesis, and various fabrication and characterization techniques that were used throughout the thesis have been discussed in detail.

Finally, in **Chapter 7**, a thorough conclusion and summary have been presented of all the work done so far, along with a short discussion of the future scope.

1.7 References:

[1] Gong C., Sun S., Zhang Y., et al. (2019), Hierarchical nanomaterials via biomolecular self-assembly and bioinspiration for energy and environmental applications, Nanoscale 11, 4147–4182 (DOI: 10.1039/C9NR00218A)

[2] Rothemund P. W. K. (2006), Folding DNA to create nanoscale shapes and patterns, Nature 440, 297–302 (DOI: 10.1038/nature04586)

[3] Luo Q., Hou C., Bai Y., et al. (2016), Protein Assembly: Versatile Approaches to Construct Highly Ordered Nanostructures, Chem. Rev. 116, 13571–13632 (DOI: 10.1021/acs.chemrev.6b00228)

[4] Ng C. C., Cheng Y. -L., Pennefather P. S. (2004), Properties of a Self-Assembled Phospholipid Membrane Supported on Lipobeads, Biophys. J. 87, 323–331 (DOI: 10.1529/biophysj.103.030627)

[5] Nasalean L., Baudrey S., Leontis N. B., et al. (2006), Controlling RNA self-assembly to form filaments, Nucleic Acids Res 34, 1381–1392 (DOI: 10.1093/nar/gkl008)

[6] Won J., Chae S. K., Kim J. H., et al. (2005), Self-assembled DNA composite membranes, J. Membr. Sci 249, 113–117 (DOI: 10.1016/j.memsci.2004.08.031)

[7] Chiti F., Dobson C. M. (2017), Protein Misfolding, Amyloid Formation, and Human Disease: A Summary of Progress Over the Last Decade, Annu. Rev. Biochem. 86, 27–68 (DOI: 10.1146/annurev-biochem-061516-045115.

[8] Tyler J. K. (2002), Chromatin assembly, FEBS J. 269, 2268–2274 (DOI: 10.1046/j.1432-1033.2002.02890.x)

[9] Kominami H., Kobayashi K., Ido S., et al. (2018), Immunoactivity of self-assembled antibodies investigated by atomic force microscopy, RSC Adv. 8, 29378–29384 (DOI: 10.1039/C8RA05423A)

[10] Froimchuk E., Carey S. T., Edwards C., et al. (2020), Self-Assembly as a Molecular Strategy to Improve Immunotherapy, Acc. Chem. Res. 53, 2534–2545 (DOI: 10.1021/acs.accounts.0c00438)

[11] Monnard P. -A., Deamer D. W. (2002), Membrane self-assembly processes: Steps toward the first cellular life, Anat. Rec 268, 196–207 (DOI: 10.1002/ar.10154)

[12] Ma P. X. (2008), Biomimetic materials for tissue engineering, Adv. Drug Deliv. Rev. 60, 184–198 (DOI: 10.1016/j.addr.2007.08.041)

[13] Bhattacharya P., Du D., Lin Y. (2014), Bioinspired nanoscale materials for biomedical and energy applications, J. R. Soc. Interface 11, 20131067 (DOI: 10.1098/rsif.2013.1067)

[14] Artero V. (2017), Bioinspired catalytic materials for energy-relevant conversions, Nat Energy 2, 1–6 (DOI: 10.1038/nenergy.2017.131)

[15] Zhang T., Ma Y., Qi L. (2012), Bioinspired colloidal materials with special optical, mechanical, and cell-mimetic functions, J. Mater. Chem. B 1, 251–264 (DOI: 10.1039/C2TB00175F)

[16] Schmid S. Y., Lachowski K., Chiang H. T., et al. (2023), Mechanisms of Biomolecular Self-Assembly Investigated Through In Situ Observations of Structures and Dynamics, Angew. Chem. Int. Ed. 62, e202309725 (DOI: 10.1002/anie.202309725)

[17] Mandelkow E., Mandelkow E. -M. (1994), Microtubule structure, Curr. Opin. Struct. Biol. 4, 171–179 (DOI: 10.1016/S0959-440X(94)90305-0)

[18] Harrison S. C., Kirchhausen T. (1983), Clathrin, cages, and coated vesicles, Cell 33, 650–652 (DOI: 10.1016/0092-8674(83)90007-7)

[19] Fotin A., Cheng Y., Sliz P., et al. (2004), Molecular model for a complete clathrin lattice from electron cryomicroscopy, Nature 432, 573–579 (DOI: 10.1038/nature03079)

[20] Branden C. I., Tooze J. 1998, Introduction to Protein Structure, 2nd ed., Garland Science, New York (DOI: 10.1201/9781136969898)

[21] Olson A. J., Bricogne G., Harrison S. C. (1983), Structure of tomato bushy stunt virus IV: The virus particle at 2·9resolution, J. Mol. Biol 171, 61–93 (DOI: 10.1016/S0022-2836(83)80314-3)

[22] Douglas T., Young M. (2006), Viruses: Making Friends with Old Foes, Science 312, 873–875 (DOI: 10.1126/science.1123223)

[23] Uchida M., Klem M. T., Allen M., et al. (2007), Biological Containers: Protein Cages as Multifunctional Nanoplatforms, Adv. Mat. 19, 1025–1042 (DOI: 10.1002/adma.200601168)

[24] Douglas T., Young M. (1998), Host–guest encapsulation of materials by assembled virus protein cages, Nature 393, 152–155 (DOI: 10.1038/30211)

[25] Douglas T., Strable E., Willits D., et al. (2002), Protein Engineering of a Viral Cage for Constrained Nanomaterials Synthesis, Adv. Mater. 14, 415–418 (DOI: 10.1002/1521-4095(20020318)14:6<415::AID-ADMA415>3.0.CO;2-W)

[26] M. Comellas-Aragonès, H. Engelkamp, V.I. Claessen, N.A.J.M. Sommerdijk, A.E. Rowan, P.C.M. Christianen, J.C. Maan, B.J.M. Verduin, J.J.L.M. Cornelissen, R.J.M. Nolte, A virus-based single-enzyme nanoreactor, Nature Nanotech 2 (2007) 635–639. https://doi.org/10.1038/nnano.2007.299.

[27] Minten I. J., Hendriks L. J. A., Nolte R. J. M., et al. (2009), Controlled Encapsulation of Multiple Proteins in Virus Capsids, J. Am. Chem. Soc. 131, 17771–17773 (DOI: 10.1021/ja907843s)

[28] Seeman N. C. (2003), DNA in a material world, Nature 421, 427–431 (DOI: 10.1038/nature01406)

[29] Yan H., Park S. H., Finkelstein G., et al. (2003), DNA-Templated Self-Assembly of Protein Arrays and Highly Conductive Nanowires, Science 301, 1882–1884 (DOI: 10.1126/science.1089389)

[30] Shih W. M., Quispe J. D., Joyce G. F. (2004), A 1.7-kilobase single-stranded DNA that folds into a nanoscale octahedron, Nature 427, 618–621 (DOI: 10.1038/nature02307)

[31] Sadowski J. P., Calvert C. R., Zhang D. Y., et al. (2014), Developmental Self-Assembly of a DNA Tetrahedron, ACS Nano 8, 3251–3259 (DOI: 10.1021/nn4038223)

[32] Yurke B., Turberfield A. J., Mills A. P., et al. (2000), A DNA-fuelled molecular machine made of DNA, Nature 406, 605–608 (DOI: 10.1038/35020524)

[33] Abu-Salah K. M., Zourob M. M., Mouffouk F., et al. (2015), DNA-Based Nanobiosensors as an Emerging Platform for Detection of Disease, Sensors 15, 14539–14568 (DOI: 10.3390/s150614539)

[34] de Vries J. W., Zhang F., Herrmann A. (2013), Drug delivery systems based on nucleic acid nanostructures, Journal of Controlled Release 172, 467–483 (DOI: 10.1016/j.jconrel.2013.05.022)

[35] Chao J., Liu H., Su S., et al. (2014), Structural DNA Nanotechnology for Intelligent Drug Delivery, Small 10, 4626–4635 (DOI: 10.1002/smll.201401309)

[36] Del Grosso E., Dallaire A. -M., Vallée-Bélisle A., et al. (2015), Enzyme-Operated DNA-Based Nanodevices, Nano Lett. 15, 8407–8411 (DOI: 10.1021/acs.nanolett.5b04566)

[37] Pinheiro A. V., Han D., Shih W. M., et al. (2011), Challenges and opportunities for structural DNA nanotechnology, Nat. Nanotechnol. 6, 763–772 (DOI: 10.1038/nnano.2011.187)

[38] Robertson J. L. (2018), The lipid bilayer membrane and its protein constituents, J. Gen. Physiol. 150, 1472–1483 (DOI: 10.1085/jgp.201812153)

[39] Akbarzadeh A., Rezaei-Sadabady R., Davaran S., et al. (2013), Liposome: classification, preparation, and applications, Nanoscale Res Lett 8, 102 (DOI: 10.1186/1556-276X-8-102)

[40] Liu P., Chen G., Zhang J. (2022), A Review of Liposomes as a Drug Delivery System: Current Status of Approved Products, Regulatory Environments, and Future Perspectives, Molecules 27, 1372 (DOI: 10.3390/molecules27041372)

[41] Katouzian I., Jafari S. M. (2019), Protein nanotubes as state-of-the-art nanocarriers: Synthesis methods, simulation and applications, J. Control. Release 303, 302–318 (DOI: 10.1016/j.jconrel.2019.04.026)

[42] Panigrahi B., Singh R. K., Suryakant U., et al. (2022), Cyclic peptides nanospheres: A '2-in-1′ self-assembled delivery system for targeting nucleus and cytoplasm, Eur. J. Pharm. Sci 171, 106125 (DOI: 10.1016/j.ejps.2022.106125)

[43] Adamcik J., Mezzenga R. (2012), Proteins Fibrils from a Polymer Physics Perspective, Macromolecules 45, 1137–1150 (DOI: 10.1021/ma202157h)

[44] Huerta-López C., Alegre-Cebollada J. (2021), Protein Hydrogels: The Swiss Army Knife for Enhanced Mechanical and Bioactive Properties of Biomaterials, Nanomaterials 11, 1656 (DOI: 10.3390/nano11071656)

[45] Hartgerink J. D., Beniash E., Stupp S. I. (2001), Self-Assembly and Mineralization of Peptide-Amphiphile Nanofibers, Science 294, 1684–1688 (DOI: 10.1126/science.1063187)

[46] Cui H., Webber M. J., Stupp S. I. (2010), Self-assembly of peptide amphiphiles: From molecules to nanostructures to biomaterials, Peptide Science 94, 1–18 (DOI: 10.1002/bip.21328)

[47] Webber M. J., Berns E. J., Stupp S. I. (2013), Supramolecular Nanofibers of Peptide Amphiphiles for Medicine, Isr. J. Chem. 53, 530–554 (DOI: 10.1002/ijch.201300046)

[48] Petka W. A., Harden J. L., McGrath K. P., et al. (1998), Reversible Hydrogels from Self-Assembling Artificial Proteins, Science 281, 389–392 (DOI: 10.1126/science.281.5375.389)

[49] Halstenberg S., Panitch A., Rizzi S., et al. (2002), Biologically Engineered Protein-graft-Poly(ethylene glycol) Hydrogels: A Cell Adhesive and Plasmin-Degradable Biosynthetic Material for Tissue Repair, Biomacromolecules 3, 710–723 (DOI: 10.1021/bm015629o)

[50] Vauthey S., Santoso S., Gong H., et al. (2002), Molecular self-assembly of surfactant-like peptides to form nanotubes and nanovesicles, Proc. Natl. Acad. Sci. U.S.A 99, 5355–5360 (DOI: 10.1073/pnas.072089599)

[51] Zhang S., Gelain F., Zhao X. (2005), Designer self-assembling peptide nanofiber scaffolds for 3D tissue cell cultures, Semin. Cancer Biol. 15, 413–420 (DOI: 10.1016/j.semcancer.2005.05.007)

[52] Segers V. F. M., Lee R. T. (2007), Local delivery of proteins and the use of self-assembling peptides, Drug Discov. Today 12, 561–568 (DOI: 10.1016/j.drudis.2007.05.003)

[53] Holmes T. C., de Lacalle S., Su X., et al. (2000), Extensive neurite outgrowth and active synapse formation on self-assembling peptide scaffolds, Proc. Natl. Acad. Sci. U.S.A 97, 6728–6733 (DOI: 10.1073/pnas.97.12.6728)

[54] Davis M. E., Motion J. P. M., Narmoneva D. A., et al. (2005), Injectable Self-Assembling Peptide Nanofibers Create Intramyocardial Microenvironments for Endothelial Cells, Circulation 111, 442–450 (DOI: 10.1161/01.CIR.0000153847.47301.80)

[55] Maury C. P. J. (2018), Amyloid and the origin of life: self-replicating catalytic amyloids as prebiotic informational and protometabolic entities, Cell. Mol. Life Sci. 75, 1499–1507 (DOI: 10.1007/s00018-018-2797-9)

[56] Frenkel-Pinter M., Samanta M., Ashkenasy G., et al. (2020), Prebiotic Peptides: Molecular Hubs in the Origin of Life, Chem. Rev. 120, 4707–4765 (DOI: 10.1021/acs.chemrev.9b00664)

[57] Castelvecchi D. (2022), Origin of life theory involving RNA–protein hybrid gets new support, Nature 605, 409–409 (DOI: 10.1038/d41586-022-01303-z)

[58] Meisl G., Xu C. K., Taylor J. D., et al. (2022), Uncovering the universality of self-replication in protein aggregation and its link to disease, Sci. Adv. 8, eabn6831 (DOI: 10.1126/sciadv.abn6831)

[59] Knowles T. P. J., Vendruscolo M., Dobson C. M. (2014), The amyloid state and its association with protein misfolding diseases, Nat Rev Mol Cell Biol 15, 384–396 (DOI: 10.1038/nrm3810)

[60] McManus J. J., Charbonneau P., Zaccarelli E., et al. (2016), The physics of protein self-assembly, Curr. Opin. Colloid Interface Sci. 22, 73–79 (DOI: 10.1016/j.cocis.2016.02.011)

[61] Opie E. L., (1901), THE RELATION OE DIABETES MELLITUS TO LESIONS OF THE PANCREAS. HYALINE DEGENERATION OF THE ISLANDS OE LANGERHANS, J Exp Med 5, 527–540 (DOI: 10.1084/jem.5.5.527)

[62] Lage J. M. M. (2006), 100 Years of Alzheimer's disease (1906–2006), J. Alzheimer's Dis 9, 15–26 (DOI: 10.3233/JAD-2006-9S303)

[63] Hamley I. W. (2007), Peptide Fibrillization, Angew. Chem. Int. Ed. 46, 8128–8147 (DOI: 10.1002/anie.200700861)

[64] Tycko R., Wickner R. B. (2013), Molecular Structures of Amyloid and Prion Fibrils: Consensus versus Controversy, Acc. Chem. Res. 46, 1487–1496 (DOI: 10.1021/ar300282r)

[65] Sipe J. D., Cohen A. S. (2000), Review: History of the Amyloid Fibril, J. Struct. Biol. 130, 88–98 (DOI: 10.1006/jsbi.2000.4221)

[66] Munishkina L. A., Fink A. L. (2007), Fluorescence as a method to reveal structures and membrane-interactions of amyloidogenic proteins, Biochim. Biophys. Acta 1768, 1862–1885 (DOI: 10.1016/j.bbamem.2007.03.015)

[67] Moran S. D., Zanni M. T. (2014), How to Get Insight into Amyloid Structure and Formation from Infrared Spectroscopy, J. Phys. Chem. Lett. 5, 1984–1993 (DOI: 10.1021/jz500794d)

[68] Tycko R. (2011), Solid-State NMR Studies of Amyloid Fibril Structure, Annual Review of Physical Chemistry 62, 279–299 (DOI: 10.1146/annurev-physchem-032210-103539)

[69] Nelson R., Sawaya M. R., Balbirnie M., et al. (2005), Structure of the cross-β spine of amyloid-like fibrils, Nature 435, 773–778 (DOI: 10.1038/nature03680)

[70] Hartl F. U., Hayer-Hartl M. (2009), Converging concepts of protein folding in vitro and in vivo, Nat Struct Mol Biol 16, 574–581. (DOI: 10.1038/nsmb.1591)

[71] Balobanov V., Chertkova R., Egorova A., et al. (2020), The Kinetics of Amyloid Fibril Formation by de Novo Protein Albebetin and Its Mutant Variants, Biomolecules 10, 241 (DOI: 10.3390/biom10020241)

[72] Khemtemourian L., Gazit E., Miranker A. (2016), Recent Insight in Islet Amyloid Polypeptide Morphology, Structure, Membrane Interaction, and Toxicity in Type 2 Diabetes, J. Diabetes Res. 2535878 (DOI: 10.1155/2016/2535878)

[73] Berger G., Berger N., Guillaud M. -H., et al. (1988), Calcitonin-like immunoreactivity of amyloid fibrils in medullary thyroid carcinomas, Vichows Archiv A Pathol Anat 412, 543–551 (DOI: 10.1007/BF00844290)

[74] Tenidis K., Waldner M., Bernhagen J., et al. (2000), Identification of a penta- and hexapeptide of islet amyloid polypeptide (IAPP) with amyloidogenic and cytotoxic properties, J. Mol. Biol. 295, 1055–1071 (DOI: 10.1006/jmbi.1999.3422)

[75] Reches M., Porat Y., Gazit E. (2002), Amyloid Fibril Formation by Pentapeptide and Tetrapeptide Fragments of Human Calcitonin, J. Biol. Chem. 277, 35475–35480 (DOI: 10.1074/jbc.M206039200)

[76] Ghadiri M. R., Granja J. R., Milligan R. A., et al. (1993), Self-assembling organic nanotubes based on a cyclic peptide architecture, Nature 366, 324–327 (DOI: 10.1038/366324a0)

[77] Reches M., Gazit E. (2003), Casting Metal Nanowires Within Discrete Self-Assembled Peptide Nanotubes, Science 300, 625–627 (DOI: 10.1126/science.1082387)

[78] Castelletto V., Ryumin P., Cramer R., et al. (2017), Self-Assembly and Anti-Amyloid Cytotoxicity Activity of Amyloid beta Peptide Derivatives, Sci Rep 7, 43637 (DOI: 10.1038/srep43637)

[79] Nguyen V., Zhu R., Jenkins K., et al. (2016), Self-assembly of diphenylalanine peptide with controlled polarization for power generation, Nat. Commun. 7, 13566 (DOI: 10.1038/ncomms13566)

[80] Yan X., Zhu P., Li J., (2010), Self-assembly and application of diphenylalanine-based nanostructures, Chem. Soc. Rev. 39, 1877–1890 (DOI: 10.1039/B915765B)

[81] Yan X., He Q., Wang K., et al. (2007), Transition of Cationic Dipeptide Nanotubes into Vesicles and Oligonucleotide Delivery, Angew. Chem. Int. Ed. 46, 2431–2434 (DOI: 10.1002/anie.200603387)

[82] Yan X., Cui Y., He Q., et al. (2008), Reversible Transitions between Peptide Nanotubes and Vesicle-Like Structures Including Theoretical Modeling Studies, Chem. Eur. J 14, 5974–5980 (DOI: 10.1002/chem.200800012)

[83] Frederix P. W. J. M., Scott G. G., Abul-Haija Y. M., et al. (2015), Exploring the sequence space for (tri-)peptide self-assembly to design and discover new hydrogels, Nat. Chem. 7, 30–37 (DOI: 10.1038/nchem.2122)

[84] Reches M., Gazit E., (2005), Self-assembly of peptide nanotubes and amyloid-like structures by charged-termini-capped diphenylalanine peptide analogues, Isr. J Chem. 45, 363–371 (DOI: 10.1560/5MC0-V3DX-KE0B-YF3J)

[85] Jeon J., Mills C. E., Shell M. S. (2013), Molecular Insights into Diphenylalanine Nanotube Assembly: All-Atom Simulations of Oligomerization, J. Phys. Chem. B 117, 3935–3943 (DOI: 10.1021/jp308280d)

[86] Do T. D., Bowers M. T. (2015), Diphenylalanine Self Assembly: Novel Ion Mobility Methods Showing the Essential Role of Water, Anal. Chem. 87, 4245–4252 (DOI: 10.1021/ac5046774)

[87] Levin A., Mason T. O., Adler-Abramovich L., et al. (2014), Ostwald's rule of stages governs structural transitions and morphology of dipeptide supramolecular polymers, Nat Commun 5, 5219 (DOI: 10.1038/ncomms6219)

[88] Hamley I. W., (2014), Peptide Nanotubes, Angew. Chem. Int. Ed. 53, 6866–6881 (DOI: 10.1002/anie.201310006)

[89] Guo C., Luo Y., Zhou R., et al. (2012), Probing the Self-Assembly Mechanism of Diphenylalanine-Based Peptide Nanovesicles and Nanotubes, ACS Nano 6, 3907–3918 (DOI: 10.1021/nn300015g)

[90] Mason T. O., Chirgadze D. Y., Levin A., et al. (2014), Expanding the Solvent Chemical Space for Self-Assembly of Dipeptide Nanostructures, ACS Nano 8, 1243–1253 (DOI: 10.1021/nn404237f)

[91] Zhu P., Yan X., Su Y., et al. (2010), Solvent-Induced Structural Transition of Self-Assembled Dipeptide: From Organogels to Microcrystals, Chem. Eur. J. 16, 3176–3183. https://doi.org/10.1002/chem.200902139.

[92] Wang Y., Huang R., Qi W., et al. (2015), Capillary Force-Driven, Hierarchical Co-Assembly of Dandelion-Like Peptide Microstructures, Small 11, 2893–2902 (DOI: 10.1002/smll.201403645)

[93] Kumar M., Ing N. L., Narang V., et al. (2018), Amino-acid-encoded biocatalytic self-assembly enables the formation of transient conducting nanostructures, Nat. Chem. 10, 696–703 (DOI: 10.1038/s41557-018-0047-2)

[94] Lee I. S., Kim K. T., Lee A. Y., et al. (2008), Concomitant Crystallization of Glycine on Patterned Substrates: The Effect of pH on the Polymorphic Outcome, Cryst. Growth Des 8, 108–113 (DOI: 10.1021/cg700890m)

[95] Imae T., Takahashi Y., Muramatsu H. (1992), Formation of fibrous molecular assemblies by amino acid surfactants in water, J. Am. Chem. Soc. 114, 3414–3419 (DOI: 10.1021/ja00035a038)

[96] Guerin S., Stapleton A., Chovan D., et al. (2018), Control of piezoelectricity in amino acids by supramolecular packing, Nat. Mater. 17, 180–186 (DOI: 10.1038/nmat5045)

[97] Makam P., Yamijala S. S. R. K. C., Tao K., et al. (2019), Non-proteinaceous hydrolase comprised of a phenylalanine metallo-supramolecular amyloid-like structure, Nat Catal 2, 977–985 (DOI: 10.1038/s41929-019-0348-x)

[98] Adler-Abramovich L., Vaks L., Carny O., et al. Phenylalanine assembly into toxic fibrils suggests amyloid etiology in phenylketonuria, Nat Chem Biol 8, 701–706 (DOI: 10.1038/nchembio.1002)

[99] Nandi S., Pyne A., Ghosh M., et al. (2020), Antagonist Effects of l-Phenylalanine and the Enantiomeric Mixture Containing d-Phenylalanine on Phospholipid Vesicle Membrane, Langmuir 36, 2459–2473 (DOI: 10.1021/acs.langmuir.9b03543)

[100] Anand B. G., Dubey K., Shekhawat D. S., et al. (2017), Intrinsic property of phenylalanine to trigger protein aggregation and hemolysis has a direct relevance to phenylketonuria, Sci Rep 7, 11146 (DOI: 10.1038/s41598-017-10911-z)

[101] Singh V., Rai R. K., Arora A., et al. (2014), Therapeutic implication of L-phenylalanine aggregation mechanism and its modulation by D-phenylalanine in phenylketonuria, Sci Rep 4, 3875 (DOI: 10.1038/srep03875)

[102] Banik D., Dutta R., Banerjee P., et al. (2016), Inhibition of Fibrillar Assemblies of l-Phenylalanine by Crown Ethers: A Potential Approach toward Phenylketonuria, J. Phys. Chem. B 120, 7662–7670 (DOI: 10.1021/acs.jpcb.6b05209)

[103] Shaham-Niv S., Adler-Abramovich L., Schnaider L., et al. (2015), Extension of the generic amyloid hypothesis to nonproteinaceous metabolite assemblies, Sci. Adv 1, e1500137 (DOI: 10.1126/sciadv.1500137)

[104] Shaham-Niv S., Rehak P., Vuković L., et al. (2017), Formation of Apoptosis-Inducing Amyloid Fibrils by Tryptophan, Isr. J. Chem. 57, 729–737 (DOI: 10.1002/ijch.201600076)

[105] Zaguri D., Kreiser T., Shaham-Niv S., et al. (2018), Antibodies towards Tyrosine Amyloid-Like Fibrils Allow Toxicity Modulation and Cellular Imaging of the Assemblies, Molecules 23, 1273. (DOI: 10.3390/molecules23061273)

[106] Banik D., Kundu S., Banerjee P., et al. (2017), Investigation of Fibril Forming Mechanisms of l-Phenylalanine and l-Tyrosine: Microscopic Insight toward Phenylketonuria and Tyrosinemia Type II, J. Phys. Chem. B 121, 1533–1543. (DOI: 10.1021/acs.jpcb.6b12220)

[107] Perween S., Chandanshive B., Kotamarthi H. C., et al. (2013), Single amino acid based self-assembled structure, Soft Matter 9, 10141–10145 (DOI: 10.1039/C3SM51054A)

[108] Do T. D., Kincannon W. M., Bowers M. T. (2015), Phenylalanine Oligomers and Fibrils: The Mechanism of Assembly and the Importance of Tetramers and Counterions, J. Am. Chem. Soc. 137, 10080–10083 (DOI: 10.1021/jacs.5b05482)

[109] German H. W., Uyaver S., Hansmann U. H. E. (2015), Self-Assembly of Phenylalanine-Based Molecules, J. Phys. Chem. A 119, 1609–1615 (DOI: 10.1021/jp5077388)

[110] Uyaver S., Hernandez H. W., Habiboglu M. G. (2018), Self-assembly of aromatic amino acids: a molecular dynamics study, Phys. Chem. Chem. Phys. 20, 30525–30536 (DOI: 10.1039/C8CP06239K)

[111] Hawe A., Sutter M., Jiskoot W. (2008), Extrinsic Fluorescent Dyes as Tools for Protein Characterization, Pharm Res 25, 1487–1499. (DOI: 10.1007/s11095-007-9516-9)

[112] Buell A. K., Dobson C. M., Knowles T. P. J., et al. (2010), Interactions between Amyloidophilic Dyes and Their Relevance to Studies of Amyloid Inhibitors, Biophys. J. 99, 3492–3497 (DOI: 10.1016/j.bpj.2010.08.074)

[113] Eisert R., Felau L., Brown L. R. (2006), Methods for enhancing the accuracy and reproducibility of Congo red and thioflavin T assays, Anal. Biochem. 353, 144–146 (DOI: 10.1016/j.ab.2006.03.015)

[114] Klunk W. E., Jacob R. F., Mason R. P. (1999), Quantifying Amyloid β-Peptide (Aβ) Aggregation Using the Congo Red-Aβ (CR–Aβ) Spectrophotometric Assay, Anal. Biochem. 266, 66–76 (DOI: 10.1006/abio.1998.2933)

[115] Jameson L. P., Smith N. W., Dzyuba S. V. (2012), Dye-Binding Assays for Evaluation of the Effects of Small Molecule Inhibitors on Amyloid (Aβ) Self-Assembly, ACS Chem. Neurosci. 3, 807–819 (DOI: 10.1021/cn300076x)

[116] Pinotsi D., Buell A. K., Dobson C. M., et al. (2013), A Label-Free, Quantitative Assay of Amyloid Fibril Growth Based on Intrinsic Fluorescence, ChemBioChem 14, 846–850. (DOI: 10.1002/cbic.201300103)

[117] Pinotsi D., Grisanti L., Mahou P., et al. (2016), Proton Transfer and Structure-Specific Fluorescence in Hydrogen Bond-Rich Protein Structures, J. Am. Chem. Soc. 138, 3046–3057 (DOI: 10.1021/jacs.5b11012)

[118] Shaham-Niv S., Arnon Z. A., Sade D., et al. (2018), Intrinsic Fluorescence of Metabolite Amyloids Allows Label-Free Monitoring of Their Formation and Dynamics in Live Cells, Angew. Chem. Int. Ed. 57, 12444–12447 (DOI: 10.1002/anie.201806565)

[119] Babar D. G., Sarkar S. (2017), Self-assembled nanotubes from single fluorescent amino acid, Appl Nanosci 7, 101–107. (DOI: 10.1007/s13204-017-0551-5)

[120] J.H. Viles, (2012), Metal ions and amyloid fiber formation in neurodegenerative diseases. Copper, zinc and iron in Alzheimer's, Parkinson's and prion diseases, Coord. Chem. Rev. 256, 2271–2284. (DOI: 10.1016/j.ccr.2012.05.003)

[121] Brown D. R. (2009), Brain proteins that mind metals: a neurodegenerative perspective, Dalton Trans. 4069–4076. (DOI: 10.1039/B822135A)

[122] Abelein A. (2023), Metal Binding of Alzheimer's Amyloid-β and Its Effect on Peptide Self-Assembly, Acc. Chem. Res. 56, 2653–2663 (DOI:10.1021/acs.accounts.3c00370)

[123] Sayre L. M., Perry G., Smith M. A. (1999), Redox metals and neu rodegenerative disease, Curr. Opin. Chem. Biol. 3, 220–225 (DOI: 10.1016/S1367-5931(99)80035-0)

[124] Lovell M. A., Robertson J. D., Teesdale W. J., et al. (1998), Copper, iron and zinc in Alzheimer's disease senile plaques, J. Neurol. Sci. 158, 47–52 (DOI: 10.1016/S0022-510X(98)00092-6)

[125] Suh S. W., Jensen K. B., Jensen M. S., et al. (2000), Histochemically-reactive zinc in amyloid plaques, angiopathy, and degenerating neurons of Alzheimer's diseased brains, Brain Research 852, 274–278 (DOI: 10.1016/S0006-8993(99)02096-X)

[126] Atwood C. S., Moir R. D., Huang X., et al. (1998), Dramatic Aggregation of Alzheimer Aβ by Cu(II) Is Induced by Conditions

Representing Physiological Acidosis, J. Biol. Chem. 273 12817–12826 (DOI: 10.1074/jbc.273.21.12817)

[127] Bush A. I., Pettingell W. H., Paradis M. D., et al. (1994), Modulation of A beta adhesiveness and secretase site cleavage by zinc., J. Biol. Chem. 269, 12152–12158 (DOI: 10.1016/S0021-9258(17)32694-7)

[128] Pradines V., Stroia A. J., Faller P. (2008), Amyloid fibrils: modulation of formation and structure by copper(II), New J. Chem. 32, 1189–1194 (DOI: 10.1039/B719556G)

[129] Raman B., Ban T., Yamaguchi K., et al. (2005), Metal Ion-dependent Effects of Clioquinol on the Fibril Growth of an Amyloid β Peptide, J. Biol. Chem. 280, 16157–16162 (DOI: 10.1074/jbc.M500309200)

[130] Ha C., Ryu J., Park C. B. (2007), Metal Ions Differentially Influence the Aggregation and Deposition of Alzheimer's β-Amyloid on a Solid Template, Biochemistry 46, 6118–6125 (DOI: 10.1021/bi7000032)

[131] Ji W., Yuan C., Zilberzwige-Tal S., et al. (2019), Metal-Ion Modulated Structural Transformation of Amyloid-Like Dipeptide Supramolecular Self-Assembly, ACS Nano 13, 7300–7309 (DOI: 10.1021/acsnano.9b03444)

[132] López de la Paz M., Goldie K., Zurdo J., et al. (2002), De novo designed peptide-based amyloid fibrils, Proc. Natl. Acad. Sci. U.S.A. 99, 16052–16057 (DOI: 10.1073/pnas.252340199)

[133] Hartgerink J. D., Beniash E., Stupp S. I., (2002), Peptide-amphiphile nanofibers: A versatile scaffold for the preparation of self-assembling materials, Proc. Natl. Acad. Sci. U.S.A. 99, 5133–5138 (DOI: 10.1073/pnas.072699999)

[134] Hoyer W., Antony T., Cherny D., et al. (2002), Dependence of α-Synuclein Aggregate Morphology on Solution Conditions, J. Mol. Biol. 322, 383–393 (DOI: 10.1016/S0022-2836(02)00775-1)

[135] Cabaleiro-Lago C., Szczepankiewicz O., Linse S., (2012), The Effect of Nanoparticles on Amyloid Aggregation Depends on the Protein Stability and Intrinsic Aggregation Rate, Langmuir 28, 1852–1857 (DOI: 10.1021/la203078w)

[136] Cabaleiro-Lago C., Quinlan-Pluck F., Lynch I., et al. (2008), Inhibition of Amyloid β Protein Fibrillation by Polymeric Nanoparticles, J. Am. Chem. Soc. 130, 15437–15443 (DOI: 10.1021/ja8041806)

[137] Yoo S. I., Yang M., Brender J. R., et al. (2011), Inhibition of Amyloid Peptide Fibrillation by Inorganic Nanoparticles: Functional Similarities with Proteins, Angew. Chem. Int. Ed. 50, 5110–5115 (DOI: 10.1002/anie.201007824)

[138] Wu W., Sun X., Yu Y., et al. (2008), TiO2 nanoparticles promote β-amyloid fibrillation in vitro, Biochem. Biophys. Res. Commun 373, 315–318 (DOI: 10.1016/j.bbrc.2008.06.035)

[139] Xu X., Ray R., Gu Y., et al. (2004), Electrophoretic Analysis and Purification of Fluorescent Single-Walled Carbon Nanotube Fragments, J. Am. Chem. Soc. 126, 12736–12737 (DOI: 10.1021/ja040082h)

[140] Bao L., Zhang Z. -L., Tian Z. -Q., et al. (2011), Electrochemical Tuning of Luminescent Carbon Nanodots: From Preparation to Luminescence Mechanism, Advanced Materials 23, 5801–5806 (DOI:10.1002/adma.201102866)

[141] Hamd-Ghadareh S., Salimi A., Fathi F., et al. (2017), An amplified comparative fluorescence resonance energy transfer immunosensing of CA125 tumor marker and ovarian cancer cells using green and economic carbon dots for bio-applications in labeling, imaging and sensing, Biosensors and Bioelectronics 96, 308–316 (DOI: 10.1016/j.bios.2017.05.003)

[142] Shao D., Lu M., Xu D., et al. (2017), Carbon dots for tracking and promoting the osteogenic differentiation of mesenchymal stem cells, Biomater. Sci. 5, 1820–1827 (DOI: 10.1039/C7BM00358G)

[143] Zhou N., Hao Z., Zhao X., et al. (2015), A novel fluorescent retrograde neural tracer: cholera toxin B conjugated carbon dots, Nanoscale 7, 15635–15642 (DOI: 10.1039/C5NR04361A)

[144] Shao X., Wang C., Wang C., et al. (2024), Novel photocatalytic carbon dots: efficiently inhibiting amyloid aggregation and quickly disaggregating amyloid aggregates, Nanoscale 16, 8074–8089 (DOI: 10.1039/D3NR06165E)

[145] Guerrero E. D., Lopez-Velazquez A. M., Ahlawat J., et al. (2021), Carbon Quantum Dots for Treatment of Amyloid Disorders, ACS Appl. Nano Mater. 4, 2423–2433 (DOI: 10.1021/acsanm.0c02792)

[146] Malishev R., Arad E., Bhunia S. K., et al. (2018), Chiral modulation of amyloid beta fibrillation and cytotoxicity by enantiomeric carbon dots, Chem. Commun. 54, 7762–7765 (DOI: 10.1039/C8CC03235A)

Chapter 2

Effect of Metal Ions on the Intrinsic Blue Fluorescence Property and Morphology of the Aromatic Amino Acid Self-Assembly

2.1 Introduction

The self-assembly of biomolecules is a ubiquitous process in nature. Among all the biomolecules, proteins and peptides are widely studied for their self-assembled structures. The self-aggregation of proteins and peptides can lead to the formation of amyloid aggregates *[1]*. It has been a major concern and an area of interest for researchers worldwide. There are many degenerative diseases, like Alzheimer's disease (AD), type II diabetes, and Parkinson's disease, which are found to be associated with the formation of amyloid structures *[2,3]*. Very recently, amyloid-like fibrillar structures with cytotoxic effects have been reported for single amino acids like phenylalanine, tryptophan, and tyrosine *[4-6]*. The self-assembly of phenylalanine plays a vital role in phenylketonuria (PKU), an inborn error of metabolism (IEM) disorder. The primary forces responsible for the amino acids to undergo self-aggregation are non-covalent interactions, including electrostatic interactions, van der Waals forces, π-π interactions, and hydrogen bonding, which play a pivotal role in the aggregation mechanism. It was reported that the fibril-forming mechanisms of phenylalanine and tyrosine are completely different *[7,8]*. Chakraborty et al. reported an aggregated "Tamarix dioica leaf"-like the fibrillar pattern of amino acid during the formation of copper nanoclusters *[9]*. Apart from the fibrillar structures, small oligomeric aggregates are often obtained as precursors of amyloid fibrils. Much interest has recently been devoted to these oligomers since their presence is linked to several neurodegenerative processes *[10,11]*.

Earlier studies have shown that pH, protein/peptide concentration, or the presence of ions can drastically influence the amyloid aggregation

process *[12,13]*. Additionally, there has been growing interest in the role of metal ions-based modulation of amyloid aggregates. Elevated concentrations of metal ions like Zn^{2+}, Cu^{2+}, and Fe^{3+} are found deposited within senile plaque deposits *[14]*. Al^{3+} has also been found in amyloid fibers at the cores of the senile plaques *[15]*. On the other hand, it was reported that Zn^{2+} stabilizes the non-fibrillar small amyloid aggregates *[16]*. Ha and co-workers reported that both Zn^{2+} and Cu^{2+} disrupt the fibrillar amyloid aggregates formation but induce the formation of amorphous amyloid aggregates *[17]*. Ye et al. have recently studied the protein nanofibrils (PNF) growth and hydrogel formation in the presence of different metal ions. Their study indicated that PNF hydrogel formation occurs faster with metal ions having lower pK_a *[18]*. All these studies may imply that metal ions can trigger or promote the aggregation of proteins or peptides.

It has been recently found that aromatic amino acids like phenylalanine, tryptophan, and tyrosine also show intrinsic blue fluorescence-like proteins and peptides upon forming amyloid structures *[19]*. Several attempts have been made to understand this unique blue fluorescence from proteins, peptides, and aromatic amino acids. Apart from proteins, peptides, amino acids, and other metabolites, the non-traditional fluorescence from macromolecular dendrimer systems has also been investigated *[20-24]*. These nonconventional luminogens (luminescence from non-aromatic moieties) are emissive in concentrated solutions and aggregated states. Luo and co-workers first reported this unique behavior as aggregation-induced emission (AIE) *[25]*. Yuan et al. proposed the unique emission behaviors of the already discussed non-traditional luminogens to be the result of unique clustering-triggered emission (CTE) *[26]*. This CTE involves the clustering of electron-rich hetero (N- and O-) atoms present in the backbones of the hyper-branched structures of the polymers. Recent research by Wang and co-workers has shown that BSA (Bovine serum albumin) exhibits unique aggregation-induced visible emission properties attributed to the clusterization of BSA proteins *[27]*. They

suggested that intra-intermolecular H-bonding, dipole-dipole interactions, and n-π^* interaction cause extended electronic delocalization and rigidified conformation, which are responsible for observed luminescence for BSA.

Our group has previously investigated the intrinsic blue fluorescence properties of both amyloid-like fibrils of aromatic amino acids and the aromatic amino acid-functionalized gold nanoparticles *[28]*. It was demonstrated that the common intrinsic optical properties in the visible range for both nanoparticles and fibrils come from the clusterization of amino acids in nanoparticles and fibrils. For amino acid-functionalized nanoparticles, the large fibrillar structures were found to be diminished upon the formation of the nanoparticles. Surprisingly, the quantum yields of the aromatic amino acid-functionalized gold nanoparticles were much higher than the blank amino acid fibrils. This observation raised a fundamental question on whether the formation of non-fibrillar amyloid-like aggregates through clusterization of amino acids causes an enhancement in the emission intensity in the case of nanoparticles or not. Recent reports indicate that several metal ions disrupt fibrillation but stabilize the formation of non-fibrillar amyloid aggregates upon interaction with peptides and proteins *[29,30]*. However, it is still unclear if the interaction between metal ions and peptide/protein and subsequent morphological change has any direct link with clusterization and the resultant clusteroluminescence. In the present work, we aim to study the influence of different metal ions (Na^+, Mg^{2+}, Ca^{2+}, Zn^{2+}, Al^{3+}, Ga^{3+}, In^{3+}, Sn^{4+}) in the formation of the self-assemblies of two aromatic amino acids namely phenylalanine and tryptophan to unravel the role of metal ions on fibrillation and the intrinsic blue fluorescence that develops during amyloid formation. The metal ions were selected systematically with the variation of their charge and size. We studied the intrinsic blue fluorescence properties of the self-assemblies using steady-state fluorescence, time-resolved decay, confocal imaging, and field emission scanning electron microscope (FESEM) imaging. Our study demonstrates the role of metal ions in the clusterization of

aromatic amino acids, resulting in a change in clusteroluminescence and the morphology of the self-assemblies.

2.2 Results and Discussion

2.2.1 Investigation of the Intrinsic Luminescence Property of Aromatic Amino Acid Self-assemblies:

Before investigating the effect of metal ions on intrinsic blue fluorescence properties of aromatic amino acid self-assemblies (A_{aa}), we studied the intrinsic photoluminescence properties of phenylalanine and tryptophan self-assemblies (A_{Phe} and A_{Trp}). The self-assemblies of amino acids show distinct emission behavior, which is in contrast to that of the monomeric state (**Figure 2.1**).

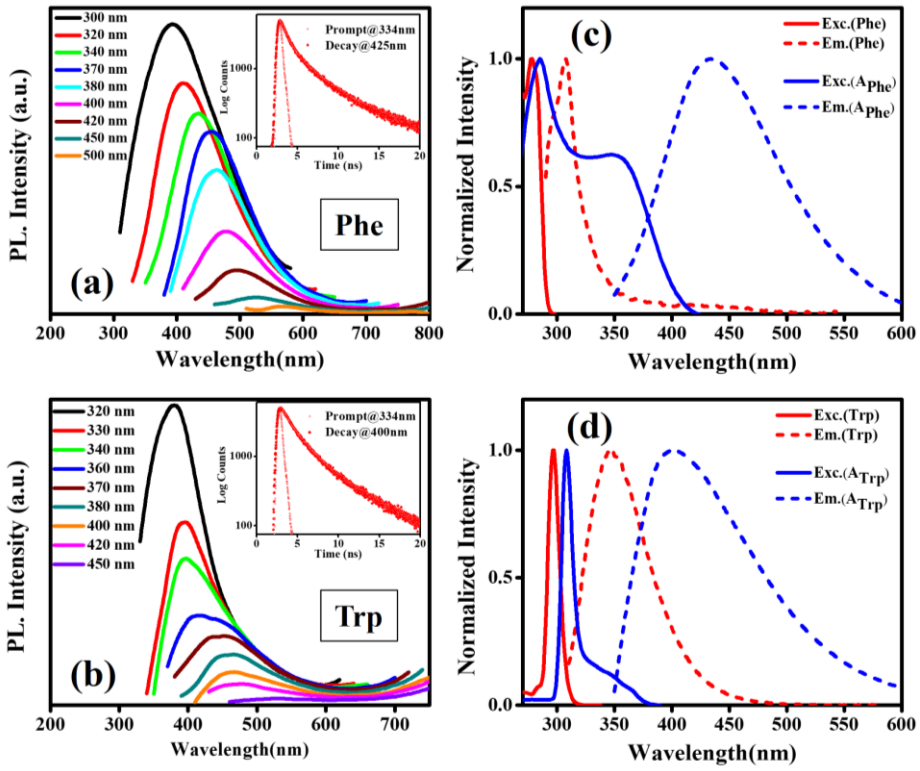

Figure 2.1 *Excitation-dependent emission spectra and time-resolved decays (inset) of A_{Phe} (a), A_{Trp} (b), and excitation-emission spectra of monomeric and self-assembly of L-Phe (c), and L-Trp (d).*

Furthermore, the amino acid self-assemblies (A_{Phe} and A_{Trp}) exhibit excitation-dependent emission spectra (**Figure 2.1a, b**). The emission maximum of the self-assemblies varies from 395 to 567 nm for A_{Phe} and

from 377 to 525 nm for A_{Trp} with increasing excitation wavelength, which emanates from diverse emissive species, and this was further confirmed by their different lifetime components (Data not shown) spanning over 2-6 ns upon excitation at 334 and 405 nm

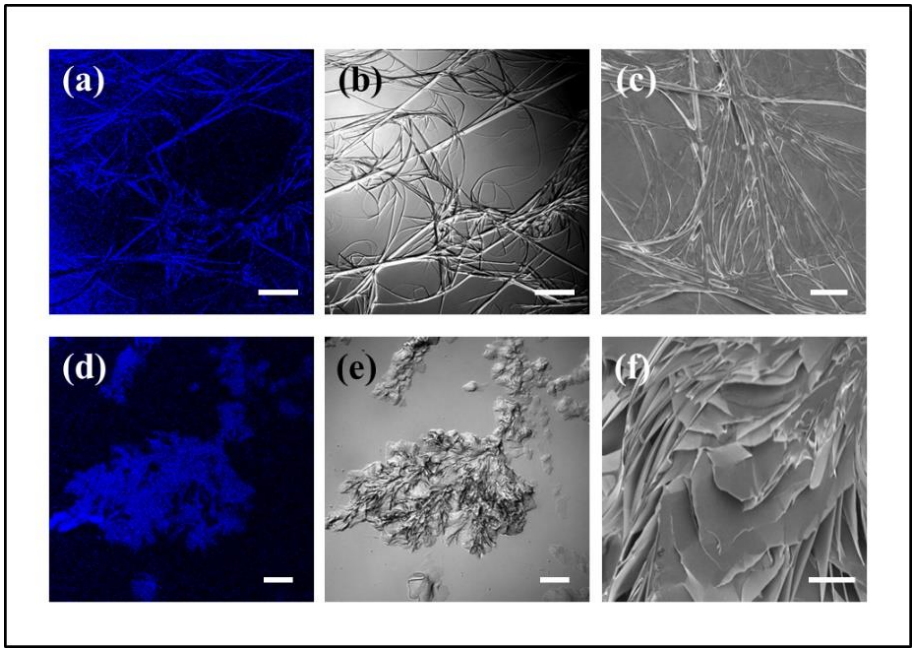

Figure 2.2 *CLSM (a,d), bright-field (b,e), and SEM (c,f) images of A_{Phe} (a-c) and A_{Trp} (d-f). Scale bar 10 µm.*

respectively. The non-exponential decay with different components resulting from different excitation wavelengths may primarily be attributed to the presence of different aggregates of amino acids. The

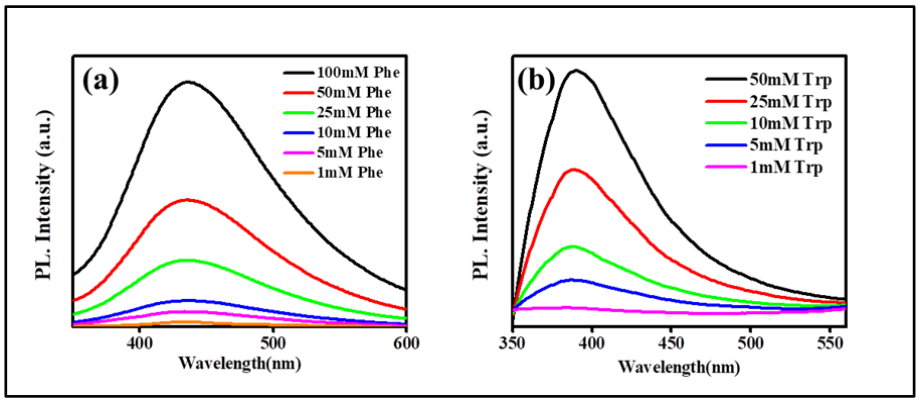

Figure 2.3 *Concentration-dependent emission spectra of L-Phe (a), and L-Trp (b), upon excitation at 340 nm.*

excitation spectra reveal a secondary peak at around 340-360 nm, indicating the formation of the aggregated states, which is believed to

be responsible for the observed emission in the visible range (**Figure 2.1c, d**). The formation of fibrillar morphology and intrinsic blue fluorescence was further confirmed by FESEM and confocal microscopy (CLSM; **Figure 2.2**). These results corroborate well with our previous report *[28]*.

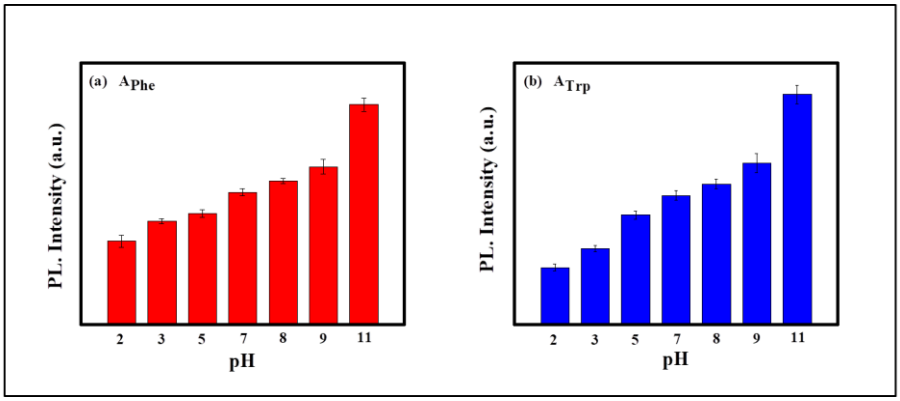

Figure 2.4 *The emission intensity of A_{Phe} (a) and A_{Trp} (b) at different pH.*

It is important to note that amino acids undergo aggregation in solution, even at room temperature, to form the self-assemblies. At higher concentrations (50 mM for L-Tryptophan and 100 mM for L-Phenylalanine), they show strong emission behavior above 400 nm

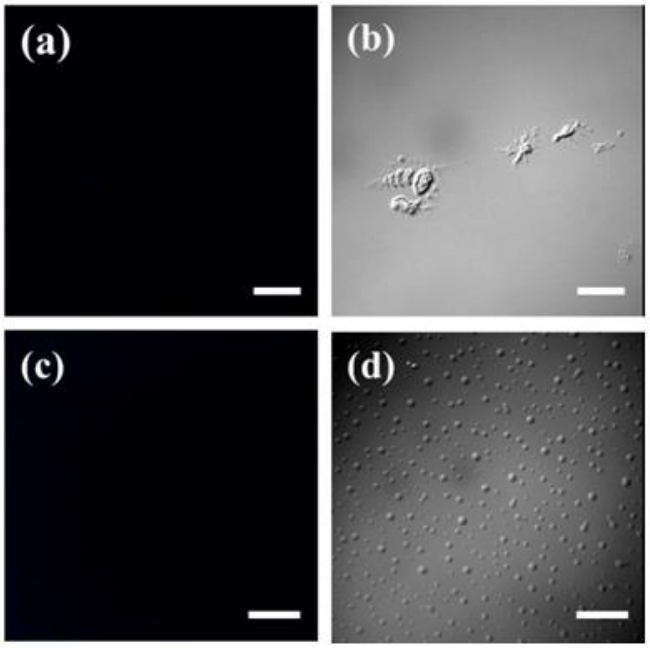

Figure 2.5 *CLSM and bright-field images of A_{Phe} (a,b) and A_{Trp} (c,d), respectively, at pH~2. Scale bar 10 µm.*

when excited at 340 nm and higher wavelengths (**Figure 2.3**). Interestingly, emission intensities decreased as the solutions were diluted up to 5 mM, and at very low concentrations (1 mM), faint emission was observed in the visible range. We previously reported that simple drying of the amino acids of 1 mM concentration led to form self-assemblies with weak fluorescence intensities captured with

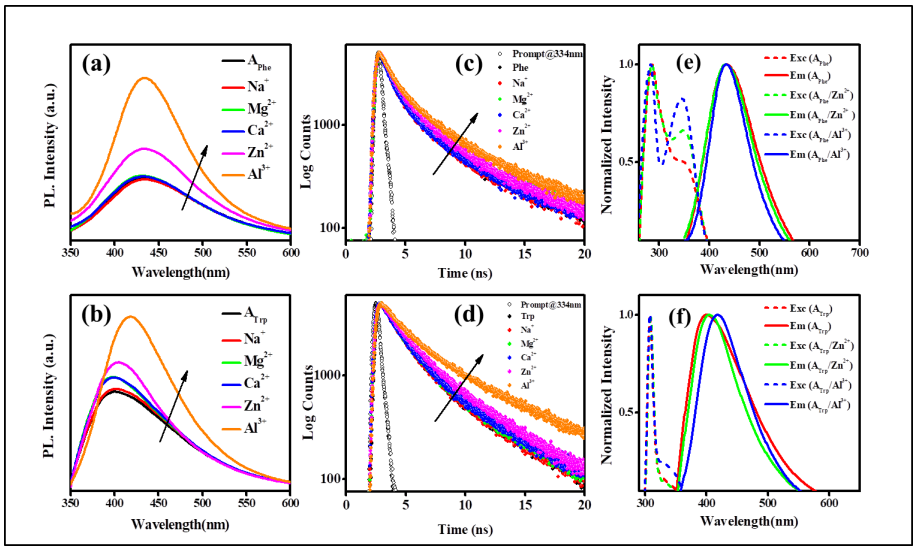

Figure 2.6 *Emission spectra (a,b) when excited at 340 nm and Time-resolved decay curves (c,d) when excited at 334 nm of A_{Phe} (a,c) and A_{Trp} (b,d) in the presence of different metal ions. Excitation-emission spectra of A_{Phe} (e) and A_{Trp} (f) in the presence of Zn^{2+} and Al^{3+}.*

confocal microscopy *[28]*. Such concentration-enhanced visible emission was recently explored by Wang and co-workers for BSA protein *[27]*, which was attributed to the clustering of NH_2, C=O, OH, and several other units with n and π electrons, leading to extended electronic delocalization and rigidified conformations in the concentrated BSA solutions. He et al. investigated the luminescence properties of maleimide and succinimide derivatives in concentrated solution and solid-state *[31]*. They proposed the formation of clusters as the origin of striking luminescence in the visible range. All these interesting results indicate a probable clusterization-triggered emission (CTE) for simple aromatic amino acids. Earlier, we reported the existence of diverse emissive aggregates formed by amino acid monomers through clusterization, and these nano-aggregates act as the

fundamental building blocks that organize into the amyloid-like fibrillar structure *[28]*. These aggregates exhibit unique luminescence behavior, which can be linked to the unusual "blue fluorescence" in the case of several proteins and peptides.

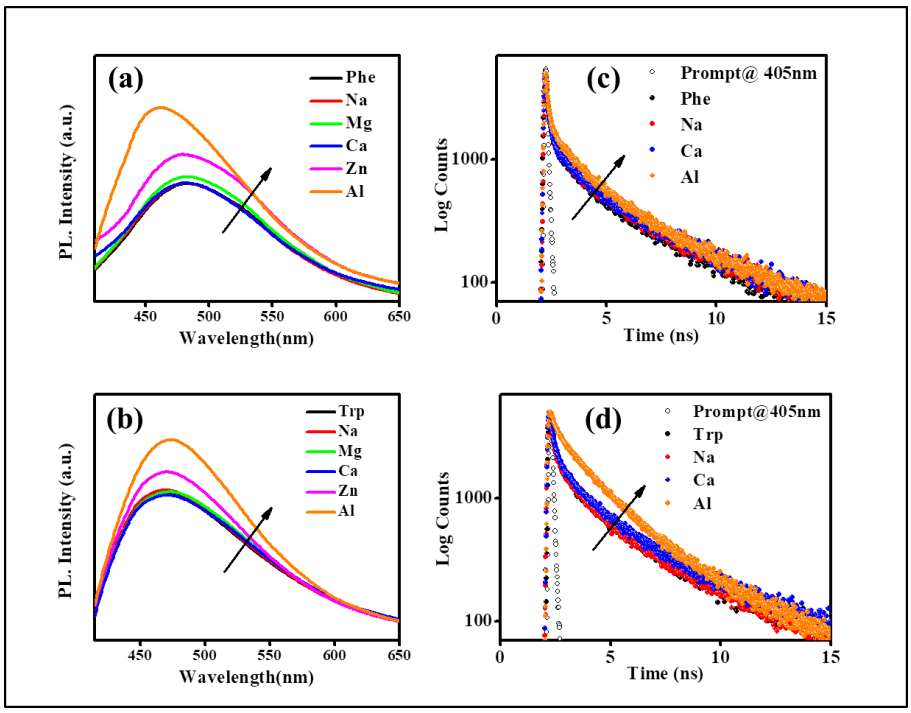

Figure 2.7 *Emission spectra (a,b) when excited at 400 nm and Time-resolved decay curves (c,d) when excited at 405 nm of* A_{Phe} *(a,c) and* A_{Trp} *(b,d) in the presence of different metal ions. For a clear depiction of time-resolved decay curves, we have omitted a few metal ions.*

2.2.2 Effect of pH on the Photophysical Properties and Morphology of the Self-assemblies:

We also studied the formation of amino acid assemblies at different pHs. It was observed that the quantum yield of A_{aa} is higher in alkaline pH and lower at acidic pH than in neutral medium (pH~7) (**Figure 2.4**). The decrease in the fluorescence intensity with decreasing pH may be attributed to the fact that at lower pH, protonation of COO- groups can result in the disruption of "through-space conjugation (TSC)" between the amino acid residues *[32]*. This observation implies that the COOH group has a significant role in forming the fluorescent aggregates. Interestingly, the confocal images at very low pH (pH~2) revealed the absence of any amyloid-like fibrillar structures, indicating that high

acidic conditions inhibit the formation of fluorescent aggregates (**Figure 2.5**). We have already reported in our previous work that clusteroluminescence arises from through-space conjugation (TSC), which is disrupted by the protonation of COO- at lower pH *[28]*.

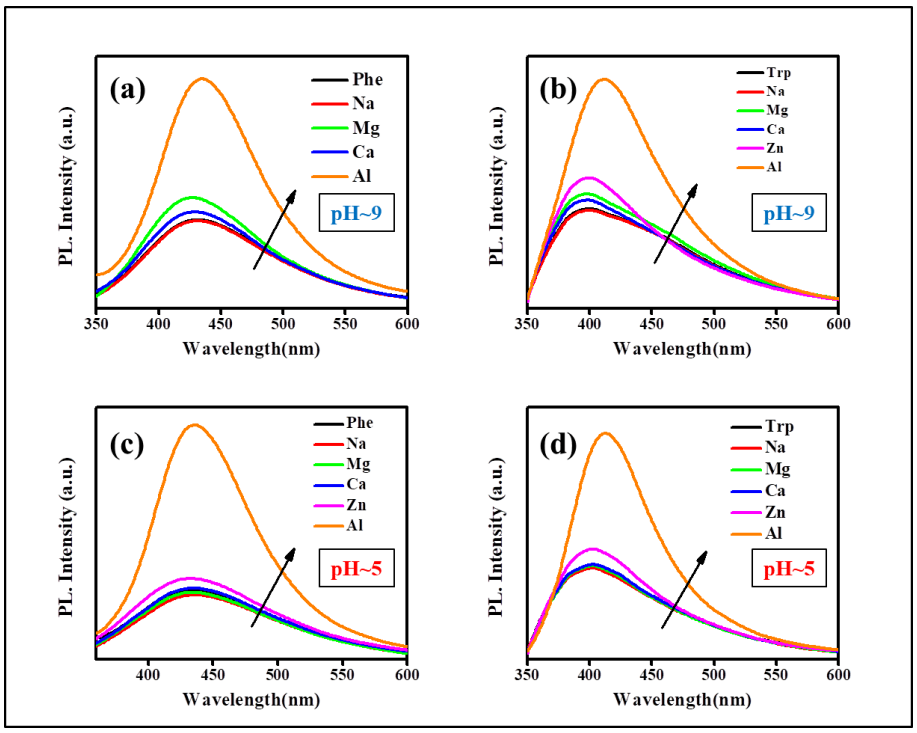

Figure 2.8 *Emission spectra of A_{Phe} (a,c) and A_{Trp} (b,d), at pH~9 (a,b) and pH~5 (c,d), respectively, in the presence of different metal ions, upon excitation at 340 nm.*

2.2.3 Effect of Metal Ions on the Photophysical Property of the Self-assemblies (A_{aa}):

After confirming the formation of the self-assemblies (A_{aa}), we investigated the effect of several metal salts on the photoluminescence property and morphology of the amino acid self-assemblies (A_{Phe} and A_{Trp}) using steady-state fluorescence and time-resolved fluorescence spectroscopy measurements. Since aromatic amino acids are among the simplest building blocks of proteins and peptides, we made a reductionist approach to simplifying the complexity of proteins and peptides. Our main objective is to understand the role of metal ions in the formation of aromatic amino acid self-assembly and the intrinsic blue fluorescence coming out of it. In this study, the metal ions (M^{n+}) were systemically selected with variable pK_a values (from basic to

acidic), which correlate to their charge and size. The monovalent Na^+ (sized 116 pm), divalent Ca^{2+}, Mg^{2+}, and Zn^{2+} (sized 114 pm, 86 pm, and 74 pm, respectively) and trivalent Al^{3+} (sized 68 pm) were

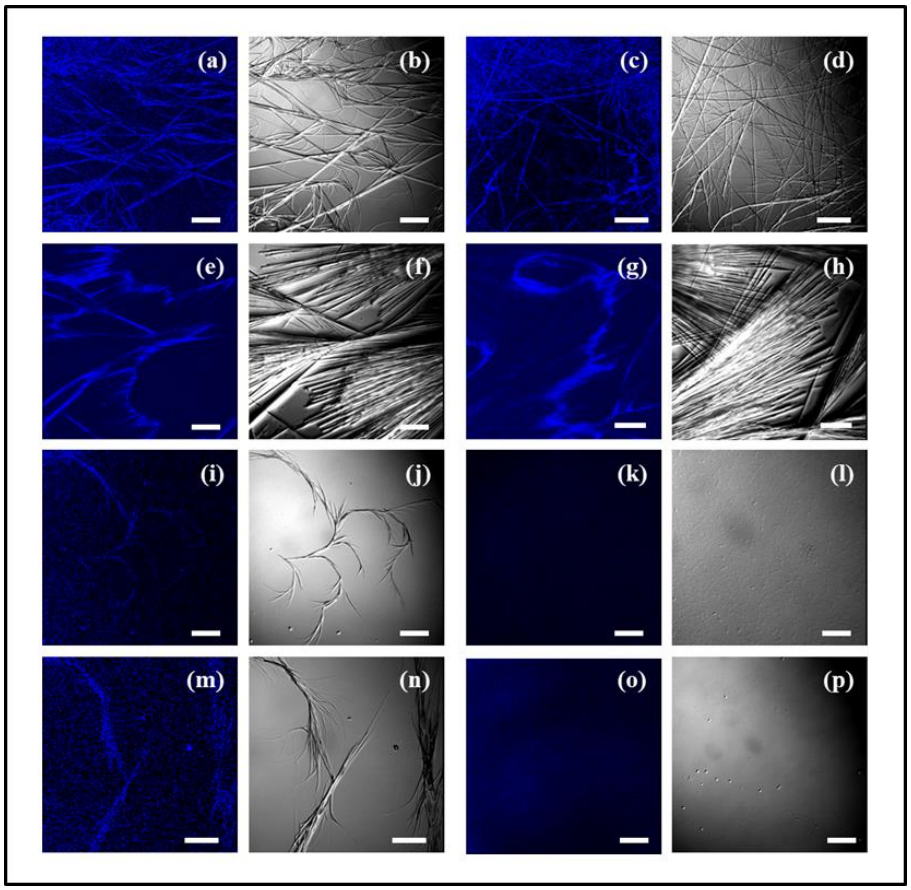

Figure 2.9 *CLSM and bright-field images of (a,b) A_{Phe}, (c,d) A_{Phe}/Na^+ (1:2), (e,f) A_{Phe}/Mg^{2+} (1:2), (g,h) A_{Phe}/Ca^{2+} (1:2), (i,j) A_{Phe}/Zn^{2+} (1:0.25), (k,l) A_{Phe}/Zn^{2+} (1:2), (m,n) A_{Phe}/Al^{3+} (1:0.25), (o,p) A_{Phe}/Al^{3+} (1:2), respectively. Scale bar 10 µm.*

considered with their corresponding pK_a values of 14, 12.7, 11.2, 9.0, and 5.0 for Na^+, Ca^{2+}, Mg^{2+}, Zn^{2+}, and Al^{3+}, respectively *[18,33]*. We measured the steady-state fluorescence properties of the self-assemblies in the presence of metal ions at a fixed molar ratio of amino acid to metal ion at 1:2. All the samples were excited at 340 and 400 nm wavelength to capture different aggregates formed due to the addition of metal ions to amino acid assemblies. At HEPES buffer medium (pH~7), all the A_{aa}/M^{n+} (1:2) except A_{aa}/Zn^{2+} (1:2) and A_{aa}/Al^{3+} (1:2) showed similar fluorescence intensities as compared to that of blank assemblies (A_{aa}) when excited at 340 nm (**Figure 2.6a, b**) and 400 nm (**Figure 2.7a, b**) respectively. The enhanced emission behavior was obtained for both

A_{aa}/Zn^{2+} (1:2) (increased by ~46.5% for A_{Phe}/Zn^{2+} and ~33% for A_{Trp}/Zn^{2+}) and A_{aa}/Al^{3+} (1:2) (increased by ~160% for A_{Phe}/Al^{3+} and ~75% for A_{Trp}/Al^{3+}) systems as compared to blank A_{aa}, upon excitation at 340 nm. The significant increase in the

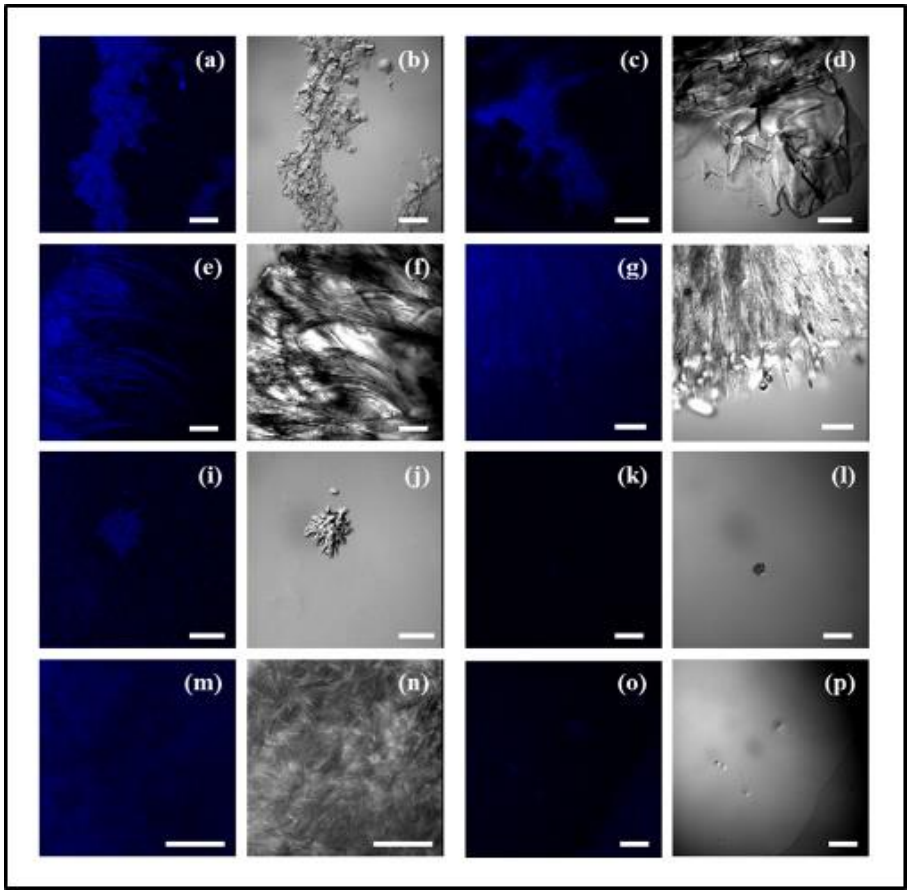

Figure 2.10 *CLSM and bright-field images of (a,b) A_{Trp}, (c,d) A_{Trp}/Na^{+} (1:2), (e,f) A_{Trp}/Mg^{2+} (1:2), (g,h) A_{Trp}/Ca^{2+} (1:2), (i,j) A_{Trp}/Zn^{2+} (1:0.25), (k,l) A_{Trp}/Zn^{2+} (1:2), (m,n) A_{Trp}/Al^{3+} (1:0.25), (o,p) A_{Trp}/Al^{3+} (1:2), respectively. Scale bar 10 µm.*

intensity implies that the fluorescent nano-aggregates might have formed to a larger extent upon the addition of bivalent Zn^{2+} and trivalent Al^{3+} ions. The formation of diverse aggregates facilitates the clusteroluminescence of amino acid assembly, which may be responsible for the observed enhancement. The excitation spectra reveal a more prominent peak at the 340-360 nm range as compared to that of blank A_{aa} assemblies, indicating the formation of more aggregates that are responsible for the intrinsic fluorescence in the visible range (**Figure 2.6e, f**). The lifetime profile reveals that upon excitation at 334 nm, there is a marginal increment in the lifetime decay in the presence of Na^{+},

Ca^{2+}, and Mg^{2+}; on the other hand, we observed a significant increment in the lifetime in the presence of Al^{3+} (**Figure 2.6c, d**). This enhanced lifetime may arise due to more rigid conformations of the emissive species present. Interestingly, the excitation at 405 nm yields a similar trend but we observed a very long component appeared as compared to the blank assembly of amino acids (**Figure 2.7c, d**).

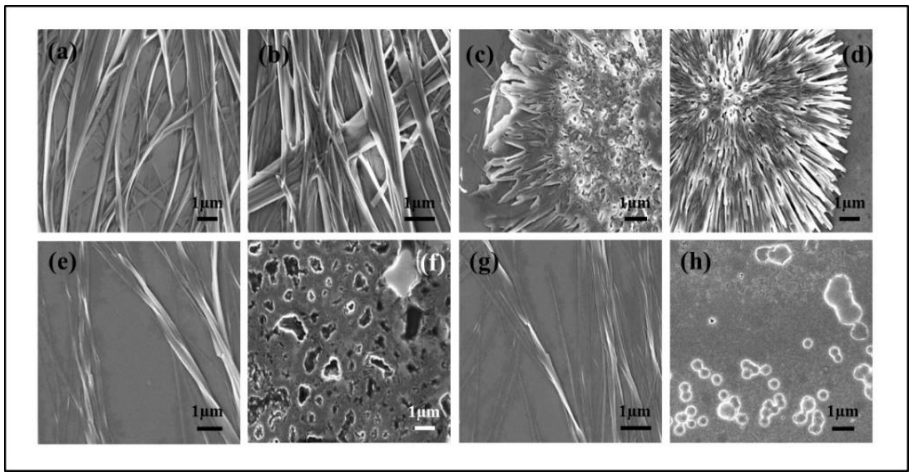

Figure 2.11 *SEM images of (a) A_{Phe}, (b) A_{Phe}/Na^{+} (1:2), (c) A_{Phe}/Mg^{2+} (1:2), (d) A_{Phe}/Ca^{2+} (1:2), (e) A_{Phe}/Zn^{2+} (1:0.25), (f) A_{Phe}/Zn^{2+} (1:2), (g) A_{Phe}/Al^{3+} (1:0.25), (h) A_{Phe}/Al^{3+} (1:2).*

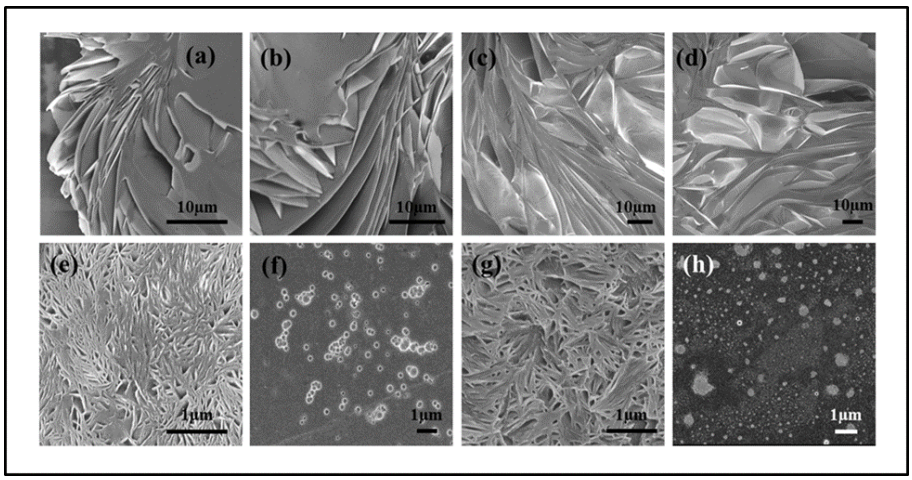

Figure 2.12 *SEM images of (a) A_{Trp}, (b) A_{Trp}/Na^{+} (1:2), (c) A_{Trp}/Mg^{2+} (1:2), (d) A_{Trp}/Ca^{2+} (1:2), (e) A_{Trp}/Zn^{2+} (1:0.25), (f) A_{Trp}/Zn^{2+} (1:2), (g) A_{Trp}/Al^{3+} (1:0.25), (h) A_{Trp}/Al^{3+} (1:2).*

It is reported that NH_3^{+} and COO^{-} of the amino acids play crucial roles in the formation of the self-assembly and the clusteroluminescence property *[34]*. We studied the steady-state fluorescence in two different

buffer mediums (acetate buffer for pH~5 and the Tris buffer for pH~9) to investigate their role in the interaction between metal ions and the A_{aa}. We observed a similar enhancement in emission intensities for both A_{Phe}/Al^{3+} (1:2) (by ~160%) and A_{Trp}/Al^{3+} (1:2) (by ~130%) at pH~9, as compared to the blank A_{aa}, upon excitation at 340 nm (**Figure 2.8a, b**). However, we observed precipitation for the

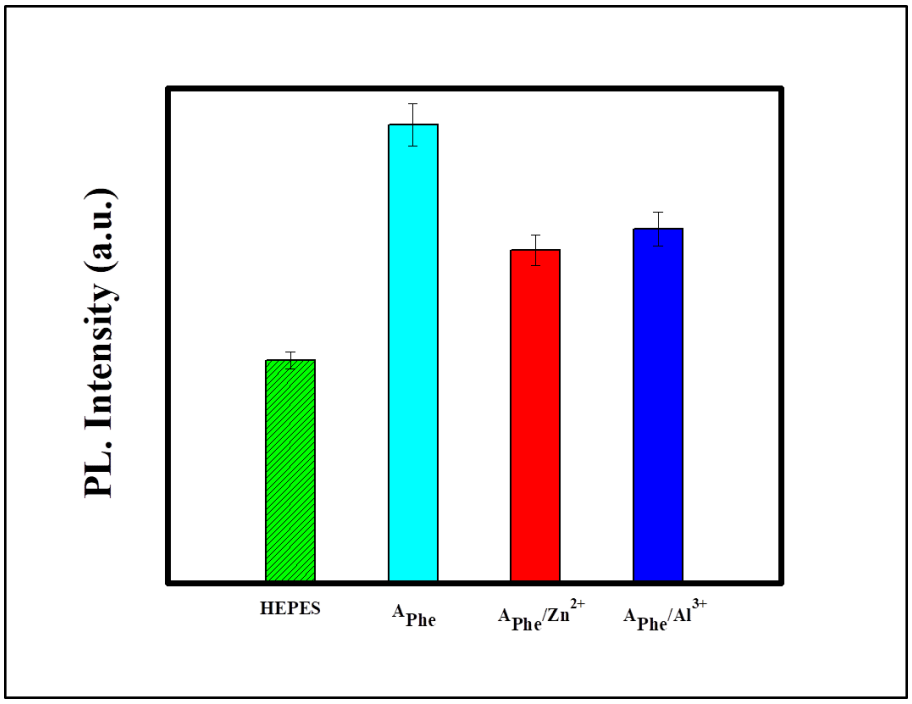

Figure 2.13 *The fluorescence intensity of ThT at 485 nm (λ_{ex} = 450 nm) in control, A_{Phe}, A_{Phe}/Zn^{2+}, and A_{Phe}/Al^{3+} systems.*

A_{Phe}/Zn^{2+} (1:2) solution, which may be associated with the formation of ZnO nanoparticles in the alkaline medium *[35]*. Interestingly, we did not find any precipitation for A_{Trp}/Zn^{2+} (1:2). We did not observe much change in the emission intensities for the A_{aa}/M^{n+} (1:2) systems, except for Al^{3+}, at pH~5, as compared to A_{aa} systems. This observation supports our previous work that lowering of pH indeed disrupts the through-space conjugation (TSC), and the metal ions (Na^{+}, Mg^{2+}, Ca^{2+}, Zn^{2+}) will not have much influence on the clusterization at lower pH region. Exceptionally for both A_{Phe}/Al^{3+} (1:2) and A_{Trp}/Al^{3+} (1:2), we got enhanced fluorescence emission at pH~5 upon excitation at 340 nm (**Figure 2.8c, d**). Therefore, it can safely be concluded that the metal ion with a high charge-to-radius ratio, such as Al^{3+}, is much more effective

in promoting clusteroluminescence than the other metal ions. In our earlier work, we have shown that gold nanoparticles facilitate the clusterization of amino acids over the nanoparticle surface, which leads to enhanced blue fluorescence *[28]*. Surprisingly, upon the formation of nanoparticles, the amyloid-like fibrillar structures of the amino acids were diminished, but enhanced fluorescence was observed. Even after the removal of nanoparticles, the nano-aggregates, with appreciable fluorescence signals, were found to exist.

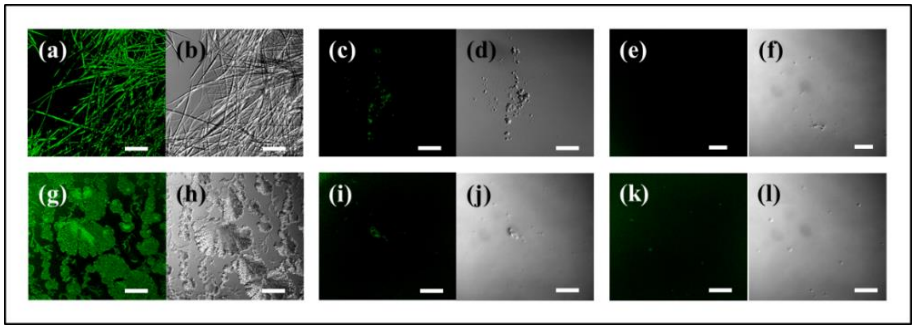

Figure 2.14 *CLSM and bright-field images of (a,b) A_{Phe}, (c,d) A_{Phe}/Zn^{2+} (1:2), (e,f) A_{Phe}/Al^{3+} (1:2), (g,h) A_{Trp}, (i,j)A_{Trp}/Zn^{2+} (1:2), (k,l) A_{Trp}/Al^{3+} (1:2), respectively, when stained with ThT. Scale bar 10 µm.*

2.2.4 Effect of Metal Ions on the Morphology of the Self-assemblies (A_{aa}):

To investigate the formation of fluorescent amyloid-like aggregates, we undertook extensive confocal microscopy (**Figure 2.9 and 2.10**) and SEM imaging (**Figure 2.11 and 2.12**) of the aromatic amino acid assemblies in the presence of metal salts. We observed that the fibrillar morphologies prevail in the presence of metal ions like Na^+, Mg^{2+}, and Ca^{2+}. Additionally, strong fluorescence signals were obtained from the assemblies. Interestingly, fibrillar morphologies were not observed for both A_{aa}/Zn^{2+} (1:2) and A_{aa}/Al^{3+} (1:2). From the confocal microscopy (**Figures 2.9 k,l,o,p and 2.10 k,l,o,p**) and SEM imaging (**Figures 2.11f,h and 2.12f,h**), it is quite evident that both Zn^{2+} and Al^{3+} inhibit the large fibrillation of the aromatic amino acids. But interestingly, we observed some very small aggregates that are formed at a large scale in the presence of Zn^{2+} and Al^{3+}. The same nano-aggregates, probably

formed due to the clusterization, systematically assemble into mature fibrillar structures and are believed to be responsible for the bright blue fluorescence of the self-assemblies (A_{aa}). Furthermore, to gain deeper insight into the effect of the concentration of the metal ions on A_{aa} (at fixed amino acid concentration), a lower concentration of the metal ions Zn^{2+} and Al^{3+} was used (amino acid to metal ion ratio of 1:0.25). We observed the existence of fibrillar structures of the aromatic amino acid assemblies along with the presence of nano-aggregates from both the CLSM images (**Figures 2.9 i,j,m,n and 2.10 i,j,m,n**) and SEM images (**Figures 2.11e,g and 2.12e,g**) for A_{aa}/Zn^{2+} (1:0.25) and A_{aa}/Al^{3+} (1:0.25). This observation indicates that at an apparent lower metal ion concentration, the metal ions Zn^{2+} and Al^{3+} partially inhibit fibrillation.

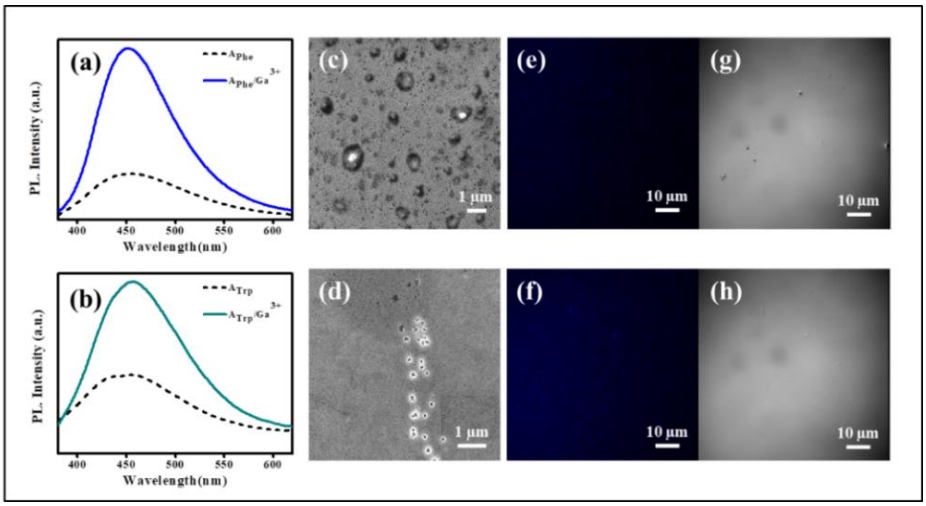

Figure 2.15 *Emission spectra upon excitation at 370 nm (a,b), SEM images (c,d), CLSM (e,f) and bright-field images (g,h) of* A_{Phe} *(a,c,e,g) and* A_{Trp} *(b,d,f,h), respectively, in presence of* Ga^{3+}.

We further investigated the effect of the metal ions Zn^{2+} and Al^{3+} on the fibrillation of phenylalanine using the Thioflavin T (ThT) binding assay. ThT exhibits remarkable fluorescence enhancement upon binding with fibrillar structures and has been widely applied in studying amyloid formation *[36]*. The steady-state fluorescence measurement showed an enhanced intensity of ThT in the presence of A_{Phe}, indicating the formation of a fibrillar structure (**Figure 2.13**). However, in the case of both A_{Phe}/Zn^{2+} (1:2) and A_{Phe}/Al^{3+} (1:2), we observed a decrease in the emission intensity compared to the signal obtained from ThT in A_{Phe}.

Confocal microscopy of the ThT-stained assemblies also showed that fibrillar structures of the respective amino acids were absent in the presence of Zn^{2+} and Al^{3+} (**Figure 2.14**). This observation supports our previous conjecture that Zn^{2+} and Al^{3+} induce inhibition of the formation of fibrillar structures. Thus, from all the imaging studies (CLSM and SEM), it is evident that in the presence of Zn^{2+} and Al^{3+}, small aggregates of aromatic amino acids are formed. The formation of these small aggregates is possibly due to the extensive clusterization of the aromatic amino acids in the presence of the metal ions Zn^{2+} and Al^{3+}, which is responsible for the observed fluorescence enhancement obtained in the steady-state fluorescence spectra. Enhancement in the fluorescence signal may be attributed to the increased local concentration of amino acids upon clusterization. Our previous work demonstrated that the local concentration of the aromatic amino acids increased many folds on the gold nanoparticle surface, providing an essential environment for aggregation *[28]*.

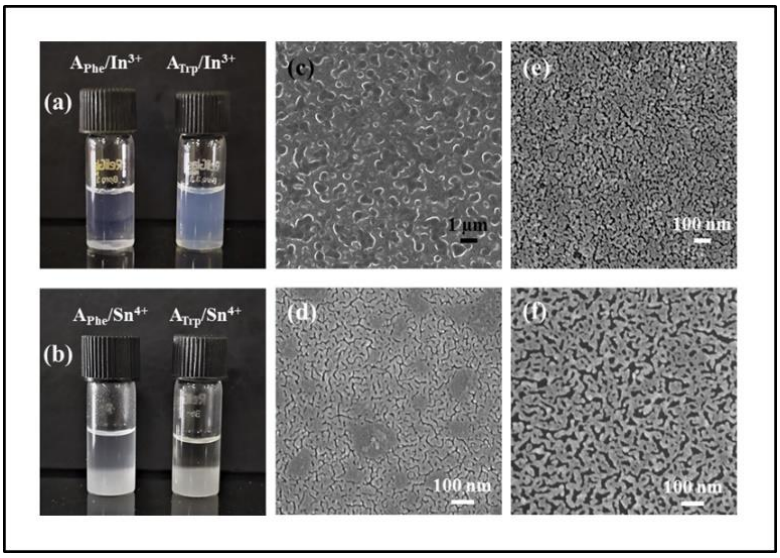

Figure 2.16 *Photographs of amino acid self-assemblies (A_{Phe}, A_{Trp}) in the presence of In^{3+} and Sn^{4+} (a,b), SEM images of A_{Phe}/In^{3+}(c), A_{Trp}/In^{3+}(d), A_{Phe}/Sn^{4+}(e), and A_{Trp}/Sn^{4+} (f).*

Now, the important question that arises is: what are the crucial parameters of some of the metal ions that induce the formation of a large number of amyloid aggregates and subsequently enhance the emission behavior? Very recently, Ye and co-workers revealed that much smaller

and curved fibrils are formed in the presence of metal ions with lower pK_a values *[18]*. In our work, we observed that in the presence of monovalent Na^+, sized 116 pm, or divalent Mg^{2+} and $Ca^{2+,}$ sized 86 pm and 114 pm, respectively, the fibrillar morphology of the self-assemblies remained almost intact. But fibrillar structures was inhibited in the presence of metal ions having higher charge and smaller size, i.e., divalent Zn^{2+} (74 pm) and trivalent Al^{3+} (68 pm). To further confirm the role of pK_a of the metal ions on the self-assemblies, the other three metal ions, Ga^{3+} sized 76 pm, In^{3+} sized 94 pm, and Sn^{4+} sized 83 pm, were selected for the investigation. These metal ions were particularly chosen for their relatively low pK_a values, i.e. 2.6, 3.9, and -0.6 for Ga^{3+}, In^{3+}, and Sn^{4+}, respectively *[18,33]*. Enhanced emission was indeed observed in the case of A_{Phe}/Ga^{3+} (1:2) (by ~250%) and A_{Trp}/Ga^{3+} (1:2) (by ~120%) when excited at 370 nm, and from SEM images and CLSM images, non-fibrillar aggregates were obtained to be present (**Figure 2.15**). Interestingly, for both A_{Phe}/In^{3+} (1:2) and A_{Trp}/In^{3+} (1:2), turbid appearance was observed (**Figure 2.16a**), and as for both A_{Phe}/Sn^{4+} (1:2) and A_{Trp}/Sn^{4+} (1:2), we observed a clear phase-separation, probably due to the precipitation of SnO_2 *[18]* (**Figure 2.16b**). From SEM images, non-fibrillar aggregates were observed (**Figure 2.16c-f**), indicating that lower pK_a values of metal ions indeed affect fibril formation. It was reported earlier that larger hydrophobic exposures of Aβ conformation induced by Zn^{2+} and Al^{3+} can significantly destabilize fibril formation *[37]*. Do et al. reported that the small hydrophobic peptide forms small aggregates under acidic conditions as at relatively low pH, electrostatic interactions between neighboring NH_3^+ and COO^- get weakened to form fibrillar structures *[38]*. Thus, the lowering of pH due to the hydrolysis of the metal ions, Zn^{2+} and Al^{3+}, may be an important factor that leads to the inhibition of fibrillar structures. But this does not imply that lowering of pH can induce the enhancement of photoluminescence behavior as we have already shown that at lower pH, emission intensities get decreased. The recent computational simulations study indicates that Zn^{2+} ions inhibit fibril formation by reducing the number of hydrogen bonds between neighboring β-sheet layers of the Aβ fibril. Additionally,

Zn^{2+} ions increase the number of water molecules located in the salt-bridge region of the amyloid fibril, which leads to the disruption of the salt-bridge region and inhibition of fibril growth *[30]*. It was also reported earlier that in the presence of both Zn^{2+} and Al^{3+}, diphenylalanine self-assembles into both nanofibrils and spherical structures, and the enhanced hydrophobic interactions induced by the strong binding between trivalent metal ions and dipeptides inhibit the assembly of spherical structures into nanofibrils *[39]*. All these factors cumulatively shed light on explaining the inhibition of the fibril formation caused by metal ions Zn^{2+} and Al^{3+}.

	FWHM			**FWHM**
A_{Phe}	115 nm		**A_{Trp}**	117 nm
A_{Phe}/Zn^{2+}	110 nm		**A_{Trp}/Zn^{2+}**	97 nm
A_{Phe}/Al^{3+}	93 nm		**A_{Trp}/Al^{3+}**	96 nm

Table 2.1 *The full width at half maxima values of A_{aa}, A_{aa}/Zn^{2+}, and A_{aa}/Al^{3+} systems (where aa = Phe and Trp).*

Very recently, it was observed that the emission behavior of gold nanoclusters enhanced drastically when metal ions (Zn^{2+}, Cd^{2+}) were incorporated in the co-assembly along with the morphological transformation *[40-42]*. The enhanced emission was attributed to the aggregation-induced emission (AIE) behavior of nanoclusters along with π-π stacking of ligands and ligand-to-metal charge transition (LMCT). Fan and co-workers previously showed an enhanced emission intensity of dipeptide self-assembly upon coordination with $Zn^{2+,}$ and it was observed that metal ions with higher nuclear charge and polarizability induce more enhancement in the emission signal *[43]*. They proposed to utilize the effects of metal coordination and π-π stacking interaction for tuning the optical properties of the assembly from the ultraviolet to the visible range. Interestingly, we have witnessed

a similar red-shift in the emission signal (**Figure 2.6b**) for A_{Trp}/Al^{3+} (1:2), which may result from the π-π stacking interaction and metal ion coordination, as these interactions reduce the excited-state energy, thereby increasing the emission wavelengths. Previously, it was observed that the emission intensity of tryptophan-based cyclo-dipeptide self-assemblies gets enhanced upon coordination with Zn^{2+}, producing a narrower peak *[44]*. The narrower emission bandwidth of the dipeptide nanoparticles may be regarded as evidence of quantum-well structure. Our study also revealed the enhanced emission intensities of the self-assemblies upon coordination with Zn^{2+} and Al^{3+}, generating peaks with full width at half maximum (FWHM) values lesser as compared to that of A_{aa} (**Figure 2.6e, f and Table 2.1**), which may stem from the formation of more confined structure. The possible dehydration of the amino acid aggregates, driven by enhanced hydrophobic interaction in the presence of a high concentration of metal ions, can lead to the increased local concentration of the amino acids, which eventually facilitates extensive clusterization. From our study, it was quite conclusive that metal ions with lower pK_a values inhibit fibril formation. Interestingly, metal ions Zn^{2+}, Al^{3+}, and Ga^{3+} not only inhibit fibril formation but also enhance the emission intensity and induce morphological change. Therefore, it can be concluded that metal ions with higher nuclear charge and smaller sizes are much more effective in promoting the clusterization of amino acids, resulting in enhanced clusteroluminescence. These metal ions induce the inhibition of the fibrillar growth of the aromatic amino acids but facilitate the formation of non-fibrillar emissive amyloid-like aggregates.

2.3 Conclusion

In summary, we thoroughly investigated the effect of different metal ions on the intrinsic blue luminescence and the structures of the self-assembly of aromatic amino acids. The emission behavior and structural morphology of amino acid aggregates were studied in detail using various spectroscopic and microscopic techniques. It was demonstrated

that the formation of diverse aggregates of amino acids and the resultant photoluminescence was strongly dependent on the charge and size of the metal ions, which can directly be correlated to their pK_a values. Monovalent Na^+ (pK_a ~14), divalent Mg^{2+}, and Ca^{2+} (pK_a ~11-12) did not significantly alter the emission behavior and morphology of the self-assemblies. On the other hand, Zn^{2+} (pK_a ~9), Al^{3+} (pK_a ~5), and Ga^{3+} (pK_a ~3) inhibited the large fibrillar structure and led to the formation of nano-aggregates. The formation of nano-aggregates, as evident from the microscopic images, was attributed to the extensive clusterization of amino acids that took place due to dehydration and enhanced hydrophobic interaction in the presence of metal ions, particularly of lower pK_a values. The clusterization and subsequent formation of diverse nano-aggregates in presence of metal ions increased the local concentration of amino acids significantly and thus enhanced the clusteroluminescence as compared to native aggregates. We believe that the metal ion-induced inhibition of fibrillation and corresponding enhanced clusteroluminescence may help us to understand the underlying mechanism of the intrinsic blue luminescence of amyloid aggregation and the effect of metal ions on it.

2.4 References

[1] Almeida Z. L., Brito R. M. M. (2020), Structure and aggregation mechanisms in amyloids, Molecules, 25, 1195 (DOI: 10.3390/molecules25051195)

[2] Knowles T. P., Vendruscolo M., Dobson, C. M. (2014), The amyloid state and its association with protein misfolding diseases, Nat Rev Mol Cell Biol 15, 384−396 (DOI: 10.1038/nrm3810)

[3] Aguzzi A., O'Connor T. (2010), Protein aggregation diseases: pathogenicity and therapeutic perspectives, Nat Rev Drug Discovery 9, 237−248 (DOI: 10.1038/nrd3050)

[4] Zaguri D., Kreiser T., Shaham-Niv S. *et al.* (2018), Antibodies towards tyrosine amyloid like fibrils allow toxicity modulation and

cellular imaging of the assemblies, Molecules 23, 1273 (DOI: 10.3390/molecules23061273)

[5] Shaham-Niv S., Rehak P., Vuković L. *et al.* (2017), Formation of apoptosis-inducing amyloid fibrils by tryptophan, Isr J Chem 57, 729−737 (DOI: 10.1002/ijch.201600076)

[6] Adler-Abramovich L., Vaks L., Carny O., *et al.* (2012), Phenylalanine assembly into toxic fibrils suggests amyloid etiology in phenylketonuria, Nat Chem Biol 8, 701−706 (DOI: 10.1038/nchembio.1002)

[7] Banik D., Dutta R., Banerjee P. *et al.* (2016), Inhibition of fibrillar assemblies of L-phenylalanine by crown ethers: A potential approach towards phenylketonuria, J Phys Chem B 120, 7662−7670 (DOI: 10.1021/acs.jpcb.6b05209)

[8] Banik D., Kundu S., Banerjee P. (2017), Investigation of fibril forming mechanisms of L-phenylalanine and L-tyrosine: Microscopic insight toward phenylketonuria and tyrosinemia type II, J Phys Chem B 121, 1533−1543 (DOI: 10.1021/acs.jpcb.6b12220)

[9] Chakraborty S., Mukherjee S. (2021), Role of small moiety of a large ligand: Tyrosine templated copper nanoclusters, J Phys Chem Lett 12, 3266−3273 (DOI: 10.1021/acs.jpclett.1c00245)

[10] Globe C. G. (2006), Common mechanisms of amyloid oligomer pathogenesis in degenerative disease, Neurobiol Aging 27, 570−575 (DOI: 10.1016/j.neurobiolaging.2005.04.017)

[11] Lambert M. P., Barlow A. K., Chromy B. A. *et al.* (1998), Diffusible, nonfibrillar ligands derived from Abeta1−42 are potent central nervous system neurotoxins, Proc Natl Acad Sci U. S. A. 95, 6448−6453 (DOI: 10.1073/pnas.95.11.6448)

[12] Li R., Wu Z., Wangb Y. *et al.* (2016), Role of pH induced structural change in protein aggregation in foam fractionation of bovine serum albumin, Biotechnol Rep 9, 46−52 (DOI: 10.1016/j.btre.2016.01.002)

[13] Klement K., Wieligmann K., Meinhardt J. *et al.* (2007), Effect of different salt ions on the propensity of aggregation and on the structure of Alzheimer's Aβ(1−40) amyloid fibrils, J Mol Biol 373, 1321−1333 (DOI: 10.1016/j.jmb.2007.08.068)

[14] Lovell M. A., Robertson J. D., Teesdale W. J. *et al.* (1998), Copper, Iron and zinc in Alzheimer's disease senile plaques, J Neurol Sci 158, 47−52 (DOI: 10.1016/S0022-510X(98)00092-6)

[15] Yumoto S., Kakimi S., Ohsaki A. *et al.* (2009), Demonstration of aluminum in amyloid fibers in the cores of senile plaques in the brains of patients with Alzheimer's disease, J Inorg Biochem 103, 1579–1584 (DOI: 10.1016/j.jinorgbio.2009.07.023)

[16] Noy D., Solomonov I., Sinkevich O. *et al.* (2008), Zinc-amyloid β interactions on a millisecond time-scale stabilize non-fibrillar Alzheimer-related species, J Am Chem Soc 130, 1376−1383 (DOI: 10.1021/ja076282l)

[17] Ha C., Ryu J., Park C. B. (2007), Metal ions differentially influence the aggregation and deposition of Alzheimer's β-amyloid on a solid template, Biochemistry 46, 6118−6125 (DOI: 10.1021/bi7000032)

[18] Ye X., Capezza A., Xiao X. *et al.* (2021), Protein nanofibrils and their hydrogel formation with metal ions, ACS Nano 15, 3, 5341–5354 (DOI: 10.1021/acsnano.0c10893)

[19] Shaham-Niv S., Arnon Z. A., Sade D. *et al.* (2018), Intrinsic fluorescence of metabolite amyloids allows label-free monitoring of their formation and dynamics in live cells, Angew Chem Int Ed 57, 12444−1244 (DOI: 10.1002/anie.201806565)

[20] Wang R., Yuan W., Zhu X. (2015), Aggregation-induced emission of non-conjugated poly(amido amine)s: Discovering, luminescent mechanism understanding and bioapplication, Chin J Polym Sci 33, 680−687 (DOI: 10.1007/s10118-015-1635-x)

[21] Wu, Liu Y., He, *et al.* (2005), Blue photoluminescence from hyperbranched poly(amino ester)s, Macromolecules 38, 9906−9909 (DOI: 10.1021/ma051407x)

[22] Wang D., Imae T., Miki M. (2007), Fluorescence emission from PAMAM and PPI dendrimers, J. Colloid Interface Sci 306, 222−227 (DOI: 10.1016/j.jcis.2006.10.025)

[23] Lin Y., Gao J., Liu H. *et al.* (2009), Synthesis and characterization of hyperbranched poly(ether amide)s with thermoresponsive property and unexpected strong blue photoluminescence, Macromolecules 42, 3237−3246 (DOI: 10.1021/ma802353f)

[24] Jayamurugan G., Umesh C. P., Jayaraman N. (2008), Inherent photoluminescence properties of poly(propyl ether imine) dendrimers, Org Lett 10, 9−12 (DOI: 10.1021/ol702635w)

[25] Luo J. D., Xie Z. L., Lam J. W. Y. *et al.* (2001), Aggregation-induced emission of 1-methyl-1,2,3,4,5-pentaphenylsilole, Chem Commun 18, 1740−1741 (DOI: 10.1039/b105159h)

[26] Zhang Yuan W., Zhang Y. (2017), Nonconventional macromolecular luminogens with aggregation-induced emission characteristics, J Polym Sci. Part A: Polym Chem 55, 560−574 (DOI: 10.1002/pola.28420)

[27] Wang Q., Dou X., Chen X. *et al.* (2019), Reevaluating protein photoluminescence: Remarkable visible luminescence upon concentration and insight into the emission mechanism, Angew Chem Int. Ed 58, 12667−12673 (DOI: 10.1002/anie.201906226)

[28] De S. K., Maity A., Chakraborty A. (2021), Underlying mechanisms for the modulation of self-assembly and the intrinsic fluorescent properties of amino acid-functionalized gold nanoparticles, Langmuir 37, 5022–5033 (DOI: 10.1021/acs.langmuir.1c00431)

[29] Faller P., Hureau C., Berthoumieu O. (2013), Role of metal ions in the self-assembly of the Alzheimer's amyloid-β peptide, Inorg Chem 52, 12193−12206 (DOI: 10.1021/ic4003059)

[30] Lee M., Kim J. I., Na S. *et al.* (2018), Metal ions affect the formation and stability of amyloid β aggregates at multiple length scales, Phys Chem Chem Phys 20, 8951−8961 (DOI: 10.1039/C7CP05072K)

[31] He B., Zhang J., Zhang J. *et al.* (2021), Clusteroluminescence from cluster excitons in small heterocyclics free of aromatic rings, Adv Sci 8, 2004299 (DOI: 10.1002/advs.202004299)

[32] Zheng S., Zhu T., Wang Y. *et al.* (2020), Accessing tunable afterglows from highly twisted nonaromatic organic AIEgens via effective through space conjugation, Angew Chem Int Ed 59, 10018−10022 (DOI: 10.1002/anie.202000655)

[33] Hawkes S. J. (1996), All positive ions give acid solutions in water, J Chem Educ 73, 516517 (DOI: 10.1021/ed073p516)

[34] Tomar D., Chaudhary S., Jena K. C. (2019), Self-assembly of L-phenylalanine amino acid: Electrostatic induced hindrance of fibril formation, RSC Adv 9, 12596−12605 (DOI: 10.1039/C9RA00268E)

[35] Wang Z., Li H., Tang F. *et al.* (2018), A facile approach for the preparation of nano-size zinc oxide in water/glycerol with extremely concentrated zinc sources, Nanoscale Res Lett 13, 1−9 (DOI: 10.1186/s11671-018-2616-0)

[36] Levine H. (1993), Thioflavine T interaction with synthetic Alzheimer's disease β-amyloid peptides: Detection of amyloid aggregation in solution, Protein Sci 2, 404−410 (DOI: 10.1002/pro.5560020312)

[37] Chen W.-T., Liao Y.-H., Yu H.-M. *et al.* (2011), Distinct effects of Zn^{2+}, Cu^{2+}, Fe^{3+}, and Al^{3+} on amyloid-β stability, oligomerization, and aggregation, J Biol Chem 286, 9646−9656 (DOI: 10.1074/jbc.M110.177246)

[38] Do T. D., LaPointe N. E., Economou N. J. *et al.* (2013), Effects of pH and charge state on peptide assembly: The YVIFL model system, J Phys Chem B 117, 10759−10768 (DOI: 10.1021/jp406066d)

[39] Ji W., Yuan C., Zilberzwige-Tal S. *et al.* (2019), Metal-ion modulated structural transformation of amyloid-like dipeptide supramolecular self assembly, ACS Nano 13, 7300−7309 (DOI: 10.1021/acsnano.9b03444)

[40] Liu J., Feng J., Yu Y. *et al.* (2020), Fabrication of a luminescent supramolecular hydrogel based on the AIE strategy of gold nanoclusters and their application as a luminescence switch, J Phys Chem C 124, 23844−23851 (DOI: 10.1021/acs.jpcc.0c07198)

[41] Shen J., Xiao Q., Sun P. *et al.* (2021), Self-assembled chiral phosphorescent microflowers from Au nanoclusters with dual-mode pH sensing and information encryption, ACS Nano 15, 4947−4955 (DOI: 10.1021/acsnano.0c09766)

[42] Zhang Y., Feng, N., Zhou S. *et al.* (2021), Fluorescent nanocomposites based on gold nanoclusters for metal ion detection and white light emitting diodes, Nanoscale 13, 4140−4150 (DOI: 10.1039/D0NR09141C)

[43] Fan Z., Sun L., Huang Y. *et al.* (2016), Bioinspired fluorescent dipeptide nanoparticles for targeted cancer cell imaging and real-time monitoring of drug release, Nat Nanotechnol 11, 388−394 (DOI: 10.1038/nnano.2015.312)

[44] Tao K., Fan Z., Sun L. *et al.* (2018), Quantum confined peptide assemblies with tunable visible to near-infrared spectral range. Nat Commun 9, 3217 (DOI: 10.1038/s41467-018-05568-9)

Chapter 3

Metal-Ion-Induced Evolution of Phenylalanine Self-Assembly: Structural Polymorphism of Novel Metastable Intermediates

3.1 Introduction

The biomolecular self-assembly, especially the self-assembly of proteins *[1-3]* and peptides *[4-6]* has attracted immensely due to their ability to form various nanostructures that are vital in different essential cellular functions *[7-13]*. However, their uncontrolled aggregation can lead to the formation of amyloid fibrillar structures, which are associated with several devastating neurodegenerative diseases like Alzheimer's disease, type II diabetes, Parkinson's disease, and many more *[14-19]*. In this context, the self-assembly of amino acids could be of high interest as they serve as the basic building block of proteins and peptides. Among all the amino acids, aromatic amino acids, especially Phenylalanine (Phe), play a key role in the formation of the amyloid fibrillar structure *[20,21]*. This is due to its higher intrinsic propensity to promote the formation of amyloid aggregates as compared to the aliphatic analogs *[21]*. The time and temperature-dependent aggregates of Phe can modulate the lipid membrane dynamics noticeably, as reported by Banerjee and co-workers *[22]*. These findings paved the way to investigate the self-assembly of Phe-based peptides *[23-30]* due to their ability to form well-ordered structures with diverse polymorphisms like toroids, ellipsoids, spheres, nanotubes, and so on *[31-34]*. As discussed above, the studies on the morphological transformations of Phe-based di- and tripeptide assemblies are well-established. However, similar studies on naturally occurring amino acids are not yet available, even though simple aromatic amino acids can form

amyloid-like self-assembled structures *[35-38]*. Additionally, the peptides employed for research are usually either N-terminally *[39-41]* or C-terminally *[42-43]* capped with protecting groups. The capping facilitates the self-assembly process's kinetically rapid and thermodynamically rigid manner, resulting in highly ordered architectures *[44]*. In this context, the self-assembly process of protected amino acids has also been recently explored *[45,46]*. However, the sequential changes in the morphology of the intermediates of amino acids during the self-assembly process in an aqueous medium are yet to be reported.

Specifically, capturing the morphology of the intermediates formed through early-stage nucleation in the aqueous medium has been the most crucial challenge with a few attempts so far *[47,48]*. This is probably due to the very fast fibrillation kinetics that result in the rapid transformation of intermediate states. So, it is essential to inhibit the fast kinetics to capture tangible images of intermediates. Recently, Yan and co-workers reported that the supramolecular nanofibrils of protected amino acids and dipeptides in the aqueous medium proceed through droplet formation *[49]*. The solute-rich metastable droplets act as nucleation precursors to produce thermodynamically stable nanofibrils. Remarkably, several metal ions also enhance the hydrophobic interaction within the medium *[50,51]*. Our earlier publication suggests that several metal ions of high charge-to-radius ratio (i.e. Zn^{2+}, Al^{3+}, Ga^{3+}, In^{3+}, and Sn^{4+}) can induce the formation of non-fibrillar oligomeric aggregates of aromatic amino acids *[52]*. This observation, however, raised the possibility of whether these metal ions could stabilize the intermediate states by enhancing different non-covalent interactions. Notably, these metal ions are known to extract water molecules. Thus, the expulsion of water molecules increases the entropy of the system *[53]*. Therefore, these metal ions could stabilize any entropy-driven intermediate states. So, in the present paper, we plan to investigate the self-assembly process of naturally occurring simple aromatic amino acid, phenylalanine, devoid of any protecting group, in the presence of

categorically chosen different divalent (Zn^{2+}, Cd^{2+}, and Hg^{2+}) and trivalent (Al^{3+}, Ga^{3+}, and In^{3+}) metal ions with a wide variety in their pK_a values (**Table 3.1**). We anticipated that these metal ions might stabilize the intermediate states by inducing hydrophobic interaction in the system during the self-assembly process. We have employed Confocal Laser Scanning Microscopy (CLSM) and Field Emission Scanning Electron Microscopy (FESEM) imaging in a time-dependent fashion to capture the development of the assembly formation from the beginning i.e., the monomeric state of amino acid till the supramolecular assembly completes. For the first time, we report the sequential formation of different nanostructures, e.g., from microsphere to toroid to fibril of Phe-assembly in the aqueous medium. It is worth mentioning that toroid and related nanostructures available in the literature were obtained by changing the concentration of Phe-based peptides and the solvent composition of polar and non-polar solvents *[31,33]*. We believe that our study here on the metal ion-induced formation of metastable states could provide a deep insight into the plethora of amino acid-based self-assembled structures and their potential wide applications in the fields of bioimaging, drug delivery, tissue engineering, biocatalysis, etc.

Metal	**Zn^{2+}**	**Cd^{2+}**	**Hg^{2+}**	**Al^{3+}**	**Ga^{3+}**	**In^{3+}**
Size (pm)	74	92	83	68	76	94
pK_a	9	10.1	3.4	5	2.6	4

Table 3.1 *Metal ions used in our study and their respective size and pK_a values*

3.2 Results and Discussion

3.2.1 Investigation of the Morphological Transformation of Blank Phe during the Self-assembly process using CLSM:

We mentioned earlier that the stability of the metastable state largely depends on the hydrophobic interaction of the amino acid. Therefore, we induced hydrophobicity in the systems by introducing metal ions to

observe the different metastable states. To eliminate any pre-existing aggregate, the Phe solution was heated to 90 °C to achieve the

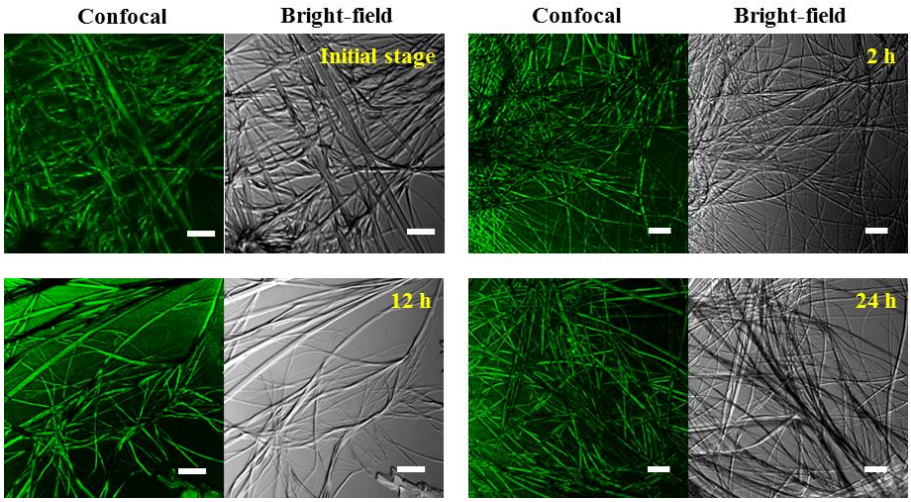

Figure 3.1 *Time-dependent CLSM (left panel) and bright-field (right panel) images of the control system (blank A_{Phe}), which showcases the absence of any intermediates; Scale bar 10 µm.*

monomeric state of the amino acid. Then, we added salts to the monomeric solution and performed the time-dependent microscopic imaging (CLSM and SEM) techniques to gain insight into the morphological changes. For the CLSM technique, we used Thioflavin T (ThT), a well-known fluorescence marker for the self-assembled fibrillar structure *[54]*, to unravel the structural evolution from metastable to stable fibril formation. It was observed that the blank A_{Phe}, in the absence of any metal ion (i.e., the control system), develops the fibrillar structure at the very initial stage. We could not capture any intermediate nanostructures for A_{Phe} (i.e., the control system) as fibrillar structures were observed from the initial stage. The observation implies the rapid transformation of the monomeric Phe to the fibrillar structure through very fast kinetics, rendering it difficult to capture the intermediates (**Figure 3.1**). Therefore, to investigate whether the different metal ions influence the fibrillation process, we first investigated the effect of different divalent metal (M^{2+}) ions, including Zn^{2+}, Cd^{2+}, and Hg^{2+}, on the self-assembled fibrillation process. It is important to mention that these metal ions belong to the same series and

are known to increase entropy by coordinating with the amino acid *[55,56]*.

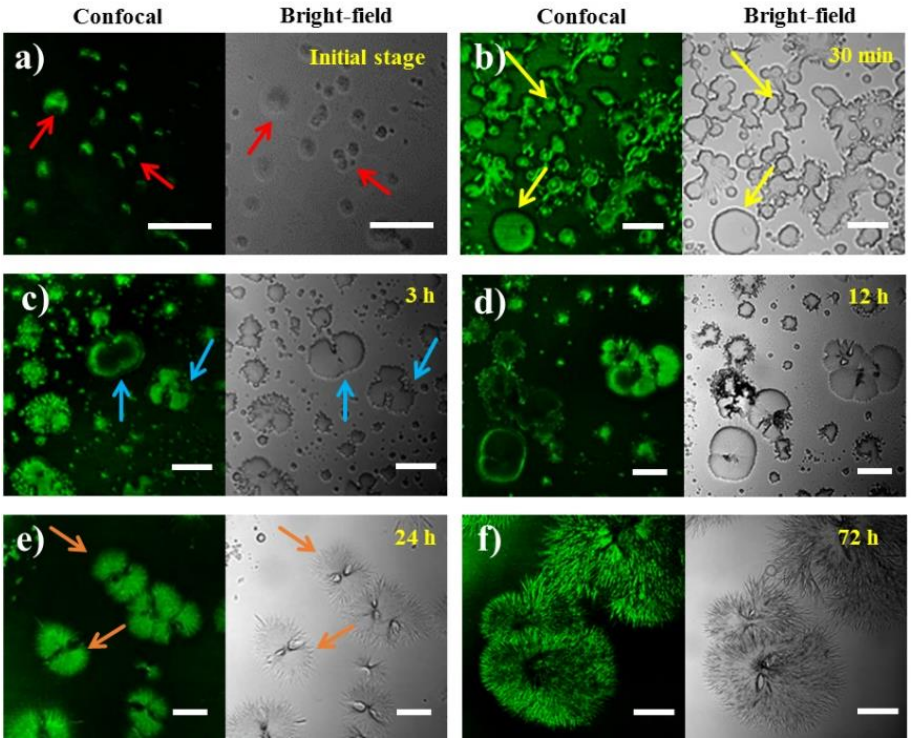

Figure 3.2 *Time-dependent CLSM (left panel) and bright-field (right panel) images of* A_{Phe}/Zn^{2+}*: a) microspheres at the initial stage, b) vesicle structures at 30 min, c) larger vesicles formation at 3 h, d) spike-like fibrils from the edges at 12 h, e) fibrillar growth in dendritic fashion at 24 h, f) formation of matured fibrils at 72 h; Scale bar 10 µm.*

3.2.2 Effect of Divalent Metal Ions on the Time-dependent Morphological Transformation of Phenylalanine Self-assembly:

In the cases of all A_{Phe}/M^{2+} systems, the monomeric Phe rapidly generated microspheres, followed by the subsequent fusion of these microspheres to vesicular structure, which further transformed into mature fibrils over time. At the initial stages of the assembly formation, orderly small aggregated structures were observed (**Figure 3.2a, 3.3a, 3.4a**; red arrows) that subsided over time due to coalescence and subsequent formation of other random intermediate structures. The formation of amino acid-rich microspheres is associated with the clusterization of amino acids at the early stages induced by the enhanced hydrophobic interaction, which is absent in the case of blank Phe. The solid microspheres transformed into larger spheres and finally into

vesicle-like structures (**Figure 3.2b** (yellow arrow), **3.3b** (blue arrow), and **3.4b**) in a time-dependent manner. The absence of signals from the very core of the structure (**Figure 3.3b**) could be because the amino acids assembled in the interfacial region and away from the core to form fibrillar structures, leaving the core

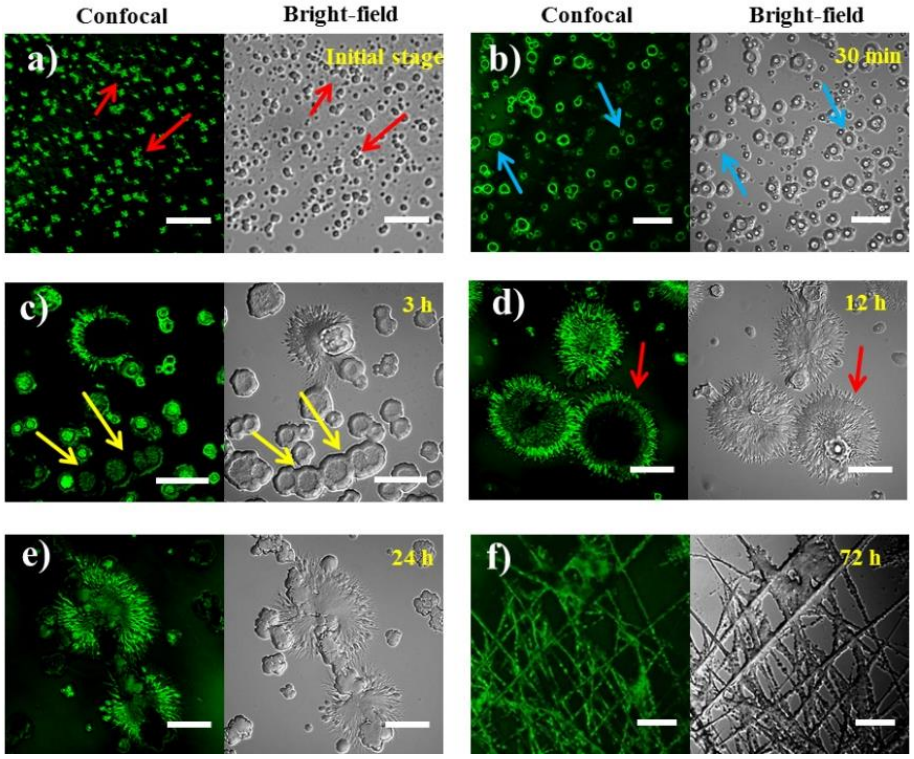

Figure 3.3 *Time-dependent CLSM (left panel) and bright-field (right panel) images of* A_{Phe}/Cd^{2+}*: a) microspheres at the initial stage, b) ring-like vesicles structures at 30 min, c) chains and fibrillar growth at 3 h, d) flower-like structures at 12 h, e) small rings to large fibrillar network transformation at 24 h, f) formation of matured fibrils; Scale bar 10 µm.*

unrecognized by ThT. In the next stage, the vesicle-like structures started to fuse (**Figure 3.2c** (blue arrow), **3.3c** (yellow arrows)) and formed larger vesicles that imitate the well-known cellular membrane-like entities (**Figure 3.3d**). We observed the generation of fibrillar structures from the edge of the vesicles (**Figure 3.2d, 3.3d**) after 12 hrs depicting the nucleation site for the amino acid clusters, which transformed into mature fibrils (**Figure 3.2e, f, and 3.3e**). The spike-

like fibrillar structures that emerged from the edges of the spherical structures were found to be more prominent in the later stages.

The coexistence of the metastable state along with the matured fibrillar structure is somehow different for different divalent metal ions. In the case of the A_{Phe}/Zn^{2+} system, the fibrils expanded in a specific

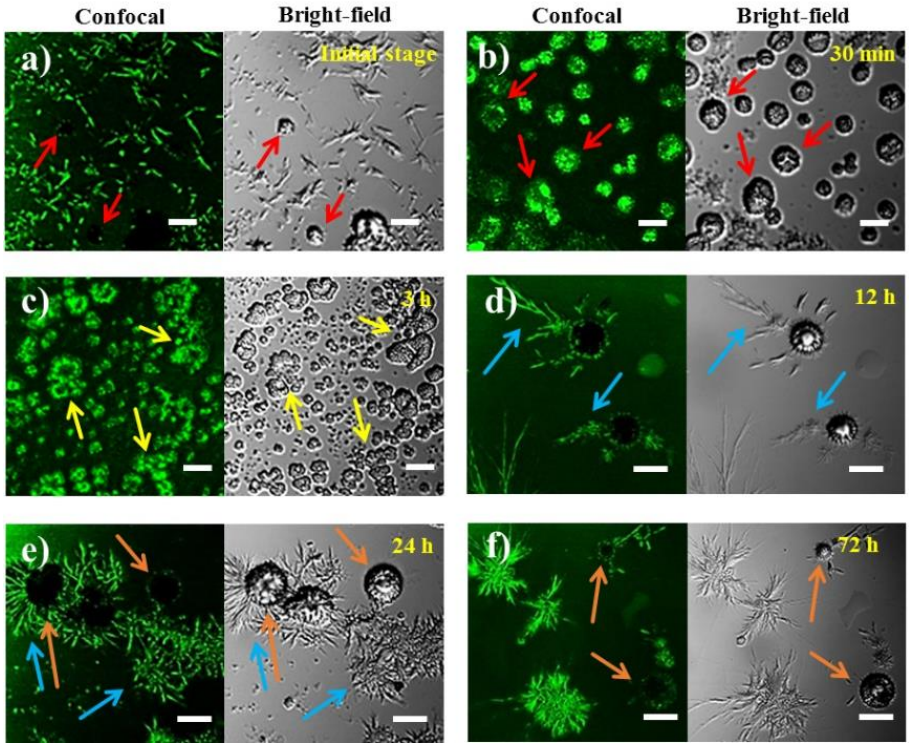

Figure 3.4 *Time-dependent CLSM (left panel) and bright-field (right panel) images of* A_{Phe}/Hg^{2+}*: a) formation of spheres at the initial stage, b) larger spherical structures at 30 min, c) further fusion at 3 h, d) formation of fibrils from the edges obtained at 12 h, e) more fibrillar growth along with the spheres at 24 h, f) formation of matured fibrils at 72 h; the existence of spherical structures (orange arrows) even at 72 h implies higher order of stability of the spheres; Scale bar 10 µm.*

orientation where the fibrillary growth was observed to take place in a dendritic fashion, sharing a common center between two distinct fibrillar structures (**Figure 3.2e** (orange arrow)). However, for the A_{Phe}/Cd^{2+} system, we observed very prominent vesicle-like structures (**Figure 3.3c**), which eventually transformed into rod-like morphology, diminishing the vesicular structure (**Figure 3.3f**). Interestingly, in the case of Hg^{2+}, we found the initially formed spherical entities to sustain over time, and vesicle structures could be observed at the final stages of

structural evolution (**Figure 3.4**). This suggests the better stability of the spherical structures in the A_{Phe}/Hg^{2+} system than the A_{Phe}/Zn^{2+} and A_{Phe}/Cd^{2+} systems. The presence of low-shielding 5d electrons increases the effective nuclear charge of Hg^{2+}, resulting in a strong covalent and static polarizability that can induce an alteration in the metal-amino acid interaction *[55]*. So, a different and unique coordination nature for Hg^{2+} is observed compared to Zn^{2+} and Cd^{2+}. Thus, the strong chelating properties of Hg^{2+} ions and specific interactions with the amino acid, compared to Cd^{2+} and Zn^{2+}, may enhance the stability of the metastable state and direct the structural assembly.

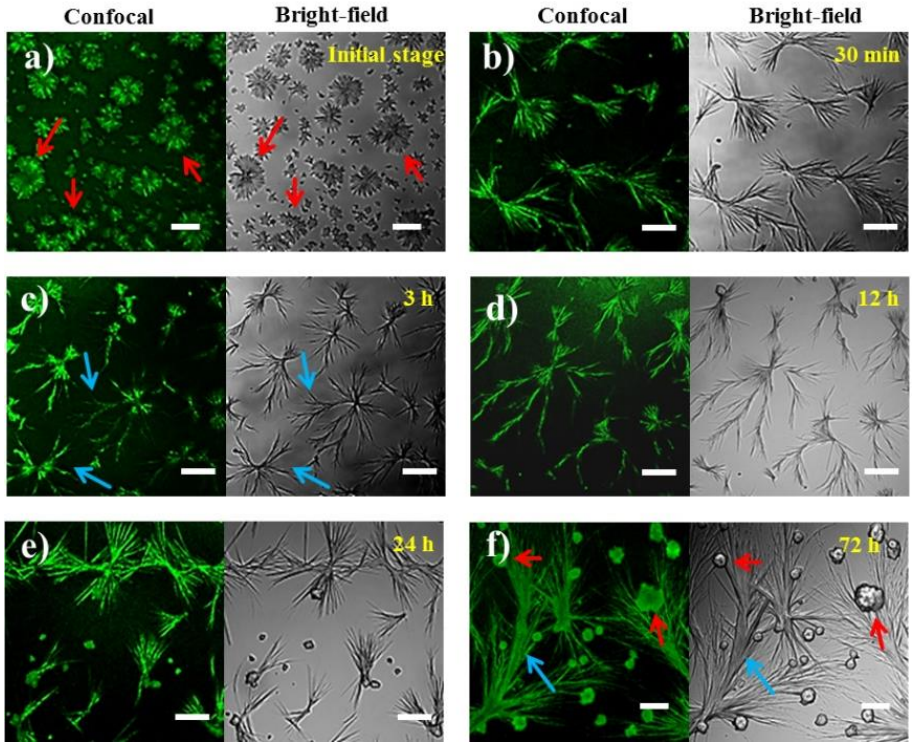

Figure 3.5 *Time-dependent CLSM (left panel) and bright-field (right panel) images of A_{Phe}/Al^{3+}: a) formation of nanoclusters and nanoflowers at the initial stage, b) generation of fibrous structures at 30 min, c) formation of fibrillar networks, d)-e) more fibrillar networks with time, f) blue arrows indicate the fibrillar structures, whereas red arrows show the existence of spherical structures even at 72 h; Scale bar 10 µm.*

3.2.3 Effect of Trivalent Metal Ions on the Time-dependent Morphological Transformation of Phenylalanine Self-assembly:

As the divalent metal ions provide important pieces of evidence for the formation of spherical metastable intermediates, this further encouraged us to investigate the impact of charge and size of trivalent metal ions on the self-assembly process of Phe using a series of trivalent metal ions, namely, Al^{3+}, Ga^{3+} and In^{3+} of the same group to get a distinct view of whether the size and effective charge of metal ions exert any influences on the self-assembly process. For the A_{Phe}/Al^{3+} system, smaller nano-aggregates along with some uniform nano-fibrillar structures initially, reminiscent of nanoflower-like

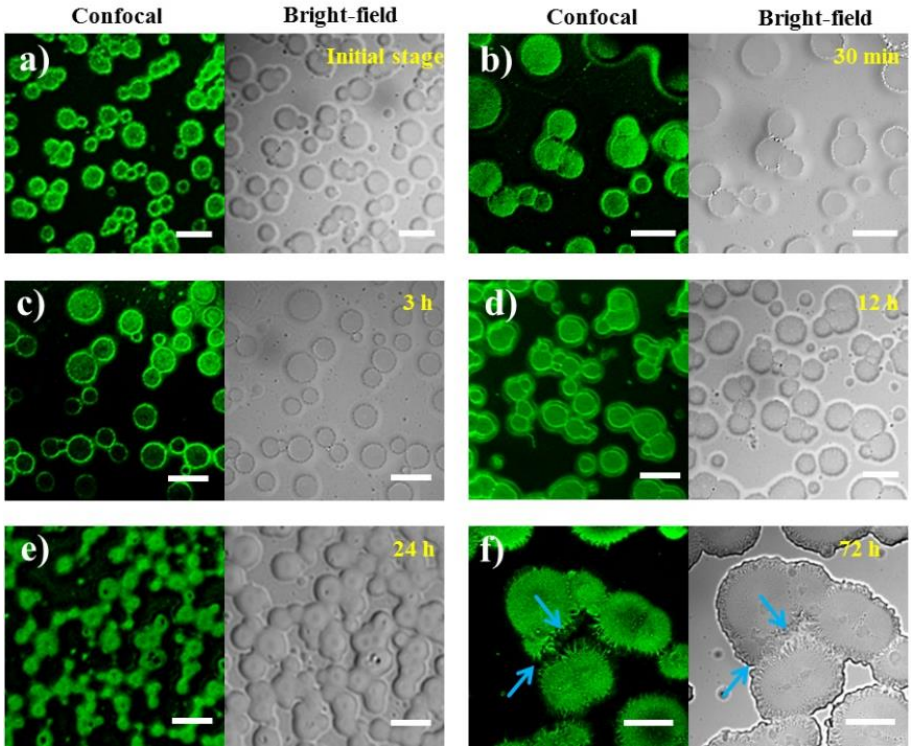

Figure 3.6 *Time-dependent CLSM (left panel) and bright-field (right panel) images of A_{Phe}/Ga^{3+}: a) spherical structures at the initial stage, b-d) fusion of the structures, e) formation of fused patchy clamps at 24 h, f) spike-like fibrils piercing through the fused patches at 72 h; Scale bar 10 µm.*

morphologies were observed (**Figure 3.5a** (red arrow)). The coexistence of both non-fibrillar spherical entities and nano-fibrillar structures implies the rapid transformation between the different morphologies in the systems. The as-obtained nanoflower structures elongated in a time-

dependent fashion to produce longer fibrils with a well-ordered network that started transforming (**Figure 3.5c** (blue arrow)) into matured fibrils. Along with matured fibrils (**Figure 3.5f** (blue arrow)), interestingly, the occurrence of spherical structures (**Figure 3.5f** (red arrow)) was observed, which is quite similar to that of in A_{Phe}/Hg^{2+} system indicating higher order of stability of the microspheres. For another trivalent metal ion, Ga^{3+}, we observed only homogeneous spherical structures generated from the very beginning (**Figure 3.6a**) of the assembly formation. And these metastable vesicles

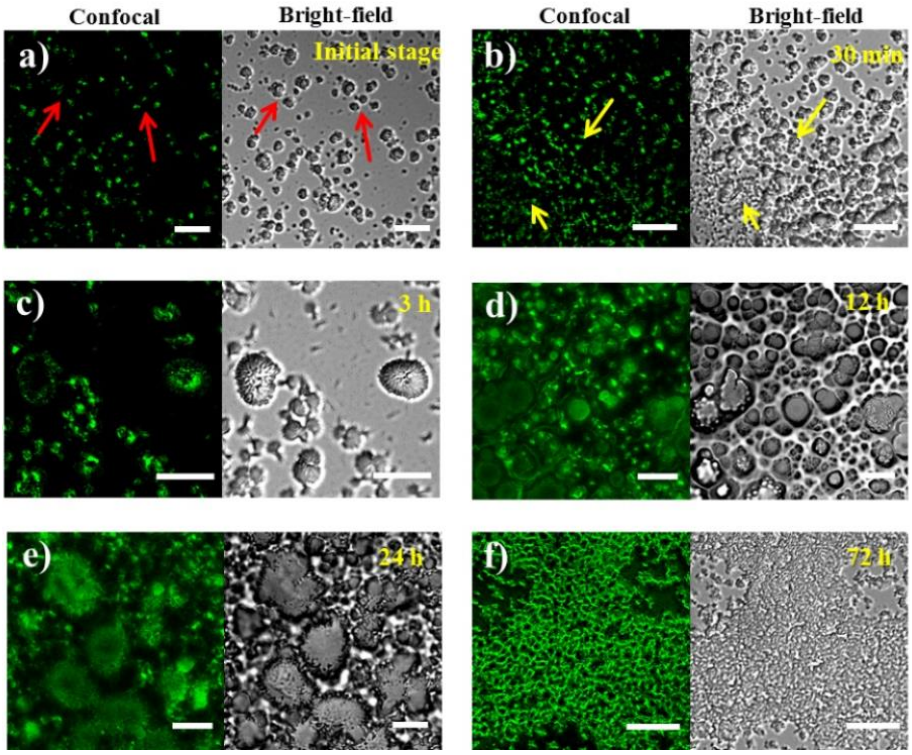

Figure 3.7 *Time-dependent CLSM (left panel) and bright-field (right panel) images of* A_{Phe}/In^{3+}*: a) red arrows indicate the formation of nanoclusters at the initial stage, b) yellow arrows show the fusion of clusters to produce spherical structures at 30 min, c-e) fusion into the formation of patchy spheres, f) formation of nanofibrils at 72 h; Scale bar 10 µm.*

were found to sustain even after 3 hrs (**Figure 3.6c**). The size of these vesicle structures is ~ 4-5 µm, which is higher than A_{Phe}/M^{2+} systems at 30 min of the self-assembly process (**Figure 3.6b**). The higher stability of the spherical structures formed in the A_{Phe}/Ga^{3+} system is attributed to the higher order of hydrophobicity induced by Ga^{3+}.

Moreover, these larger vesicles may have higher stability against fusion due to lower surface curvature. However, we found these spheres to coalesce, producing patchy clumps after 24 hrs (**Figure 3.6e**), and we could witness the presence of spike-like fibrils piercing through the spheres at 72 hrs (**Figure 3.6f** (blue arrow)). As observed in the images, the fused spheres were connected through these fibrils. In the presence of another trivalent ion, In^{3+}, we observed the existence of small nanoclusters at the initial stages (**Figure 3.7a** (red arrow)) that fused sequentially to obtain larger spherical structures (**Figure 3.7b** (yellow arrow)). The microspheres of the A_{Phe}/In^{3+} system seem to possess more patchy clumps than A_{Phe}/Ga^{3+} (**Figure 3.7e**), indicating a higher tendency of the spheres to undergo fusion. The fused structures took a much longer time compared to other systems to transform into the nano-fibrillar network.

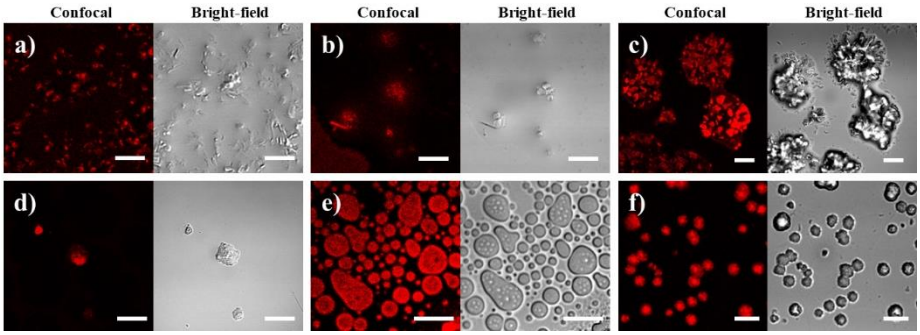

Figure 3.8 *Confocal laser scanning microscopy images of Nile Red incorporated A_{Phe} assemblies, in the presence of a) Zn^{2+}, b) Cd^{2+}, c) Hg^{2+}, d) Al^{3+}, e) Ga^{3+}, and f) In^{3+} at the initial state of the assembly formation; Scale bar 10 µm.*

To gain further insights into the formation of the early-stage metastable state, we investigated the CLSM images at different stages of the assembly formation using another dye, namely Nile red. The Nile red is used to unravel the morphological transformation that occurs due to the hydrophobic interaction *[57]*. In the early stages, strong fluorescence signals were obtained from the tiny spherical aggregates of all the metal-amino acid systems. However, the signal was much more prominent for Ga^{3+} and In^{3+} (**Figure 3.8e, f**) revealing that the initial spherical structures were stabilized by hydrophobic interactions. The structures obtained from the images of A_{Phe}/Ga^{3+} looked like droplets, which

corroborate well with that reported by Yan and co-workers *[49]*. With time-lapse, the signals became weaker and it was almost difficult to obtain any signals from the structures formed in the later stage of the self-assembly process indicating other non-covalent interactions, such as π-π stacking, hydrogen bonding etc. to be more dominant over hydrophobic interaction in the course of formation of assembly (**Figure 3.9**).

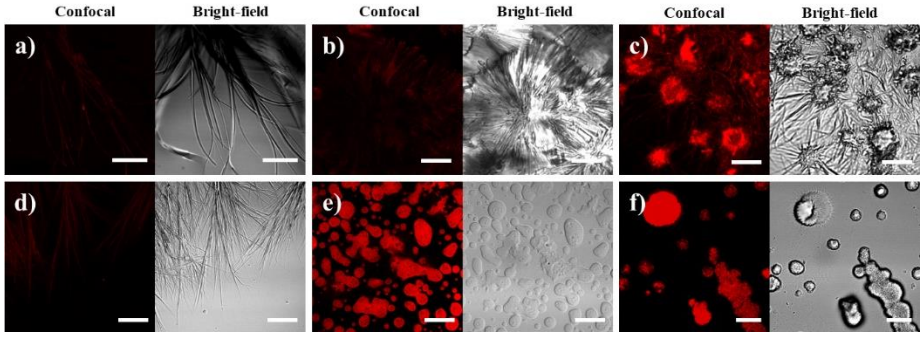

Figure 3.9 *Confocal laser scanning microscopy images of Nile Red incorporated A_{Phe} assemblies in the presence of a) Zn^{2+}, b) Cd^{2+}, c) Hg^{2+}, d) Al^{3+}, e) Ga^{3+}, and f) In^{3+} at the later stage of the assembly formation; Scale bar 10 µm.*

3.2.4 Investigation of the Structural Transformation using FESEM:

Although the CLSM images revealed the time evolution development of morphologies and droplet formation. However, the limitation of CLSM techniques is that it only illuminates the signal from fluorescent dye, necessitating additional morphological examination. Therefore, we employed the FESEM imaging technology to focus on the metastable states developed during the morphological evolution of metal-Phe complexes to mature fibrils. It was observed that the A_{Phe}/Zn^{2+} system developed homogeneously spherical structures at the beginning (**Figure 3.10a**). The formation of solid spheres may be associated with initial hydrophobic interaction induced by the metal-amino acid coordination. With increasing time, other molecular interactions, such as hydrogen bonding, π- π stacking etc., dominate over hydrophobic interaction. As a result, structural evolution from spheres to the semi-fused vesicle-like structure was observed after 3 hrs (**Figure 3.10b**). We found that the vesicle structure has a close resemblance to the toroid structure. Along

with this transformation, the generation of spike-like fibrillar entities was observed from the surface as well as within the vesicles. The vesicles fused further to form a network of vesicular structures connected through the fibrils. After 24 hrs, these networks became more prominent and the formation of nanofibrils can be witnessed within the structures (**Figure 3.10c**), which clearly indicates the initial solid spheres to be the nucleation centres for the amino acid that transforms into fibrillar structures.

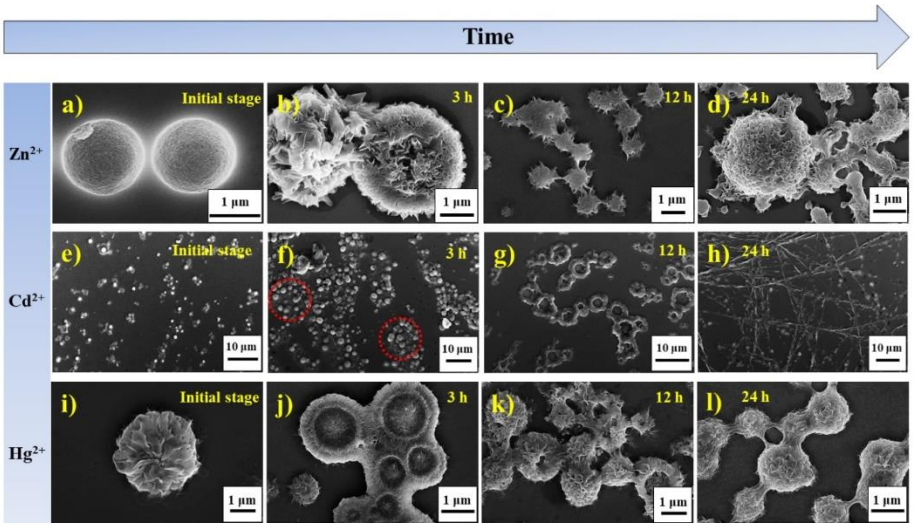

Figure 3.10 *Time-dependent morphological evolution of A_{Phe}/Zn^{2+} (a-d), A_{Phe}/Cd^{2+} (e-h), A_{Phe}/Hg^{2+} (i-l) observed using FESEM imaging technique at initial stage (a, e, i), at 3 h (b, f, j), at 12 h (c, g, k) and after formation of mature fibril at 24 h (d, h, l).*

For the A_{Phe}/Cd^{2+} system (**Figure 3.10e-h**) the microspheres (**Figure 3.10e**) were not as homogeneously spherical as we observed for the A_{Phe}/Zn^{2+} system. These microspheres then clustered together, as shown by the red circle (**Figure 3.10f**). These clustered structures were further transformed into a well-known toroid structure with time (**Figure 3.10g**). Earlier works reported the formation of toroidal structures in the case of dipeptides and tripeptides by varying the solvent composition *[32,58]*. To the best of our knowledge, this is the first direct observation of the toroidal structures formed by amino acids in aqueous medium as one of the meta-stable states. The studies on several peptides and polymers indicated that the formation of rod-like structures at the early stages, which attains half-toroid or banana-like shape, eventually

transforms into toroids through end-to-end cyclization *[59]*. Our study not only provides the very first evidence of toroid formation in the case of phenylalanine in aqueous medium but rather indicates a different mechanism for the structural evolution of the toroids. The images (**Figure 3.10g, h**) reveal that with increasing time, these toroids tended to form a chain-like network, which fused further to the formation of matured fibrils. Interestingly, we also observed lump-like structures along the fibrils,

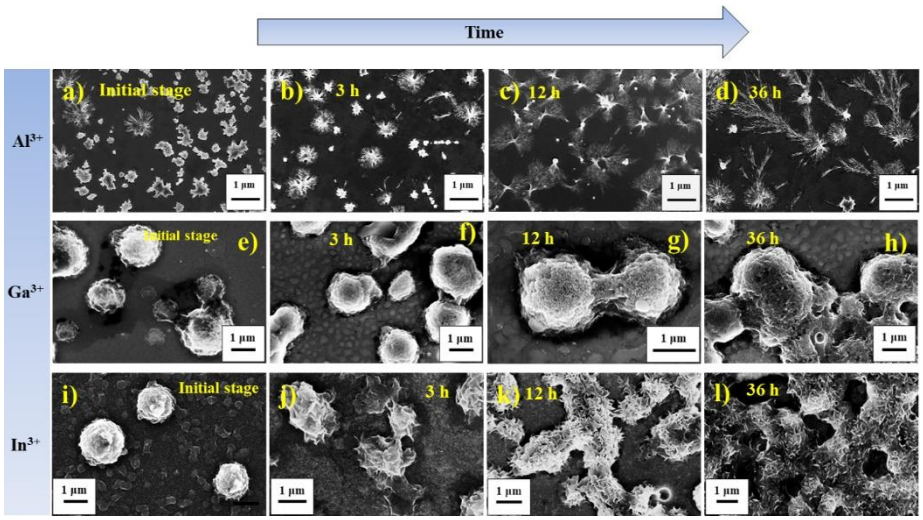

Figure 3.11 *Time-dependent morphological evolution of A_{Phe}/Al^{3+} (a-d), A_{Phe}/Ga^{3+} (e-h), A_{Phe}/In^{3+} (i-l) observed using FESEM imaging technique at initial stage (a, e, i), at 3 h (b, f, j), at 12 h (c, g, k) and at 36 h (d, h, l).*

indicating that the linked toroid chains may act as nucleation sites for the fibrils (**Figure 3.10h**). Although the A_{Phe}/Hg^{2+} system followed morphological changes (**Figure 3.10i-l**) similar to those of the A_{Phe}/Cd^{2+} system, the toroid formation and subsequent fusion were notably more prominent in the former system. The toroids were found to be interconnected by nanofibrils that were generated around the microsphere discussed earlier. This is attributed to the fact that Hg^{2+} forms a stronger complex with amino acids compared to Cd^{2+}.

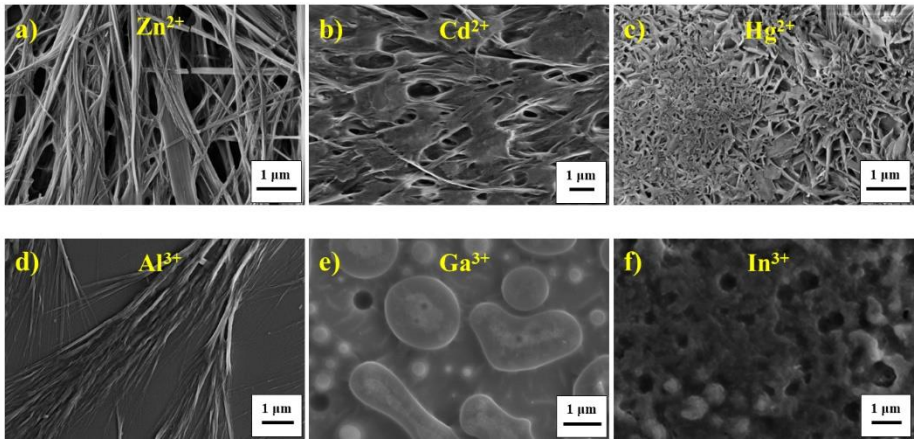

Figure 3.12 *FESEM images of A_{Phe} in the presence of Zn^{2+} (a), Cd^{2+} (b), Hg^{2+} (c), Al^{3+} (d), Ga^{3+} (e), and In^{3+} (f), respectively, at 120 h.*

Alteration in metal ions enabled the formation of metastable microstructures with completely different morphologies, as reflected in the present study. For example, the A_{Phe}/Al^{3+} system generated different morphology (**Figure 3.11a-d**) in the intermediate stage from A_{Phe}/Ga^{3+} (**Figure 3.11e-h**) and A_{Phe}/In^{3+} (**Figure 3.11i-l**). In the first scenario, i.e., for the A_{Phe}/Al^{3+} system, we observed a flower-like morphology (**Figure 3.11a**), which is in accordance with the result

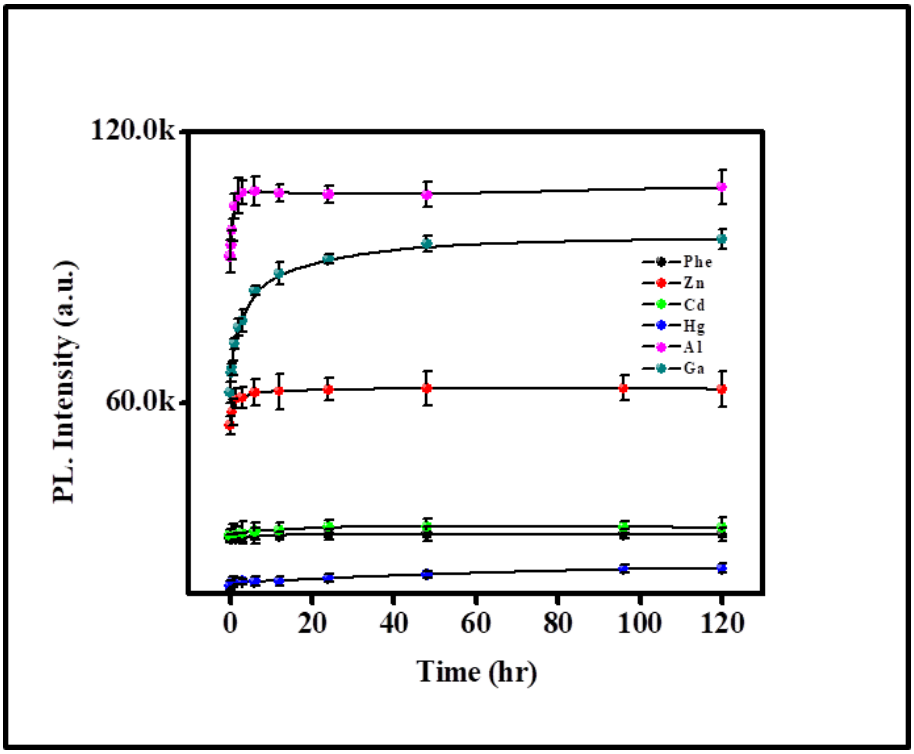

Figure 3.13 *Time-dependent fluorescence intensity curve during the structural evolution for A_{Phe} system (with and without different metal ions)*

obtained from CLSM images. On the other hand, in the latter cases, very stable microspheres (**Figure 3.11e**) and vesicle-like structures (**Figure 3.11i**) were found, which could sustain for a much longer period due to the slower nucleation rate than other systems studied in this work. Remarkably, even at 120 hrs, we could observe the presence of non-fibrillar spherical or vesicular structures for Ga^{3+} and In^{3+} incorporated systems (**Figure 3.12e, f**), whereas matured fibrils can be obtained for the rest of the cases (**Figure 3.12a-d**) studied here. In the absence of metal ions, the self-assembly process of A_{Phe} is so rapid that capturing the metastable states by imaging techniques is quite challenging. The metal ions can drastically slow down the assembly process. This enables the metastable spheres or vesicles to gain stability due to hydrophobic interactions induced by the metal ions *[49]*. The formation of compact

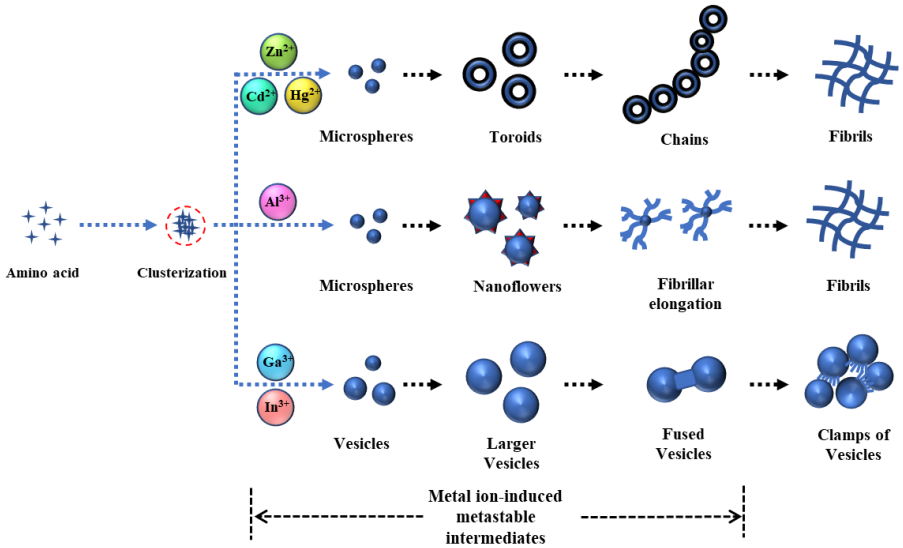

Scheme 3.1 *Evolution of the self-assembly of phenylalanine in the presence of various divalent and trivalent metal ions.*

microspheres in the initial stages takes place due to the dehydration of the amino acid nanoclusters driven by hydrophobic Phe···Phe interaction, which is primarily dominated by side-chain aromatic ring···aromatic ring interaction and is much stronger than Phe···solvent interaction *[33]*. The process is favored by entropy, which is likely to originate from the expulsion of water from the liquid droplets and microspheres. Since compact packing decreases the conformational

degrees of freedom, such an entropy-driven process must be governed by metal ion coordination, and the resultant removal of water is the major driving force for the formation of metastable intermediates *[49]*. However, with time, in the case of divalent metal ions, the Phe···solvent interaction dominates, which results in the transformation from a microsphere to a hollow (toroid) structure [33]. This process should be entropically unfavorable as interaction with solvent molecules increases. However, it is facilitated by the fibrillar growth around the microsphere. In the case of A_{Phe}/M^{2+}, the toroids undergo fusion to form the matured fibrils for a longer time. On the other hand, for trivalent metal ions, because of very high hydrophobic interaction, the microspheres could sustain a long time and were found to be interconnected before forming matured fibrils. We have depicted the mechanism through **Scheme 3.1**.

3.2.5 Effect of Metal Ions on the Time-dependent Emission Properties of the Self-assemblies:

Furthermore, the local concentration of amino acid would be varied widely under the influence of different metal ions, which may further induce the formation of different structures. Previous studies on concentration-dependent structural analysis of diphenylalanine revealed several nano-architectures like the toroid, ellipsoid, discoid vesicles, nanotubes, and others *[31]*. The time-dependent fluorescence of the self-assemblies was monitored further to get insights into the metal ion-induced clusteroluminescence of amino acids (**Figure 3.13-3.19**).

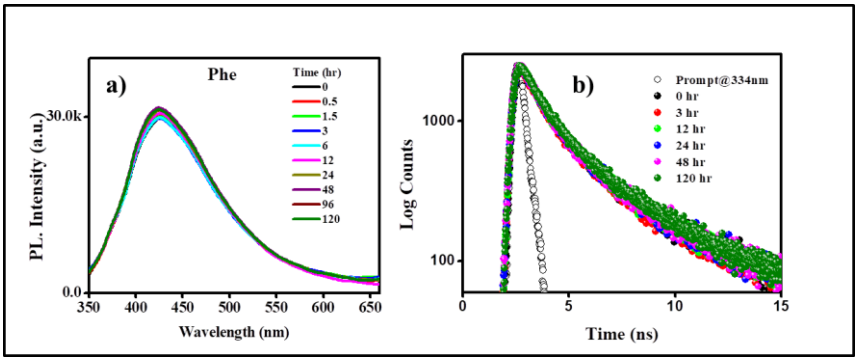

Figure 3.14 *Time-dependent fluorescence measurements of A_{Phe} system: a) steady-state fluorescence spectra, b) lifetime profiles.*

It was observed that the emission intensities of the self-assembly in the presence of metal ions (when excited at 340 nm) went on increasing before reaching the lag phase (**Figure 3.15-3.19**). More prominent enhancement with time was observed for A_{Phe}/Hg^{2+} (**Figure 3.17a**) and A_{Phe}/Ga^{3+} (**Figure 3.19a**) systems.

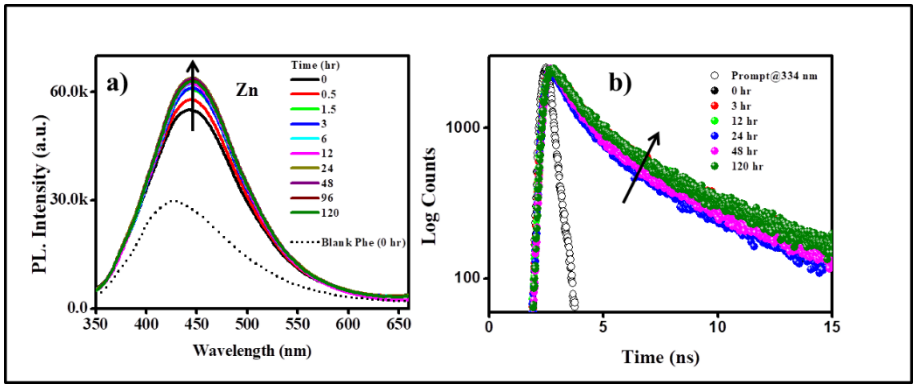

Figure 3.15 *Time-dependent fluorescence measurements of A_{Phe}/Zn^{2+} system: a) steady-state fluorescence spectra, b) lifetime profiles.*

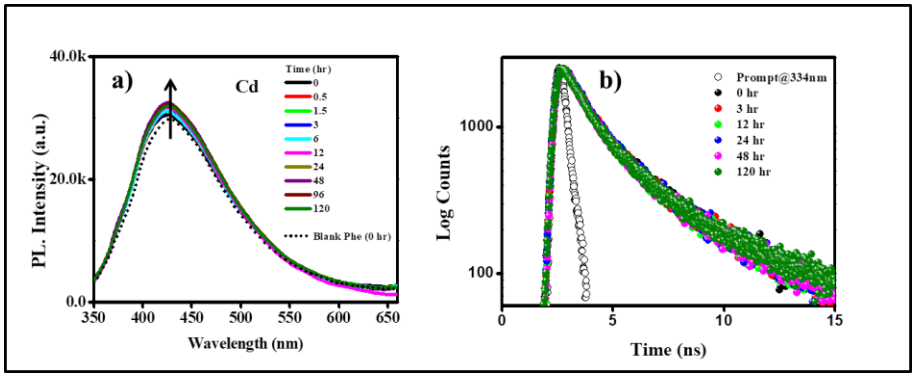

Figure 3.16 *Time-dependent fluorescence measurements of A_{Phe}/Cd^{2+} system: a) steady-state fluorescence spectra, b) lifetime profiles.*

The monitored enhancement of the fluorescence can be attributed to the clustering-triggered emission (CTE) due to the metal ion-induced clusterization of amino acids, as reported in our previous work *[52]*. The introduction of metal ions yields a longer lag time, indicating that the self-assembly process has slowed down. Therefore, various intermediates were observed using microscopic techniques. Interestingly, for A_{Phe}/Cd^{2+} (**Figure 3.16a**), the increment in the emission intensity was negligible, which may be due to the quenching effect exerted by Cd^{2+}. Although the emission intensity of A_{Phe}/Hg^{2+} was less compared to blank A_{Phe}. However, a gradual increment in

luminescence intensities can be observed for A_{Phe}/Hg^{2+}. The fluorescence quenching by heavy metal ions, Cd^{2+} and Hg^{2+}, can be associated with the effect known as the external heavy atom effect (EHE) *[60]*.

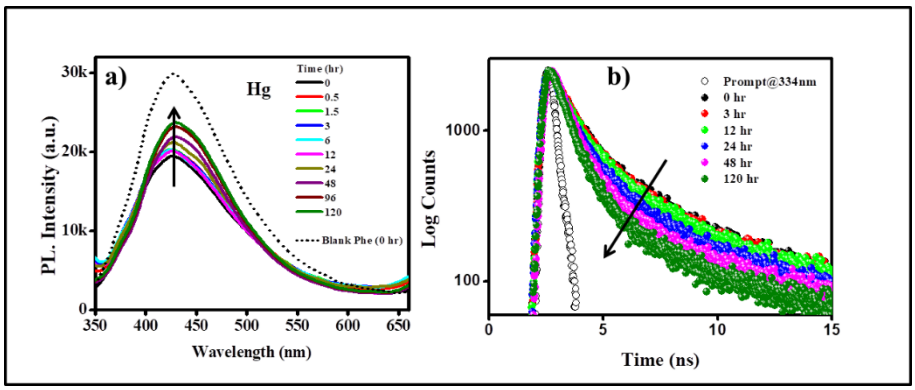

Figure 3.17 *Time-dependent fluorescence measurements of A_{Phe}/Hg^{2+} system: a) steady-state fluorescence spectra, b) lifetime profiles.*

The fluorescence intensity of A_{Phe} in the presence of Zn^{2+} and Cd^{2+} ions reached the plateau after 24 hours. This explains why we observed fibrillar structures for both A_{Phe}/Zn^{2+} (**Figure 3.2**) and A_{Phe}/Cd^{2+} (**Figure 3.3**) at later stages. Interestingly, faster saturation was observed in the case of the A_{Phe}/Al^{3+} system, indicating faster clusterization of amino acids, whereas more time was required for the A_{Phe}/Ga^{3+} system. The faster clusterization can be associated with the nano-fibrillar growth observed from the edges of the nanoflowers (**Figure 3.5**). On the contrary, the longer lag time for A_{Phe}/Ga^{3+} is probably due to the existence of vesicles for quite a long time.

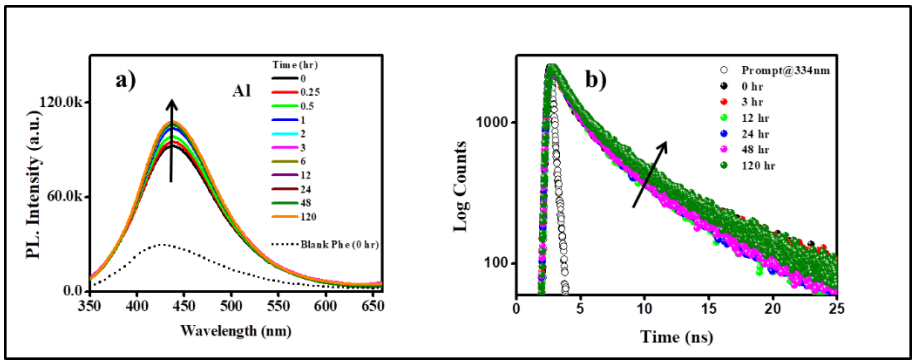

Figure 3.18 *Time-dependent fluorescence measurements of A_{Phe}/Al^{3+} system: a) steady-state fluorescence spectra, b) lifetime profiles.*

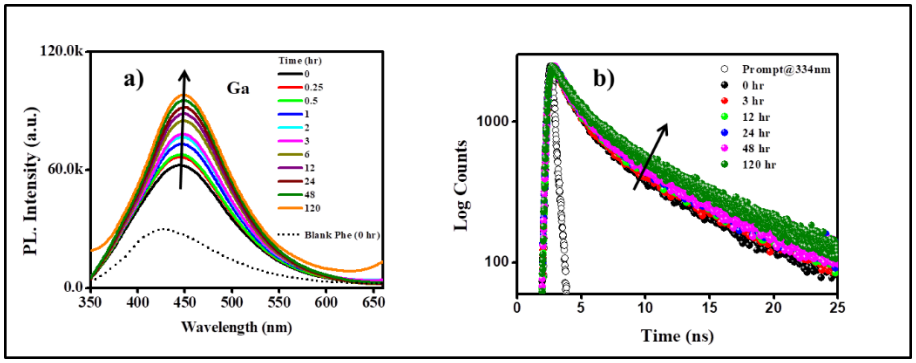

Figure 3.19 *Time-dependent fluorescence measurements of A_{Phe}/Ga^{3+} system: a) steady-state fluorescence spectra, b) lifetime profiles.*

From the lifetime profiles upon excitation at 334 nm, we observe a significant increment in the lifetimes in the presence of Zn^{2+} (**Figure 3.15b**), Al^{3+} (**Figure 3.18b**), and Ga^{3+} (**Figure 3.19b**), as compared to the blank A_{Phe} (**Figure 3.14b**). The enhanced lifetimes may arise due to more rigid conformations due to the clusterization of amino acids. The gradual increase in the lifetimes for A_{Phe}/Ga^{3+} can be associated with more clusterization of amino acids and subsequent rigidity of the vesicles formed. The continuous decrease in the lifetime of A_{Phe}/Hg^{2+} (**Figure 3.17b**) can be witnessed and can be correlated with the stable complex formation between Hg^{2+} and phenylalanine, leading to extensive dynamic quenching. In the presence of metal ions, the strong hydrophobic Phe···Phe interaction enhances the local concentration, resulting in more compact stacking of the aromatic side-chains of Phe. The initial densely packed microstructures were much more stabilized by trivalent ions and could sustain a much longer time due to repulsive Phe···solvent interaction *[33]*. This explains why we observed initial microspheres and subsequent toroid structure and their fusion in the presence of divalent ions and lack of prominent toroid structures in the presence of trivalent ions. Previous work on protein nanofibril upon interaction with several metal ions of variable pK_a values has established the effect of hydrolysis of the ions and subsequent stabilization of the hydrogel *[61]*. Smaller and polyvalent metal ions have a greater ability to get hydrolyzed to form hydroxides or oxides, readily producing hydronium ions in the medium. This led to a decrease in the effective concentration of ions that would support the hydrogel and disrupt the

gel formation, as witnessed. Our previous work *[52]* suggested that hydrolysis of metal ions Zn^{2+} and Al^{3+} can disrupt the electrostatic interaction between the neighboring NH_3^+ and COO^- thus slowing down the fibrillation process. However, non-fibrillar spherical structures can be stabilized due to the hydrophobic interaction between the metal ions and amino acids. Similar results were obtained when other metal ions analogous to Zn^{2+} and Al^{3+} were introduced to the system. Thus, we conclude that the metal ions of higher charge-to-radius ratio that possess acidic pK_a values, e.g., Hg^{2+} and Ga^{3+}, inhibit the very fast kinetics of fibril formation, making it possible to capture intermediates of different morphology at different times.

3.3 Conclusion

In conclusion, divalent and trivalent metal ions were found to stabilize the intermediate states during the self-assembly process of phenylalanine by increasing the hydrophobic interaction. At the very beginning stage of assembly, entropy favored droplet and microsphere formation took place owing to the strong hydrophobic Phe···Phe interaction and metal coordination with amino acids. The microspheres, at the later stage of the self-assembly process, subsequently transformed into different intermediate structures, such as vesicles, flowers, toroids, etc., due to Phe···solvent interaction. For trivalent metal ions, the spherical nano-aggregates formed at the initial stage were much stabilized and could sustain more times due to stronger hydrophobic interaction than for divalent metal ions.

3.4 References

[1] Whyburn G. P., Li Y., Huang Y. (2008), Protein and protein assembly based material structures, J Mater Chem 18, 3755−3762 (DOI: 10.1039/b807421f)

[2] Lai Y. T., Reading E., Hura G. L. *et al.* (2014), Structure of a designed protein cage that self-assembles into a highly porous cube, Nat Chem 6, 1065−1071 (DOI: 10.1038/nchem.2107)

[3] Acosta S., Ye Z., Aparicio C. *et al.* (2020), Dual Self-assembled nanostructures from intrinsically disordered protein polymers with LCST behavior and antimicrobial peptides, Biomacromolecules 21, 4043−4052 (DOI: 10.1021/acs.biomac.0c00865)

[4] Cui H., Webber M. J., Stupp, S. I. (2010), Self-assembly of peptide amphiphiles: from molecules to nanostructures to biomaterials, Biopolymers 94, 1−18 (DOI: 10.1002/bip.21328)

[5] Webber M. J., Newcomb C. J., Bitton R. *et al.* (2011), Switching of self-assembly in a peptide nanostructure with a specific enzyme, Soft Matter 7, 9665−9672.

[6] Mondal S., Adler-Abramovich L., Lampel A. *et al.* (2015), Formation of functional super-helical assemblies by constrained single heptad repeat, Nat Commun 6, 8615 (DOI: 10.1039/c1sm05610g)

[7] Yi M., Tan W., Guo J. *et al.* (2021), Enzymatic noncovalent synthesis of peptide assemblies generates multimolecular crowding in cells for biomedical applications, Chem Commun 57, 12870−12879 (DOI: 10.1039/D1CC05565H)

[8] Jeena M. T., Palanikumar L., Go E. M. *et al.* (2017), Mitochondria localization induced self-assembly of peptide amphiphiles for cellular dysfunction, Nat. Commun. 8, 26−36 (DOI: 10.1038/s41467-017-00047-z)

[9] Wang H., Feng Z., Xu B. (2019), Assemblies of peptides in a complex environment and their applications, Angew Chem Int Ed 58, 10423−10432 (DOI: 10.1002/anie.201814552)

[10] Flynn G. C., Chappell T. G., Rothman J.E. (1989), Peptide binding and release by proteins implicated as catalysts of protein assembly, Science 245, 385−390 (DOI: 10.1126/science.2756425)

[11] Xiao X., Wang X., Wang Y. *et al.* (2018), Multi-functional peptide–microRNA nanocomplex for targeted microRNA delivery and function imaging, Chem. Eur. J. 24, 2277−2285 (DOI: 10.1002/chem.201705695)

[12] Yan X., He Q., Wang K. *et al.* (2007), Transition of cationic dipeptide nanotubes into vesicles and oligonucleotide delivery, Angew. Chem., Int. Ed. 119, 2483−2486 (DOI: 10.1002/ange.200603387)

[13] Ruff Y., Moyer T., Newcomb C. J. *et al.* (2013), Precision templating with DNA of a virus-like particle with peptide nanostructures, J. Am. Chem. Soc. 135, 6211−6219 (DOI: 10.1021/ja4008003)

[14] Ross C. A., Poirier M. A. (2004), Protein aggregation and neurodegenerative disease, Nat. Med. 10, S10−17 (DOI: 10.1038/nm1066)

[15] Bernstein S. L., Dupuis N. F., Lazo N. D. *et al.* (2009), Amyloid-β protein oligomerization and the importance of tetramers and dodecamers in the aetiology of Alzheimer's disease, Nat. Chem. 1, 326–331 (DOI: 10.1038/nchem.247)

[16] Adamcik J., Jung J.-M., Flakowski J. *et al.* (2010), Understanding amyloid aggregation by statistical analysis of atomic force microscopy images, Nat. Nanotechnol. 5, 423−428 (DOI: 10.1038/nnano.2010.59)

[17] Gazit E. (2007), Self assembly of short aromatic peptides into amyloid fibrils and related nanostructures, Prion 1, 32−35 (DOI: 10.4161/pri.1.1.4095)

[18] Knowles T. P., Vendruscolo M., Dobson C. M. (2014), The amyloid state and its association with protein misfolding diseases, Nat. Rev. Mol. Cell Biol. 15, 384−396 (DOI: 10.1038/nrm3810)

[19] Mehta A. K., Lu K., Childers W. S. *et al.* (2008), Facial symmetry in protein self-assembly, J. Am. Chem. Soc. 130, 9829–9835 (DOI: 10.1021/ja801511n)

[20] Azriel R., Gazit E. (2001), Analysis of the minimal amyloid-forming fragment of the islet amyloid polypeptide, J. Biol. Chem. 276, 34156–34161 (DOI: 10.1074/jbc.M102883200)

[21] Pawar A. P., Dubay K. F., Zurdo J. *et al.* (2005), Prediction of "aggregation-prone" and "aggregation-susceptible" regions in proteins associated with neurodegenerative diseases, J. Mol. Biol. 350, 379−392 (DOI: 10.1016/j.jmb.2005.04.016)

[22] Banerjee P., Rajak K., Nandi P. K. *et al.* (2020), Aging-dependent morphological crystallinity determines membrane activity of l-phenylalanine self-assembles, J. Phys. Chem. Lett. 11, 8585−8591 (DOI: 10.1021/acs.jpclett.0c01831)

[23] Reches M., Gazit E. (2003), Casting metal nanowires within discrete self-assembled peptide nanotubes, Science 300, 625−627 (DOI: 10.1126/science.1082387)

[24] Han T. H., Ok T., Kim J. *et al.* (2010), Bionanosphere lithography via hierarchical peptide self-assembly of aromatic triphenylalanine, Small 6, 945–951 (DOI: 10.1002/smll.200902050)

[25] Guo C., Luo Y., Zhou R. *et al.* (2014), Triphenylalanine peptides self-assemble into nanospheres and nanorods that are different from the nanovesicles and nanotubes formed by diphenylalanine peptides. Nanoscale 6, 2800–2811 (DOI: 10.1039/c3nr02505e)

[26] Azuri I., Adler-Abramovich L., Gazit E. *et al.* (2014), Why are diphenylalanine-based peptide nanostructures so rigid? Insights from first principles calculations, J. Am. Chem. Soc. 136, 963–969 (DOI: 10.1021/ja408713x)

[27] Garcia A. M., Melchionna M., Bellotto O. *et al.* (2021), Nanoscale assembly of functional peptides with divergent programming elements, ACS Nano 15, 3015–3025 (DOI: 10.1021/acsnano.0c09386)

[28] Basavalingappa V., Bera S., Xue B. *et al.* (2020), Diphenylalanine-derivative peptide assemblies with increased aromaticity exhibit metal-like rigidity and high piezoelectricity, ACS Nano 14, 7025–7037 (DOI: 10.1021/acsnano.0c01654)

[29] Li Q., Jia Y., Dai L. *et al.* (2015), Controlled rod nanostructured assembly of diphenylalanine and their optical waveguide properties, ACS Nano 9, 2689–2695 (DOI: 10.1021/acsnano.5b00623)

[30] Yan X., Cui Y., He Q. *et al.* (2008), Organogels based on self-assembly of diphenylalanine peptide and their application to immobilize quantum dots, Chem. Mater. 20, 1522–1526 (DOI: 10.1021/cm702931b)

[31] Guo C., Luo Y., Zhou R. *et al.* (2012), Probing the self-assembly mechanism of diphenylalanine-based peptide nanovesicles and nanotubes, ACS Nano 6, 3907–3918 (DOI: 10.1021/nn300015g)

[32] Guo C., Arnon Z. A., Qi R. *et al.* (2016), Expanding the nanoarchitectural diversity through aromatic di-and tri-peptide coassembly: Nanostructures and molecular mechanisms, ACS Nano 10, 8316–8324 (DOI: 10.1021/acsnano.6b02739)

[33] Mayans E., Casanovas J., Gil, A. M. *et al.* (2017), Diversity and hierarchy in supramolecular assemblies of triphenylalanine: from laminated helical ribbons to toroids, Langmuir 33, 4036–4048 (DOI: 10.1021/acs.langmuir.7b00622)

[34] Tamamis P., Adler-Abramovich L., Reches M. *et al.* (2009), Self-assembly of phenylalanine oligopeptides: insights from experiments and simulations, Biophys. J. 96, 5020–5029 (DOI: 10.1016/j.bpj.2009.03.026)

[35] Adler-Abramovich L., Vaks L., Carny O. *et al.* (2012), Phenylalanine assembly into toxic fibrils suggests amyloid etiology in phenylketonuria, Nat. Chem. Biol. 8, 701 (DOI: 10.1038/nchembio.1002)

[36] Shaham-Niv S., Rehak P., Vuković L. *et al.* (2017), Formation of apoptosis-inducing amyloid fibrils by tryptophan, Isr. J. Chem. 57, 729–737 (DOI: 10.1002/ijch.201600076)

[37] Zaguri D., Kreiser T., Shaham-Niv S. *et al.* (2018), Antibodies towards tyrosine amyloid-like fibrils allow toxicity modulation and cellular imaging of the assemblies, Molecules 23, 1273 (DOI: 10.3390/molecules23061273)

[38] Banik D., Kundu S., Banerjee P. *et al.* (2017), Investigation of fibril forming mechanisms of l-phenylalanine and l-tyrosine: microscopic insight toward phenylketonuria and tyrosinemia type II, J. Phys. Chem. B 121, 1533–1543 (DOI: 10.1021/acs.jpcb.6b12220)

[39] Adler-Abramovich L., Kol N., Yanai I. *et al.* (2010), Self-assembled organic nanostructures with metallic-like stiffness, Angew. Chem., Int. Ed. 49, 9939–9942 (DOI: 10.1002/anie.201002037)

[40] Jayawarna V., Ali M., Jowitt T. A. *et al.* (2006), Nanostructured hydrogels for three-dimensional cell culture through self-assembly of fluorenylmethoxycarbonyl–dipeptides, Adv. Mater. 18, 611–614 (DOI: 10.1002/adma.200501522)

[41] Chronopoulou L., Sennato S., Bordi F. *et al.* (2014), Designing unconventional Fmoc-peptide-based biomaterials: structure and related properties, Soft Matter 10, 1944–1952 (DOI: 10.1039/c3sm52457d)

[42] Martí D., Mayans E., Gil A. M. *et al.* (2018), Amyloid-like fibrils from a diphenylalanine capped with an aromatic fluorenyl, Langmuir 34, 15551–15559 (DOI: 10.1021/acs.langmuir.8b03378)

[43] Mayans E., Ballano G., Casanovas J. *et al.* (2016), Hierarchical self-assembly of di, tri-and tetraphenylalanine peptides capped with two fluorenyl functionalities: from polymorphs to dendrites, Soft Matter 12, 5475–5488 (DOI: 10.1039/C6SM00337K)

[44] Tao K., Levin A., Adler-Abramovich L. *et al.* (2016), Fmoc-modified amino acids and short peptides: simple bio-inspired building blocks for the fabrication of functional materials, Chem. Soc. Rev. 45, 3935–3953 (DOI: 10.1039/C5CS00889A)

[45] Xie Y. Y., Qin X. T., Feng, J. Y. *et al.* (2021), A self-assembled amino acid-based hydrogel with broad-spectrum antibacterial activity, J. Mater. Sci. 56, 7626–7636 (DOI: 10.1007/s10853-021-05801-9)

[46] Xie Y. Y., Zhang Y. W., Qin X. T. *et al.* (2020), Structure-dependent antibacterial activity of amino acid-based supramolecular hydrogels, Colloids Surf. B 193, 111099 (DOI: 10.1016/j.colsurfb.2020.111099)

[47] Levin A., Mason T. O., Adler-Abramovich L. *et al.* (2014), Ostwald's rule of stages governs structural transitions and morphology of dipeptide supramolecular polymers, Nat. Commun. 5, 5219 (DOI: 10.1038/ncomms6219)

[48] Chen S. W., Drakulic S., Deas E. *et al.* (2015), Structural characterization of toxic oligomers that are kinetically trapped during α-synuclein fibril formation, Proc. Natl. Acad. Sci. U. S. A. 112, E1994–E2003 (DOI: 10.1073/pnas.1421204112)

[49] Yuan C., Levin A., Chen W. *et al.* (2019), Nucleation and growth of amino acid and peptide supramolecular polymers through liquid–

liquid phase separation, Angew. Chem., Int. Ed. 58, 18116–18123 (DOI: 10.1002/anie.201911782)

[50] Ji W., Yuan C., Zilberzwige-Tal S. *et al.* (2019), Metal-ion modulated structural transformation of amyloid-like dipeptide supramolecular self-assembly, ACS Nano 13, 7300–7309 (DOI: 10.1021/acsnano.9b03444)

[51] Li S., Zou Q., Li Y. *et al.* (2018), Smart peptide-based supramolecular photodynamic metallo-nanodrugs designed by multicomponent coordination self-assembly, J. Am. Chem. Soc. 140, 10794–10802 (DOI: 10.1021/jacs.8b04912)

[52] Bagchi D., Maity A., De S. K. *et al.* (2021), Effect of metal ions on the intrinsic blue fluorescence property and morphology of aromatic amino acid self-assembly, J. Phys. Chem. B 125, 12436–12445 (DOI: 10.1021/acs.jpcb.1c07392)

[53] Lee M., Kim J. I., Na S. *et al.* (2018), Metal ions affect the formation and stability of amyloid β aggregates at multiple length scales, Phys. Chem. Chem. Phys. 20, 8951–8961 (DOI: 10.1039/C7CP05072K)

[54] Levine H. III (1993), Thioflavine T interaction with synthetic Alzheimer's disease β-amyloid peptides: detection of amyloid aggregation in solution, Protein Sci. 2, 404–410 (DOI: 10.1002/pro.5560020312)

[55] Ropo M., Blum V., Baldauf C. (2016), Trends for isolated amino acids and dipeptides: conformation, divalent ion binding, and remarkable similarity of binding to calcium and lead, Sci. Rep. 6, 3577 (DOI: 10.1038/srep35772)

[56] Erdoğan H. (2021), Cation-based approach to morphological diversity of diphenylalanine dipeptide structures, Soft Matter 17, 5221–5230 (DOI: 10.1039/D1SM00083G)

[57] Wang J., Yuan C., Han Y. *et al.* (2017), Trace water as prominent factor to induce peptide self-assembly: dynamic evolution and governing interactions in ionic liquids, Small 13, 1702175 (DOI: 10.1002/smll.201702175)

[58] Brown N., Lei J., Zhan C. *et al.* (2018), Structural polymorphism in a self-assembled tri-aromatic peptide system, ACS Nano 12, 3253–3262 (DOI: 10.1021/acsnano.7b07723)

[59] Yang C., Gao L., Lin J. *et al.* (2017), Toroid formation through a supramolecular "cyclization reaction" of rodlike micelles, Angew. Chem., Int. Ed. 56, 5546–5550 (DOI: 10.1002/anie.201701978)

[60] Kemlo J. A., Shepherd T. M. (1977), Quenching of excited singlet states by metal ions, Chem. Phys. Lett. 47, 158–162 (DOI: 10.1016/0009-2614(77)85329-3)

[61] Ye X., Capezza A., Xiao X. *et al.* (2021), Protein nanofibrils and their hydrogel formation with metal ions. ACS Nano 15, 5341–5354 (DOI: 10.1021/acsnano.0c10893)

Chapter 4

Metal Ions-Induced Unusual Stability of the Metastable Vesicle-like Intermediates Evolving in the Self-Assembly Process of Phenylalanine: Prominent Role of Surface Charge Inversion

4.1 Introduction

The origin of cellular life in the prebiotic environment was an intriguing phenomenon in nature. Therefore, it has been the most fundamental area of research *[1-3]*. Especially explaining the emergence of life-like behavior from the mixture of several molecules remains the most crucial challenge. Several attempts have been made over the past few decades to understand the underlying mechanism of cellular organization *[4-7]*. For this purpose, compartmentalization has become one of the most fundamental hallmarks *[8,9]*. These compartments can play an essential role in bringing together the biomolecules of interest. Being intrigued by this, researchers have focused on designing various protocells as these could have provided the desired compartments that perhaps facilitated the formation of living cells from abiotic systems *[10,11]*. Different types of protocells have been explored, where the compartments are surrounded mainly by membranes of lipids, fatty acids, block copolymers, and so on *[12-14]*. However, the major disadvantages of these membrane-enclosed protocells are the uncertainty in the prebiotic synthesis of the membrane components and the selective permeability of the biomolecules in the systems that restrict their utility. Thus, compartments without membrane components would be beneficial for designing effective protocells. These membraneless protocells are formed spontaneously, where the solute-rich condensed phase separates itself from the solute-depleted aqueous phase *[15]*. The

selective accumulation and dynamic cargo exchange make these membraneless compartments attractive for designing various protocells *[16,17]*. Further, enhanced solute concentration and a distinct environment inside the compartments help to accelerate several important bio-reactions *[18]*. The protocells formed by biomolecular self-organization are of immense interest because they are often used as the research model to design biological compartments for understanding the origin of life *[19-21]*. Among all biomolecules, the self-assembly of proteins and peptides is very important and ubiquitous because of various nanostructures with important cellular organizations and functions *[22-24]*. However, the uncontrolled aggregation of proteins and peptides can lead to several neurodegenerative diseases *[25,26]*. Recent studies have shown that the proteins or peptides undergo phase separation to form nano-fibrillar self-aggregates *[27-29]*. The formation of solute-rich intermediates is one of the key steps in the process *[30,31]*. These act as nucleation precursors that transform into thermodynamically favorable fibrillar structures. Therefore, tuning the stability of the various intermediates is of great importance as it can be utilized as the membraneless compartments.

In this regard, a reductionist approach must be targeted at understanding the self-assembly of the amino acids, as they serve as the simplest building blocks of proteins or peptides. Although aromatic amino acids, especially phenylalanine, can self-assemble to form fibrillar networks *[32-34]*, it was not clear how the transformation of monomeric amino acids into fibrils proceeds through intermediates. Recently, Yuan et al. proposed that the formation of supramolecular nanofibrils of small peptides and amino acids proceeds through the solute-rich liquid droplets *[30]*, which are further stabilized by the enhanced hydrophobicity due to coordination with metal. Our previous work revealed that several bivalent and trivalent metal ions could successfully slow down the fibrillation kinetics, and as a result, various metastable intermediates of unique morphologies such as nano-spheres (Zn^{2+}), toroids (Cd^{2+}, Hg^{2+}), nano-flowers (Al^{3+}), and vesicles (Ga^{3+}, In^{3+}) were

observed *[35]* that further transformed into matured fibrils, indicating that the fibrillation process is thermodynamically more favored. The intermediates in the naturally occurring amino acids were found to be less stable for a longer period owing to the insufficient hydrophobic interactions that rendered the transformation of the intermediates to the fibrillar network. The introduction of a protecting group, such as carboxybenzyl (Z) or 9-fluorenylmethoxycarbonyl (Fmoc), induces a higher order of hydrophobic and π-π stacking interactions *[36,37]* and may help in stabilizing the intermediates. The most important issue regarding the intermediates not well reported in the literature is the crucial role of the surface charges of the intermediates that take place with time during the evolution of the intermediate. It has already been reported *[38]* that the local pairing of ions and carboxyl groups and protonation in the presence of these metal ions alter the surface charges of the proteins. Therefore, the alteration in surface charge with time may play a crucial role in stabilizing the intermediates of different morphology.

Keeping all these possibilities in mind, we have investigated the evolution of the self-assembly process of carboxybenzyl (Z) protected phenylalanine (ZF) as a function of time in the presence of different metal ions by live imaging to capture the morphology of the intermediates that develops at various time. We measured the surface charge of the system at different times to correlate the stability of the intermediates. Furthermore, it is suggested that the intrinsically disordered regions in proteins are enriched with aromatic (tyrosine, phenylalanine) and charged (lysine, arginine, aspartic acid, glutamic acid) amino acid residues and can drive the self-assembly process of peptides and proteins. Apart from metal ions, we have also investigated the roles of several polar amino acids in driving the aggregation process of ZF. Stabilizing intermediates formed in the self-assembly process of the amino acid can provide a novel approach that may facilitate the design of membraneless compartments.

4.2 Results and Discussion

4.2.1 Effect of Concentration and General Characterisation of the ZF Self-assembly:

We start our investigation by monitoring the self-assembly process of blank ZF. The self-assembly of ZF was prepared by dissolving the ZF molecules in ethanol to create a molecular reservoir prior to the addition of water *[39]*. To understand the self-assembly behavior of ZF, different sets with variable concentrations of ZF were prepared,

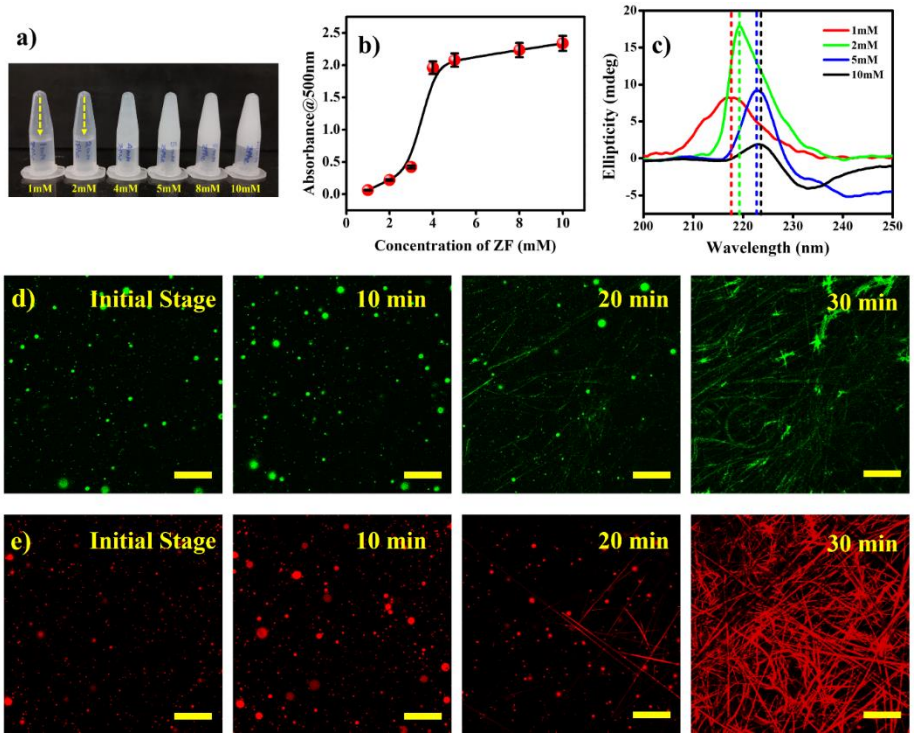

Figure 4.1 *(a) Photographs of the ZF solutions at different concentrations, (b) Turbidity measured at 500 nm (Error = ±5 %), (c) CD spectra of ZF at different concentrations, Time-dependent CLSM images of 10 mM ZF self-assembly using (d) ThT, and (e) Nile red. The scale bar is 20 μm.*

and their physical appearance was determined (**Figure 4.1a**). Visible phase separation or turbidity appeared at and beyond 4 mM of ZF, and this was further verified by measuring the turbidity (absorbance at 500 nm) that showcased abrupt enhancement of absorbance (**Figure 4.1b**). The turbid solution at or above 4 mM transformed into self-supporting hydrogels (**Figure 4.1a**) with the progression of time. However, in our

previous work *[35]*, we could not observe such turbidity appearing in the solution containing Phe self-assembly, indicating the non-occurrence of any phase separation. The monomeric Phe turned into fibrillar structures without the occurrence of stable intermediates. This can be attributed to the lower π electron densities and lower phase separation propensities of Phe-containing dipeptide *[40]*.

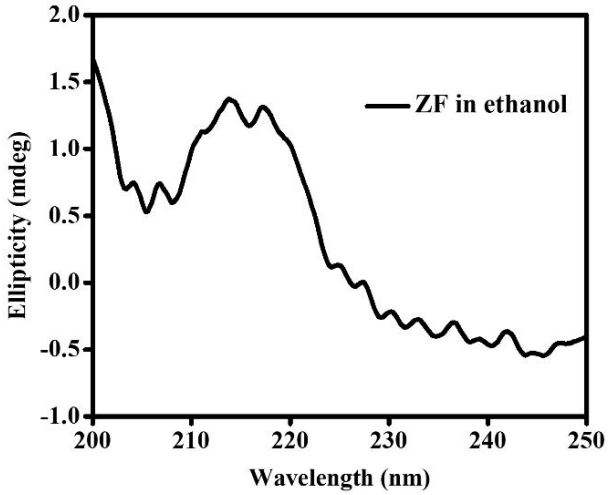

Figure 4.2 *CD spectrum of the monomeric ZF solution (0.1 mM in ethanol). It indicates a positive peak centered at around 212 nm.*

We employed the CD spectra of ZF at different concentrations to shed light on the self-aggregation process. The CD spectra revealed that the positive peak centered at 217 nm for diluted ZF solution (1 mM) shifted towards a higher wavelength (219 nm) with a higher absorbance value when the concentration was enhanced to 2 mM (**Figure 4.1c**). The appearance of this peak is attributed to the transition involving the carboxyl group (n-π^*) and benzene ring (π-π^*) present in the molecule *[41,42]*. The higher ellipticity and the change in peak position compared to those of monomeric ZF (**Figure 4.2**) indicate the formation of higher-ordered structures of ZF in a concentration-dependent manner *[43]*. A different pattern of spectra with more red-shifted positive peaks at the region 222-225 nm and a negative peak (233 nm) was observed at a higher concentration (5-10 mM). These significant positive and negative Cotton effects can be correlated to the structural change of monomeric ZF to well-ordered self-assembly *[44]*. Several phenylalanine-based

peptides are known to form structures rich in β-sheet *[45,46]*. Thus, further investigation into morphological transition was very much needed.

4.2.2 Investigation of Morphological Transformation of ZF Self-assembly:

To study the morphological changes with phase separation, we first employed optical microscopy (OM) for different concentrations of

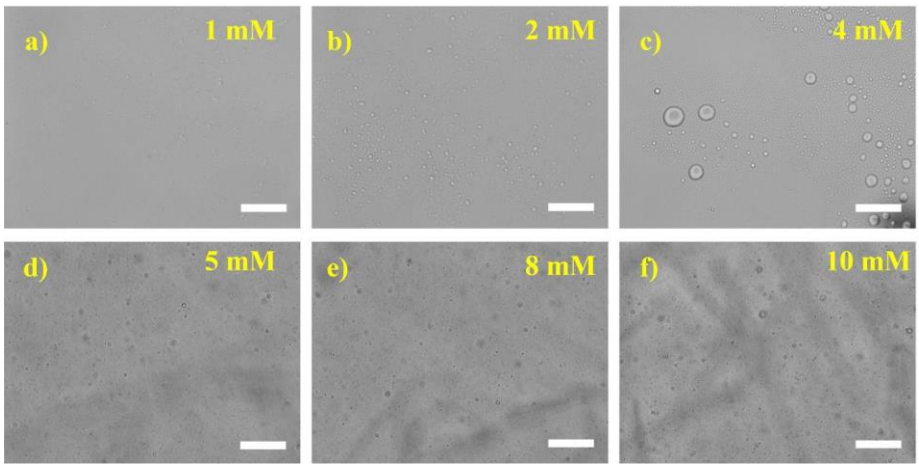

Figure 4.3 *Optical microscopy images of different sets with increasing ZF concentrations. At the early stages, discrete, tiny clusters were found for 1-2 mM (a,b), and microspheres were found for 4-10 mM (d-f) of ZF. Scale bar* 20 μm.

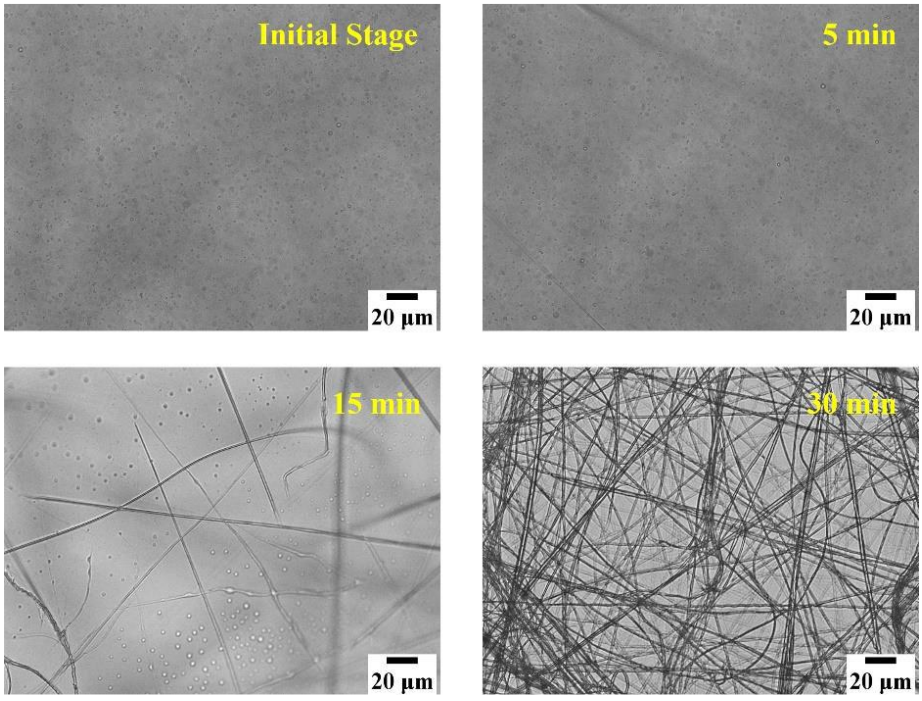

Figure 4.4 *Optical microscopy images of 10 mM ZF at different times indicate the evolution of fibrils from microspheres at the later stages of the self-assembly process.*

blank ZF, followed by confocal imaging. The OM images revealed the presence of non-fibrillar uniform spherical structures with sizes ranging from nano to micrometer at the initial stages of self-assembly for 4-10 mM of ZF (**Figure 4.3**). These metastable structures underwent coalescence and transformed into rodlike fibrillar morphologies with the progression of time (**Figure 4.4**). Surprisingly, for lower concentrations of ZF (1 or 2 mM), almost no definite structures appeared, and in some cases, discrete, irregular, and less spherical structures were found (**Figures 4.3a, b**) due to insufficient molecular interaction.

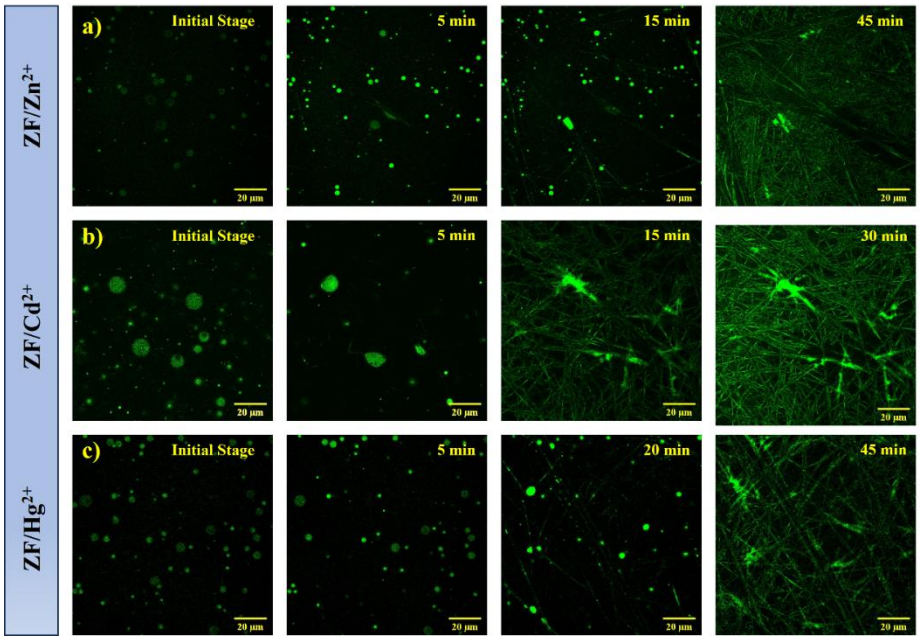

Figure 4.5 *Time-dependent CLSM images of ZF self-assembly using ThT, in the presence of metal ions, (a) Zn^{2+}, (b) Cd^{2+}, (c) Hg^{2+}; Scale bar 20 µm.*

Recently, Yuan and coworkers depicted that the multistep de-solvation of peptides directs the self-assembly process through liquid-liquid phase separation *[39]*. Introducing a poor solvent induces phase separation by partial de-solvation of the good solvent, and the hydrophobic interaction drives the formation of solute-rich spherical vesicular metastable aggregates. These metastable spheres served as the nucleation precursors for the fibril formation after a certain period. Favorable changes in entropy drove the rapid transformation of monomeric amino

acids to spherical vesicle-like intermediates. This entropy contribution originating from the expulsion of solvent molecules is associated with the conformational degrees of freedom *[30]*. Furthermore, the transformation of phase-separated nano aggregates into nanofibrils may stem from the organized and ordered packing of molecules through multiple intermolecular hydrogen bonds. The initially obtained microspheres were reported to be formed by extensive hydrophobic interaction, whereas the dynamic evolution into fibrils was assisted predominantly by π-π interactions *[30]*.

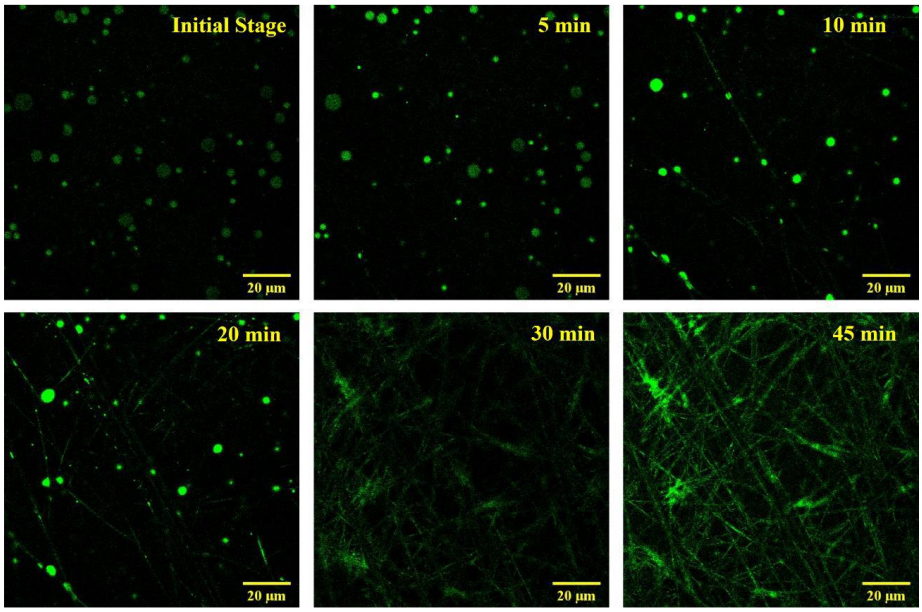

Figure 4.6 *Time-dependent CLSM images of ZF/Mg^{2+} system using ThT as a dye. Initially, tiny microspheres were formed, which further transformed into matured fibrils; Scale bar 20 µm.*

The OM imaging of blank ZF was followed by time-lapse Confocal Laser Scanning Microscopy (CLSM) imaging using Thioflavin T (ThT) and Nile red (NR) *[47-51]* at a fixed ZF concentration (10 mM). At the early stage of the self-assembly, both the ThT (**Figure 4.1d**) and NR (**Figure 4.1e**) showed strong fluorescence signals from the microspheres of blank ZF. This indicates that the π-π and hydrophobic interactions are the main driving force behind the amino acid microsphere formation. The signals became more prominent with time due to enhanced π-π and

hydrophobic interactions. Fibrillar structures started to emerge after a

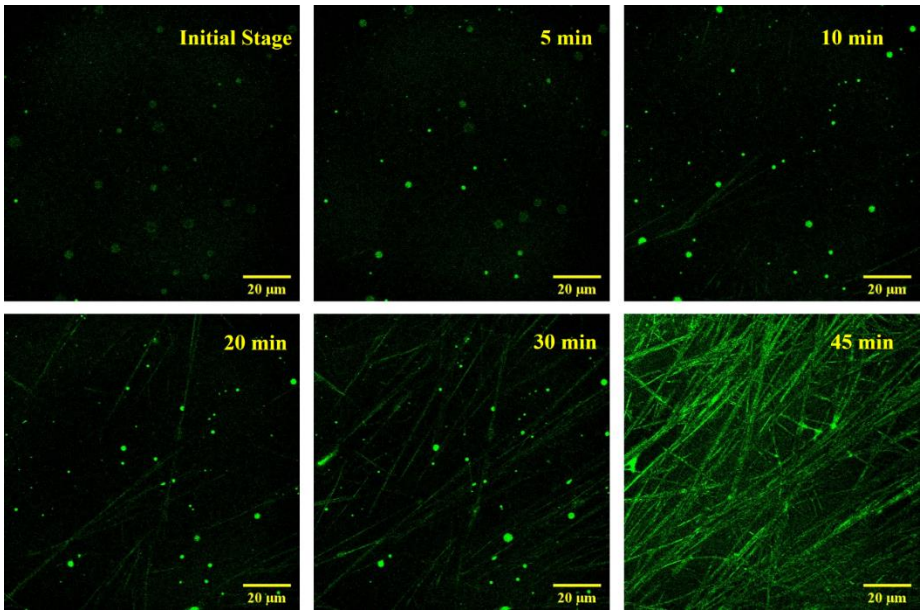

Figure 4.7 *Time-dependent CLSM images of ZF/Ca^{2+} system using ThT as a dye. Initially, tiny microspheres were formed, which further transformed into matured fibrils; Scale bar 20 µm.*

certain time as the initially obtained vesicle like microspheres (or the amino acid compartments) started to fuse with these fibrils. The spheres moved fast during the initial period but became immobilized as they fused with fibrils in a time-dependent fashion. Finally, only fibrillar structures were obtained with signals within the structures, as all the spheres merged with the fibrils. Fibrillar structures remained even when the samples were kept and dried after 45 min.

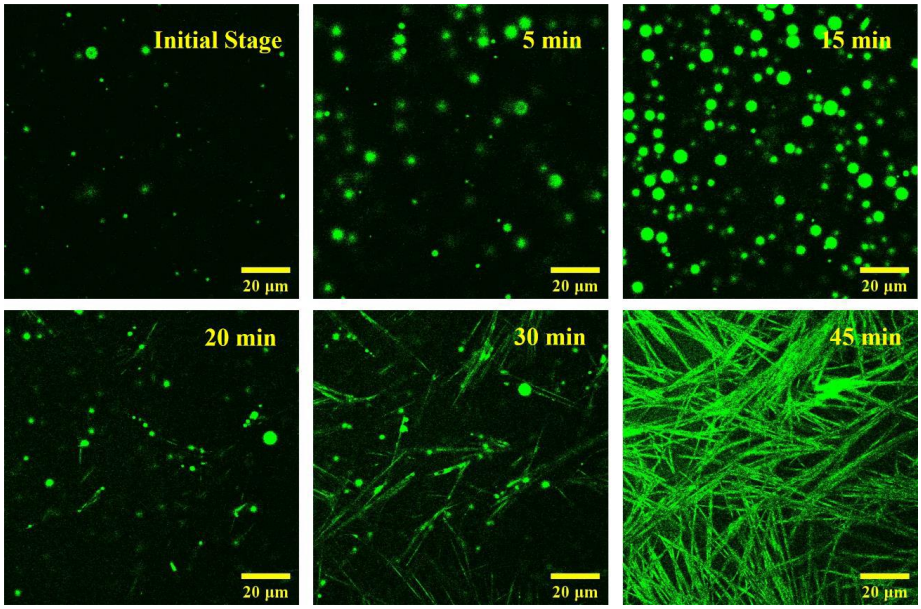

Figure 4.8 *Time-dependent CLSM images of ZF/La^{3+} system using ThT as a dye. Initially, tiny microspheres were formed, which further transformed into matured fibrils; Scale bar 20 µm.*

4.2.3 Effect of Bivalent Metal Ions on the ZF Self-assembly:

As the fibrillation kinetic of blank ZF generated some metastable spherical intermediates, one can expect that different bivalent or trivalent metal ions may further stabilize these intermediate structures by enhanced hydrophobic interaction and coordination with ZF. Previously, in the case of naturally occurring phenylalanine, the transformation of solid and compact spherical structures into various structures, such as doughnut-like toroid structures (Cd^{2+} and Hg^{2+}), was obtained *[35]* and explained as an interplay between the Phe-Phe and Phe-solvent interactions *[52]*. However, in this work, no such alteration in the physical appearance was obtained in the ZF self-assembly in the presence of bivalent metal ions such as Mg^{2+}, Ca^{2+}, Zn^{2+}, Cd^{2+}, and Hg^{2+}. The solutions became turbid as soon as the metal salts were added, and gelation was observed over time. The CLSM images of the ZF/M^{2+} systems showed that the initially formed spherical vesicle-like intermediates were metastable and transformed into fibrillar structures with strong ThT signals (**Figures 4.5-4.7**).

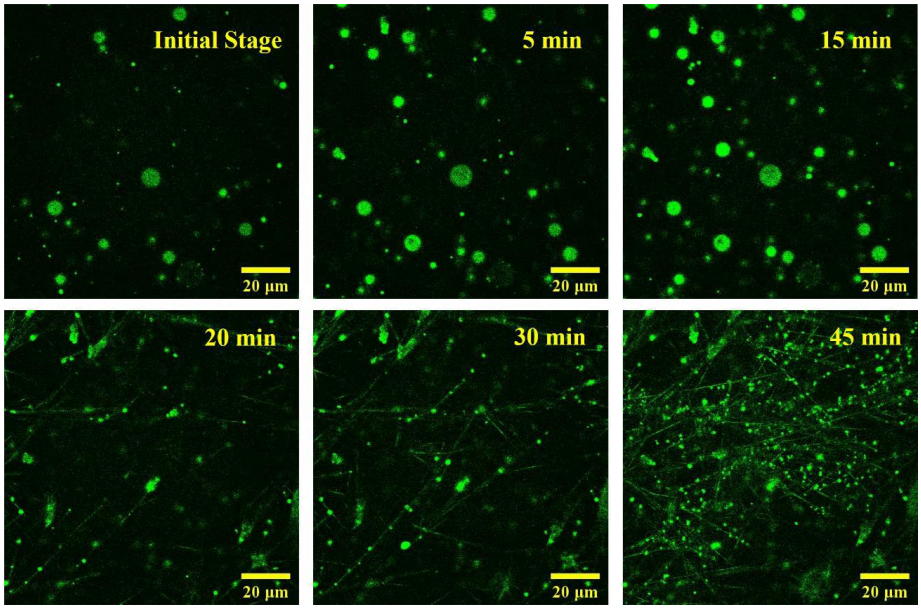

Figure 4.9 *Time-lapse CLSM images of ZF/Y^{3+} system using ThT as a dye. Initially, tiny microspheres were formed, which further transformed into matured fibrils; Scale bar 20 µm.*

These findings indicate that these bivalent metal ions do not drastically interfere with the self-assembly process of ZF. Unlike Phe, where a few bivalent metal ions (Zn^{2+}, Cd^{2+}, Hg^{2+}) generated various nanostructures of metastable intermediates, they could not alter the kinetics for ZF. This is likely since the ZF molecules are extensively hydrophobic. Their dominant hydrophobicity does not allow the water molecules to penetrate the spherical structures. Coordination with metal ions can only exert the expulsion of water, thus further helping to maintain the metastable states of the spheres. These spheres act as the nucleation center to generate fibrillar networks. For Phe/M^{2+} systems, the fibrillar networks are eventually developed by passing through various metastable intermediates. However, this was difficult for the ZF/M^{2+} system. In the latter case, we observed only micro-spheres before they transformed into fibrils. Thus, bivalent metal ions cannot drive similar morphological transformations for ZF (as compared to Phe), where the participation of solvent molecules is largely needed. Other factors for the inability of these bivalent metal ions will be discussed later.

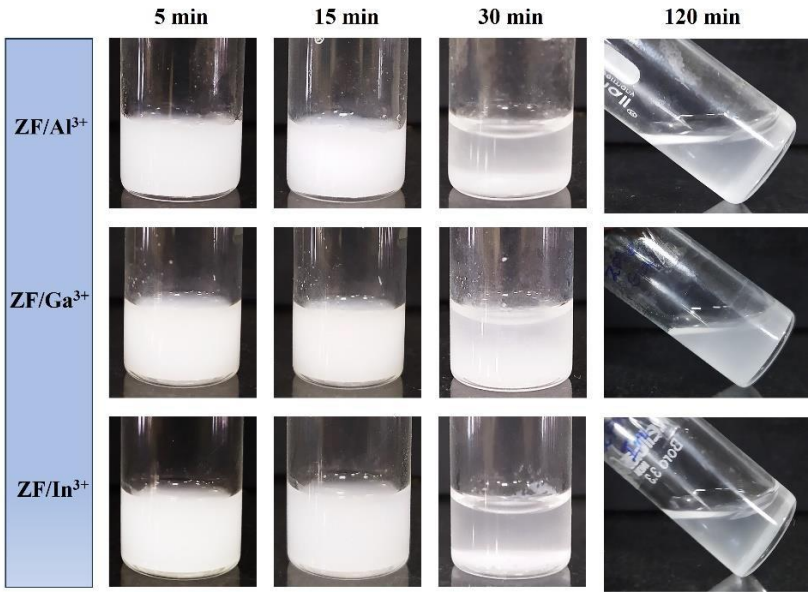

Figure 4.10 *Photographs of ZF in the presence of Al^{3+}, Ga^{3+}, and In^{3+} at different times. No gelation can be observed in these solutions as they remain fluid after 120 min.*

4.2.4 Effect of Trivalent Metal Ions on the ZF Self-assembly:

Next, we investigated the effects of trivalent metal ions, La^{3+}, Y^{3+}, Al^{3+}, Ga^{3+}, and In^{3+} on the ZF self-assembly. La^{3+} and Y^{3+} yielded results similar to that of bivalent metal ions with no striking changes (**Figure 4.8, 4.9**). Surprisingly, when we added the metal ions Al^{3+}, Ga^{3+}, or In^{3+} to the ethanolic ZF solution during the rapid mixing process, the solutions could not form hydrogels (**Figure 4.10**), unlike what happened in the case of blank ZF and in the presence of bivalent metal ions. The

solutions only remained turbid persistently from the

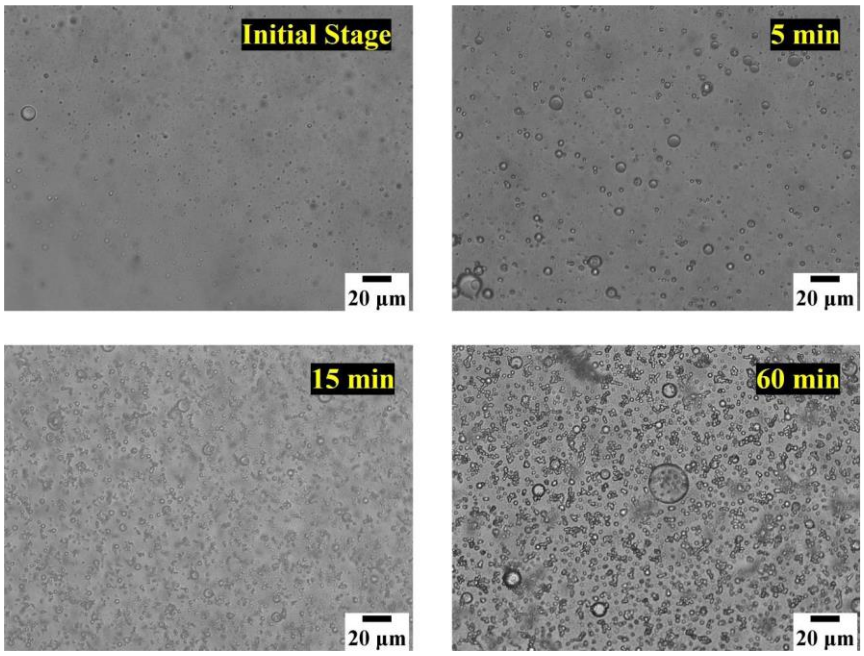

Figure 4.11 *Time-lapse optical microscopy (OM) images of ZF/Al^{3+} depict the formation of microspheres at the early stage of structure formation. Over time, these more spherical structures were formed. Surprisingly, no fibrillar structures were obtained even after 60 min.*

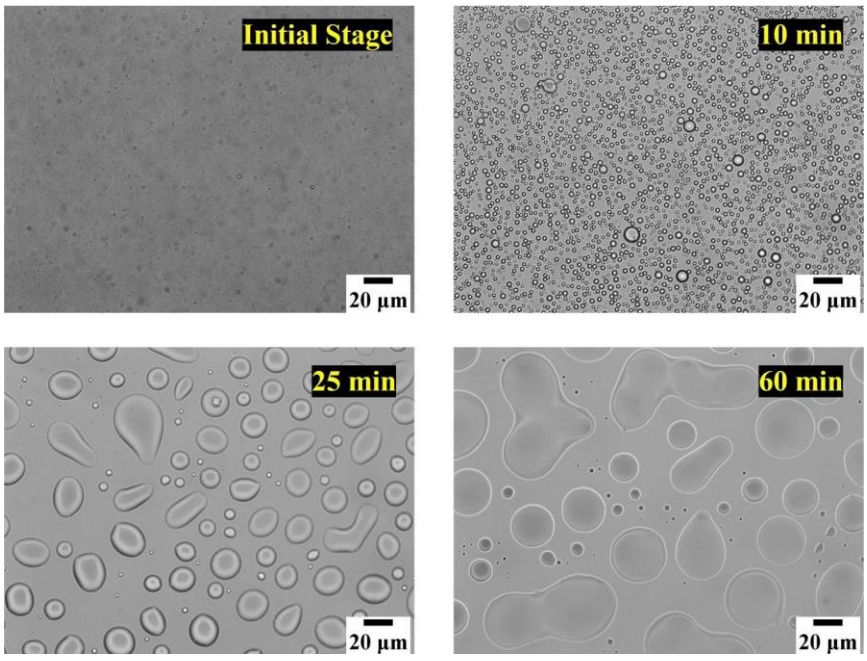

Figure 4.12 *Time-lapse OM images of ZF/Ga^{3+} depict the formation of microspheres. Over time, these structures tend to fuse and become larger in size. Surprisingly, no fibrillar structures were obtained even after 60 min.*

very early stage during rapid mixing till the end. The time-dependent OM images revealed that the initially formed vesicular spheres tended to fuse (**Figure 4.11-4.13**). A gradual increase in the size of the spheres was observed over the period. The spheres underwent coalescence to obtain larger spherical structures. Unlike the blank ZF, no fibrillar networks were obtained for these systems, even after a prolonged incubation period. Time-lapse CLSM images showed that microspheres were formed at the early stage of self-assembly for the ZF/Al^{3+} system. More spherical aggregates were generated as time progressed with strong emission signals from ThT (**Figure 4.14a**) and Nile red (**Figure 4.14b**). It is attributed to the enhanced hydrophobic and π-π interactions caused by metal-amino acid coordination. Similar phenomena were observed for ZF/Ga^{3+} (**Figures 4.15**) and ZF/In^{3+} (**Figures 4.14c, d**). The live images revealed that the vesicle-like microspheres were slowly moving compared to those obtained for blank ZF. This is probably due to the consequence of forming a comparatively denser phase-separated assembly.

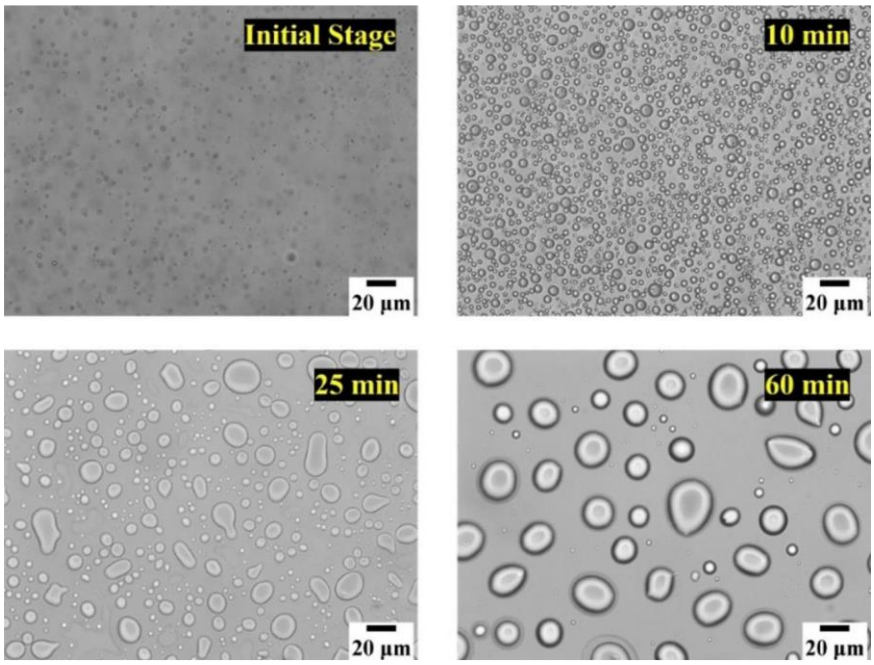

Figure 4.13 *Time-lapse OM images of ZF/In^{3+} depict the formation of microspheres. Over time, these structures tend to fuse and become larger in size. Surprisingly, no fibrillar structures were obtained even after 60 min.*

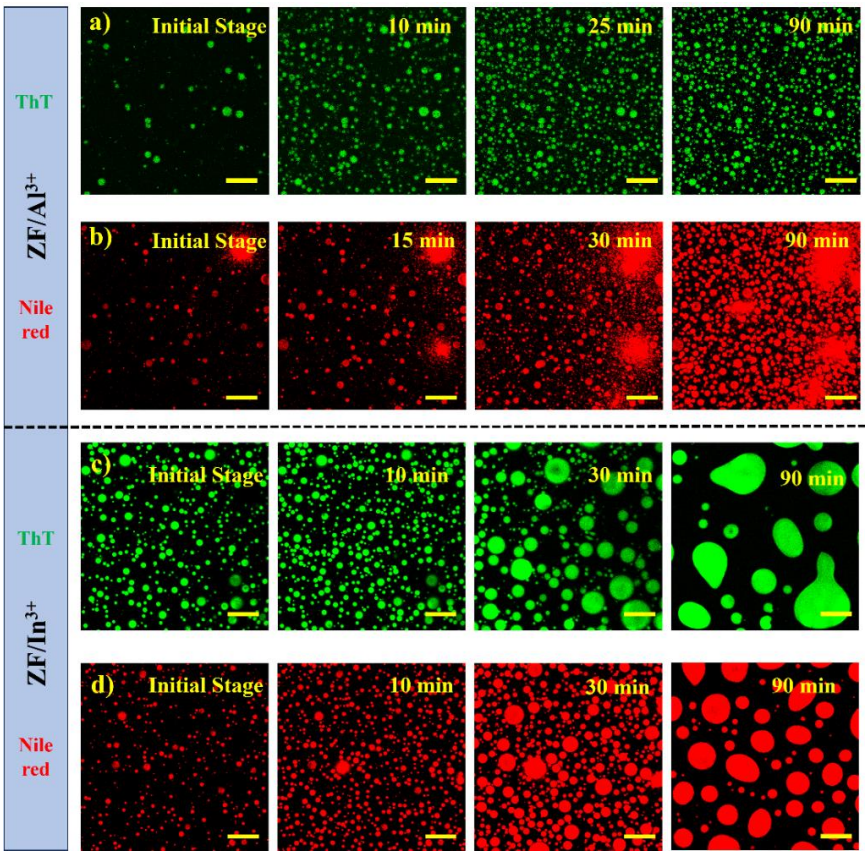

Figure 4.14 *Time-dependent CLSM images of ZF/Al^{3+} self-assembly using (a) ThT and (b) Nile red. With time, more microspheres were obtained as compared to the initial stage. The spheres were stable, and no fibrillar structures were found. Time-dependent CLSM images (snapshots from the live imaging) of ZF/In^{3+} self-assembly using (c) ThT and (d) Nile red. The initially obtained spheres fused with time to form larger spheres, but no fibrillar structures were observed. Scale bar 20 µm.*

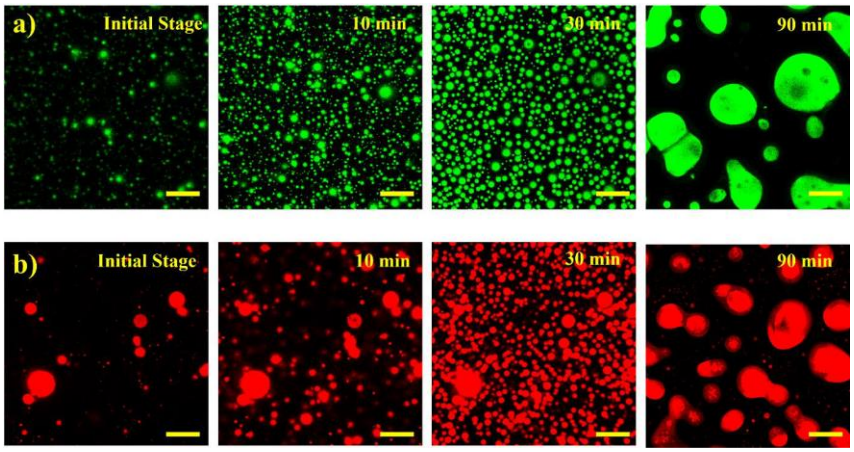

Figure 4.15 *Time-lapse CLSM images of ZF/Ga^{3+} system using (a) ThT and (b) Nile red. Initially, microspheres were formed, and eventually, the fusion of these spherical structures was found with subsequent fusion. The images were taken as snapshots during live imaging at different intervals. Scale bar 20 µm.*

Interestingly, rapid coalescence of microspheres was observed at the later stage for ZF/Ga^{3+} and ZF/In^{3+}. No fibrillar structures were observed in any of the samples, even when the samples were kept and dried after 90 min (**Figures 4.14, 4.15**). These metal ion-induced intermediates were stable even after 1 week (**Figure 4.16**). Furthermore, the previously observed CD pattern of ZF (**Figure 4.1c**) was completely absent in ZF/M^{3+} assemblies (**Figure 4.17**) clearly indicate that these trivalent ions inhibit the fibrillar structures by stabilizing the metastable intermediates for a longer period.

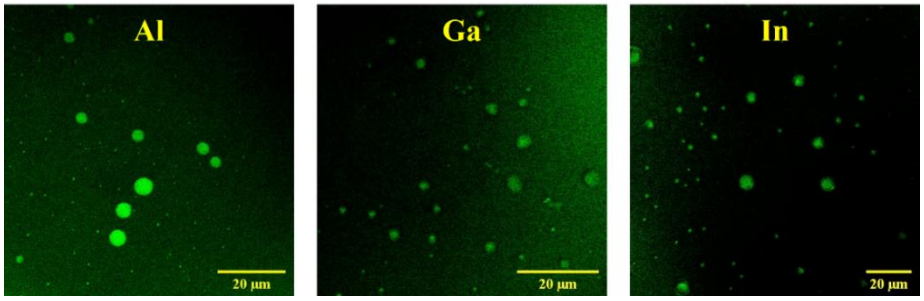

Figure 4.16 *CLSM images of ThT incorporated ZF/Al^{3+}, ZF/Ga^{3+}, and ZF/In^{3+} systems after seven days of incubation.*

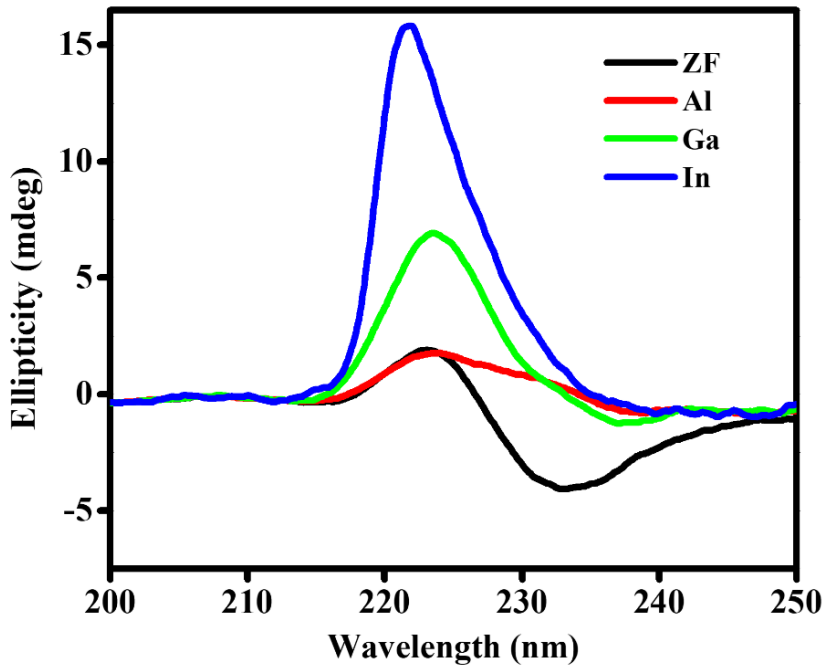

Figure 4.17 *CD spectra of ZF self-assemblies in the presence of trivalent Al^{3+}, Ga^{3+}, and In^{3+} ions.*

4.2.5 Effect of Initial Incubation Temperature on the ZF Self-assembly:

The effect of initial incubation temperature *[53]* on the ZF and ZF/M^{3+} self-assembly was also investigated using turbidity measurements and optical microscopy. We have investigated the thermodynamic and kinetic stability of the metastable intermediates (formed in the absence and presence of trivalent metal ions Al^{3+}, Ga^{3+}, and In^{3+}) at different initial incubation temperatures ranging from 20 ℃ to 80 ℃ for 60 min *[53]*. From the turbidity measurements (absorbance obtained at 500 nm), it was observed that the ZF solutions, in the absence and presence of the mentioned trivalent metal ions, became turbid at all the incubation temperatures (**Figure 4.18**). The turbidity was comparatively less as the incubation temperature was increased. Moreover, the turbidity of blank ZF remained almost intact with respect to time for all the incubation temperatures. Surprisingly, the absorbance values decreased with time for ZF/M^{3+} due to phase separation and sedimentation.

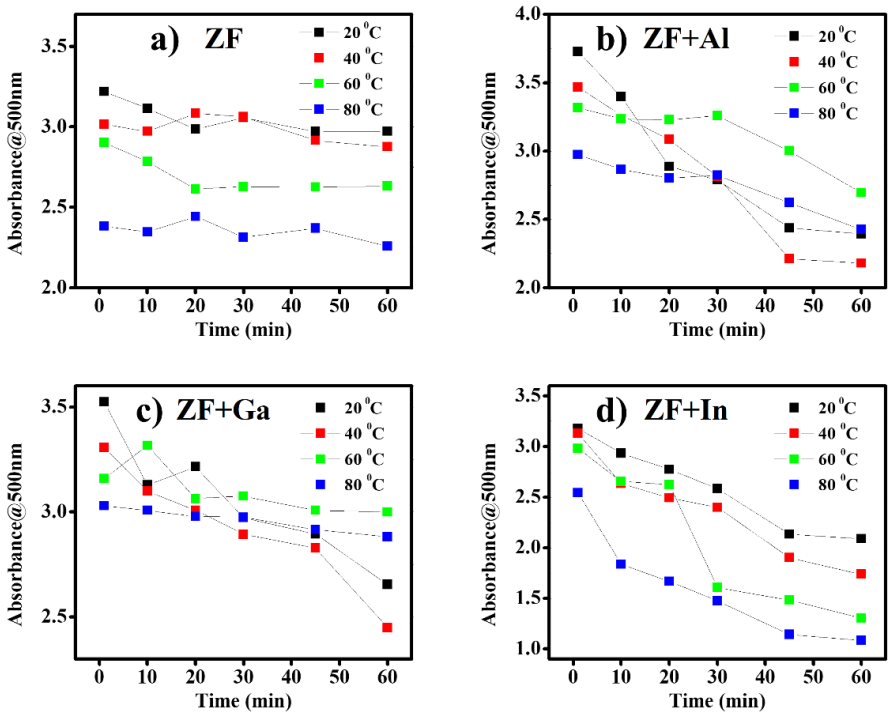

Figure 4.18 *Turbidity was measured (absorbance@500 nm) for 60 min at different initial incubation temperatures for (a) ZF, (b)ZF/Al^{3+}, (c) ZF/Ga^{3+}, and (d) ZF/In^{3+}.*

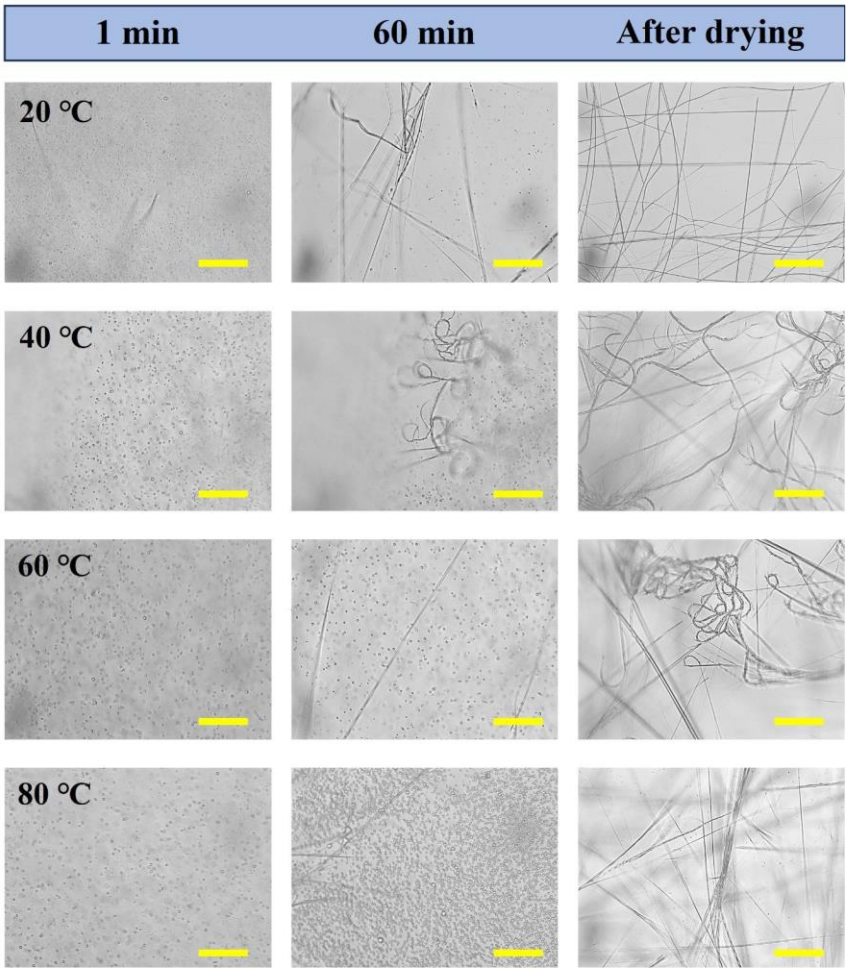

Figure 4.19 *OM images of structural evolution of ZF at different initial incubation temperatures at very initial stage, after 60 min, and after drying. Scale bar 20 µm.*

From the OM images, micro-spherical structures were observed for all the samples at the very initial stage for different incubation temperatures (**Figures 4.19-4.22**). At high temperatures (40, 60, and 80 °C) and after 1h incubation, the spheres increased in size. For blank ZF, we observed the formation of fibrillar structures along with the spheres after 1h of incubation at all the different incubation temperatures (**Figure 4.19**). However, only fibrillar morphology was obtained when the blank ZF samples were dried. We also found out that although the ZF solution incubated at 20 °C turned into hydrogel after 1h, it could not form a gel at higher incubation temperatures (40, 60, and 80 °C).

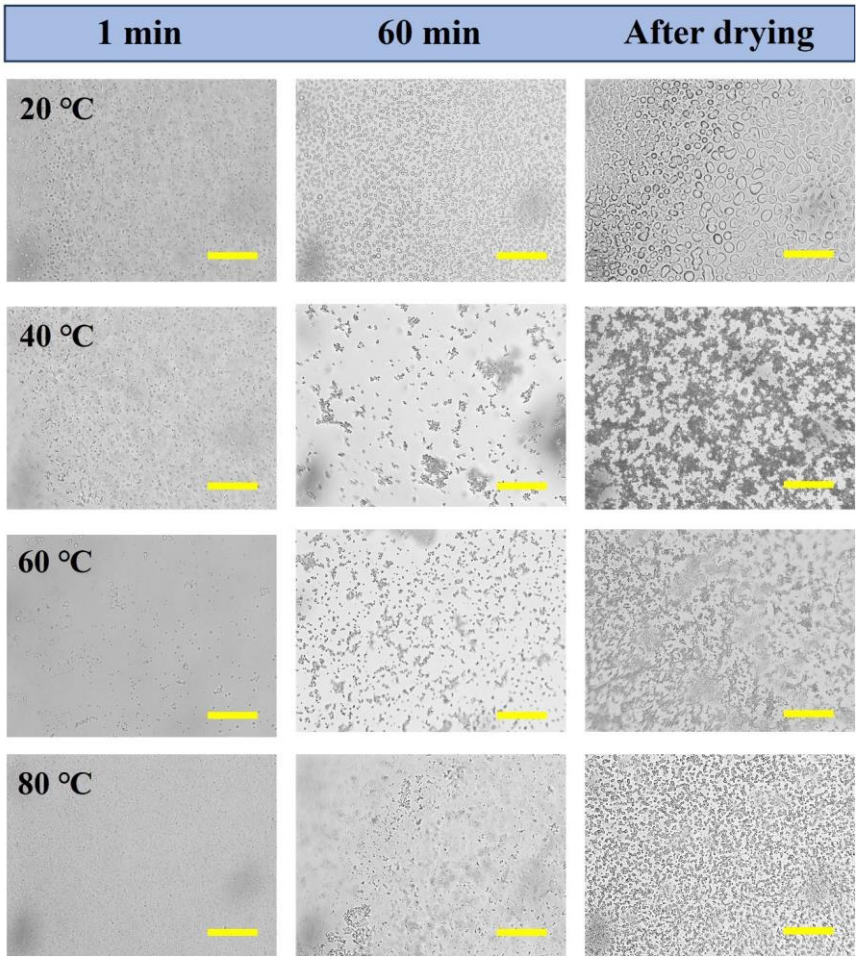

Figure 4.20 *OM images of structural evolution of ZF/Al^{3+} at different initial incubation temperatures at the very initial stage, after 60 min, and after drying. Scale bar 20 μm.*

Surprisingly, the ZF/M^{3+} (M= Al/Ga/In) systems could not form hydrogels even at low temperatures like 20 ℃. From OM images, larger spherical structures were observed in the presence of these metal ions at the initial stages as well as after 1h incubation (**Figures 4.20-4.22**). However, distorted spherical structures and non-fibrillar aggregates were obtained for ZF/Al^{3+} at higher temperatures (40 ℃ and above) (**Figure 4.20**). This is probably due to the violent molecular thermal motions that the structures could not maintain the spherical shape and become deformed *[53]*. Furthermore, non-fibrillar larger spherical vesicles were obtained upon drying all the ZF/M^{3+} samples. This clearly implies that trivalent metal ions strongly inhibit the fibrillation of ZF at

all the different incubation temperatures by stabilizing the metastable intermediate vesicles and suppressing the gelation of ZF.

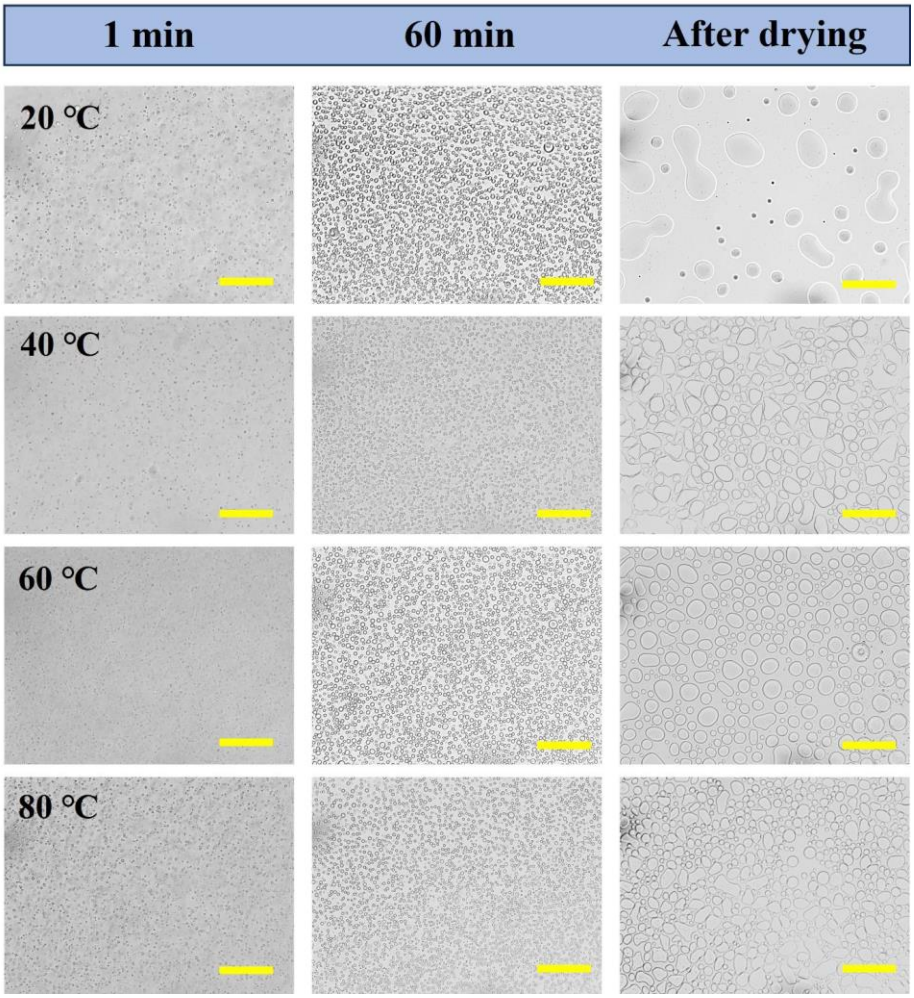

Figure 4.21 *OM images of structural evolution of ZF/Ga^{3+} at different initial incubation temperatures at very initial stage, after 60 min, and after drying. Scale bar 20 μm.*

4.2.6 Exploring the Formation and Unusual Stability of the Intermediates:

We took FTIR data to gain insight into metal ion-ZF coordination that helps the formation of the various intermediates during morphological evolution self-assembly. Characteristic absorption peaks at 3326 cm^{-1} for -OH and at the range 3100-2900 cm^{-1} for -NH and -CH were obtained in solid ZF powder (**Figure 4.23a**) *[54]*. The weakening and broadening of these bands in the ZF self-assembly demonstrate the presence of

multiple intermolecular H-bonding between ZF molecules during the structural transition *[30]*.

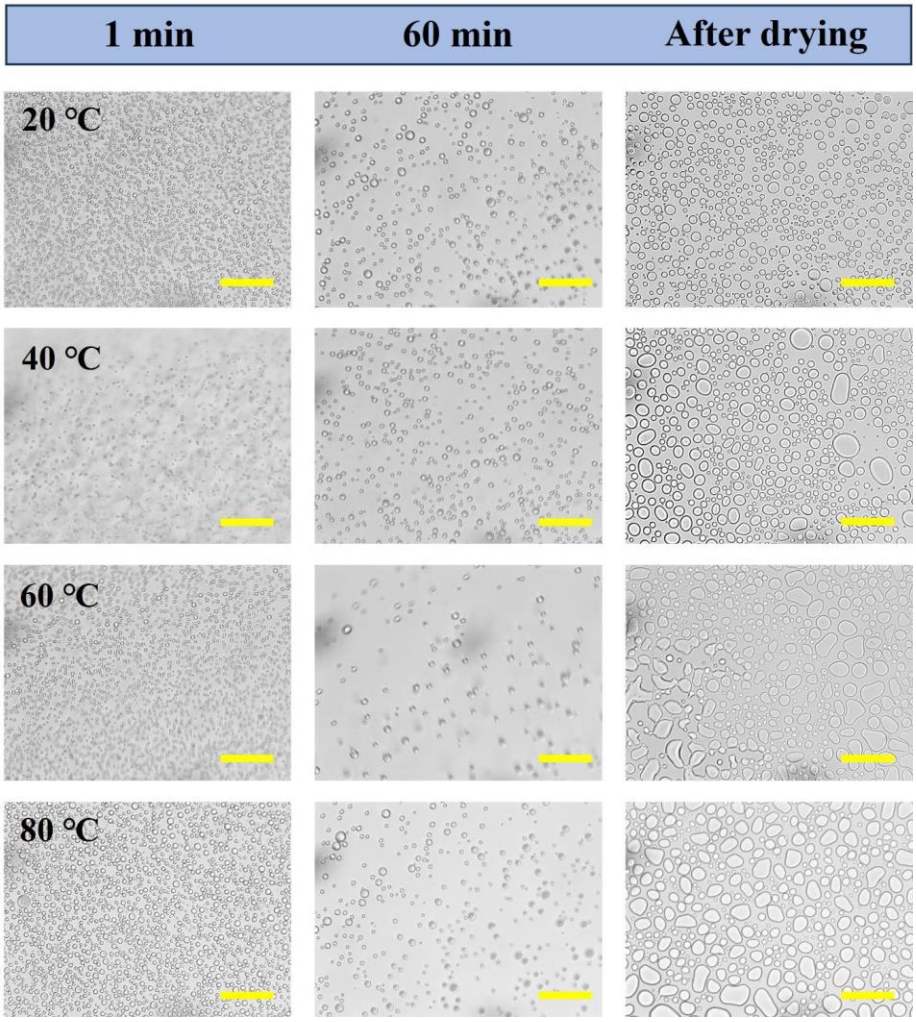

Figure 4.22 *OM images of structural evolution of ZF/In^{3+} at different initial incubation temperature at very initial stage, after 60 min, and after drying. Scale bar 20 μm.*

The weakening of C=O stretching at 1690 cm^{-1} also suggests the role of carbonyl C=O of the carboxylic acid group during assembly formation. The O-H stretching vibration was further broadened when several metal ions (Mg^{2+}, Cd^{2+}, Y^{3+}, La^{3+}, In^{3+}) were added (**Figures 4.23b, c, d**). This indicates that the metal ions coordinate with the hydroxyl from the carboxylic acid group. Additionally, the peak splitting in ZF/Al^{3+} and ZF/Ga^{3+} indicates the occurrence of different modes of interactions (**Figure 4.23e**). The 1700-1500 cm^{-1} region was previously assigned to the stretching vibration of amide I and the bending peak of amide II for dipeptides and Fmoc-protected amino acids *[44,55]*. The stretching

vibration band for carbonyl at 1703 cm^{-1} red-shifted in the presence of metal ions. The band became weak for ZF/Ca^{2+} and ZF/Hg^{2+}, whereas splitting was observed in trivalent metal ions (Y^{3+}, Al^{3+}, Ga^{3+}, In^{3+}). Altogether, the data suggests a better coordination ability of the metal ions with the carbonyl groups of amide and carboxylic acids.

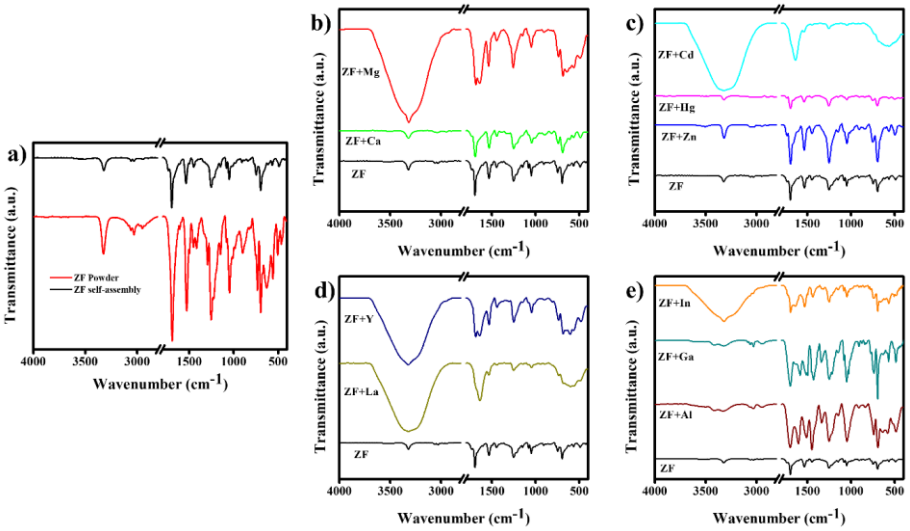

Figure 4.23 *FTIR spectra of (a) the ZF molecule and ZF self-assembly, (b) and (c) in the presence of bivalent metal ions, (d) and (e) in the presence of trivalent metal ions.*

4.2.7 Effect of Surface Charge on the Unusual Stability of the Intermediates:

Despite the IR data providing a better insight into the metal ion-amino acid coordination, it cannot properly explain the specificity of certain metal ions to the formation and stabilization of vesicular structures. Therefore, further study was required to validate the effect of metal ions on the stability of amino acid vesicle-like intermediates. One of the most crucial factors that control the phase behavior of proteins and peptides is the charge modification on the protein surface. Proteins, like BSA, do not show phase separation but can undergo phase separation under the influence of multivalent metal ions *[56]*. So, to quantify the role of metal ions, we measured the zeta potential of the self-assembly with and without metal ions at different time intervals (**Figure 4.24**). At the very initial stages, the high negative surface charge (-30 mV) indicates the colloidal stability of the microspheres. Although the ZF molecule is

predominantly hydrophobic, the rapid change in the surrounding environment due to the addition of water into ethanolic ZF solution during self-assembly can cause ionization/deprotonation of carboxylic acid groups so that water can partially solvate the carboxylate. The carboxylates orient themselves to the outer surfaces of the microspheres, as evident from the negative zeta potential values of the initial ZF spherical aggregates. The structures were stable as long as the zeta potential remained negative. However, with time, the extent of surface charge decreases and reaches almost zero value (-0.21 mV) after 60 min. When the spheres did not bear any net charge, there were enhanced intermolecular interactions driven by strong hydrophobic and π-π interactions that resulted in the aggregation of microspheres and subsequent formation of the fibrillar network. The surface charge neutralization accounts for the morphological transformation from metastable intermediates to thermodynamically stable fibrillar structures.

In the presence of bivalent metal ions (Mg^{2+}, Ca^{2+}, Zn^{2+}, Cd^{2+}, Hg^{2+}) and a few trivalent metal ions (La^{3+} and Y^{3+}), the trend in the zeta potential values did not change much as compared to that of blank ZF, as all the systems showed near-zero charge after 60 min incubation. Surprisingly, upon the addition of trivalent Al^{3+}, Ga^{3+}, and In^{3+}, the positive zeta potential values were obtained from the very initial stages. The zeta values increased with time and became stable (10.61 ± 4.2, 10.92 ± 3.4, 10.84 ± 4 mV, respectively) after 60 min of the incubation period. The unusual stability of the microspheres in presence of Al^{3+}, Ga^{3+}, and In^{3+}, stems from the charge inversion of the amino acid condensates. But, La^{3+} and Y^{3+} were unable to cause the same; therefore, they were unable to stabilize the spherical vesicle-like intermediates against time. One of the plausible reasons is that Y^{3+} can maintain a broad phase-separated regime for BSA protein as compared to Al^{3+} and Fe^{3+} *[38]*, indicating that Y^{3+} has less ability to inverse the charge of a system from negative to positive. It acts as a neutral ion and can only reduce the negative charge to zero value and maintain the broad phase-separated regime.

Further we found a possible trend upon correlating the pK_a of the metal ions *[57]* with the zeta potential of the metal-amino acid systems. The acidic metal ions with lower pK_a values can sufficiently stabilize the intermediates by causing the charge inversion from negative to positive indicating the accumulation of metal ions or their hydroxide on the surface of the spheres through electrostatic attraction *[58]*. Moreover, the addition of acidic metal ions can subsequently lower the pH of the solution. So, the argument may arise whether the pH plays any role in stabilizing the spherical structures. We investigated the ZF self-assembly without any metal ions but lowering the pH. A similar observation to blank ZF self-assembly indicated that only lowering pH cannot stabilize the structures. Therefore, it is safe to conclude that the binding of ZF to the trivalent metal ions greatly enhances the stability of the spherical intermediates.

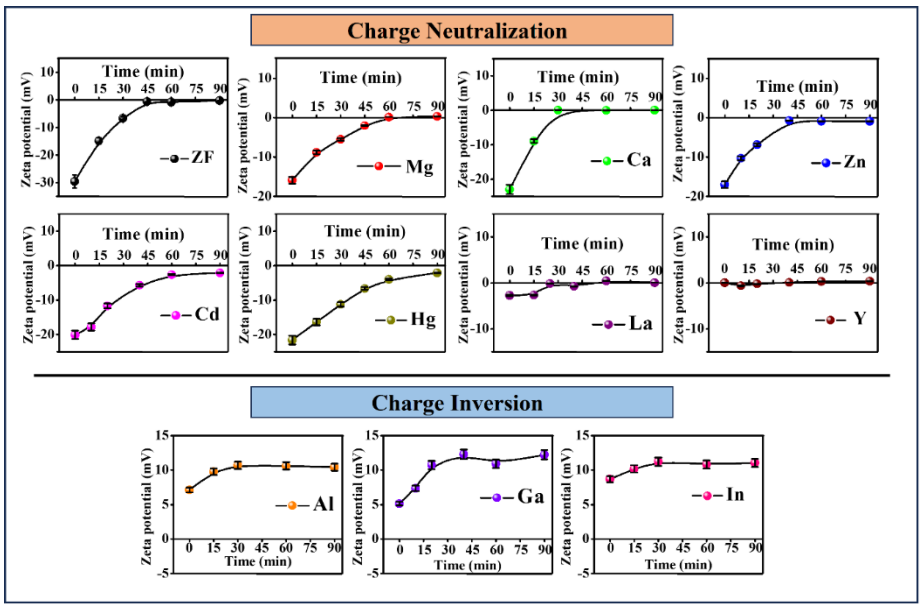

Figure 4.24 *Zeta-potential values of ZF self-assembly in the absence and presence of various metal ions at different time intervals (Error = ±5 %).*

The metal ion binding with amino acid clusters can also be associated with a favorable change in entropy. Before binding, the trivalent metal ion and the carboxylate binding site of ZF microspheres should be surrounded by hydration shells *[59]*. Upon metal binding with the carboxylate group, a large number of water molecules from the

hydration shells are supposed to be released. Other than this factor, the contribution of ion-coordination can be an ion-specific decisive factor. A previous study indicates that when trivalent metal ions induce protein phase separation, it is not solely due to the protein hydration (aggregation of proteins followed by the solvent release) *[60]*. It is to be noted that the trivalent metal ions with lower pK_a can organize more water molecules *[61]*. Therefore, during the binding, they can contribute largely to increase the entropy of the system leading to the extensive stabilization of the metal-bound spheres as observed in this work. Additionally, cation bridges, which are formed between proteins due to the metal ion binding can sufficiently release water molecules and provide additional entropic contributions *[59]*. The excess stability of the spherical intermediates can further be established by the metal ion bridging to the amino acid compartments.

4.2.8 The Effect of Charged Amino Acids on the ZF Self-assembly:

Among many factors, the interactions between aromatic hydrophobic amino acid and charged amino acid residues play a crucial role in the phase-separation process of proteins and peptides *[62]*. We, therefore, studied the effect of charged amino acids on the self-assembly process of the ZF. When an aqueous solution of arginine (Arg) or lysine (Lys) was injected into the ethanolic ZF solution, the solutions became transparent (**Figure 4.25a**) with a very low turbidity level (**Figure 4.25b**). Both the solutions remain in the fluid phase, as observed from the inverted tube. The OM and CLSM images revealed that the number of microspheres was significantly reduced in both ZF/Arg and ZF/Lys systems (**Figures 4.25c, e**) compared to the blank ZF solution. While the ZF/Arg system formed discrete spherical structures, the ZF/Lys transformed into typical fibrillar structures with time.

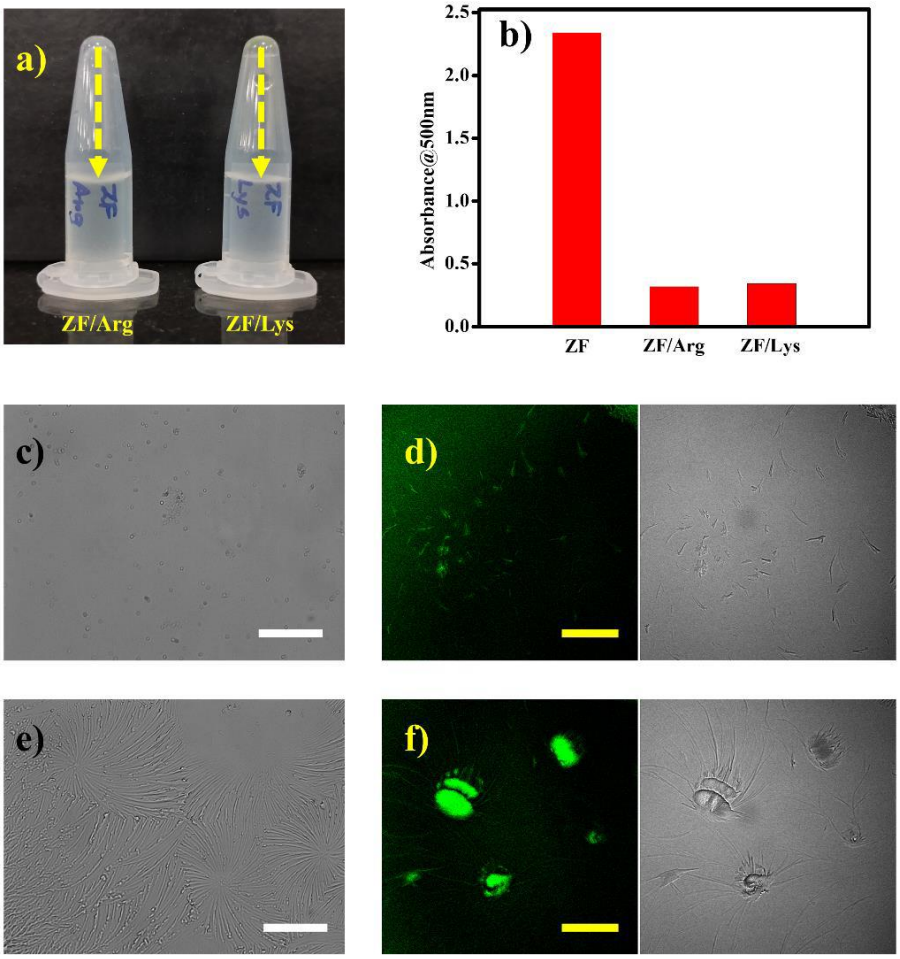

Figure 4.25 *(a) Photographs of ZF/Arg and ZF/Lys self-assemblies showing no hydrogel formation, (b) Turbidity measured at 500 nm comparing ZF self-assembly with ZF/Arg and ZF/Lys, (c) OM and (d) CLSM/Bright field images of ZF/Arg, (e) OM and (f) CLSM/Bright field images of ZF/Lys. Both the CLSM images were taken using ThT dye. Scale bar 20 µm for (c) and (e), 10 µm for (d) and (f).*

Further heterogeneous clusters were obtained for ZF/Arg, and fibrillar morphology was obtained for ZF/Lys after drying the sample (**Figures 4.25d, f**). Since both amino acids (Arg and Lys) contain a net positive charge in the solution, they should interact with ZF in a similar way as metal ions do. Instead, these amino acids strongly inhibited the phase separation of ZF, probably by increasing the solubility of ZF molecules in the solution. It is reported that Arg and Lys can participate in strong cation-π interactions with the aromatic side chains of proteins and peptides *[63]*. If cation-π interactions take place in the present case, it could sufficiently suppress the usual ZF-ZF interaction required for the ZF self-aggregation. This possibility inhibited the usual phase

separation, as reflected in the reduced turbidity of the ZF/Arg and ZF/Lys systems (**Figure 4.25b**). However, the interaction with Arg was found to be stronger compared to that of Lys, as the former can strongly inhibit the fibrillation of ZF. Previous reports have shown that arginine can interrupt protein-protein interactions and increase the solubility of proteins and other solutes *[64,65]*. The presence of the guanidium group is crucial for the Arg to interact with ZF through π- π interaction. This Arg-ZF interaction must have effectively inhibited the usual ZF-ZF-attracting interaction and subsequent fibrillation.

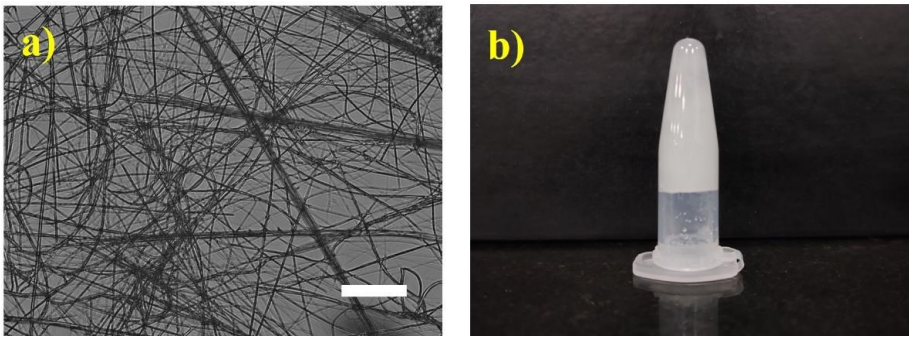

Figure 4.26 *(a) OM image of ZF/Asp; Scale bar 20 μm, (b) Photograph showing hydrogel formation for ZF/Asp.*

We have also investigated the effect of aspartic acid (Asp) on the self-assembly of ZF. It was observed that Asp could not stabilize the intermediates as they transformed into fibrils (**Figure 4.26a**), and subsequent hydrogel formation was observed (**Figure 4.26b**). This is because negatively charged aspartate in the aqueous solution did not interact with the negatively charged ZF microspheres. So, no further alteration in the self-assembly was obtained. We also studied the effect of anions on the ZF self-assembly process. We investigated the aggregation process of ZF in the presence of potassium salts of chloride, carbonate, and phosphate (**Figure 4.27**). In the presence of chloride ions, the turbidity obtained was similar to that of blank ZF assembly. The OM images revealed the presence of microspheres at the initial stages that transformed into fibrillar structures after a certain period of time. Surprisingly, in the presence of carbonate and phosphate salts, the solutions became transparent with low turbidity.

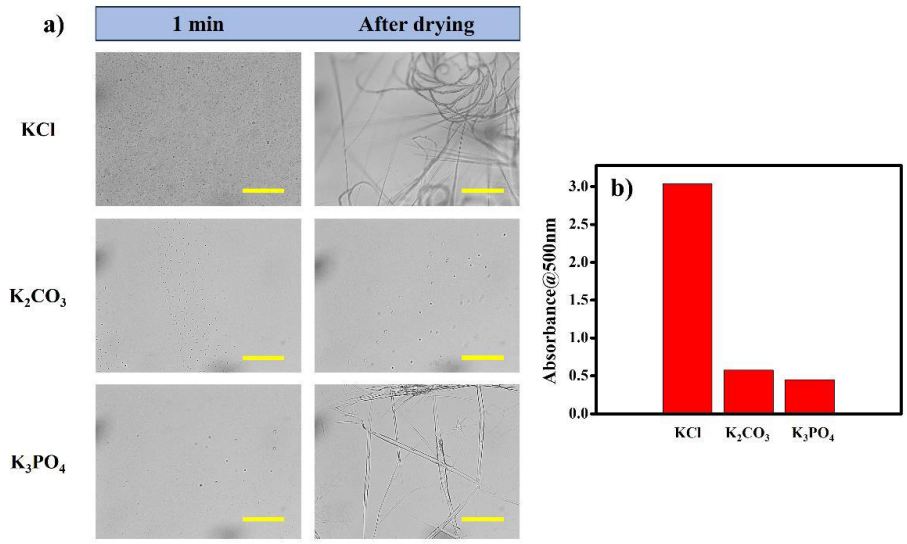

Figure 4.27 *(a) OM images and (b) turbidity measurements of ZF in presence of different anions; Scale bar 20 µm.*

Furthermore, the formation of microspheres was inhibited, and no fibrillar structures were found for ZF/carbonate, whereas some spherical intermediates were obtained for ZF/phosphate that transformed into less dense fibrils. Thus, the basic salts subsequently suppress the droplet formation by enhancing the solubility of ZF. This is due to the basic nature of potassium carbonate and potassium phosphate, and the pH of the solution is enhanced when these salts are added in an aqueous medium. Therefore, ideally, the ZF molecules will carry a net negative charge in the medium, and the electrostatic repulsion between molecules inhibits the self-assembly process. This can further support the observation found in the case of basic amino acids arginine and lysine.

4.3 Conclusion

In summary, we studied the formation of metastable intermediates in the self-assembly process ZF in the presence of several bivalent and trivalent metal ions. The blank ZF was found to form the fibrillar network passing through vesicle-like spherical intermediates after phase separation. The bivalent metal ions like Mg^{2+}, Ca^{2+}, Zn^{2+}, Cd^{2+}, and Hg^{2+} did not affect the fibrillation kinetics. On the contrary, a few specific trivalent metal ions, Al^{3+}, Ga^{3+}, and In^{3+}, were found to stabilize the

early-stage vesicle-type intermediates and completely inhibited the fibril formation. The metal ions-stabilized microspheres did not undergo coalescence and remained stable for more than seven days. The unusual stability of the vesicle-like intermediates in the presence of selective metal ions has been rationalized with the metal ion coordination, metal ion-specific entropy factor, and excess hydrophobicity induced by the trivalent metal ions. Other than these factors, we observed from the time-lapse surface charge measurements that the charge inversion of the microspheres from initial negative to positive values induced by the trivalent metal ions played a governing role in stabilizing the metastable intermediates.

4.4 References

[1] Orgel L. E. (1994), The Origin of Life on the Earth, Sci. Am. 271, 76– 83 (DOI: 10.1038/scientificamerican1094-76)

[2] Orgel L. E. (1998), The Origin of Life - A Review of Facts and Speculations, Trends Biochem. Sci. 23, 491–495 (DOI: 10.1016/S0968-0004(98)01300-0)

[3] Urey H. (1952), On the Early Chemical History of the Earth and the Origin of Life, Proc. Natl. Acad. Sci. U. S. A. 38, 351–363 (DOI: 10.1073/pnas.38.4.351)

[4] Weber S. C., Brangwynne, C. P. (2012), Getting RNA and Protein in Phase, Cell 149, 1188–1191 (DOI: 10.1016/j.cell.2012.05.022)

[5] Mitrea D. M., Kriwacki R. W. (2016), Phase Separation in Biology; Functional Organization of a Higher Order, Cell Commun. Signaling 14, 1–20 (DOI: 10.1186/s12964-015-0125-7)

[6] Pressman A., Blanco C., Chen I. A. (2015), The RNA World as a Model System to Study the Origin of Life, Curr. Biol. 25, R953–R963 (DOI: 10.1016/j.cub.2015.06.016)

[7] Schrum J. P., Zhu T. F., Szostak J. W. (2010), The Origins of Cellular Life, Cold Spring Harb. Perspect. Biol. 2, a002212 (DOI: 10.1101/cshperspect.a002212)

[8] Buddingh' B. C., van Hest J. C. M. (2017), Artificial Cells: Synthetic Compartments with Life-Like Functionality and Adaptivity, Acc. Chem. Res. 50, 769–777 (DOI: 10.1021/acs.accounts.6b00512)

[9] Laflamme G., Mekhail K. (2020), Biomolecular Condensates as Arbiters of Biochemical Reactions inside the Nucleus, Commun. Biol. 3, 773 (DOI: 10.1038/s42003-020-01517-9)

[10] Dzieciol A. J., Mann S. (2012), Designs for Life: Protocell Models in the Laboratory, Chem. Soc. Rev. 41, 79–85 (DOI: 10.1039/C1CS15211D)

[11] Gozen I., Koksal E. S., Poldsalu I. *et al.* (2022), Protocells: Milestones and Recent Advances, Small 18, e2106624 (DOI: 10.1002/smll.202106624)

[12] Wang A., Szostak J. W. (2019), Lipid Constituents of Model Protocell Membranes, Emerging Top. Life Sci. 3, 537–542 (DOI: 10.1042/ETLS20190021)

[13] Mansy S. S., Schrum J. P., Krishnamurthy M. *et al.* (2008), Template-Directed Synthesis of a Genetic Polymer in a Model Protocell, Nature 454, 122–125 (DOI: 10.1038/nature07018)

[14] Meyer C. E., Abram S. L., Craciun I. *et al.* (2020), Biomolecule-Polymer Hybrid Compartments: Combining the Best of Both Worlds, Phys. Chem. Chem. Phys. 22, 11197–11218 (DOI: 10.1039/D0CP00693A)

[15] van Haren M. H., Nakashima K. K., Spruijt E. (2020), Coacervate-Based Protocells: Integration of Life-Like Properties in a Droplet, J. Syst. Chem. 8, 107–120

[16] Yewdall N. A., André A. A. M., Lu T. *et al.* (2021), Coacervates as Models of Membraneless Organelles, Curr. Opin. Colloid Interface Sci. 52, 101416 (DOI: 10.1016/j.cocis.2020.101416)

[17] Donau C., Späth F., Sosson M. *et al.* (2020), Active Coacervate Droplets as a Model for Membraneless Organelles and Protocells, Nat. Commun. 11, 5167 (DOI: 10.1038/s41467-020-18815-9)

[18] Love C., Steinkühler J., Gonzales D. T. *et al.* (2020), Reversible pH-Responsive Coacervate Formation in Lipid Vesicles Activates Dormant Enzymatic Reactions, Angew. Chem. Int. Ed. 59, 5950–5957 (DOI: 10.1002/anie.201914893)

[19] Yuan C., Ji W., Xing R. *et al.* (2019), Hierarchically Oriented Organization in Supramolecular Peptide Crystals, Nat. Rev. Chem. 3, 567–588 (DOI: 10.1038/s41570-019-0129-8)

[20] Wang J., Liu K., Xing R. (2016), Peptide Self-Assembly: Thermodynamics and Kinetics, Chem. Soc. Rev. 45, 5589–5604 (DOI: 10.1039/C6CS00176A)

[21] Sun H., Li Y., Yu S. *et al.* (2020), Hierarchical Self-Assembly of Proteins Through Rationally Designed Supramolecular Interfaces, Front. Bioeng. Biotechnol. 8, 295 (DOI: 10.3389/fbioe.2020.00295)

[22] Haines L. A., Rajagopal K., Ozbas B. *et al.* (2005), Light-Activated Hydrogel Formation via the Triggered Folding and Self-Assembly of a Designed Peptide, J. Am. Chem. Soc. 127, 17025–17029 (DOI: 10.1021/ja054719o)

[23] Rudra J. S., Tian Y. F., Jung J. P. *et al.* (2010), A Self-Assembling Peptide Acting as an Immune Adjuvant, Proc. Natl. Acad. Sci. U. S. A. 107, 622–627 (DOI: 10.1073/pnas.0912124107)

[24] Peressotti S., Koehl G. E., Goding J. A. *et al.* (2021), Self-Assembling Hydrogel Structures for Neural Tissue Repair, ACS Biomater. Sci. Eng. 7, 4136–4163 (DOI: 10.1021/acsbiomaterials.1c00030)

[25] Nguyen P. H., Sterpone F., Derreumaux P. (2022), Self-Assembly of Amyloid-Beta (Aβ) Peptides from Solution to Near In Vivo Conditions, J. Phys. Chem. B 126, 10317–10326 (DOI: 10.1021/acs.jpcb.2c06375)

[26] John T., Martin L. L., Abel B. (2023), Peptide Self-Assembly into Amyloid Fibrils at Hard and Soft Interfaces—From Corona Formation to Membrane Activity, Macromol. Biosci. 23, 2200576 (DOI: 10.1002/mabi.202200576)

[27] Xing Y., Nandakumar A., Kakinen A. *et al.* (2021), Amyloid Aggregation under the Lens of Liquid-Liquid Phase Separation, J. Phys. Chem. Lett. 12, 368–378 (DOI: 10.1021/acs.jpclett.0c02567)

[28] Lipiński W. P., Zehnder J., Abbas M. *et al.* (2023), Fibrils Emerging from Droplets: Molecular Guiding Principles behind Phase Transitions of a Short Peptide-Based Condensate Studied by Solid-State NMR, Chem. Eur. J. 29, e202301159 (DOI: 10.1002/chem.202301159)

[29] Dada S. T., Hardenberg M. C., Toprakcioglu Z. *et al.* (2023), Spontaneous Nucleation and Fast Aggregate-Dependent Proliferation of α-Synuclein Aggregates within Liquid Condensates at Neutral pH, Proc. Natl. Acad. Sci. U. S. A. 120, e2208792120 (DOI: 10.1073/pnas.2208792120)

[30] Yuan C., Levin A., Chen W. *et al.* (2019), Nucleation and Growth of Amino Acid and Peptide Supramolecular Polymers through Liquid-Liquid Phase Separation, Angew. Chem., Int. Ed. 58, 18116–18123 (DOI: 10.1002/anie.201911782)

[31] Levin A., Mason T. O., Adler-Abramovich L. *et al.* (2014), Ostwald's Rule of Stages Governs Structural Transitions and Morphology of Dipeptide Supramolecular Polymers, Nat. Commun. 5, 5219–5227 (DOI: 10.1038/ncomms6219)

[32] Adler-Abramovich L., Vaks L., Carny O. *et al.* (2012), Phenylalanine Assembly into Toxic Fibrils Suggests Amyloid Etiology

in Phenylketonuria, Nat. Chem. Biol. 8, 701–706 (DOI: 10.1038/nchembio.1002)

[33] Do T. D., Kincannon W. M., Bowers M. T. *et al.* (2015), Phenylalanine Oligomers and Fibrils: The Mechanism of Assembly and the Importance of Tetramers and Counterions, J. Am. Chem. Soc. 137, 10080–10083 (DOI: 10.1021/jacs.5b05482)

[34] Banik D., Dutta R., Banerjee P. *et al.* (2016), Inhibition of Fibrillar Assemblies of L-Phenylalanine by Crown Ethers: A Potential Approach toward Phenylketonuria, J. Phys. Chem. B 120, 7662–7670 (DOI: 10.1021/acs.jpcb.6b05209)

[35] Bagchi D., Maity A., De S. K. et al. (2022), Metal-Ion-Induced Evolution of Phenylalanine Self-Assembly: Structural Polymorphism of Novel Metastable Intermediates, J. Phys. Chem. Lett. 13, 10409–10417 (DOI: 10.1021/acs.jpclett.2c02882)

[36] Tao K., Levin A., Adler-Abramovich L. *et al.* (2016), Fmoc-Modified Amino Acids and Short Peptides: Simple Bio-Inspired Building Blocks for the Fabrication of Functional Materials, Chem. Soc. Rev. 45, 3935–3953 (DOI: 10.1039/C5CS00889A)

[37] Basavalingappa V., Bera S., Xue B. *et al.* (2019), Mechanically Rigid Supramolecular Assemblies Formed from an Fmoc-Guanine Conjugated Peptide Nucleic Acid, Nat. Commun. 10, 5256 (DOI: 10.1038/s41467-019-13250-x)

[38] Roosen-Runge F., Heck B. S., Zhang F. *et al.* (2013), Interplay of pH and Binding of Multivalent Metal Ions: Charge Inversion and Reentrant Condensation in Protein Solutions, J. Phys. Chem. B 117, 5777–5787 (DOI: 10.1021/jp401874t)

[39] Yuan C., Xing R., Cui J. *et al.* (2024), Multistep Desolvation as a Fundamental Principle Governing Peptide Self-Assembly Through Liquid–Liquid Phase Separation, CCS Chem. 6, 255–265 (DOI: 10.31635/ccschem.023.202302990)

[40] Tang Y., Bera S., Yao Y. *et al.* (2021), Prediction and Characterization of Liquid-Liquid Phase Separation of Minimalistic Peptides, Cell Rep. Phys. Sci. 2, 100579–100596 (DOI: 10.1016/j.xcrp.2021.100579)

[41] Perween S., Chandanshive B., Kotamarthi H. C. *et al.* (2013), Single Amino Acid Based Self-Assembled Structure, Soft Matter 9, 10141–10145 (DOI: 10.1039/c3sm51054a)

[42] Krysmann M. J., Castelletto V., Kelarakis A. *et al.* (2008), Self-Assembly and Hydrogelation of an Amyloid Peptide Fragment, Biochemistry 47, 4597–4605 (DOI: 10.1021/bi8000616)

[43] Tomar D., Chaudhary S., Jena K. C. (2019), Self-assembly of L-Phenylalanine Amino Acid: Electrostatic Induced Hindrance of Fibril Formation, RSC Adv. 9, 12596–12605 (DOI: 10.1039/C9RA00268E)

[44] Ji W., Yuan C., Zilberzwige-Tal S. *et al.* (2019), Metal-Ion Modulated Structural Transformation of Amyloid-Like Dipeptide Supramolecular Self-Assembly, ACS Nano 13, 7300−7309 (DOI: 10.1021/acsnano.9b03444)

[45] Smith A. M., Williams R. J., Tang C. *et al.* (2008), Fmoc-Diphenylalanine Self Assembles to A Hydrogel via A Novel Architecture based on pi-pi Interlocked Beta-Sheets, Adv. Mater. 20, 37–41 (DOI: 10.1002/adma.200701221)

[46] Shlomo Z., Vinod T. P., Jelinek R. *et al.* (2015), Stacking Interactions by Two Phe Side Chains Stabilize and Orient Assemblies of Even the Minimal Amphiphilic β-Sheet Motif, Chem. Commun. 51, 3154–3157 (DOI: 10.1039/C4CC09673H)

[47] Layek S., Bera N., Nandi P. K. *et al.* (2023), Insights into the Strong Emission Enhancement of Molecular Rotor Thioflavin T in Aqueous Cellulose Nanocrystal Dispersion: White Light Generation in Protein and Micellar Media, Langmuir 39, 8083–8090 (DOI: 10.1021/acs.langmuir.3c00401)

[48] Harel M., Sonoda L. K., Silman I. *et al.* (2008), Crystal Structure of Thioflavin-T Bound to the Peripheral Site of Torpedo Californica Acetylcholinesterase Reveals How Thioflavin-T Acts as a Sensitive Fluorescent Reporter of Ligand Binding to the Acylation Site, J. Am. Chem. Soc. 130, 7856–7861 (DOI: 10.1021/ja7109822)

[49] Babenko V., Dzwolak W. (2011), Thioflavin T Forms a Non-Fluorescent Complex with α-Helical Poly-L-Glutamic Acid, Chem. Commun. 47, 10686–10688 (DOI: 10.1039/c1cc14230e)

[50] Wolfe L. S., Calabrese M. F., Nath A. *et al.* (2010), Protein-Induced Photophysical Changes to the Amyloid Indicator Dye Thioflavin T, Proc. Natl. Acad. Sci. U. S. A. 107, 16863–16868 (DOI: 10.1073/pnas.1002867107)

[51] Wang J., Yuan C., Han Y. *et al.* (2017), Trace Water as Prominent Factor to Induce Peptide Self-Assembly: Dynamic Evolution and Governing Interactions in Ionic Liquids, Small 13, 1702175 (DOI: 10.1002/smll.201702175)

[52] Mayans E., Casanovas J., Gil A. M. *et al.* (2017), Diversity and Hierarchy in Supramolecular Assemblies of Triphenylalanine: From Laminated Helical Ribbons to Toroids, Langmuir 33, 4036–4048 (DOI: 10.1021/acs.langmuir.7b00622)

[53] Zhou P., Xing R., Li Q. *et al.* (2023), Steering Phase-Separated Droplets to Control Fibrillar Network Evolution of Supramolecular Peptide Hydrogels, Matter 6, 1945–1963 (DOI: 10.1016/j.matt.2023.03.029)

[54] Zheng X., Xu K., Wang Y. *et al.* (2018), Study of Hydrogen Explosion Control Measures by Using L-Phenylalanine for Aluminum Wet Dust Removal Systems, RSC Adv. 8, 41308–41316 (DOI: 10.1039/C8RA08587K)

[55] Ma M., Wang T., Liu R. et al. (2023), A Novel Green Amino Acid Derivative Hydrogel with Multi-Stimulus Responsiveness, Colloid Polym. Sci. 301, 569–576 (DOI: 10.1007/s00396-023-05095-0)

[56] Matsarskaia O., Roosen-Runge F., Lotze G. et al. (2018), Tuning Phase Transitions of Aqueous Protein Solutions by Multivalent Cations, Phys. Chem. Chem. Phys. 20, 27214–27225 (DOI: 10.1039/C8CP05884A)

[57] Hawkes S. J. (1996), All Positive Ions Give Acid Solutions in Water. J. Chem. Educ. 73, 516–517 (DOI: 10.1021/ed073p516)

[58] Schubert J., Radeke C., Fery A. *et al.* (2019), The Role of pH, Metal Ions and Their Hydroxides in Charge Reversal of Protein-Coated Nanoparticles, Phys. Chem. Chem. Phys. 21, 11011–11018 (DOI: 10.1039/C8CP05946B)

[59] Matsarskaia O., Braun M. K., Roosen-Runge F. *et al.* (2016), Cation-Induced Hydration Effects Cause Lower Critical Solution Temperature Behavior in Protein Solutions, J. Phys. Chem. B 120, 7731–7736 (DOI: 10.1021/acs.jpcb.6b04506)

[60] Saha R., Mitra R. K. (2022), Trivalent Cation-Induced Phase Separation in Proteins: Ion Specific Contribution in Hydration Also Counts, Phys. Chem. Chem. Phys. 24, 23661–23668 (DOI: 10.1039/D2CP01061E)

[61] Ye X., Capezza A., Xiao X. *et al.* (2021), Protein Nanofibrils and Their Hydrogel Formation with Metal Ions, ACS Nano 15, 5341–5354 (DOI: 10.1021/acsnano.0c10893)

[62] Leshem A. B., Sloan-Dennison S., Massarano T. et al. (2023), Biomolecular Condensates Formed by Designer Minimalistic Peptides. Nat. Commun. 14, 421 (DOI: 10.1038/s41467-023-36060-8)

[63] Krainer G., Welsh T. J., Joseph J. A. *et al.* (2021), Reentrant Liquid Condensate Phase of Proteins is Stabilized by Hydrophobic and Non-

Ionic Interactions. Nat. Commun. 12, 1085 (DOI: 10.1038/s41467-021-21181-9)

[64] Arakawa T., Kita Y., Koyama, A. H. (2008), Solubility Enhancement of Gluten and Organic Compounds by Arginine, Int. J. Pharm. 355, 220–223 (DOI: 10.1016/j.ijpharm.2007.12.009)

[65] Ariki R., Hirano A., Arakawa T. *et al.* (2011), Arginine Increases the Solubility of Alkyl Gallates through Interaction with the Aromatic Ring, J. Biochem. 149, 389–394 (DOI: 10.1093/jb/mvr004)

Chapter 5

Distinct and Dynamic Emission Behavior of Hydrophobic Carbon Dots during the Biomolecular Self-Assembly Process

5.1 Introduction

The self-assembly of biomolecules is a ubiquitous process in nature. It has fascinated the research community over the past few years *[1–3]*. The self-aggregation process of biomolecules allows individual molecules to form supramolecular architectures with various important biological functions *[4,5]*. In this regard, the self-assembly of proteins or peptides is of greater interest because of their biological importance *[6–9]*. Additionally, they have been utilized to serve as a research model to understand the origin of life *[10–12]*. However, their uncontrolled aggregation can lead to the formation of amyloid fibrillar networks, which are associated with several major neurodegenerative diseases like Alzheimer's disease, type II diabetes, Parkinson's disease, and so on *[13–15]*. Thus, the quest for monitoring and understanding the molecular mechanisms governing self-assembly formation is of great urgency.

It was observed that the formation of supramolecular self-assembly proceeds through a series of microscopic steps, including various stages of nucleation events *[16,17]*. During these events, the proteins and peptides undergo phase separation to generate solute-rich and solute-depleted phases *[18–20]*. The solute-rich phases act as nucleation precursors that finally transform into stable fibrillar structures. These membraneless solute-rich condensates of proteins and peptides have also been correlated to fatal diseases *[21,22]*. To monitor the fibrillation process of proteins and peptides, Thioflavin T (ThT) has been widely used as the most common and reliable fluorescent marker *[23–25]* as it shows a massive enhancement in its fluorescent signal upon binding to

amyloid fibrils *[26,27]*. However, ThT itself can promote amyloid aggregation *[28]* and can affect the self-assembly of dipeptides *[29]*. Additionally, the lack of interaction of ThT with amyloid oligomers and protofibrils is also a major disadvantage of using ThT *[30]*. Besides ThT, Nile red has also been used as an amyloid marker *[31]*. However, the lack of solubility in an aqueous medium is a major disadvantage of using this dye. Thus, a different type of fluorescent system with distinct emission behavior in the different steps of the assembly process may be useful in efficiently monitoring the self-assembly kinetics.

A different type of fluorescent marker can be utilized to overcome these issues. In this regard, previous reports suggest that phase-separated peptide condensates can encapsulate large payloads, including nanoparticles *[32,33]*. Therefore, we sought to investigate the self-assembly dynamics of amino acids from initial droplet-like condensates to fibrillar structures by exploiting the emission behavior of carbon-based fluorescent nanoparticles or carbon dots (CDs) encapsulated in the biomolecular compartments. Although several carbon dots have been reported that can inhibit the protein or peptide fibrillation process *[34,35]*. However, monitoring self-assembly dynamics with the progression of time using carbon dots is not available in the literature. Carbon dots (CD), owing to their multicolor photoluminescence, high stability, easy preparation, biocompatibility, and non-toxicity, have several advantages over conventional dyes in applications like bioimaging *[36,37]*, sensors *[38]*, optoelectrical devices *[39,40]*, etc. Therefore, a suitable carbon dot that does not hamper the fibrillation process can be an excellent marker for self-assembly kinetics. To this date, a CD-based sensor that could show distinct emissions, detectable using the naked eye in different stages of the biomolecular self-assembly process, has not been reported. In this context, our previous report on the emission behavior of a carbon dot is very promising (**Scheme 5.1a**) *[41]*. The highly hydrophobic carbon dot (HCD) exhibited distinctly different emission behavior in non-aggregated and aggregated forms due to the restriction of intramolecular rotation (RIR) of the S-S bond. We

successfully exploited the CD's special characteristic to identify different lipid phases.

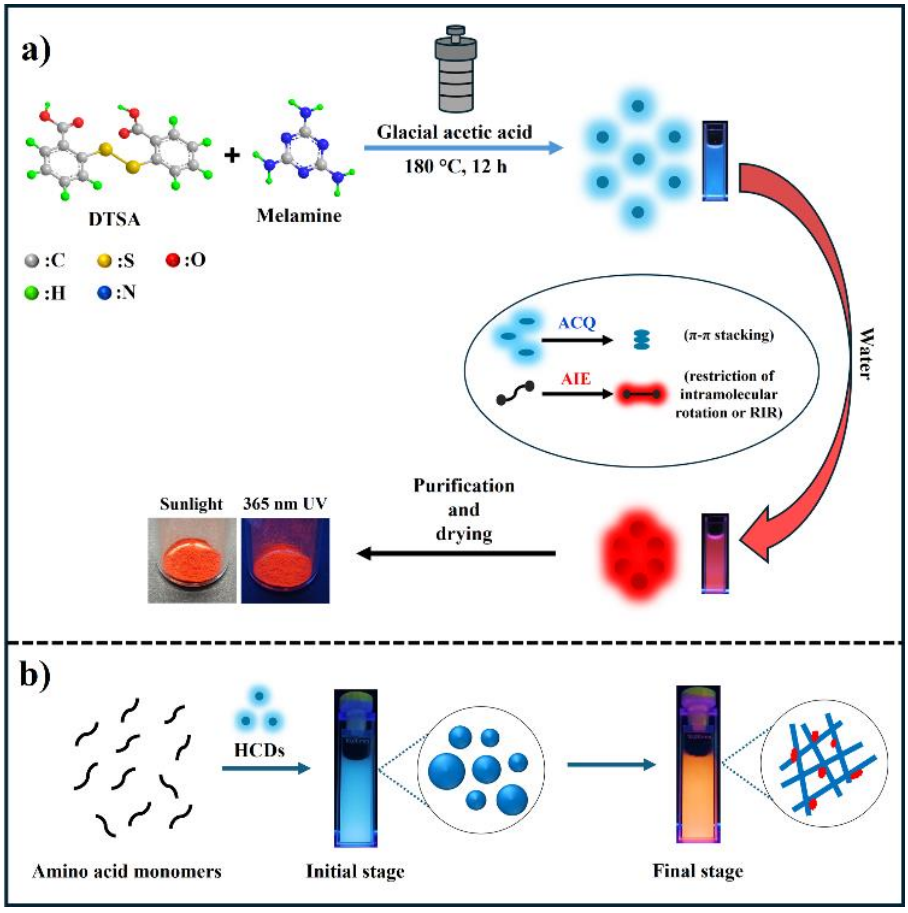

Scheme 5.1 *a) Pictorial representation of the HCD synthesis pathway and the emission principle of the HCD, b) Schematic illustration of the emission behavior of the HCD during the dynamic self-assembly process of the amino acid.*

In this current manuscript, for the first time, we exploit the unique and distinct emission behavior of this HCD in a time-dependent manner to capture the self-assembly dynamics of the amino acid. We demonstrate that the distinct emission of the HCD can be visualized through the naked eye under a UV lamp during the morphological evolution of the amino acid self-assembly. The time-dependent change in the emission profile of the carbon dots can monitor the structural transformation of the amino acid condensates into the fibrillar network (**Scheme 5.1b**). Furthermore, the HCD can also detect microenvironmental changes in the self-assembly kinetics under influential factors like the concentration of amino acids and the presence of multivalent metal ions, which can be observed through the naked eye under a UV lamp.

5.2 Results and Discussion

5.2.1 Synthesis and Characterization of the Hydrophobic Carbon Dot (HCD):

The hydrophobic carbon dots were first prepared by a one-pot solvothermal process using melamine and dithiosalicylic acid (DTSA) in the glacial acetic acid medium *[42]*. The HR-TEM and AFM images of HCDs present a size distribution between 2.5 and 10 nm, with an average size of ~4.25 nm (**Figure 5.1a-c**). HR-TEM also indicates the lattice spacing of 0.221 nm, which corresponds to the (100) plane of graphite, indicating the graphite-like structures *[42]*. The surface functional groups and the chemical structures of the HCD were characterized by the Fourier transform infrared spectroscopy (FTIR) (**Figure 5.2**) and X-ray photoelectron spectroscopy (XPS) (**Figure 5.3**). The FTIR spectra (**Figure 5.2**) show that the surface contains methylene (2966 and 2860 cm^{-1}), S-H (2650 cm^{-1}), amide carbonyl (1668 cm^{-1}), C=C (1456 cm^{-1}), C-N (1407 cm^{-1}), aromatic C-NH (1257 cm^{-1}), C-S (686 cm^{-1}) and S-S (489 cm^{-1}) groups. Additionally, the FTIR spectra of the precursors, i.e., melamine and DTSA, exhibit characteristic peaks for amino (3462 and 3414 cm^{-1}) and hydroxyl (3587 cm^{-1}). However, these hydrophilic groups almost disappeared in HCD after amidation and carbonization, accounting for the hydrophobic nature of the as-prepared carbon dots.

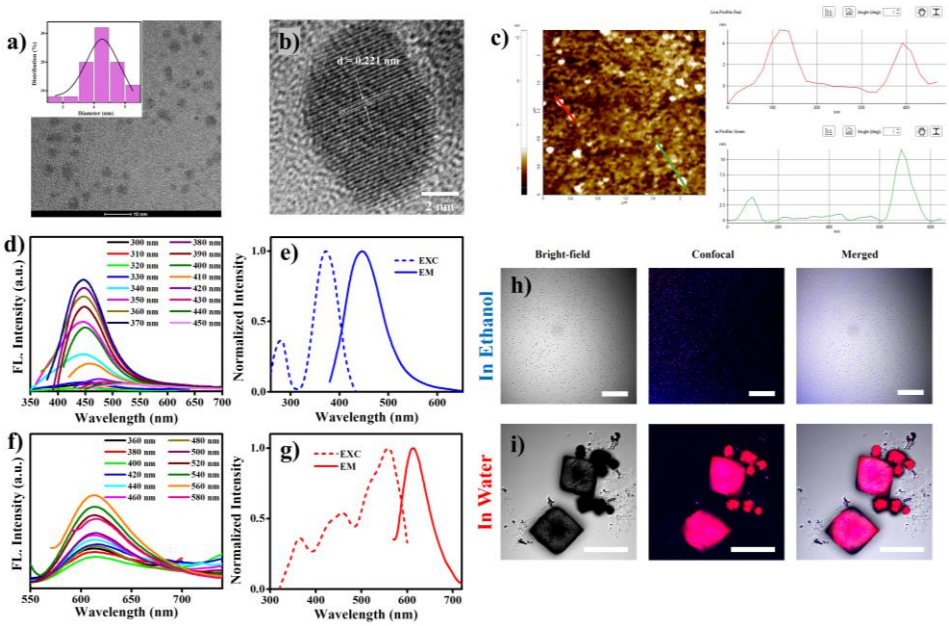

Figure 5.1 *Basic characterization of the HCD. a-b) High-resolution TEM (HR-TEM) image (inset: particle size distribution obtained from the image), c) AFM image with height profiles, Excitation-dependent emission and excitation-emission spectra of HCD in d-e) acetic acid, f-g) solid state, Bright-field, confocal and merged images of HCD in i) ethanol and j) water. The scale bar is 10 nm (a), 2 nm (b), 20 μm (i-j).*

The full XPS spectra (**Figure 5.3**) display five typical peaks at 164.08, 228.08, 284.08, 399.08, and 532.08 eV for S 2p, S 2s, C 1s, N 1s, and O 1s, respectively. This suggests that HCDs contain C, N, O, and S elements, and their atomic ratio was found to be 74.07%, 1.77%, 14.99%, and 9.17%, respectively. The high-resolution XPS spectrum of the C 1s band was deconvoluted into three binding energy peaks, 284.68, 285.29, and 288.78 eV, which are assigned to the C-C/C=C, C-N/C-O, and C=O/C=N, respectively. The O 1s spectra contain two peaks, 531.78 and 533.28 eV, for C=O and COH/ C-O-C band, respectively. The N 1s band exhibits two peaks at 398.28 and 400.08 eV, respectively, which is assigned to the pyridinic C3-N and pyrrolic C2-N-H groups. The S 2p band shows three peaks at 163.58, 164.08, and 164.78 eV, corresponding to the S-C, S-H, and S-S, respectively. Therefore, the spectra indicate the successful incorporation of N and S atoms into the HCDs, and the surface of the HCDs is covered with C, N, O, and S-containing heterocycles.

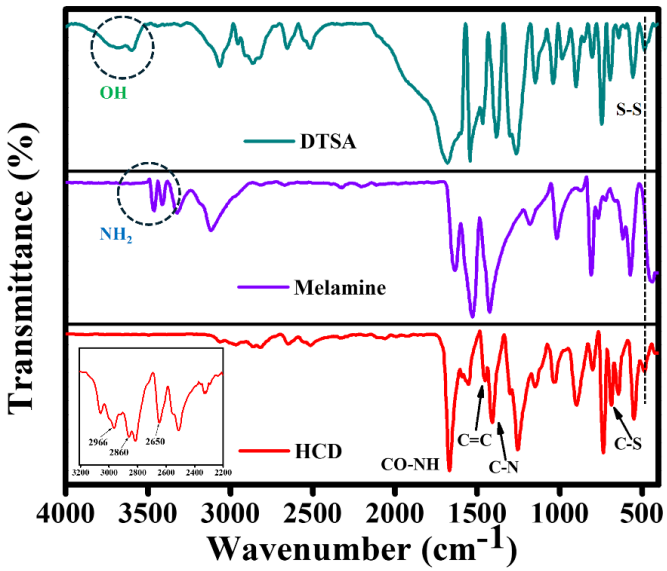

Figure 5.2 *FTIR spectra of DTSA, melamine and HCD.*

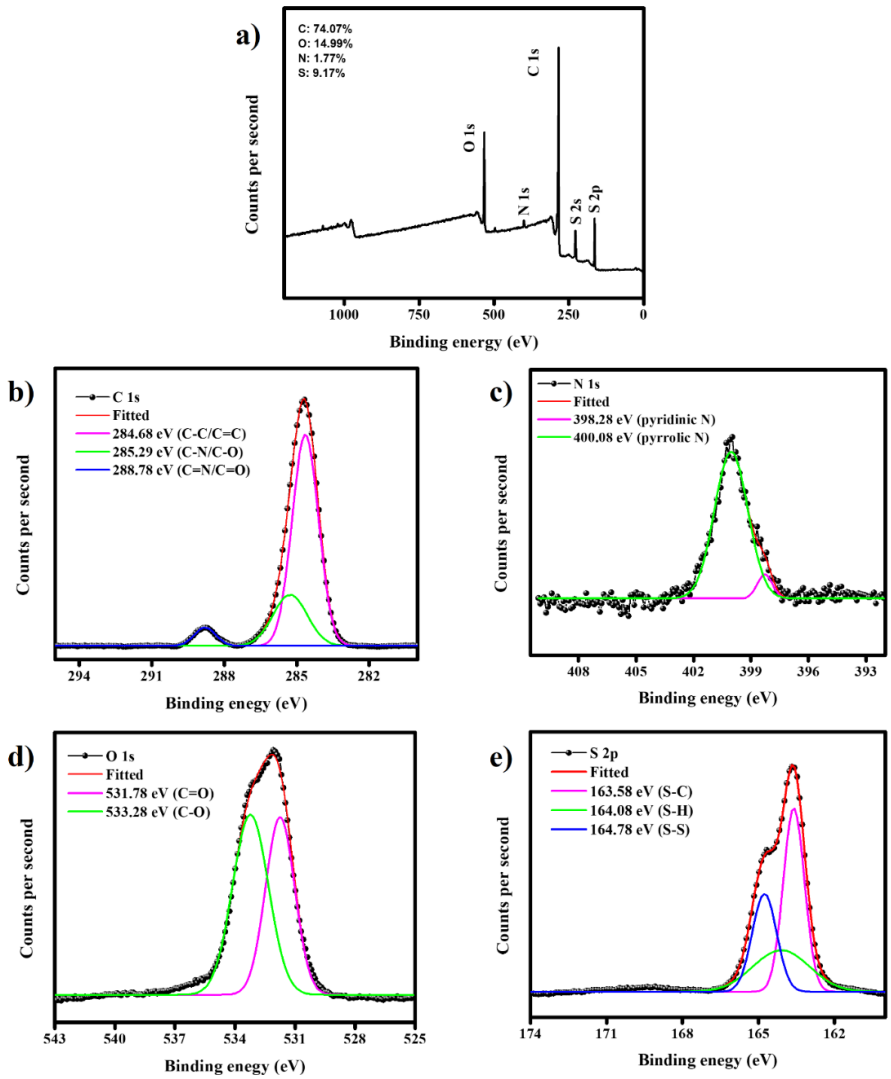

Figure 5.3 *a) XPS spectrum and high-resolution b) C 1s, c) N 1s, d) O 1s, and e) S 2p spectra of HCD.*

5.2.2 Photophysical Properties and Mechanism Behind Distinct Emission Behavior of the HCD:

The as-prepared HCD in acetic acid absorbs at 317 nm, corresponding to the π-π* transitions of the C=C in the graphitized core (**Figure 5.4a**). In other solvents with higher polarity, the absorption of this band decreases, and a broad secondary peak at the 450-550 nm region emerges, with maximum broadening in water. This secondary peak is attributed to the n–π* transitions of the surface states that contain C=O/C=N, C–O, and C−S structures, as reported in the earlier works *[42–44]*. The HCD exhibits a typical excitation-dependent emission feature in acetic acid, with the maximum intensity at 447 nm when

excited at 370 nm (**Figures 5.1d, e**). The quantum yield of HCD in acetic acid is estimated to be 5.82%. The solvent-dependent emission

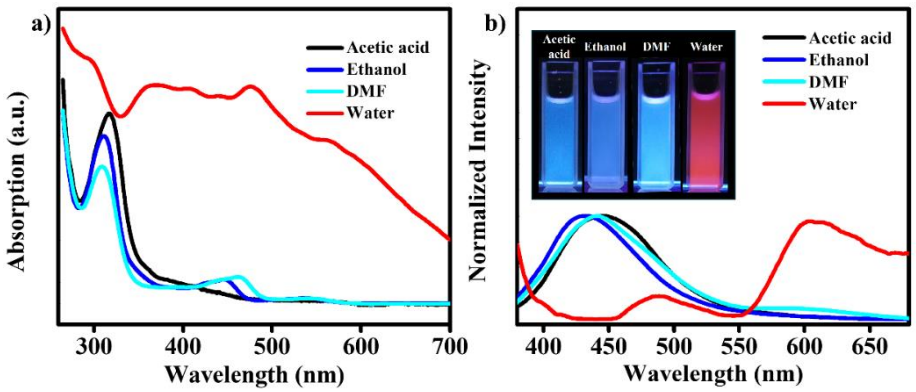

Figure 5.4 *a) UV-vis absorption spectra, b) normalized emission spectra of HCD in different solvents of varying polarity (inset: photographs of the HCD in different solvents using 365 nm UV lamp).*

spectra of HCD revealed a prominent red emission with increasing solvent polarity (**Figure 5.4b**). The appearance of turbidity in the aqueous solution of the HCD indicates an aggregative nature of the carbon dots in the water. This is further supported by the distinct red emission of the HCD powder under different excitation wavelengths, which shows an excitation independence phenomenon with an intense red emission at 610 nm upon excitation at 560 nm (**Figures 5.1f, g**).

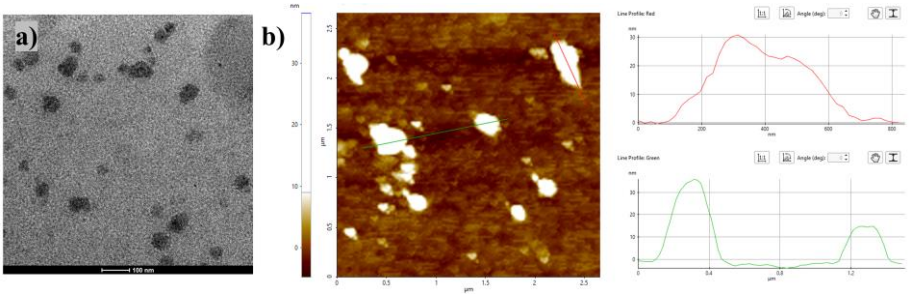

Figure 5.5 *a) TEM and b) AFM image with the height profile of the aggregated HCDs in water medium.*

The excitation-dependent emissions of HCDs in acetic acid solution arise from the graphitized carbon cores, whereas the excitation-independent red emission may arise from the surface states *[44,45]*. The graphitized cores of the carbon dots are responsible for the blue fluorescence, which is dominant in non-polar environments. However, in water, the surface hydrophobicity of the carbon dots drives them to form aggregates, leading to an extensive π-π stacking of the graphitized

cores and results in the quenched blue emission because of ACQ (aggregation-caused quenching). At the same time, the stacked conjugated structures of the aggregates limit the free self-rotation (restriction of intramolecular rotation or RIR) of the disulfide bond, resulting in the red AIE in water similar to the powdered HCD (**Scheme 5.1a**). The HR-TEM and AFM images of HCD in water

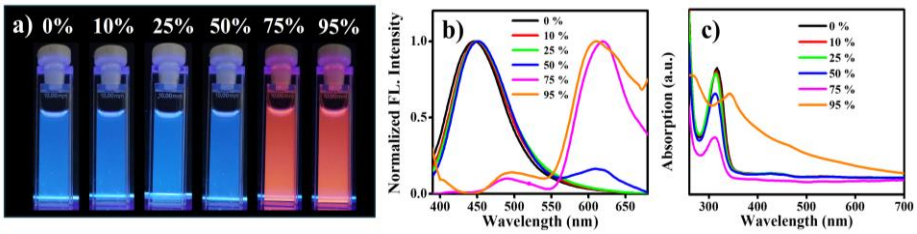

Figure 5.6 *a) Visual images using 365 nm UV lamp, b) fluorescence spectra, and c) absorption spectra of HCD in different water % in ethanol.*

indicate the formation of aggregates (**Figure 5.5**), and the confocal laser scanning microscopy (CLSM) images show the strong red emission from the HCD aggregates in water (**Figures 5.1i, j**). We have also investigated the effect of water fraction by adding water to the ethanolic HCD solution. Visual images (using a 365 nm UV lamp) in **Figure 5.6a** show the emission color of the HCD at different water fractions. HCD in pure ethanol shows blue emission. The emission color remains the same when water accounts for 10-50 %. However, at higher water % (from 75 %), the solutions turned turbid as solid HCD started to separate the solid powder out, resulting in the aggregated state and the red AIE emission. Therefore, the emission intensity gradually increases in the red region with the addition of water (**Figure 5.6b**). The trend in the absorption values (**Figure 5.6c**) with increasing water fraction reveals that with the addition of water, the absorbance at 310 nm decreases. In comparison, a red-shifted absorbance at 450-460 nm appears and continues increasing. In summary, the blue emission dominates in low water fractions, but red AIE emission becomes prominent in higher water content. This trend indicates the presence of strong π-π stacking interactions in HCDs.

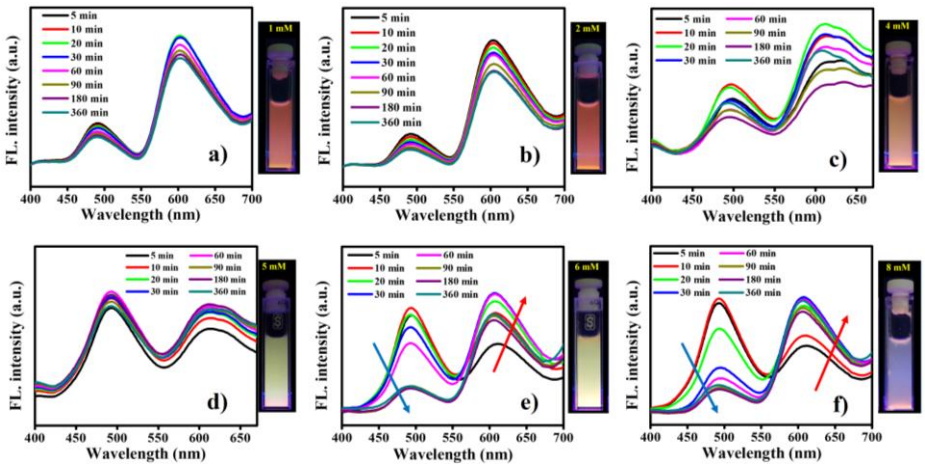

Figure 5.7 *Time-dependent emission behavior of HCD in a) 1 mM, b) 2 mM, c) 4 mM, d) 5 mM, e) 6 mM, and f) 8 mM of ZF. The visual images indicate the emission color at the initial stage of the self-assembly process.*

5.2.3 Distinct Emission Behavior of the HCD During the ZF Self-assembly Process:

Once the study of the photophysical properties of the HCD in conventional solvents was completed, we focused on the utility of the HCDs to capture the self-assembly dynamics of amino acids. We used carboxybenzyl (Z)-protected phenylalanine (ZF) as a model system. We have recently reported the self-aggregation process of ZF that passes through the formation of spherical metastable intermediates and finally transforms into stable fibrillar structures *[46]*. The formation of spherical structures was promoted by enhanced molecular interactions like hydrophobic and π-π interactions between ZF molecules. The spherical aggregates showed high encapsulation efficiency for small aromatic and hydrophobic dyes like ThT and Nile red. However, as mentioned before, using these dyes to monitor the dynamics has its own limitations. Therefore, we seek to encapsulate the HCD into the hydrophobically driven structures and monitor its photophysical changes during the gradual formation of the ZF self-assembly. To do this, we first monitored the emission behavior of the HCD at different ZF concentrations. The emission spectra and visual images (**Figure 5.7)** showed that the 1 and 2 mM ZF solutions were predominantly red emissive (605 nm), and this feature did not change much with time (**Figures 5.7a, b**). This indicates that the carbon dot remains in

aggregated form in the solution at low concentrations of amino acids as there are insufficient hydrophobic compartments of amino acids. Surprisingly, for 4 mM or higher concentrations of ZF, the emission intensities at the blue region were relatively stronger than that of 1 and 2 mM ZF (**Figures 5.7c-f**). Accordingly, the visual images showed a mixture of blue and red emissions, leading to various colorations under the 365 UV lamp, like orange, greenish-yellow, and violet, with increasing ZF concentration. At lower ZF concentrations (1-2 mM), the HCDs would form aggregates in the presence of many water molecules in solutions, explaining the red emission in the 1-2 mM ZF systems. However, when ZF concentration is high (4 mM or higher), the phase separation forms hydrophobic compartments, which would easily sequester the monomeric HCDs through hydrophobic and π-π interactions. As a result, the blue emission of the HCD is predominantly enhanced. Interestingly, the strong blue signal can be observed from the initial stage of the assembly formation at 8 mM ZF. However, with time, the blue emission decreases, and an increment in the signal intensities is observed in the red region. The change in the emission behavior can be accounted for by the dynamic transformation of the turbid solution of solid-like amino acid aggregates into the stable hydrogel. Thus, this carbon dot can be a potential indicator for successfully monitoring the self-assembly dynamics of amino acids.

5.2.4 Time-dependent Distinct Emission Behavior of the HCD During the ZF Self-assembly:

We further measured the emission intensities and lifetime of the carbon dots in a time-dependent manner in 10 mM ZF to gain deeper insight into the environment inside the amino acid aggregates and their structural transformation. **Figure 5.8** reveals that the emission intensities and the lifetimes of blank HCD in the aqueous medium remain the same over time. However, during the self-assembly of ZF, HCD exhibits intense blue emission at ~ 480 nm with a very negligible emission in the red region (~ 600 nm) at the initial stage (**Figure 5.9a**). The blue luminescence can be easily observed with the naked eye using

a UV lamp (**Figure 5.9b**). The turbid solutions started to transform into the hydrogel with the progression of time, following a diminish in the intensity at ~ 480 nm (**Figure 5.9a**, blue arrow). On the other hand, the signal from the red region (~600 nm) became prominent (**Figure 5.9a**, red arrow) with time. Interestingly, the lifetimes of HCD collected at both the blue region (480 nm) and the

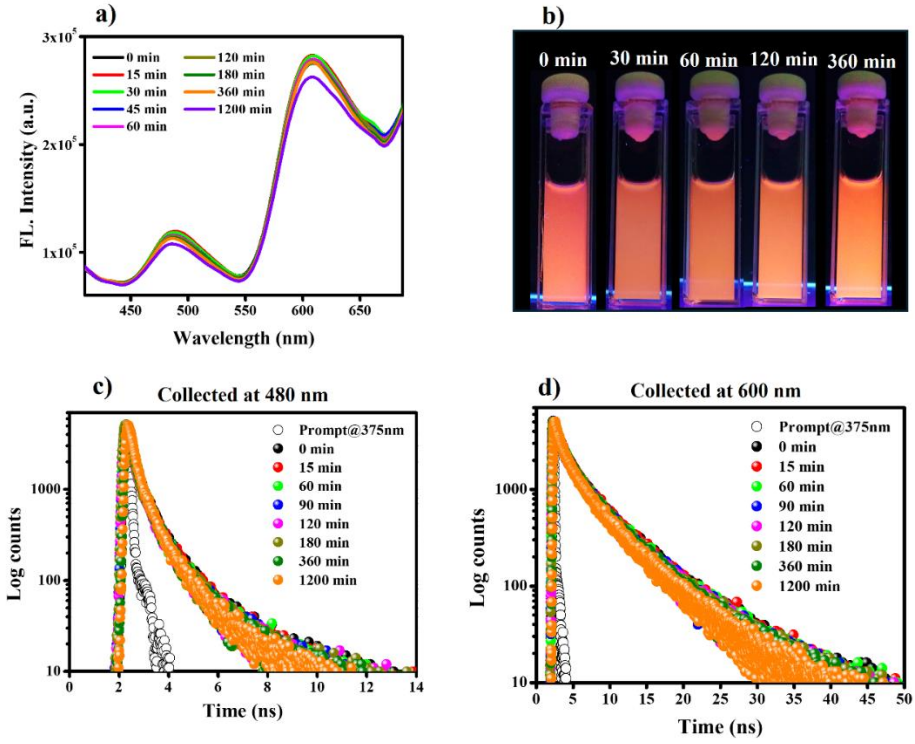

Figure 5.8 *a) Time-dependent emission spectra of the HCD upon excitation at 365 nm, b) photographs of the HCD at different times under a 365 nm UV lamp, Time-resolved decay of HCD collected at c) 480 nm, and d) 600 nm, at different time intervals.*

red region (600 nm) was also enhanced in the HCD-ZF system as compared to the pristine HCD (**Figures 5.9c, d**). This indicates that the HCDs experience a better-confined environment in the amino acid compartments. Surprisingly, with time, the lifetime at 480 nm decreases (**Figure 5.9c**, blue arrow), whereas the lifetime increases at the red region (600 nm, **Table 5.1**) for HCD-ZF (**Figure 5.9d**, black arrow). This observation is attributed to the RIR of the S-S bond of the carbon dots in a more rigid environment with time as the ZF self-assembly transformed into the rigid hydrogel. We have also investigated the emission behavior of a conventional carbon dot, CAY CD (synthesized from citric acid and tyrosine) *[33]* during the ZF self-assembly process.

The blue emission of the CAY CD did not alter much, and we did not observe any distinct emission behavior like that of HCD (**Figure 5.10**). This further supports the notion that the restricted S-S bond of the HCD plays a vital role in exhibiting distinct red emissions.

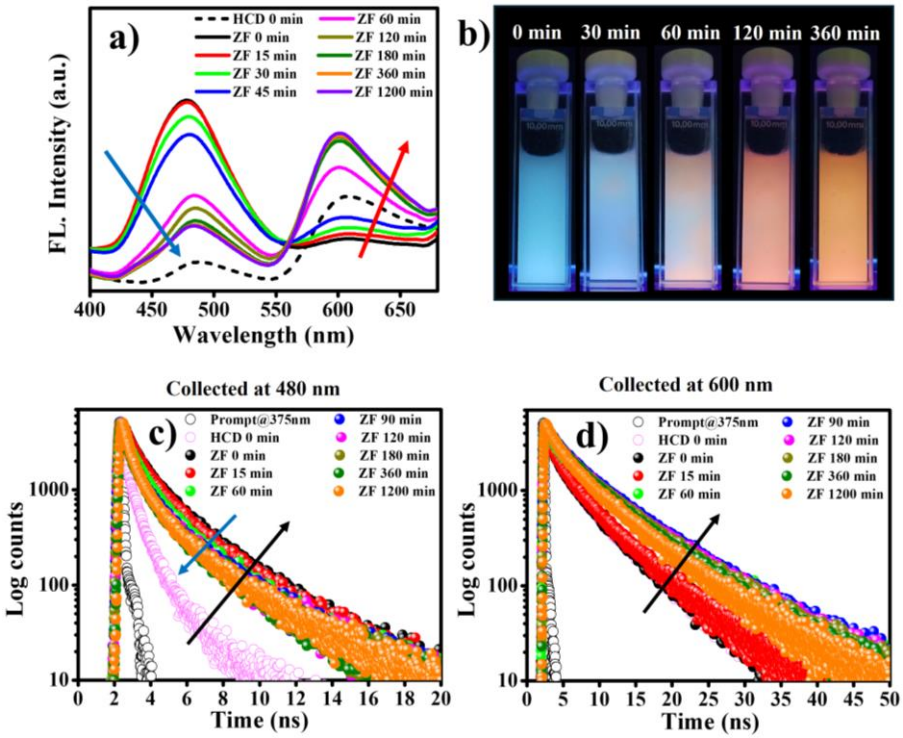

Figure 5.9 *a) Fluorescence spectra of the HCD-ZF with time upon excitation at 365 nm, the blue arrow indicates the decrease and the red arrow indicates the increase in the blue and red emission, respectively, b) visual images of the HCD-ZF at different times under a 365 nm UV lamp, Time-resolved decay of HCD-ZF collected at c) 480 nm, and d) 600 nm, at different time intervals.*

Sample	Incubation Time	χ^2	a_1	τ_1 (ns)	a_2	τ_2 (ns)	a_3	τ_3 (ns)	<τ> (ns)
HCD	0 min	1.042	0.35	2.151	0.20	6.608	0.45	0.385	**2.270**
HCD-ZF	0 min	1.060	0.31	2.460	0.19	6.823	0.50	0.418	**2.276**
	15 min	1.005	0.32	2.434	0.21	6.852	0.48	0.423	**2.391**
	60 min	1.052	0.35	3.329	0.30	8.955	0.35	0.603	**4.081**
	120 min	1.004	0.36	3.654	0.30	9.033	0.34	0.746	**4.640**
	180 min	1.042	0.38	3.854	0.31	8.969	0.31	0.862	**4.503**
	360 min	1.010	0.38	3.688	0.30	8.582	0.33	0.805	**4.212**
	1200 min	1.062	0.38	3.376	0.29	8.231	0.34	0.801	**3.911**

Table 5.1 *Time-dependent lifetime data of HCD in ZF self-assembly collected at 600 nm upon excitation at 482 nm.*

Therefore, in summary, we observed an initial strong blue emission of the HCD eventually turned into a strong red fluorescence when ZF

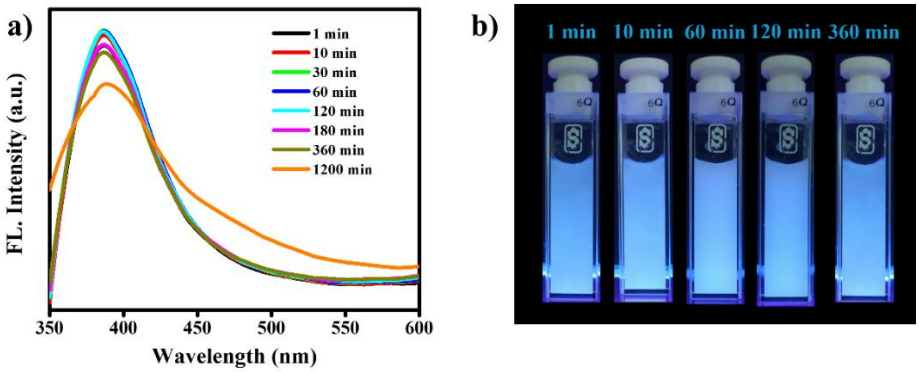

Figure 5.10 *a) Time-dependent emission spectra of CAY CD in ZF self-assembly, b) Visual images at different times under a 365 nm UV lamp.*

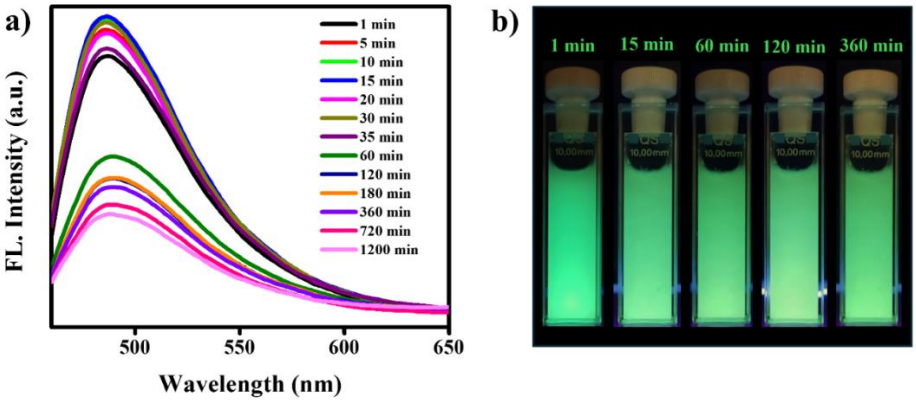

Figure 5.11 *a) Time-dependent emission spectra of ThT in ZF self-assembly, b) Visual images at different times under a 365 nm UV lamp.*

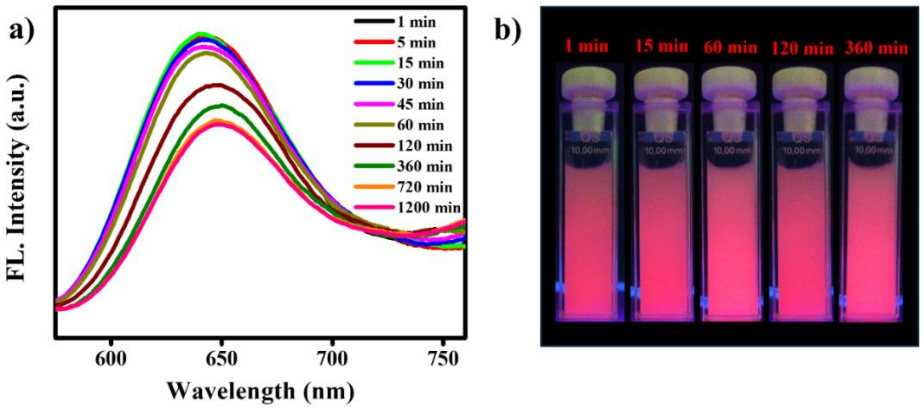

Figure 5.12 *a) Time-dependent emission spectra of the Nile red in ZF self-assembly, b) visual images at different times under a 365 nm UV lamp.*

hydrogel was formed, as the solution transformed into the fibrillar networks with the progression of time. This unique feature of the HCD makes it a more suitable and promising candidate for monitoring the self-assembly dynamics over conventional dyes like ThT and Nile red, as they do not show distinct emission behavior that can be observed with the naked eye (**Figures 5.11 and 5.12**).

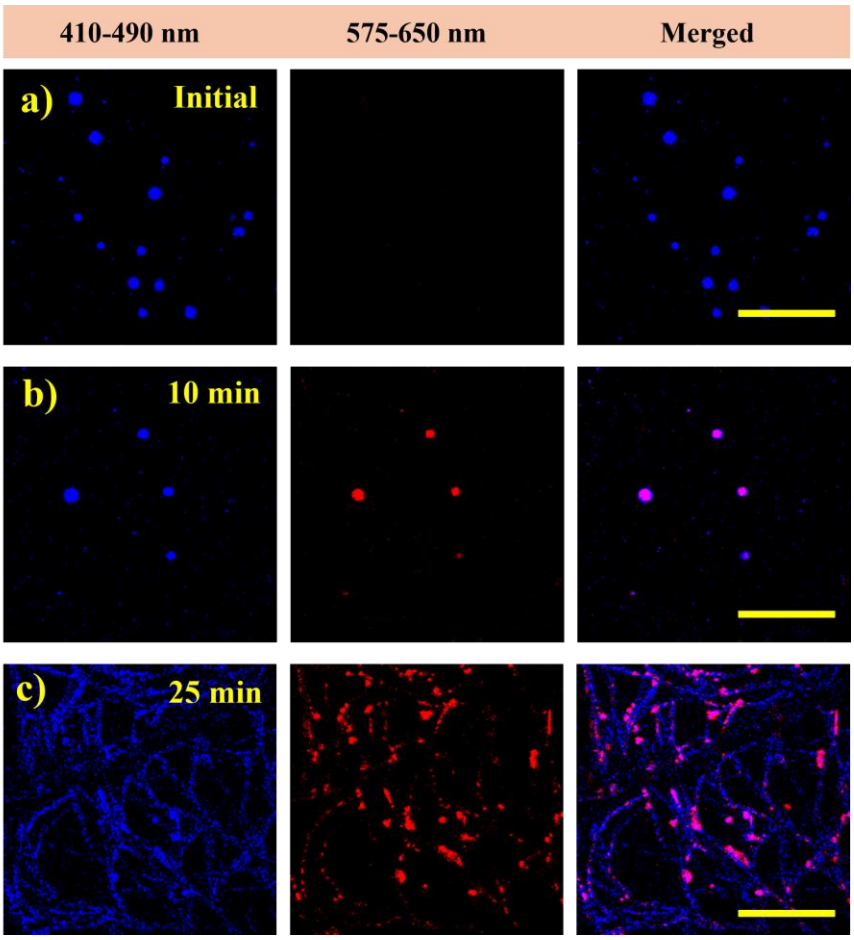

Figure 5.13 *Confocal laser scanning microscopy (CLSM) images of the HCD-ZF self-assembly at a) initial stage, b) after 10 min, and c) after 25 min. The CLSM images were recorded upon excitation at 405 nm with emission filter EM 410/490 (blue) and EM 575/650 (red). The scale bar corresponds to 20 μm.*

We utilized the CLSM imaging technique (λ_{ex} = 405 nm) to observe the morphological transition of the HCD-ZF system. The live CLSM imaging (**Figures 5.13a-c**) affirms the presence of amino acid droplets in the early stage of the assembly formation *[46]*. The encapsulation of the HCDs in the amino acid condensates is confirmed by the significant blue signals from the HCD-ZF assembly at the initial phase. However, we found no signal using the emission filter 575-650 nm (red region) at

this stage. The red signals were observed only in the later stages, and finally, all the spherical structures fused, and fibrillar structures formed after 25 min. The blue emission was observed from the fibrils, whereas some random aggregated red emissive chunks were present along the fibrillar structures. The observation implies that the initially formed hydrophobic amino acid condensates could successfully encapsulate the monomeric carbon dots, as revealed by the strong blue signals. The HCDs partitioning results from hydrophobic and π-π interactions between the carbon dots and aromatic side chain of cbz-phenylalanine (ZF). Some carbon dots formed aggregates during the dynamic structural transformation and fusion of the droplets, hence leading to the enhanced red emission observed within the structures. Since the carbon dots are several nanometers in size, the thin fibrillar structures could only take up the monomeric HCDs, rendering blue emission preferentially within the fibrils. Although it is difficult to explain why there is a gradual decrease in the blue emission (**Figure 5.9a**) using CLSM, it could be due to the partial aggregation of the carbon dots when encapsulated within the fibrils and exposed to water. This would lead to π-π stacking interactions of the graphitized core and eventual quenching of the blue fluorescence *[42, 47]*. HCDs that could not be taken inside the fibrils formed aggregates in contact with the water and could be found on the outer interface adjacent to the fibrils exhibiting strong red emissions.

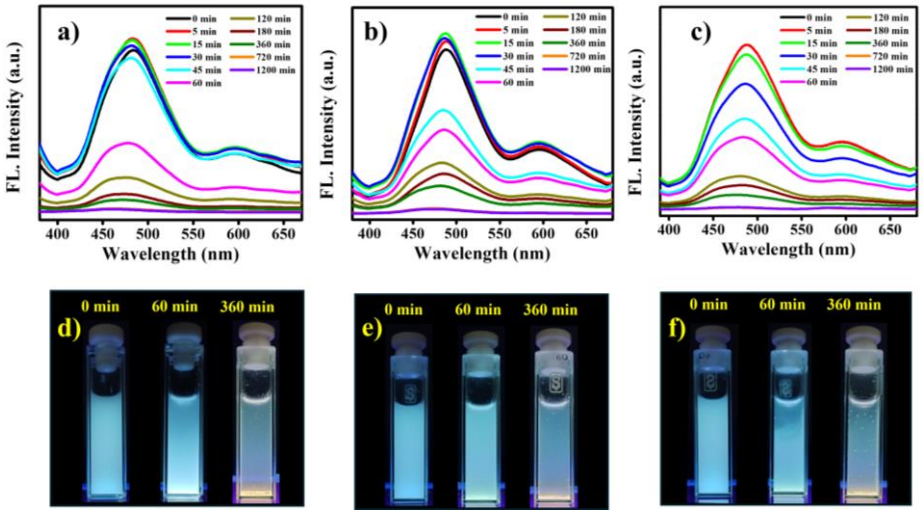

Figure 5.14 *Time-dependent fluorescence spectra HCD in a) ZF/Al^{3+}, b) ZF/Ga^{3+}, and c) ZF/In^{3+} systems upon excitation at 365 nm. Visual images (using the 365 nm UV lamp) of HCD incorporated d) ZF/Al^{3+}, e) ZF/Ga^{3+}, and f) ZF/In^{3+} systems at different time intervals.*

5.2.5 Detection of the Metastable Intermediates using the Distinct Emission of the HCD:

We further envisioned that the blue and red emission of the encapsulated HCDs could be exploited to capture the intermediate states of the amino acid aggregates stabilized by different metal ions *[48]* as these intermediates are more stable compartments and offer more hydrophobic environments. For this purpose, we introduced trivalent metal ions Al^{3+}, Ga^{3+}, and In^{3+}, which are reported to stabilize the metastable droplets through metal-amino acid coordination and surface charge inversion of the initially obtained droplets *[46]*. It was observed that, similar to ZF; the HCDs show blue emission in the metal ion-ZF systems at the initial stage (**Figures 5.14a-c**). Although the intensities at 480 nm are very high compared to that of ZF. This enhanced emission can be attributed to enhanced hydrophobic and π-π interactions experienced by the carbon dots inside the condensates. With time, no alteration in the emission behavior is observed as the red emission signal at ~600 nm remains less prominent (**Figures 5.14d-f**). These distinct emission behaviors of the HCDs in ZF and ZF/M^{3+} systems indicate the presence of more stable hydrophobic environments in metal-induced amino acid compartments. In the case of ZF, a dynamic change in the emission signals is observed (from blue to red), while the stable blue emission persists for metal ions incorporated in ZF. The overall intensity of the HCDs in ZF/M^{3+} decreases after a certain time. This is due to the macroscopic phase separation of the aggregates along with the carbon dots incorporated within the droplets. The phasing out of carbon dots results in quenched fluorescence signals after a certain time. CLSM images indicated strong blue and green signals (using emission filters 410-480 nm and 490-560 nm, respectively) with moderate red emission (emission filter 575-650 nm) from the spherical condensates (**Figure**

5.15). This indicates the incorporation of the HCDs into the structures as negligible signals are obtained from the background.

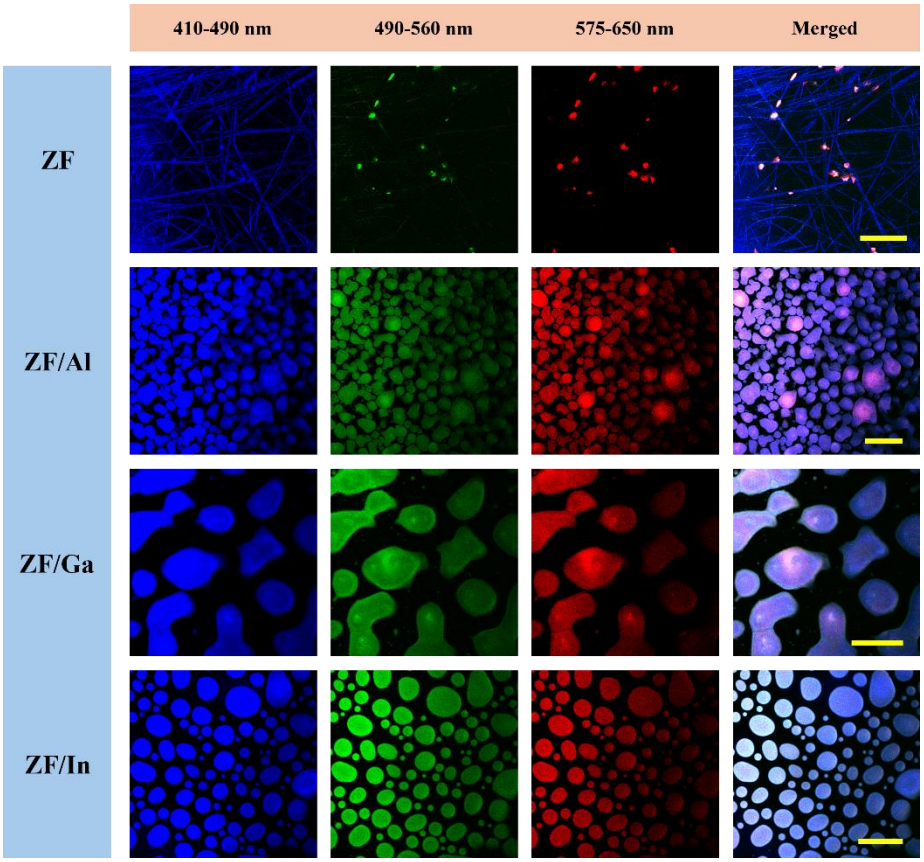

Figure 5.15 *Confocal laser scanning microscopy (CLSM) images of the HCD incorporated ZF, ZF/Al^{3+}, ZF/Ga^{3+}, and ZF/In^{3+}. The CLSM images were recorded upon excitation at 405 nm with emission filter EM 410/490 (blue), EM 490/560 (green), and EM 575/650 (red). The scale bar corresponds to 20 μm.*

Furthermore, the merged images showcase that the overall emission lies in the blue region for the ZF/M^{3+}, confirming the presence of monomeric HCDs inside these hydrophobic compartments. For the HCD-ZF system, red emission can be observed from the small aggregates adjacent to the fibrillar networks. However, for ZF/M^{3+} systems, the HCD shows the red signals within the structures. This may arise due to the formation of some aggregates of HCDs as an inherent property of the HCDs to exhibit red fluorescence in the solid state (as the samples were analyzed after drop casting). Additionally, the red emission of the carbon dots can also be associated with the RIR of the S-S bond due to the incorporation of HCDs into the condensates and immobilization through stronger hydrophobic and π-π interactions inside the compartments. A similar phenomenon was observed earlier when the

RIR of the symmetrical heterocycles of HCDs in the lipid bilayer of the ordered phase rendered the red emission *[41]*.

5.3 Conclusion

In summary, the unique emission behavior of the hydrophobic carbon dot (HCD) was utilized to monitor the self-assembly dynamics of an aromatic amino acid. The HCD exhibits distinct emission behavior in different stages of the amino acid self-assembly process that can be detectable even by the naked eye. The transformation of the amino acids from initial droplet-like spherical structures to hydrogels having fibrillar morphology can be monitored by the striking change in the emission behavior of the HCD in a time-dependent fashion. The HCD exhibits blue emission from the hydrophobic droplets at the initial stages, whereas its emission changes strikingly to red upon forming a fibrillar network in ZF-based hydrogel. Thus, the HCD has the potential to become an excellent biomarker to monitor the self-assembly dynamics of biomolecules. Unlike traditional dyes (like Thioflavin-T, Nile red, etc.), this HCD exhibits widely different emission (blue and red) behavior in different dynamic stages of the self-assembly process, which can be visible to the bare eye under a UV lamp. The carbon dots exhibited stable blue emission in a more hydrophobic environment when we inhibited the fibrillation pathway by incorporating metal ions into the amino acid self-assembly. Thus, the HCD can be developed as a stimuli-responsive tool to monitor the biomolecular self-assembly processes, as well as the change in the microenvironments surrounding the biomolecules.

5.4 References

[1] Schmid S. Y., Lachowski K., Chiang H. T., *et al.* (2023), Mechanisms of Biomolecular Self-Assembly Investigated Through in Situ Observations of Structures and Dynamics, Angew. Chem. Int. Ed. 62, e202309725 (DOI: 10.1002/anie.202309725)

[2] Gong C., Sun S., Zhang Y., *et al.* (2019) Hierarchical nanomaterials via biomolecular self-assembly and bioinspiration for

energy and environmental applications, Nanoscale 11, 4147–4182 (DOI: 10.1039/c9nr00218a)

[3] Petrescu D. S., Zahr O. K., Abu-Baker I., *et al.* (2022), Biomolecular Self-Assembly of Nanorings on a Viral Protein Template, Biomacromolecules 2022, 23, 3407–3416 (DOI: 10.1021/acs.biomac.2c00535)

[4] Wang J., Li H., Xu B., *et al.* (2021), Biological functions of supramolecular assemblies of small molecules in the cellular environment, RSC Chem. Biol. 2, 289–305 (DOI: 10.1039/d0cb00219d)

[5] Okesola B. O., Wu Y., Derkus B., *et al.* (2019), Supramolecular Self-Assembly to Control Structural and Biological Properties of Multicomponent Hydrogels, Chem. Mater. 31, 7883–7897 (DOI: 10.1021/acs.chemmater.9b01882)

[6] Rodrigues de Almeida N., Han Y., Perez J., *et al.* (2019), Design, Synthesis, and Nanostructure-Dependent Antibacterial Activity of Cationic Peptide Amphiphiles, ACS Appl. Mater. Interfaces 11, 2790–2801 (DOI: 10.1021/acsami.8b17808)

[7] Chibh S., Kour A., Yadav N., *et al.* (2020), Redox-Responsive Dipeptide Nanostructures toward Targeted Cancer Therapy, ACS Omega 5, 3365–3375 (DOI: 10.1021/acsomega.9b03547)

[8] Tao K., Xue B., Li Q., *et al.* (2019), Stable and optoelectronic dipeptide assemblies for power harvesting, Mater. Today 30, 10–16 (DOI: 10.1016/j.mattod.2019.04.002)

[9] Sun B., Tao K., Jia Y., *et al.* (2019), Photoactive properties of supramolecular assembled short peptides, Chem. Soc. Rev. 2019, 48, 4387–4400 (DOI: 10.1039/c9cs00085b)

[10] Greenwald J., Kwiatkowski W., Riek R., *et al.* (2018), Peptide Amyloids in the Origin of Life, J. Mol. Biol. 430, 3735–3750 (DOI: 10.1016/j.jmb.2018.05.046)

[11] Tagami S., Li P. (2023), The origin of life: RNA and protein co-evolution on the ancient Earth, Dev. Growth Differ. 65, 167–174 (DOI: 10.1111/dgd.12845)

[12] Frenkel-Pinter M., Samanta M., Ashkenasy G., *et al.* (2020), Prebiotic Peptides: Molecular Hubs in the Origin of Life, Chem. Rev. 120, 4707–4765 (DOI: 10.1021/acs.chemrev.9b00664)

[13] Nguyen Phuong. H., Sterpone F., Derreumaux P., (2022), Self-Assembly of Amyloid-Beta (Aβ) Peptides from Solution to Near In Vivo Conditions, J. Phys. Chem. B 126, 10317–10326 (DOI: 10.1021/acs.jpcb.2c06375)

[14] John T., Martin L. L., Abel B., *et al.* (2023), Peptide Self-Assembly into Amyloid Fibrils at Hard and Soft Interfaces—From Corona Formation to Membrane Activity, Macromol. Biosci. 23, 2200576 (DOI: 10.1002/mabi.202200576)

[15] Ohgita T., Namba N., Kono H., *et al.* (2022), Mechanisms of enhanced aggregation and fibril formation of Parkinson's disease-related variants of α-synuclein, Sci. Rep. 12, 6770 (DOI: 10.1038/s41598-022-10789-6)

[16] Cohen S. I. A., Vendruscolo M., Dobson C. M., *et al.* (2012), From Macroscopic Measurements to Microscopic Mechanisms of Protein Aggregation, J. Mol. Biol. 2012, 421, 160–171 (DOI: 10.1016/j.jmb.2012.02.031)

[17] Knowles T. P. J., Vendruscolo M., Dobson C. M. (2014), The Amyloid State and its Association with Protein Misfolding Diseases, Nat. Rev. Mol. Cell Biol. 15, 384–396 (DOI: 10.1038/nrm3810)

[18] Yuan C., Levin A., Chen W., *et al.* (2019), Nucleation and Growth of Amino Acid and Peptide Supramolecular Polymers through Liquid–Liquid Phase Separation, Angew. Chem. Int. Ed., 58, 18116–18123 (DOI: 10.1002/anie.201911782)

[19] Xing Y., Nandakumar A., Kakinen A., *et al.* (2021), Amyloid Aggregation under the Lens of Liquid–Liquid Phase Separation, J. Phys. Chem. Lett. 12, 368–378 (DOI: 10.1021/acs.jpclett.0c02567)

[20] Rengifo R. F., Sementilli A., Kim Y., *et al.* (2020), Liquid-Like Phases Preorder Peptides for Supramolecular Assembly, ChemSystemsChem 2, e2000007 (DOI: 10.1002/syst.202000007)

[21] Shin Y., Brangwynne C. P. (2017), Liquid Phase Condensation in Cell Physiology and Disease, Science 357, eaaf4382 (DOI: 10.1126/science.aaf4382)

[22] Ray S., Singh N., Kumar R., *et al.* (2020), α-Synuclein Aggregation Nucleates Through Liquid–liquid Phase Separation, Nat. Chem. 12, 705–716 (DOI: 10.1038/s41557-020-0465-9)

[23] Ban T., Hamada D., Hasegawa K., *et al.* (2003), Direct Observation of Amyloid Fibril Growth Monitored by Thioflavin T Fluorescence * 210, J. Biol. Chem. 278, 16462–16465 (DOI: 10.1074/jbc.C300049200)

[24] Sabaté R., Saupe S. J. (2007), Thioflavin T Fluorescence Anisotropy: An Alternative Technique for the Study of Amyloid Aggregation, Biochem. Biophys. Res. Commun. 360, 135–138 (DOI: 10.1016/j.bbrc.2007.06.063)

[25] Naiki H., Higuchi K., Hosokawa M., *et al.* (1989), Fluorometric Determination of Amyloid Fibrils in vitro using the Fluorescent Dye, Thioflavine T, Anal. Biochem. 177, 244–249 (DOI: 10.1016/0003-2697(89)90046-8)

[26] Groenning M. (2010), Binding Mode of Thioflavin T and Other Molecular Probes in the Context of Amyloid Fibrils—Current Status, J. Chem. Biol. 3, 1–18 (DOI: 10.1007/s12154-009-0027-5)

[27] Amdursky N., Erez Y., Huppert D., *et al.* (2012), Molecular Rotors: What Lies Behind the High Sensitivity of the Thioflavin-T

Fluorescent Marker, Acc. Chem. Res. 45, 1548–1557 (DOI: 10.1021/ar300053p)

[28] D'Amico M., Di Carlo M. G., Groenning M., *et al.* (2012), Thioflavin T Promotes Aβ(1–40) Amyloid Fibrils Formation, J. Phys. Chem. Lett. 3, 1596–1601 (DOI: 10.1021/jz300412v)

[29] Tikhonova T. N., Rovnyagina N. N., Arnon Z. A., *et al.* (2021), Mechanical Enhancement and Kinetics Regulation of Fmoc-Diphenylalanine Hydrogels by Thioflavin T, Angew. Chem. Int. Ed. 60, 25339–25345 (DOI: 10.1002/anie.202107063)

[30] Reinke A. A., Abulwerdi G. A., Gestwicki J. E. (2010), Quantifying Prefibrillar Amyloids in vitro by Using a "Thioflavin-Like" Spectroscopic Method, ChemBioChem 11, 1889–1895 (DOI: 10.1002/cbic.201000358)

[31] Mishra R., Sjölander D., Hammarström P. (2011), Spectroscopic Characterization of Diverse Amyloid Fibrils in vitro by the Fluorescent Dye Nile Red, Mol. Biosyst. 7, 1232–1240 (DOI: 10.1039/c0mb00236d)

[32] Kojima K., Tomita S., Kamimura M., Fluorescence Imaging of Nanoparticle Uptake into Liquid-Liquid Phase-Separated Droplets, ChemPlusChem 2023, 88, e202300207 (DOI: 10.1002/cplu.202300207)

[33] Gaash D., Dewan S., Leshem A. B., *et al.* (2023), Modulating the Optical Properties of Carbon Dots by Peptide Condensates, Chem. Commun. 59, 12298–12301 (DOI: 10.1039/d3cc03945e)

[34] Bloch D. N., Zichri S. B., Kolusheva S., *et al.* (2020), Tyrosine Carbon Dots Inhibit Fibrillation and Toxicity of the Human Islet Amyloid Polypeptide, Nanoscale Adv. 2, 5866–5873 (DOI: 10.1039/d0na00870b)

[35] Li S., Wang L., Chusuei C. C., *et al.* (2015), Nontoxic Carbon Dots Potently Inhibit Human Insulin Fibrillation, Chem. Mater. 27, 1764–1771 (DOI: 10.1021/cm504572b)

[36] Xu K. -F., Jia H. -R., Wang Z., *et al.* (2023), See the Unseen: Red-Emissive Carbon Dots for Visualizing the Nucleolar Structures in Two Model Animals and In Vivo Drug Toxicity, Small 19, 2205890 (DOI: 10.1002/smll.202205890)

[37] Jiang L., Cai H., Zhou W., *et al.* (2023), RNA-Targeting Carbon Dots for Live-Cell Imaging of Granule Dynamics, Adv. Mater. 35, 2210776 (DOI: 10.1002/adma.202210776)

[38] Li T., Li X., Zheng Y., *et al.* (2023), Phosphorescent Carbon Dots as Long-Lived Donors to Develop an Energy Transfer-Based Sensing Platform, Anal. Chem. 95, 2445–2451 (DOI: 10.1021/acs.analchem.2c04639)

[39] Hu G., Wang Y., Zhang S., *et al.* (2023), Rational Synthesis of Silane-functionalized Carbon Dots with High-efficiency Full-color Solid-state Fluorescence for Light Emitting Diodes, Carbon 203, 1–10 (DOI: 10.1016/j.carbon.2022.11.048)

[40] An Y., Liu C., Chen M., *et al.* (2023), Solid-State Carbon Dots with Tunable Fluorescence via Surface Substitution: Effect of Alkyl Moieties on Fluorescence Characteristics, ACS Sustain. Chem. Eng. 11, 23–28 (DOI: 10.1021/acssuschemeng.2c06131)

[41] De S. K., Maity A., Bagchi D., *et al.* (2021), Lipid Phase Dependent Distinct Emission Behaviour of Hydrophobic Carbon Dots: C-dot Based Membrane Probes, Chem. Commun. 57, 9080–9083 (DOI: 10.1039/d1CC01941d)

[42] Yang H., Liu Y., Guo Z., *et al.* (2019), Hydrophobic Carbon dots with Blue Dispersed Emission and Red Aggregation-induced Emission, Nat. Commun. 10, 1789 (DOI: 10.1038/s41467-019-09830-6)

[43] Mao X., Zhao X., Hu H., *et al.* (2023), Hydrophobic Carbon Dots with Aggregation-Induced Emission for Multistage Anticounterfeiting, ACS Appl. Nano Mater. 6, 20346–20354 (10.1021/acsanm.3c04391)

[44] Wang Y., Guo R., Wang F., *et al.* (2024), Chiral Aggregation-Induced Emission Carbon Dot-Based Multicolor and Near-Infrared Circularly Polarized Delayed Fluorescence via a Light-Harvesting System, J. Phys. Chem. Lett. 15, 2049–2056 (DOI: 10.1021/acs.jpclett.3c03497)

[45] Chen Y., Zheng M., Xiao Y., *et al.* (2016), A Self-Quenching-Resistant Carbon-Dot Powder with Tunable Solid-State Fluorescence and Construction of Dual-Fluorescence Morphologies for White Light-Emission, Adv. Mater. 28, 312–318 (DOI: 10.1002/adma.201503380)

[46] Bagchi D., Maity A., Chakraborty A. (2024), Metal Ion-Induced Unusual Stability of the Metastable Vesicle-like Intermediates Evolving during the Self-Assembly of Phenylalanine: Prominent Role of Surface Charge Inversion, J. Phys. Chem. Lett. 15, 4468–4476 (DOI: 10.1021/acs.jpclett.4c00444)

[47] Ooyama Y., Yoshikawa S., Watanabe S., *et al.* (2006), Molecular Design of Novel Non-planar Heteropolycyclic Fluorophores with Bulky Substituents: Convenient Synthesis and Solid-state Fluorescence Characterization, Org. Biomol. Chem. 4, 3406–3409 (DOI: 10.1039/b607891e)

[48] Bagchi D., Maity A., De S. K., *et al.* (2022), Metal-Ion-Induced Evolution of Phenylalanine Self-Assembly: Structural Polymorphism of Novel Metastable Intermediates, J. Phys. Chem. Lett. 13, 10409–10417 (DOI: 10.1021/acs.jpclett.2c02882)

Chapter 6

Materials, Methods, and Instrumentation

6.1 Materials

The amino acids, namely L-Phenylalanine, L-Tryptophan, L-Tyrosine, cbz-L-Phenylalanine (ZF), L-arginine (Arg), L-lysine (Lys), and L-aspartic acid (Asp) were purchased from Sisco Research Laboratories. Sodium hydroxide, Tris buffer, Sodium acetate, Citric acid, Acetic acid, Ethanol, DMF, and Milli-Q were purchased from Merck. Thioflavin T (ThT), 4-(2- hydroxyethyl)-1-piperazineethanesulfonic acid (HEPES), Nile red, DTSA, Melamine and the chloride salts (i.e., NaCl, KCl, K_2CO_3, K_3PO_4, $MgCl_2$, $CaCl_2$, $ZnCl_2$, $CdCl_2$, $HgCl_2$, $LaCl_3$, YCl_3, $AlCl_3$, $GaCl_3$, $InCl_3$, and $SnCl_4$) were all purchased from Sigma-Aldrich. All chemicals were used as received without further purification.

6.2 Methods

Chapter 2

6.2.1 Preparation of the Self-Assembly of the Aromatic Amino Acids. Aromatic amino acids phenylalanine (20 mM or ~3.3 mg/mL), and tryptophan (20 mM or ~4 mg/mL) were dissolved in buffer medium (Acetate buffer for pH~5, HEPES buffer for pH~7, Tris buffer for pH~9) and heated to 90 °C for 2 hours to ascertain the monomeric state, followed by gradual cooling of the solution at room temperature for 24 hours without any disturbance, resulting in the formation of amyloid-like fibrillar structure *[1-3]*. For the synthesis of self-assembly/metal ion conjugates, different metal ions were added as their respective chloride salts before incubating at room temperature.

6.2.2 Thioflavin T Fluorescence. The formation and inhibition of fibrillar structure in the solution phase were monitored by measuring the

intensity of Thioflavin T (ThT). The concentration of ThT was maintained at 20 µM for all the samples.

Chapter 3

6.2.3 Preparation of the Self-Assembly of the Phenylalanine. Aromatic amino acid phenylalanine (20 mM or ~3.3 mg/mL) was dissolved in a HEPES buffer medium of pH~7 and heated to 90 °C for 2 hours to ascertain the monomeric state, followed by gradual cooling of the solution at room temperature, which results in the formation of amyloid-like fibrillar structure *[4]*. To synthesize self-assembly/metal ion conjugates, different metal ions were added at a concentration of 5 mM as their respective chloride salts to the pre-heated amino acid solution.

Chapter 4

6.2.4 Preparation of ZF self-assembly. For the formation of ZF self-assembly, typically, the required amount of ZF (~3mg for 10 mM) was dissolved in 50 µL of ethanol to create the molecular reservoir. Then, 950 µL of water was added rapidly to form the self-assembled structures. All the experiments were performed after the rapid mixing. The metal salts were added after they were dissolved in water at a concentration of 5 mM. The metal ion-containing aqueous solution was rapidly added to the ethanolic ZF solution to obtain metal-incorporated ZF assembly.

Chapter 5

6.2.5 Preparation of Hydrophobic Carbon Dots (HCDs). The hydrophobic carbon dots were prepared using the previously reported method *[5]*. Briefly, 100.8 mg melamine and 272 mg dithiosalicylic acid (DTSA) were dissolved into 20 mL acetic acid with ultrasonic treatment. Then, the solution was transferred into a 40 mL Teflon-lined autoclave and kept at 180 °C for 12 h in an air oven. After the solvothermal treatment, the as-prepared HCD solution was added to 1 L of boiled water to form HCD powder, and the residual raw materials and solvent

were washed out. Finally, purified red-colored HCD powder was achieved through vacuum filtration.

6.2.6 Preparation of citric acid-tyrosine carbon dots (CAY CD). The carbon dots were prepared using a previously reported method *[6]*. 2 g of tyrosine and citric acid were mixed in a molar ratio of 6:1 and solubilized in 10 mL water by titrating 32% HCl until the solution became clear. The solution was treated hydrothermally in a Teflon-lined autoclave at 200°C for 17 hours. The formed fluorescent dark solution was purified by centrifugation at 8000 RPM for 15 minutes, filtration of the supernatant via 220 nm Syringe filters, and 2-day dialysis in water. The solution was lyophilized until dried. The dark powder obtained was solubilized in DDW at a 1 mg/ml concentration for further characterization.

6.2.7 Preparation of HCD incorporated ZF self-assembly. The ZF self-assembly was allowed to form according to the protocol previously reported *[7]*. Typically, the required amount of ZF was dissolved in ethanol to create the molecular reservoir, and water was added rapidly to form the self-assembled structures. The amount of ethanol was fixed at 5% (v/v). The HCD and ZF were dissolved in the ethanol before water was added to the ethanolic solution. All the experiments were performed after the rapid mixing. The concentration of metal ions was fixed at 5 mM. The metal ion-containing aqueous solution was rapidly added to the ethanolic ZF-HCD solution to obtain metal-incorporated ZF assembly.

6.3 Instrumentation

6.3.1 Steady-State Fluorescence Measurements. Steady-state fluorescence spectra of all the solutions were recorded using a Fluoromax-4p spectrofluorometer from Horiba JobinYvon (model: FM-100). All fluorescence emission spectra were analyzed using OriginPro 8.1 software. The fluorescence spectra were corrected for the

instrument's spectral sensitivity. We maintained the temperature (T) at 25 °C throughout all experiments.

The fluorescence quantum yield (QY) was estimated relative to Quinine Sulfate (∅_ST) in a water medium by using the following equation:

$$\emptyset_S = \emptyset_{ST}(I_S/I_{ST})(\eta_S^2/\eta_{ST}^2)(A_{ST}/A_S) \quad 6.1$$

Here ∅ is the QY, I is the integrated fluorescence intensity, η is the refractive index of the solvent, and A is the optical density. The subscript "ST" stands for standard, and "S" stands for the sample.

6.3.2 Time-Resolved Fluorescence Measurements. Lifetime measurements of all the solutions were performed by using a picosecond TCSPC (time-correlated single-photon counting) machine from Horiba (Fluorocube-01-NL). We used a filter on the emission side to eliminate the scattered light. The signals were collected at magic-angle (54.75°) polarization by a photomultiplier tube (TBX-07C) detector having an instrument response function of ~560 ps. The data analysis was performed using the IBH DAS Version 6 decay analysis software. In all of the experiments, we maintained the temperature (T) at 25 °C. The decays were fitted with a multi-exponential function.

$$D(t) = \sum_{i=1}^{n} a_i \exp\left(\frac{-t}{\tau_i}\right) \quad 6.2$$

where, $D(t)$ denotes the normalized fluorescence decay and a_i is the normalized amplitude of the decay components τ_i. The quality of the fit was judged by reduced chi-square (χ^2) values and the corresponding residual distribution. The acceptable fit has a χ^2 near unity.

6.3.3 Confocal Laser Scanning Microscopy (CLSM). For the confocal imaging of the samples, we used a confocal microscope from OLYMPUS, model no. IX-83. Multiline Ar laser (gas laser) with a desired excitation wavelength (405, 488, 559 nm). An aliquot of the freshly prepared sample was drop-casted on a clean cover slip and kept in a vacuum desiccator to remove the solvent. Then, the sample-containing cover slip was fixed by a glass slide in a sandwiched manner by using transparent nail polish before imaging. For live imaging, a

particular area of the coverslips containing the samples was monitored for 30 min, followed by monitoring the same area after a certain period of time (at 45 or 90 min). The snapshots from the movies were provided in the figures. ImageJ software was used to process all the images with linear adjustments of brightness and contrast. All imaging studies were performed at room temperature.

6.3.4 Field Emission Scanning Electron Microscopy (FESEM). The field emission scanning electron microscopic study was performed by using a JEOL-7610 F Plus in Chapter 2 and a ZEISS Supra55 field-emission scanning electron microscope in Chapter 3. The freshly prepared solutions were dried on glass slides under the vacuum and coated with gold for FESEM analysis with an opening voltage of 5-10 kV.

6.3.5 Turbidity assay. The turbidity was measured by the absorption at 500 nm for the samples, recorded using a Varian UV−vis spectrophotometer (Cary 100 Bio) in a quartz cuvette (10×10 mm^2).

6.3.6 Circular dichroism (CD) Spectroscopy. CD spectra were recorded at 25 °C using a JASCO J-815 spectropolarimeter. The spectra were recorded in a quartz cell (path length: 1 mm) within the 250-200 nm range with a data pitch of 0.1 nm. The bandwidth was set at 1 nm, the scanning speed was 20 nm min^{-1}, and the response time was 1 s. Before running the sample, respective solvent systems were run to correct the baseline.

6.3.7 Optical Microscopy (OM). For time-lapse optical microscopy imaging, an aliquot of the freshly prepared sample was drop-casted on a clean coverslip, and the experiments were performed. All the samples were visualized using the Dewinter Crown Trinocular microscope.

6.3.8 Fourier transform infrared (FTIR) Spectroscopy. Fourier transform infrared (FTIR) spectra (range: 4000 to 400 cm^{-1}) were conducted on the BRUKER ALPHA II instrument, and background compensation with air was performed before recording experimental sample spectra.

6.3.9 Zeta Potential Measurements. The zeta potential of the ZF solutions with or without metal ions was measured using a Nano Plus particle size analyzer (NanoPlus-3 model). An aliquot of the sample was injected into the capillary chamber, and the zeta potential was measured. Surfactants and Milli-Q water were used to clean the capillary chamber after each measurement. Each sample was measured three times for better reproducibility of the result.

6.3.10 High-resolution transmission electron microscopy (HR-TEM). High-resolution transmission electron microscopy images were taken by using a field emission gun transmission electron microscope (Model: Tecnai G2, F30) with an acceleration voltage of 300 kV. The diluted solutions of the samples were dried on a carbon-coated copper grid by slow evaporation in the air at room temperature before measurements.

6.3.11 Atomic Force Microscopy (AFM). AFM images were recorded to characterize the carbon dots in tapping mode using the NX-10 PARK system. The samples were dropcast on a freshly cleaved mica surface and dried under vacuum.

6.3.12 X-ray Photoelectron Spectroscopy (XPS). The XPS measurements were conducted using the Thermofisher Nexsa XPS instrument. Spectra were acquired using the Al-Kα monochromatic X-ray source. The vacuum pressure in the analyzing chamber was maintained at ~1x10-7 mbar during the acquisition process. The survey spectra were collected with a pass energy of 200 eV with a dwell time of 10 ms.

6.4 References

[1] Zaguri D., Kreiser T., Shaham-Niv S. *et al.* (2018), Antibodies towards tyrosine amyloid like fibrils allow toxicity modulation and cellular imaging of the assemblies, Molecules 23, 1273 (DOI: 10.3390/molecules23061273)

[2] Shaham-Niv S., Rehak P., Vuković L. *et al.* (2017), Formation of apoptosis-inducing amyloid fibrils by tryptophan, Isr J Chem 57, 729−737 (DOI: 10.1002/ijch.201600076)

[3] Adler-Abramovich L., Vaks L., Carny O., *et al.* (2012), Phenylalanine assembly into toxic fibrils suggests amyloid etiology in phenylketonuria, Nat Chem Biol 8, 701−706 (DOI: 10.1038/nchembio.1002)

[4] Bagchi D., Maity A., De S. K. *et al.* (2021), Effect of metal ions on the intrinsic blue fluorescence property and morphology of aromatic amino acid self-assembly, J. Phys. Chem. B 125, 12436–12445 (DOI: 10.1021/acs.jpcb.1c07392)

[5] Yang H., Liu Y., Guo Z., *et al.* (2019), Hydrophobic Carbon dots with Blue Dispersed Emission and Red Aggregation-induced Emission, Nat. Commun. 10, 1789 (DOI: 10.1038/s41467-019-09830-6)

[6] Gaash D., Dewan S., Leshem A. B., *et al.* (2023), Modulating the Optical Properties of Carbon Dots by Peptide Condensates, Chem. Commun. 59, 12298–12301 (DOI: 10.1039/d3cc03945e)

[7] Bagchi D., Maity A., Chakraborty A. (2024), Metal Ion-Induced Unusual Stability of the Metastable Vesicle-like Intermediates Evolving during the Self-Assembly of Phenylalanine: Prominent Role of Surface Charge Inversion, J. Phys. Chem. Lett. 15, 4468–4476 (DOI: 10.1021/acs.jpclett.4c00444)

Chapter 7

Conclusion and Future Aspects

7.1 Conclusion

In this thesis, we have discussed the effects of different external stimuli, like the presence of bivalent and trivalent metal ions, pH, temperature, etc., on the self-assembly process of aromatic amino acids. Our study demonstrates that the usual fibrillation of aromatic amino acids, phenylalanine, and tryptophan, gets affected by the presence of metal ions having higher charge-to-radius ratio. The inhibition of the large fibrillation of aromatic amino acids and the formation of small nonfibrillar aggregates is attributed to the extensive clusterization of amino acids that takes place due to dehydration and enhanced hydrophobic interaction in the presence of metal ions. These metal ions can successively slow down the fibril formation kinetics, thereby stabilizing the metastable intermediates of different and unique morphologies like droplets, spheres, vesicles, flowers, toroids, and so on. Trivalent metal ions can stabilize these intermediates more as compared to the bivalent ones. The unusual stability of the vesicle-like intermediates in the presence of selective metal ions is well rationalized with the metal ion coordination, metal ion-specific entropy factor, and excess hydrophobicity induced by the trivalent metal ions. Furthermore, the effect of surface charge inversion caused by these metal ions also plays a crucial role in their excessive stability.

Thus, monitoring the self-assembly process and detection of the intermediates formed during the self-assembly is quite important. In this thesis, we have also made an attempt to utilize the carbon dots as a probe to monitor the biomolecular self-assembly process. For the first time, we have observed that the hydrophobic carbon dot exhibits distinct emission behavior at different stages of the self-assembly process of amino acids, which can be observed through the naked eye under a UV

lamp. Therefore, this carbon dot can successfully detect the presence of prefibrillar intermediates and fibrillar networks via distinct emissions. Our study may facilitate in understanding the self-assembly of simple biomolecular building blocks, i.e., amino acids. It can further help us to get a better insight into the understanding of the self-assembly of complex systems like peptides and proteins.

7.2 Future Aspects

The self-assembly of the simplest elementary biomolecules is a very fundamental process in biology. Apart from the formation of various self-assembled nanostructures with a wide range of biofunctions, uncontrolled aggregation is problematic in many aspects. Therefore, it is important to study the self-assembly process of aromatic amino acids, the simplest building blocks of proteins and peptides to get insight into the mechanism and possible way to tune the self-aggregation process.

Our study reveals that the bivalent and trivalent metal ions with a higher charge-to-radius ratio can sufficiently slow down the fibrillation of amino acids, and metastable intermediates with various morphologies are obtained. The amino acids-based nanostructures can be a good substitute for therapeutic delivery due to their good biocompatibility, functionalization, and ease of synthesis. In the future, the metastable structures can also be utilized as drug delivery systems, nanoreactors, tissue engineering, and so on. We have also explored the potential of carbon dots to monitor the self-assembly of amino acids, which can be useful for bioimaging and monitoring the dynamics of other complex biomolecular self-aggregation processes. In the future, a new class of carbon dots can be designed for bioimaging and monitoring the biomolecular self-assembly.